Organometallic complexes featuring oligo-phenylene ethnylene ligands

Wan Mohamed Zin, an Mohd Khairul

Durham University

ORGANOMETALLIC COMPLEXES FEATURING OLIGO-PHENYLENE ETHYNYLENE LIGANDS

WAN MOHD KHAIRUL WAN MOHAMED ZIN

BSC (HONS.) (UNIPUTRAMALAYSIA), MSC (DUNELM), AMRSC

USTINOV COLLEGE

DEPARTMENT OF CHEMISTRY

DURHAM UNIVERSITY

A Thesis submitted for the degree of Doctor of Philosophy at the Durham University

September 2007

To Mek and Wae,

For simply being the most amazing and wonderful people I have ever met in my life….

STATEMENT OF COPYRIGHT

DECLARATION

The work described in this thesis was carried out in the Department of Chemistry at the University of Durham between October 2004 and August 2007. All the work was carried out by the author unless otherwise stated and has not previously been submitted for a degree at this or any other university.

FINANCIAL SUPPORT

The financial support of the studies is fully supported by Human Resources Development (Science and Technology Division), Ministry of Science, Technology and Innovation Malaysia Fellowship.

Accompanying Compact Disc

Associated .cif files for the molecular structures, extra experimental data, the bond lengths (Å) and angles (°) not discussed in the thesis.

Memorandum

The following conferences and symposia were attended during the period of study

♦ **Materials Chemistry Forum; MC7: Functional Materials for the 21st Century**

University of Edinburgh, UK 5-8th July 2005

♦ **Departmental 2nd Year PG Symposium**

Durham University, Durham, UK 4th May 2006

Talk given entitled. *'Homo and Heterometallic Clusters Complexes Featuring Oligo-Phenylenene Ethynylene As Ligands'*

♦ **Chianti Meeting on Inorganic Electrochemistry**

Certosa di Pontignano, Siena, Italy 15-20th July 2006

Poster Presented entitled. *'Novel Organometallic Complexes Featuring Conjugated Oligo-ethynylbenzene Derivatives As Ligands'.*

♦ **XXII International Conference on Organometallic Chemistry,**

Zaragoza, Spain 23-28th July 2006.

Poster Presented entitled. *'Novel Homo- And Heterometallic Cluster Complexes Featuring Conjugated Oligo-Ethynylbenzene Derivatives As Ligands'.*

♦ **Royal Society Discussion Meeting: Mixed Valency in Chemistry, Physics and Biology.**

Royal Society of Chemistry, Burlington House, London, UK 19-20th March 2007

♦ **Departmental 3rd Year PG Symposium**

Durham University, Durham, UK 5th and 14th May 2007

Poster presented and Talk Given entitled. *'Transition Metal Acetylide Complexes Featuring Oligo-Ethynyl Benzene Derivatives As Ligands'.*

The Following Publications are based on work described on this thesis:

W. M. Khairul, L. Porrès, D. Albesa-Jové, M. S. Senn, M. Jones, D. P. Lydon, J. A. K. Howard, A. Beeby, T. B. Marder, P. J. Low, **'Metal-Terminated Molecular Wires'**, *Journal of Cluster Chemistry*, 2006, **17**, 65.

M. A. Fox, R. L. Roberts, W. M. Khairul, F. Hartl, P. J. Low, **'Spectroscopic properties and electronic structure of 17-electron half-sandwich monoruthenium acetylide complexes, $[Ru(C{\equiv}CAr)(L_2)Cp']^+$ (Ar = phenyl, p-tolyl, 1-naphthyl, 9-anthryl; $L_2 = (PPh_3)_2$, Cp' = Cp; L_2 = dppe; Cp' = Cp*)'**, *Journal of Organometallic Chemistry*, 2007, **692**, 3277.

W. M. Khairul, D. Albesa-Jové, D. S. Yufit, M. R. Al-Haddad, J. C. Collings, F. Hartl, J. A. K. Howard, T. B. Marder, P. J. Low, **'The syntheses, structures and redox properties of phosphine-gold(I) and triruthenium carbonyl cluster derivatives of tolans'**, *Inorganica Chimica Acta*, 2007, article in press.

TABLE of CONTENTS

CHAPTER 3

'Synthesis and Structural Characterisation of Gold(I) Oligo-phenylene ethynylene Complexes'

CHAPTER 4

'Synthesis, Structural and Electronic Properties of Half-Sandwich Ruthenium Oligo-Phenylene Ethynylene Complexes'

CHAPTER 6

Novel Transmetallations From Simple Gold(I) Acetylide Moieties'

CHAPTER 7

Conclusions and Future Work

Abstract

Organometallic Complexes Featuring Oligo-Phenylene Ethynylene Ligands

Wan Mohd Khairul Wan Mohamed Zin

Durham University, 2007

This thesis describes the synthesis and analysis of organometallic complexes that feature oligo-phenylene ethynylene based ligands. **Chapter 1** introduces the general topic of molecular electronics and provides a general overview of the interest in phenylene ethynylene systems as foundation architectures for molecular wires. The role of metal complexes in molecular electronics and the application of the cluster - surface analogy to the study of model systems is also described.

Chapter 2 describes the synthesis of oligo-phenylene ethynylene pro-ligands of the general form $Me_3SiC{\equiv}CC_6H_4C{\equiv}CC_6H_4R$ (**1-5**), in which R is either an electron donor (Me, OMe) or acceptor (CO_2Me, NO_2, CN). The compounds were synthesised either *via* Sonogashira Pd/Cu cross-coupling reactions or *via* the nucleophilic attack of benzoquinones by lithiated acetylide anions and subsequent reduction. The desilylation of these compounds afforded the terminal alkynes $HC{\equiv}CC_6H_4C{\equiv}CC_6H_4R$ (**6-10**). Furthermore, the extended "three-ring" 1,4-bis(phenyl ethynylbenzene) derivatives $Me_3SiC{\equiv}CC_6H_4C{\equiv}CC_6H_4C{\equiv}C_6H_4C{\equiv}CSiMe_3$, **11** and $Me_3SiC{\equiv}CC_6H_4C{\equiv}CC_6(OMe)_2(H)_2C{\equiv}C_6H_4C{\equiv}CSiMe_3$, **13** and the terminal alkyne $HC{\equiv}CC_6H_4C{\equiv}CC_6(OMe)_2(H)_2C{\equiv}C_6H_4C{\equiv}CH$, (**14**) have also been prepared. These compounds were fully spectroscopically characterised and in the case of **14** the molecular structure analysis is discussed.

Chapter 3 discusses the synthesis of the gold(I) oligo-phenylene ethynylene complexes The complexes were prepared by treating the ligands precursors **1-5** with $AuCl(PL_3)$ (L = Ph or Cy) in the presence of NaOMe to afford complexes $Au(C{\equiv}CC_6H_4C{\equiv}CC_6H_4R)PPh_3$ [R = Me (**15**), **OMe** (**16**), CO_2Me (**17**), NO_2 (**18**) and

CN (**19**) and $Au(C{\equiv}CC_6H_4C{\equiv}CC_6H_4R)PCy_3$ [R = Me (**20**), OMe (**21**) and NO_2 (**22**)]. The "three-ring" complexes $\{Au(PPh_3)\}_2(\mu\text{-}C{\equiv}CC_6H_4C{\equiv}CC_6H_4C{\equiv}C_6H_4C{\equiv}C)$, **23** and $\{Au(PPh_3)\}_2(\mu\text{-}C{\equiv}CC_6H_4C{\equiv}CC_6(OMe)_2H_2C{\equiv}C_6H_4C{\equiv}C)$, **24** were also prepared. These complexes were spectroscopically characterised and molecular structural analyses reveal intermolecular interactions between the phenylene ethynylene portion of the molecules in the solid state, but not aurophilic interactions.

Chapter 4 examines the synthesis of half-sandwich $Ru(L_2)Cp'$ [$L = PPh_3$, Cp' = Cp ; L_2 = dppe, Cp' = Cp*) acetylide complexes derived from simple phenyl, tolan and oligo(phenylene ethynylene) based acetylenes. The electrochemical properties of these complexes have been explored, as have some of the molecular structural details.

Chapter 5 describes the synthesis of some cluster complexes. The gold acetylide complexes $Au(C{\equiv}CC_6H_4C{\equiv}CC_6H_4R)(PPh_3)$ react readily with $Ru_3(CO)_{10}(\mu\text{-dppm})$ to afford phenylene ethynylene derivatives $Ru_3(\mu\text{-}AuPPh_3)(\mu\text{-}C_2C_6H_4C{\equiv}CC_6H_4\text{-}R)(\mu\text{-dppm})(CO)_7$ (**38-42**) in which the conjugated organic moiety is "end-capped" by the cluster and an R group that is either electron donating or withdrawing (R = Me, OMe, CO_2Me, NO_2, CN). The clusters **38-42** are linked to the hydrido clusters $Ru_3(\mu\text{-}H)(\mu\text{-}C_2C_6H_4C{\equiv}CC_6H_4R)(CO)_7$ (**36** and **37**) through the well-known isolobal relationship between H and $Au(PR_3)$. In addition, the bis-cluster $\{Ru_3(\mu\text{-dppm})(CO)_7\}_2\{(\mu\text{-}AuPPh_3)\}_2(\mu\text{-}C_2C_6H_4C{\equiv}CC_6H_4C{\equiv}CC_6H_4C_2)$ (**43**) has also been prepared. All the clusters reported in this chapter were crystallographically determined. Structural, spectroscopic, photophysical and electrochemical studies were conducted and have revealed little electronic interaction between the remote substituent and the organometallic end-caps.

Chapter 6 explores the novel, preparative scale stoichiometric transmetallation reactions involving the simple $Au(C{\equiv}CR)(PPh_3)$ (R = Ph or C_6H_4Me) complexes. These gold(I) complexes have been treated with several inorganic and organometallic compounds MXL_n [M = metal, L_n = supporting ligands, X = halide], to afforded the corresponding metal-acetylide complexes $M(C{\equiv}CR)L_n$, with

representative examples featuring metals from Groups *8-11*. The acetylide products were fully characterised by usual spectroscopic methods including the molecular structural analysis.

Chapter 7 concludes the general summary of the thesis and discusses briefly the findings achieved in each chapter and the vital role of oligo-phenyelene ethynylenes ligands in the construction of numerous organometallic complexes which show interesting and promising properties for the molecular wires development. In addition, further future work is also proposed on other systems that feature this ligands.

Acknowledgements

Completing a PhD is a life experience that I would never forget. A lot of things came in my life during my studies, things that make me who I am today and wonderful experiences and meeting great people are a few things that worth priceless life experiences. Alhamdulillah, praise to Allah Almighty for His help and blessings, without Him I would not reach this far.

First and foremost I would like to address my deepest gratitude to Dr Paul James Low for not only for his kind supervisions throughout my studies but also a great mentor and always being patient with me. His guidance and help in different sorts of challenges while I am here that definitely nothing in this world is the same with the things that he has done. He taught me not only the knowledge in chemistry but also what the meaning of life. Thank you so much Paul, I do not know how on earth that I can pay you.

To the past and present members of the 'Low's Extended Family' in CY 100, thank you so much for you all for the priceless and precious friendships. I'd like to thank all the postdocs in the group namely Dr Donocadh Patrick Lydon, Dr Mark Edward Smith, Dr Mark Alexander Fox, Dr Howard James Spencer and Dr Xing Li. The deepest thank goes to Donocadh and Mark for their patience of guiding me in numerous challenges through my PhD. I also would like to acknowledge these amazing people in the group for making the life in the lab really enjoyable, thanks to Dr Rachel Louise Roberts, Mr Julian Dominic Farmer, Mr Oliver Alexander Dale, Miss Helen Elizabeth Coxon, Mr Neil John Brown, Prisca Eckert (University of Würzburg), Dr Pillar Cea, Miss Anna Villares and Mr Gorka Pera (University of Zaragoza).

This thesis would not be completed without a continuous support and help from Prof Todd B. Marder and his research groups in CY 52 throughout my studies, thank you for accepting me in the group from the beginning of my studies and at the end period of my PhD. A big thank you goes to Dr Jon C. Collings, Dr Richard Ward, Mr Brian

Hall, Dr Ibraheem Mkhalid, Mrs Maha Al-Haddad, Miss Kittiya Wongkhan, Mr Tay Meng Guan, Mr Jonathan Barnard, and Mr Marco Guttierez Crestani.

My thanks also go to Dr Frantisek Hartl (University of Amsterdam) for his brilliant collaboration in the electrochemical work and also to Prof. Michael I. Bruce and Dr Natasha N. Zaitseva (University of Adelaide) for their advices and guidance in the general synthetic work. It is an honour to meet all of you and the help and guidance in the studies is much appreciated. My thank also goes to Dr Andy Beeby's research group especially to Dr Karen Samantha Findlay, and Dr Laurent Porrés for their collaboration and helping me understanding what is photophysics actually means !

I also want to take this opportunity to thank my beloved parents Wan Mohamed Zin Wan Ahmad and Rokiah Awang and all my family back home for their continuous love, support, trust in me and brave enough to allow me to be in the other part of the world. I will never forget your strong spirit and believe in me for the rest of my life.

The thesis never be completed without the help from the 'backbone' of the Chemistry Department, my gratitude also goes to all the departmental analytical and the technical staff, you guys are great bunch of people and it is an honour to meet and work with all of you, thank you for all the help and guidance. I also would like to acknowledge the departmental academics for the help during the periods of my studies. The thesis never be completed without a hard work of our gifted crystallographers, thanks to Dr Dima S. Yufit and Dr David Albesa-Jovè for being so patience with me in solving the crystals.

To all my good friends, thank you all for accepting me as who I am, thanks for the lifetime precious friendships and you all just like my own brothers and sisters to me. Thanks for the patience, help, time and guidance while I am here. These special people mean a lot to me in life, Mr Michel Katris, Dr Matthew William Cartwright, Dr Carly Elizabeth Anderson, Miss Eleanor Monica Higgins, Mr Andrzej Jan Tadeusiak, Miss Louise Rebecca Harrison, Miss Emma Louise Parks, Mr Oliver

David Cunningham and Mr Christopher Luke Bailey. To my other friends who I have not mentioned here, thanks you all for the priceless friendships too.

To the sponsor of the studies, without the fellowship it is impossible for me to be here and enjoying these precious experiences. I would like to thank Ministry of Science, Technology and Innovation Malaysia for the scholarship under the 'Human Resources Development (Science and Technology Division) Fellowship. The financial support means a lot to me.

'Alah Bisa Tegal Biasa'

Wan Mohd Khairul Wan Mohamed Zin,
Deparrment of Chemistry, Durham University,
August 2007.

ABBREVIATIONS

General:

°	degrees
°C	degrees Celcius
Δ	reflux/difference
Å	angstrom
A	acceptor
Anth	anthracene
Ar	aryl groups
B	organic bridge
BPEB	1,4-bis(phenylethynyl)benzene
ca.	circa
cm	centimetres
Cp	cyclopentadienyl
Cp*	pentamethylcyclopentadienyl
CV	cyclic voltammetry
Cy	cyclohexyl
D	donor
DCTB	*trans*-2-[3-(4-*tert*-Butylphenyl)-2-methyl-2-propenylidene]malonitrile
DBU	1,8-diazabicyclo[5.4.0]undec-7-ene
dppe	1,2-bis(diphenylphosphino)ethane
dppm	bis(diphenylphosphino)methane
EC	electrochemical
edn.	Edition
Et	ethyl
EtOH	ethanol
Fc	ferrocene
Fc*	pentamethylferrocene
h	hour(s)
HOMO	highest occupied molecular orbital
HOSO	highest occupied single orbital

I/V	current voltage curve
J	Joules
IR	infrared
K	Kelvin
L	generic 2 electron ligand
LB	Langmuir-Blodgett
LUMO	lowest unoccupied molecular orbital
LUSO	lowest uncoccupied single orbital
M	metal/molarity
Me	methyl
MeCN	acetonitrile
MeOH	methanol
MeS	methylthiolate
mg	milligrams
MHz	megahertz
min	minutes
ml	millilitres
mmol	milimoles
MO	molecular orbitals
Mv	milivolts
MV	mixed-valence
Naph	naphthalene
NMR	nuclear aromatic resonance
ns	nanosecond(s)
NLO	nonlinear optical
nm	nanometres
Occ	occupancy
Ome	methoxy
OLED	organic light emitting diodes
OPE	oligo-phenyelene ethynylene
OTTLE	optically transparent thin-layer eelctrode
Ph	phenyl

ppm	part per million
^{i}Pr	isopropyl, -CH(Me)$_2$
R	general organic group
RT	room temperature
SAM	Self-Assembled Monolayer
SCE	saturated calomel electrode
$SiMe_3$	trimethylsilyl group
STM	Scanning Tunnelling Microscope
TMS	trimethylsilyl
TMSA	trimethylsilylacetylene
TEA	triethylamine
THF	tetrahydrofuran
TLC	thin layer chromatography
tol	*para*-tolyl, -C_6H_4Me
UV-vis-NIR	ultra violet-visible-near infrared
X	halide/substituents

NMR:

d	doublet
dds	doublet-of-doublet(s)
dt	doublet-of-triplet
Hz	hertz
m	multiplet
$^{n}J_{IJ}$	n bond coupling constant between nuclei I and J
ppm	part per million
s	singlet
t	triplet
δ	chemical shift

IR:

br	broad
cm^{-1}	wavenumbers (reciprocal centimetres)

m	medium
s	strong
sh	shoulder
w	weak

Mass Spectrometry:

EI	electron impact
ES	electrospray
M	molecular ion
m/z	mass per unit charge
MALDI-TOF	Matrix-assisted laser desorption/ionisation-time of flight

UV-Vis-NIR:

Abs	absorbance
LMCT	ligand-to-metal charge transfer
MLCT	metal-to-ligand charger transfer
TCSPC	time correlated single photon counting
ε	extinction coefficient
λ	wavelength

Electrochemistry:

A	amperes
CE	counter electrode
E	potential
En	potential of n^{th} redox process
$E_{1/2}$	half-wave potential
Ea	anodic potential
Ec	cathodic potential
I	current
ia	anodic peak current

ic	cathodic peak current
irr.	irreversible
Kc	comproportionation constant
DFT	density functional theory
TD-DFT	time-dependence density functional theory
V	volt(s)
ΔE	potential difference

1.1. Introduction to Molecular Electronics

Single molecules that have the ability or potential to be utilised as a self-contained electronic devices have attracted attention for the past few decades. It is a widely held hope that suitably functionalised molecules may be able to not only act as electronic components on a miniature scale but might also provide routes to novel device architectures. Amongst the most profound of the early investigations lies the work of Aviram and Ratner in 1974. They are arguably responsible for invigorating the field of molecular electronics by first proposing a unimolecular rectifier based on a Donor-Acceptor (D-A) architecture. [1] However, this proposal was premature in terms of both the chemical synthesis of such rectifying molecules and the fabrication of a device from these molecules, which involving the vertical stacking of molecules to give nanometre-scale thick organic monolayers sandwiched between two metal electrodes; such careful control over the bulk assembly of molecular was incredibly technically challenging at the time.

Fortunately developments in chemical synthesis and self-assembly methods have enabled these challenging experiments to be carried out in more recent times. For an example in 1997, Metzger and co-workers realised rectification through Langmuir-Blodgett (LB) multilayers and monolayers of hexadecylquinolinium tricyanoquinodimethanide. [2,3] Later Read found that instead of using LB films, the proposed conjugated oligomers with precisely controlled lengths as molecular devices using self-assembly techniques. Nevertheless, to electrically contact these functionalised rigid-rod conjugated oligomers with lengths on the order of nanometre is technically challenging. [4]

However, whilst the unimolecular rectifier project was arguably the starting point for much molecular electronics research in the later decades of the 20th Century, other applications and molecular electronic functions have emerged in more recent times. At the time of writing, the most widely investigated roles for the electronic properties of molecules within devices are: molecular wires, in which a molecule acts as a conduit for charge that is more effective than the transmission through space; [5]

molecular memories and signal processing, in which the electronic properties of a molecule are influenced by a a secondary property such as a non-linear optical effect, to permit signal processing and readable memory applications, [6-9] as a cheaper alternative materials to conventional solid state semi-conductors, in which the electronic properties of the bulk material is exploited to perform function. [10,11] Of these various roles and applications, exploration of use of molecules as wires, which are the simplest of electrical devices is particularly suited to the development of some fundamental understanding and techniques required for the realisation of molecule-scale electronics.

Several types of molecules have been suggested as 'molecular wires' and they all have the same key requirements. The most obvious is that they have to be electron or hole conducting in order to carry a current through the circuit. Thus the wire provides a pathway for transport of the electrons from one reservoir to another that is more efficient than electron transport through space. A molecular wire therefore may be defined as a 'one dimensional molecule allowing a through-bridge exchange of an electron/hole between its remote ends/terminal groups, themselves able to exchange electrons with the outside world.' [12] Some of the molecules that have been examined to as potential molecular wires are porphyrin oligomers, [13,14] nucleic acid strands, [15,16] carbon nanotubes [17] as well as conjugated organic molecules [18,19] and redox-active metal complexes. [20]

Quantification of the properties of a wire has been approached in different ways that generally depend on the technique used to analyse the wire properties. Measurements have been carried out of the rate of electron transfer across the wire using spectroscopic techniques, whilst techniques employing a Scanning Tunnelling Microscope (STM) (**Figure 1.1**) have been used to obtain current–voltage characteristics and to classify wires as metallic or semiconducting. Conjugated molecules, comprising alternating single and double (or triple) carbon–carbon bonds, can conduct electrons through their π-system, and this has been the basis of many wires. The wire must also be linear and of a defined length in order to span the gap between two components in the circuit. [21,22]

Mechanically controllable break junctions were originally used to study conductance quantisation. Reed and co-workers were the first to apply this technique to measure electronic transport through a single benzene-1,4-dithiol molecule. [4] Kergueris and co workers employed a fabricated break junction to study transport through oligothiophene molecules. [23] A vertical electrode method, which was first developed by Ralls, [24] was applied by Zhou to study 4-thioacetylbiphenyl molecules. [25] This technique realises the direct and robust metal-molecule contacts and allows for the variable temperature measurements, leading to the further understanding of metal-SAM contacts. [11,26] Nevertheless, the issues surrounding the contribution of the metal-molecule contact to the overall function of a molecular electronic device remains a topic for lively debate and intense investigation.

Meanwhile, the discovery of the scanning tunnelling microscope (STM) opened a new horizon for the study of molecular scale electronics. (**Figure 1.1**) This device is used for imaging, probing and manipulation of the single molecules. [5,27,28] For an example, the first demonstration of conductivity measurements using scanning tunnelling microscope (STM).was carried out by Bumm and co workers who used the STM to measure electron transport through individual molecules (or perhaps bundles of molecules) which were isolated in an insulating alkanethiol matrix.

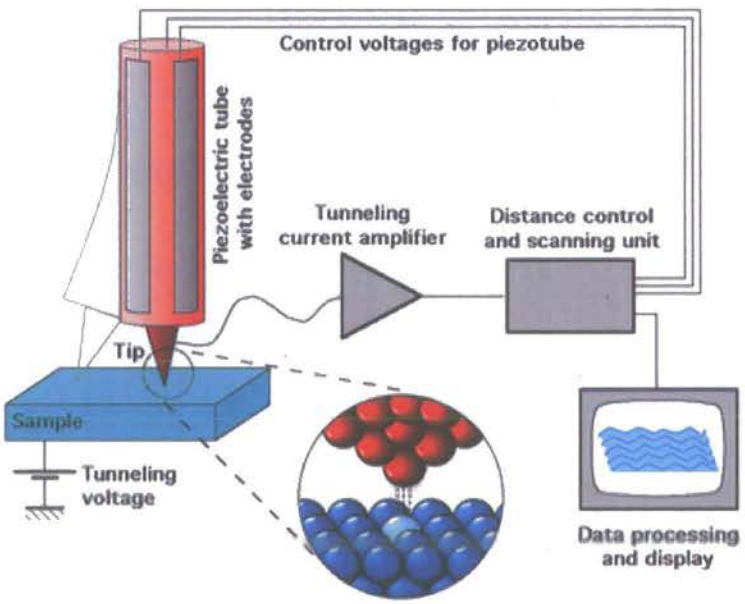

Figure 1.1. The design of Scanning Tunelling Miscroscope (STM). [29]

To improve contact between the molecules of interest and the STM tip a metallic nanoclusters, usually gold, have been self-assembled on top of the conjugated molecules of interest by Dorogi [30] and many others. [31-33] In this way, for example, the $I(V)$ characteristics of xylene-dithiol has been determined using a STM tip placed above gold cluster on a xylene-dithiol SAM covered gold surface. An intriguing avenue of current research is centred on the synthesis and properties of "insulated" molecular wires, in which a p-conjugated "core" is contained within a sheath of saturated organic material. [34-38]

In addition to research focusing on the electrical characterisation of conducting molecules, investigations of molecules with the ability to behave as switches have been ongoing for a considerable period of time. These lines of investigation were probably inspired by the idea of controlled current flow (rectification) developed by Aviram and Ratner [1] in 1974, which was elaborated upon by Aviram who proposed a molecular spiro switch in 1988. [39] Hopfield and co-workers also developed a molecular shift register to be used in molecular electronics memories. [40] Molecular switching concepts are now well developed with much of the work being directed towards the use of a controlled change in molecular geometry, and hence conjugation pathways, to influence the conductivity of the molecule in question. [41-45]

Recently, there are growing number of research project involving the experimental results on switching and memory behaviour been reported in memory devices. Collier and co workers have reported irreversible switch with a low current density involving LB film. [46]

The combination of these molecular elements of wires, switches and memories to create nanoscale devices with more complex functionality is the next step in the further development of molecular electronics. Nevertheless, the production of new molecular materials for applications in the various areas summarised by the term "molecular electronics" is an on-going and challenging process.

1.2 Oligo(phenylene ethynylene)s

One interesting branch of molecular electronics concern the properties and applications of rigid-rod, π-conjugated systems such as the 1,4-bis(phenylethynyl)benzene (BPEB) derivatives (**Figure 1.2**), and related oligomeric derivatives (OPE). These compounds which feature acetylenic substructures, display interesting structural, electronic, non-linear optical and luminescent properties. Similar motifs have attracted considerable attention in recent years as a conduit for electronic effects between molecular probe groups and consequently as a potential molecular framework from which to construct a range of molecular components for electronics. [4,47-54]

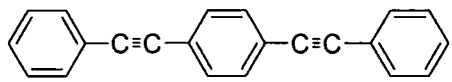

Figure 1.2. 1,4-bis(phenylethynyl)benzene.

The conjugated π-system offered by ethynyl-aromatic structures, such as 1,4-bis(phenylethynyl)benzene, has led to the development of molecular wire architectures and these fascinating properties may be directly attributed to the extended, linear π-conjugation along the principal molecular axis. [5,55,56] The concept of molecular switching through control over the relative orientation of the phenylene rings has been hotly debated in the literature, [50,57-64] with the low energy barrier to rotation proving to be a challenging obstacle that is yet to be overcome. [65]

One major advantage of building electronic devices based on OPEs is that these conjugated organic molecules can be prepared with a precise length by exploiting a range of known organic chemical reactions in their synthesis. For an example, not so long ago, Tour prepared an OPE that has a length of 128 Å (**Figure 1.3**). [52]

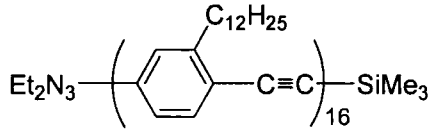

Figure 1.3. An example of an oligo(phenylene ethynylene) (OPE). [52]

In principle, oligomers are synthesised by joining one molecular unit repeatedly to itself a few times. This repeated unit is the equivalent of the unit cell in the solid state and is referred to as a monomer. Different from the more commonly encountered polymers that generally consist of strands of large molecules with varying length, structure and morphology, oligomers are synthesized as precisely controlled processes producing well defined chains. [66,67] In conjugated oligomers, in addition to the σ-framework that establishes the structure of molecules, π electrons are delocalized along the molecule. Within the context of single molecules for electronics, the best known example of conjugated oligomers are phenylene ethynylenes derivatives system that feature wire-like properties.[49,68-76]

The preparation of conjugated molecules of defined length and constitution is vital for the realisation of both molecules and polymers suitable for use as materials for molecular-scale electronics, organic luminescent devices, and nonlinear optical (NLO) media. [77,78] The ability to tailor organic molecular structure using organic synthetic techniques provides great versatility to modulate the properties of these molecules toward various applications. Conjugated oligomers of precise length and constitution have received considerable attention both as models for analogous bulk polymers and as candidates for molecular wires and molecular scale electronic devices. [79] Shape persistent oligo(phenyleneethynylenes) (OPEs) appear especially attractive for their excellent main-chain rigidity and interesting electronic characteristics. Several synthetic methods including solution and solid phase synthesis have been reported for preparing oligophenyleneethynylenes. The most common apparoach is through the reaction of a terminal alkyne with an aryl halide *via* a Sonogashira cross-coupling reaction [80] or by use of the benzoquinone carbon centres. [81-84] In most of the reported methods, isolation of environmentally sensitive terminal alkynes or bis(terminal alkynes) for use as intermediates is necessary, although protecting group strategies are becoming more widely employed. [85-87]

1.3. The Role of Metal Complexes in Molecular Electronics

Once the wire has been synthesised the key problem is how to attach this wire into a system in which it can be tested and eventually integrated into a circuit. In addition to the methods outlined above, the incorporation of transition metals which poses different redox state at each end of the molecular wire candidate can also allow the concept of "conductivity" of the wire to be tested thoroughly as shown in **Figure 1.4**. The best studied examples are dinuclear transition metal complexes. [12]

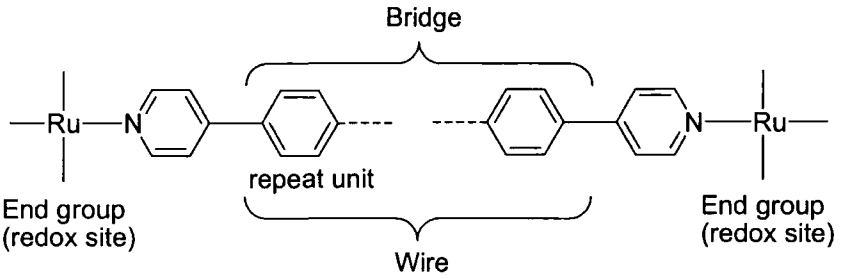

Figure 1.4. Schematic illustration of a molecular wire incorporated into a mixed valence system. [88]

The metal centres act as donor and acceptor sites for electrons transfer across the bridge or wire. These donor-bridge-acceptor systems have the advantage of generating the electron in-situ so there is no need to connect the molecule to a macroscopic system. The key requirement is that there is good overlap between the d-orbitals of the metal and the π-orbitals of the bridging segments so that there is delocalisation from one metal to the other, allowing the transfer of the electrons. However, the rate at which these electrons are transferred can be related to the properties of the wire for an example, the length and the degree of conjugation. [88] The properties of these mixed valence systems is usually assessed by analysis of the inter-valence charge transfer transition that results from photo-induced electron transfer between the two end units. The timescale of the transition and intensity and shape of the absorption band provides quantitative information on the extent coupling between the two metals, which can provide information relate to the efficiency of the wire. [21,89-91] Needless to say a wide range of bridging ligands including polyenes, polyynes and polyphenylenes have been studied for their electron transfer (ET) ability between two redox active metals.

Creutz and Taube are the pioneers in the field of mixed-valence metal complex, through their detailed studies of what is now known as the Creutz-Taube ion (**Figure 1.5**) [92,93] The ion has overall 5+ charge, with one ruthenium nominally in the 2+ oxidation state and the other in 3+ state. The interpretation of the electronic spectra of this mixed-valence (MV) compound has led to a greater understanding of the electron transfer process. Of the many conclusions that can be drawn, critical to the design of metal complexes for use in molecular electronics is the recognition that the coupling between the metal d-orbitals and the p-orbitals of the bridge is largely responsible for the magnitude of the bridge-mediated interaction between the metal centres.

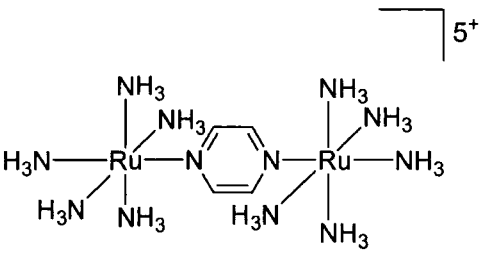

Figure 1.5. The Creutz-Taube ion. [92,93]

In seeking to design complexes which display strong metal-metal interactions metal acetylide complexes have come under close scrutiny as a result of the sensitivity of the metal-acetylide p-bonding interactions to both the nature of the metal and the acetylide substituents. [94-97] Consequently, the chemistry of metal complexes featuring alkyne and acetylide ligands which poses rigid-rod backbone, high stability and possible π-conjugation along the long molecular axis has long been thought useful in molecular electronics. [98-103] Some metal alkynyl complexes offer additional useful in physical properties including liquid crystallinity. [104-108]

It is has been demonstrated that physical properties of the metal acetylide polymers especially in oligo(phenylene ethynylene) derivatives may posses the extended π-conjugation along the polymer backbone due to the overlap of metal dπ and alkyne pπ orbitals, thus, these polymers may have similar optical and electronic properties to the conjugated organic polymers. [101] This in turn motivates the design of new monomeric models in order to evaluate the 'communication' between two metal centres, '**M1**' made possible by an organic bridge (**Figure 1.6a**), according to the

nature of the metal-bridge linkage. The influence of an additional metal fragment '**M2**' in the conjugated organic chain (**Figure 1.6b**) on the properties of these systems is also bring a great interest. [109]

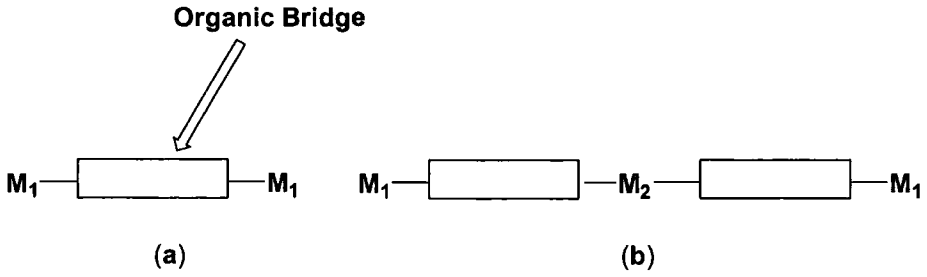

Figure 1.6. The simple schematic diagram of the representation design of monomeric model for metal-organic linkage.

As discussed above, the arylene ethynylene motif has attracted considerable attention in recent years as a conduit for electronic effects between molecular probe groups, and consequently as a potential molecular framework from which to construct a range of molecular components or materials for electronics, [110-112] or optic applications. [113,114] Most of the studies in which the phenylene ethynylene motif has been incorporated with organometallic and inorganic molecular probes have concentrated on the properties of mono-metallic species, and take advantage of the energy or electron transfer events, or magnetic interactions, that can be observed between the metal termini as a means of assessing the metal-ligand interaction, and hence provide a prelude for studies of the efficacy of organic bridge as a conduit for these processes. [115-118] Similar monometallics moieties have been incorporated with conjugated phenylene ethynylene ligands for use in the production of metallopolymers. [99,119,120] whilst in the case of gold(I) complexes, the linear coordination chemistry, together with the linearity of the C≡C bond in alkynyl ligands, make alkynylgold(I) complexes attractive candidate for the design of linear-chain metal containing polymers with the extended backbone electronic conjugation. [121] Multimetallic end-caps to phenylene ethynylene moieties, especially those larger than 1,4-diethynyl aromatics, are, however, less common.

1.4. Introduction to Metal Carbonyl Cluster Chemistry

Although many studies have been directed towards understanding the molecular factors that might influence the wire-like properties of ethynyl aromatic structures, much less is known about the metal-molecule interface which is critical to the interface of molecular components with the macroscopic world. While the cluster-surface analogy has fallen into disuse, transition metal clusters do offer convenience structural models of binding of molecules to surfaces. [122,123] The binding of alkyne derivatives to clusters is different from the mononuclear metal centres and the novel structures that formed may give clues for the surface chemistry. For an example, some time ago Adam and co-workers carried out some investigations of the cluster chemistry of a simple phenylene ethynylene derivative and the reported results of a study of the binding modes of a thiol terminated 1,4-bis(phenylethynyl)benzene to osmium clusters. [124]

Carbon chain complexes with cluster capping groups usually involve the terminal carbon atom of the chain being attached to all three metal atoms by between one and three σ-type bonds, the μ_3-η^1 mode (**Figure 1.7a**). Such capping groups include $M_3(\mu\text{-}H)_3\text{-}(CO)_9$ (M = Ru, Os), $Co_3(CO)_9$ and $M_3Cp'_3$ (M = Co, Rh, Ir; Cp' = Cp, Cp*). However there are far fewer examples of complexes in which a Cn chain is attached by two of the carbon atoms in a μ_3-η^3 mode (**Figure 1.7b**).

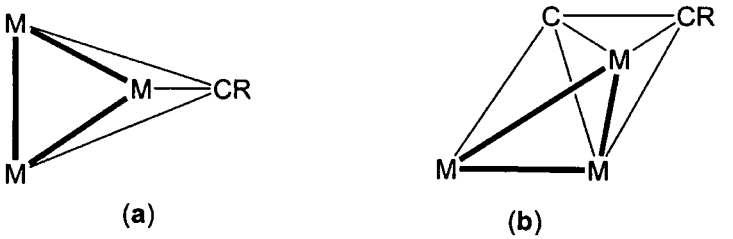

Figure 1.7. The attachment of terminal carbon to the metal atoms by (**a**) μ_3-η^1 mode and (**b**) μ_3-η^3.

Numerous di- and tri- metal carbonyl complexes are known to react readily with alkynes to give heteronuclear complexes. [125,126] Thus, the poly-ynediyl M-(C≡C)n-M and polyynyl complexes M-(C≡C)n-H are becoming precursors for cluster compounds containing a one dimensional carbon chain, with adduct formation

typically occurring at the least hindered alkyne linkage. [127] This interaction to multiple metal centres serves to stabilise the unstable poly-ynyl compounds. The common route of the formation of these clusters is via initial formation of η^2-alkyne complex, which subsequently interacts with other metal atoms of the cluster, and therefore attached to the all three metal atoms. Bruce and co-workers have demonstrated this initial formation of a μ_3-η^2-alkyne cluster and subsequent hydrogen migration to the cluster to give a hydrido-alkynyl complex. [128] To give a wide idea about the mechanism, **Scheme 1.1** shows an example of this procedure. The reaction between $Ru_3(CO)_{10}(NCMe)_2$ with the C_4 complex $W(C{\equiv}CC{\equiv}CH)(CO)_3Cp$ afforded the μ_3-alkyne complex, $Ru_3\{\mu_3\text{-}\eta^2\text{-}HC_2C{\equiv}C[W(CO)_3Cp]\}(\mu\text{-}CO)(CO)_9$ in 40 % yield. [129] The bridging CO ligand was easily identified in the IR spectrum as a weak band at 1879 cm^{-1}, while in the ^1H NMR spectrum of (≡CH) proton was observed at δ 7.86 ppm. This complex was readily converted into the corresponding hydrido-alkyl cluster, $Ru_3(\mu\text{-}H)\{\mu_3\text{-}C_2C{\equiv}C[W(CO)_3Cp]\}(CO)_9$ by briefly heated at reflux in benzene (**Scheme 1.1**). The ^1H NMR spectrum of this complex contained the metallohydride resonance at δ-20.33 ppm. [129]

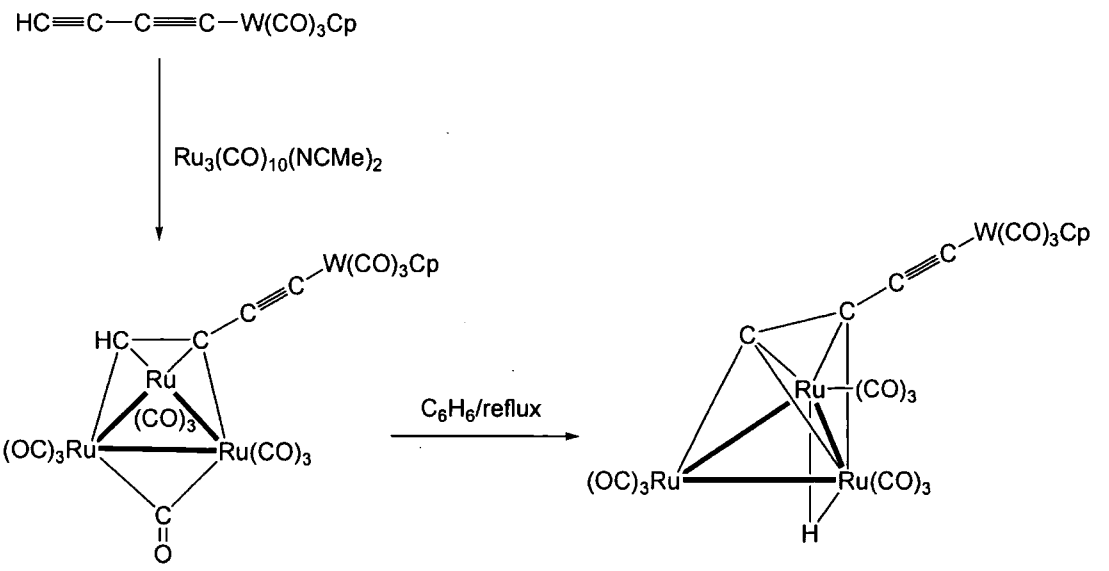

Scheme 1.1. The preparation of $Ru_3\{\mu_3\text{-}\eta^2\text{-}HC_2C{\equiv}C[W(CO)_3Cp]\}(\mu\text{-}CO)(CO)_9$ and $Ru_3(\mu\text{-}H)\{\mu_3\text{-}C_2C{\equiv}C[W(CO)_3Cp]\}(CO)_9$. [129]

The isolobal nature of the hydride and the $\{Au(PR_3)\}^+$ species has enabled the rational synthesis of new gold containing clusters in which the cluster cores differ structurally from examples such as those shown in **Scheme 1.1** only by the replacement of the hydride ligand by the $\{Au(PR_3)\}^+$ moiety. [130,131] Therefore the reaction between $Ru_3(\mu\text{-dppm})(CO)_{10}$ and $Au(C_2Ph)\{P(tol)_3\}$ in THF has afforded the heteronuclear cluster of $AuRu_3(\mu_3\text{-}C_2Ph)(\mu\text{-dppm})(CO)_7\{P(tol)_3\}$ in 92 % yield as shown in **Scheme 1.2**. [132]

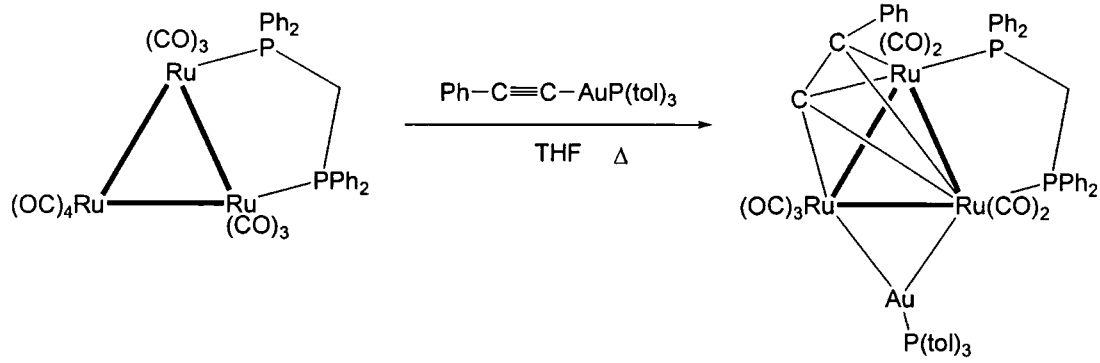

Scheme 1.2. The preparation of $AuRu_3(\mu_3\text{-}C_2Ph)(\mu\text{-dppm})(CO)_7\{P(tol)_3\}$. [132]

Complexes containing more than one cluster located at the termini of a linear conjugated ligand may serve as mimics for molecular wires suspended between two macroscopic interfaces. Such species have been prepared by reacting poly-yne species with greater than one equivalent of the metal carbonyl. For instance, the reaction between $Ru_3(\mu\text{-dppm})(CO)_{10}$ and $\{Au[P(tol)_3]\}_2\{\mu\text{-}C{\equiv}CC{\equiv}C)$ in THF generated a mixture clusters of $\{AuRu_3(CO)_9[P(tol)_3]\}_2(\mu_3, \eta^2{:}\mu_3, \eta^2\text{-}C_2C_2)$ and the monocluster complex $AuRu_3\{\mu_3, \eta^2\text{-}C_2C{\equiv}CAu[P(tol)_3]\}(CO)_9\{P(tol)_3\}$ in 10 and 31 % yield respectively (**Scheme 1.3**). The ^{31}P NMR spectra contained signals at δ 59.9 ppm for the symmetrical di-cluster complex and at δ 40.0 ppm and 59.5 ppm for $C{\equiv}CAu\{P(tol)_3\}$ and $Ru_3Au\{P(tol)_3\}$ respectively in mono-cluster complex. [133]

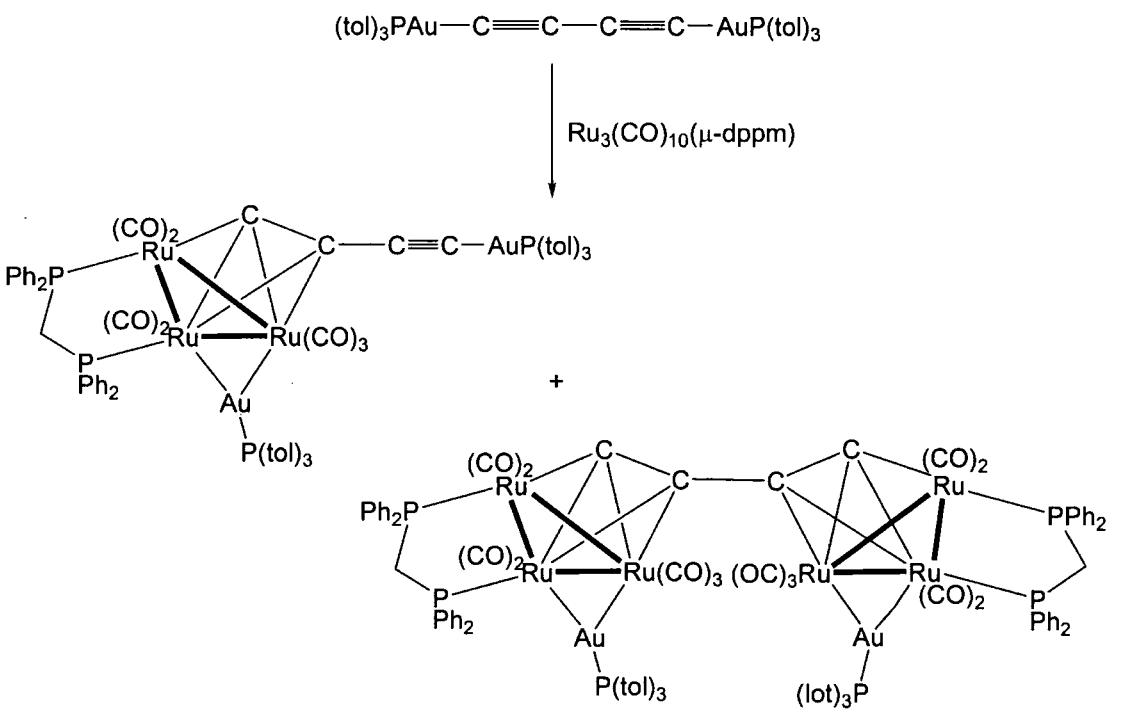

Scheme 1.3. The preparation of $AuRu_3(CO)_9[P(tol)_3]\}_2(\mu_3, \eta^2{:}\mu_3, \eta^2\text{-}C_2C_2)$ and the monocluster complex $AuRu_3\{\mu_3, \eta^2\text{-}C_2C{\equiv}CAu[P(tol)_3]\}(CO)_9\{P(tol)_3$. [133]

In this thesis, reactions of terminal alkynes and gold(I)tripheylphosphine of oligo(phenylene ethynylene) ligands with $Ru_3(\mu\text{-dppm})(CO)_{10}$ are described and these clusters are fully characterised spectroscopically, structurally and investigations of their photophysical and electrochemical properties are also have been carried out.

1.5. The Aims and Objectives of the Thesis

While the preparation of a simple metal complexes containing conjugated ligand system that feature one aryl groups are widely developed, there are few examples of complexes featuring oligo(phenylene ethynylene ligands. The most general aim of this thesis is to explore the synthesis, characterisation and properties of conjugated molecular systems featuring different metal groups and oligo(phenylene ethynylene) as ligands. The studies described herein include the synthetic approach, spectroscopic characterisations, photophysical properties, crystallographic studies, and in some cases computational studies will be described.

Chapter 2 of the thesis presents a discussion of the preparation and characterisation of the oligo(phenylene ethynylene) pro-ligand. These pro-ligands have been prepared by typical Sonogashira Pd/Cu cross-coupling reaction or *via* the electrophilicity of carbonyl carbon centres in benzoquinone. In addition, different electron donating or withdrawing groups are also have been introduced and the capacity of the OPE fragment to transmit this electronic information to the remote metal centre is investigated. The effect of the length of the molecular backbone has also been investigated. Thus, the synthesis of the extended "three-ring" ligands derived from the prototypical 1,4-bis(phenyl ethynyl)benzene is also described.

In **Chapter 3** the use of the pro-ligands in the preparation of gold(I) phenylene ethynylene complexes with phosphine co-ligands (PPh_3 and PCy_3) will be presented. The structures of these complexes in the solid state have been determined, along with their photophysical properties which can be compared with the properties of simpler conjugated systems.

Chapter 4 details the chemistry of ruthenium complexes, and contains details of the electrochemistry of the complexes that containing these OPE ligands. By the attachment of the electron rich $Ru(PPh_3)_2Cp$ and Ru(dppe)Cp* fragments to the OPE based fragments, a new series of redox active complexes has been prepared. The key idea is to investigate the role of the molecular backbone of the ligands and the influence of various electron donating and withdrawing groups in these properties. The Chapter contains details of electrochemical studies (cyclic voltammetry), IR spectroelectrochemistry, UV-vis-NIR spectroelectrochemistry, and DFT calculations studies for selected complexes.

In **Chapter 5**, several complexes in which clusters containing bridging hydride ligands "end-cap" the phenylene ethynylene motif have been prepared. The isolobal analogy of hydride and ($AuPR_3$) has also led to of the preparation of similar clusters with a μ-$Au(PR_3)$ centre to be prepared. These clusters have been fully studied spectroscopically and structurally. Further studies electrochemical and photophysical methods are also described. The results obtained have been compared with those

from the ligand precursors and the role of the clusters core as well as the ligands in the molecular structure revealed.

Transmetallation is a process of increasing importance in the area of transition metals in organic synthesis, but has been a little studied and poorly understood. In the final chapter (**Chapter 6**) of the thesis, the readily availability complexes $Au(C{\equiv}CR)(PPh_3)$ (R = Ph, or C_6H_4Me) have been used in the preparation of several acetylide complexes, via transmetallation of the acetylide fragment from gold. In addition, simple reactions have been carried out to investigate the mechanism involved in the formation of these complexes.

1.6. References

1. A. Aviram, M. A. Ratner, *Chem. Phys. Lett.*, 1974, **29**, 277.
2. R. M. Metzger, B. Chen, U. Holpfner, M. V. Lakshmikantham, D. Vuillaume, T. Kawai, X. Wu, H. Tachibana, T. V. Hughes, H. Sakurai, J. W. Baldwin, C. Hosch, M. P. Cava, L. Brehmer, G. J. Ashwell, *J. Am. Chem. Soc.*, 1997, **119**, 10455.
3. R. M. Metzger, *Chem Rev.*, 2003, **103**, 3803.
4. M. A. Reed, C. Zhou, C. J. Muller, T. P. Burgin, J. M. Tour, *Science*, 1997, **278**, 252.
5. L. A. Bumm, J. J. Arnold, M. T. Cygan, T. D. Dunbar, T. P. Burgin, L. Jones, D. L. Allara, J. M. Tour, P. S. Weiss, *Science*, 1996, **271**, 1705.
6. A. P. de Silva, H. Q. N. Gunaratne, C. P. McCoy, *Nature*, 1993, **364**, 42.
7. A. P. de Silva, H. Q. N. Gunaratne, G. E. M. Maguire, *J. Chem. Soc., Chem. Commun.*, 1994, 1213.
8. A. P. de Silva, I. M. Dixon, H. Q. N. Gunaratne, T. Gunnlaugsson, P. R. S. Maxwell, T. E. Rice, *J. Am. Chem. Soc.*, 1999, **121**, 1393.
9. S. Uchiyama, N. Kawai, A. P. de Silva, K. Iwai, *J. Am. Chem. Soc.*, 2004, **126**, 3032.
10. M. C. Petty, M. R. Bryce, D. Bloor eds., *Introduction to Molecular Electronics*, Edward Arnold, 1995, London.
11. J. Chen, L. C. Calvet, M. A. Reed, D. W. Carr, D. S. Grubisha, D. W. Bennet, *Chem. Phys. Lett.*, 1999, **313**, 741.
12. F. Paul, C. Lapinte, *Coord. Chem. Rev.*, 1998, **178-180**, 431.
13. H. L. Anderson, *Chem. Commun.*, 1999, 2323.
14. J. R. Reimers, L. E. Hall, M. J. Crossley, N. S. Hush, *J. Phys. Chem. A*, 1999, **103**, 4385.
15. H. –W. Fink, C. Schonenberger, *Nature*, 1999, **398**, 407.
16. M. W. Grinstaff, *Angew. Chem. Int. Ed.*, 1999, **38**, 3629.
17. J. Kong, N. R. Franklin, C. W. Zhou, M. G. Chapline, S. Peng, K. J. Cho, H. J. Dai, *Science,* 2000, **287**, 622.
18. K. J. Donovan, S. Spagnoli, *Chem. Phys.*, 1999, **247**, 293.

19. S. Huang, J. M. Tour, *J. Am. Chem. Soc.*, 1999, **121**, 4908
20. P. J. Low, *Dalton Trans.*, 2005, 2821.
21. N. Robertson, C. A. McGowan, *Chem. Soc. Rev.*, 2003, **32**, 96.
22. M. D. Ward, *J. Chem. Educ.*, 2001, **78**, 321.
23. C. Kergueris, J. –P. Bourgoin, S. Palacin, D. Esteve, C. Urbina, M. Magoga, C. Joachim, *Phys. Rev. B*, 1999, **59**, 12505.
24. K. S. Rall, R. A. Buhrman, T. C. Tiberio, *Appl. Phys. Lett.*, 1989, **55**, 2429.
25. C. Zhou, M. R. Deshpande, M. A. Reed, L. Jones II, J. M. Tour, *Appl. Phys. Lett.*, 1997, **71**, 611.
26. J. Chen. M. A. Reed, A. M. Rawlett, J. M. Tour, *Science,* 1999, **286**, 1550.
27. D. M. Eigler, E. K. Schweizer, *Nature*, 1990, **344**, 524.
28. G. Binnig, H. Rohner, C. Gerber, H. Weibel, *Phys. Rev. Lett.*, 1982, **49**, 57.
29. http://www.iap.tuwien.ac.at/www/surface/STM_Gallery/.
30. M. Dorogi, J. Gomez, R. Osifchin, R. P. Andres, R. Reifenberger, *Phys. Rev. B*, 1995, **52**, 9071.
31. B. K. Min, W. T. Wallace, D. W. Goodman, *Surface Science*, 2006, **600**, L7.
32. N. K. Chaki, P. Singh, C. W. Dharmadhikari, K. P. Vijayamohanan, *Langmuir*, 2004, **20**, 10208.
33. C. E. J. Mitchell, A. Howard, M. Carney, R. G. Egdell, *Surface Science*, 2001, **490**, 196.
34. P. N. Taylor, A. J. Hagan, H. L. Anderson, *Org. Biomol. Chem.*, 2003, **1**, 3851
35. F. Cacialli, J. S. Wilson, J. J. Michels, C. Daniel, C. Silva, R. H. Friend, N. Severin, P. Samorì, J. P. Rabe, M. J. O'Connell, P. N. Taylor, H. L. Anderson, *Nature Materials*, 2002, **1**, 160.
36. P. N. Taylor, M. J. O'Connell, L. A. McNeill, M. J. Hall, R. T. Aplin, H. L. Anderson, *Angew. Chem. Int. Ed.*, 2000, **39**, 19, 3456.
37. K. –I. Yoshida, T. Shimomura, K. Ito, R. Hayakawa, *Langmuir*, 1999, **15**, 910.
38. J. Stahl, J. C. Bohling, E. B. Bauer, T. B. Peters, W. Mohr, J. M. Martin-Alvarez, F. Hampel, J. A. Gladysz, *Angew. Chem. Int. Ed.*, 2002, **41**, 11, 1872.

39. A. Aviram, *J. Am. Chem. Soc.*, 1988, **110**, 5687.
40. J. J. Hopefield, J. Nelson, D. Beratan, *Science*, 1988, **241**, 817.
41. A. C. Benniston, A. Harriman, *Angew. Chem. Int. Ed.*, 1993, **32**, 10, 1459.
42. V. Goulle, A. Harriman, J.-M. Lehn, *J. Chem. Soc., Chem. Commun.*, 1993, 1034.
43. L. Gobi, P. Seiler, F. Diederich, *Angew. Chem. Int. Ed.*, 1999, **38**, 5, 674.
44. V. Balzani, M. Gómez-López, J. F. Studdart, *Acc. Chem. Res.*, 1998, **31**, 405.
45. M. Seward, R. B. Hopkins, W. Sauerer, S. -W. Tam, F. Diederich, *J. Am. Chem. Soc.*, 1990, **112**, 1783.
46. C. P. Collier, E. W. Wong, M. Belohradský, F. M. Raymo, J. F. Stoddard, P. J. Kuekes, R. S. Williams, J. R. Heath, *Science*, 1999, **285**, 391.
47. E. Negishi, L. Anastasia, *Chem Rev.*, 2003, **103**, 1979.
48. P. F. H. Schwab, M. D. Levin, J. Michl, *Chem. Rev.*, 1999, **99**, 1863.
49. U. H. F. Bunz, *Chem. Rev.*, 2000, **100**, 1605.
50. A. Beeby, K. Findlay, P. J. Low, T. B. Marder, *J. Am. Chem. Soc.*, 2002, **124**, 8280.
51. U. H. F. Bunz, *Acc. Chem. Res.*, 2001, **34**, 998.
52. J. M. Tour, *Chem. Rev.*, 1996, **96**, 537.
53. M. T. Cygan, T. D. Dunbar, J. J. Arnold, L. A. Bumm, N. F. Shedlock, T. P. Burgin. C. Jones II, J. M. Tour, P. S. Weiss, *J. Am. Chem. Soc.*, 1998, **120**, 2721.
54. D. K. James, J. M. Tour, *Adrich Chimica Acta*, 2006, **39**, 47.
55. J. M. Seminario, A. G. Zacarias, J. M. Tour, *J. Am. Chem. Soc.*, 1998, **120**, 3970.
56. J. Cornill, Y. Karkazi, J. L. Bredas, *J. Am. Chem. Soc.*, 2002, **124**, 3516.
57. C. E. Godinez, G. Zepeda, M. A. Garcia-Garibay, *J. Am. Chem. Soc.*, 2002, **124**, 4701.
58. Z. Dominguez, H. Dang, M. J. Strouse, M. A. Garcia-Garibay, *J. Am. Chem. Soc.*, 2002, **124**, 7719.
59. Z. Dominguez, T. -A. V. Khuong, H. Dang, C. N. Sanrame, J. E. Nunez, M. A. Garcia-Garibay, *J. Am. Chem. Soc.*, 2003, **125**, 8827.

60. C. E. Godinez, G. Zepeda, C. J. Mortko, H. Dang, M. A. Garcia-Garibay, *J. Org. Chem.*, 2004, **69**, 1652.

61. (a) S. D. Karlen, M. A. Garcia-Garibay, *Chem. Commun.*, 2005, 189, (b) S. D. Karlen, R. Oritz, O. L. Chapman, M. A. Garcia-Garibay, *J. Am. Chem. Soc.*, 2005, **127**, 6554.

62. S. D. Karlen, C. E. Godinez, M. A. Garcia-Garibay, *Org. Lett.*, 2006, **8**, 3417.

63. T.-A. V. Khuong, H. Dang, P. D. Jarowski, E. F. Maverick, M. A. Garcia-Garibay, *J. Am. Chem. Soc.*, 2007, **129**, 839.

64. A. Beeby, K. S. Findlay, P. J. Low, T. B. Marder, P. Matousek, A. W. Parker, S. R. Rutter, M. Towrie, *Chem., Commun.*, 2003, 2406.

65. S. J. Greaves, E. L. Flynn, E. L. Futcher, E. Wrede, D. P. Lydon, P. J. Low, S. R. Rutter, A. Beeby, *J. Phys. Chem. A*, 2006, **110**, 2114.

66. J. S. Schumm, D. L. Pearson, J. M. Tour, *Angew. Chem. Int. Ed.*, 1994, **33**, 1360.

67. J. M. Tour, R. Wu, J. S. Schumm, *J. Am. Chem. Soc.*, 1991, **113**, 7064.

68. D. J. Armit, G. T. Crisp, *J. Org. Chem.*, 2006, **71**, 3417.

69. C. D. Zangmeister, S. W. Robey, R. D. van Zee, Y. Yao, J. M. Tour, *J. Am. Chem. Soc.*, 2004, **126**, 3420.

70. L. Cheng, J. Yang, Y. Yao, D. W. Prince Jnr., S. M. Dirk, J. M. Tour, *Langmuir*, 2004, **20**, 1335.

71. D. W. Prince Jnr., S. M. Dirk, F. Maya, J. M. Tour, *Tetrahedron*, 2003, **59**, 2497.

72. Y. Morisaki, Y. Chujo, *Macromolecules*, 2002, **35**, 587.

73. D. V. Kosynkin, J. M. Tour, *Org. Lett.*, 2001, **3**, 993.

74. C. J. Yu, Y. Chong, J. F. Kayyem, M. Gozin, *J. Org. Chem.*, 1999, **64**, 2070.

75. S. Fraysse, C. Coudret, J. –P. Launay, *Tetrahedron Lett.*, 1998, **39**, 7873.

76. D. L. Pearson, J. M. Tour, *J. Org. Chem.*, 1997, **62**, 1376

77. R. E. Martin, F. Diederich, *Angew. Chem. Int. Ed.* 1999, **38**, 1350.

78. K. Müllen, G. Wegner, eds., *Electronic Materials: The Oligomer Approach*; Wiley-VCH: Weinheim, 1998.

79. T. Gu, J. Nierengarten, *Tetrahedron Lett.*, 2001, **42**, 3175.

80. K. Sonogashira, Y. Tohda, N. Hagihara, *Tetrahedron Lett.*, 1975, **16**, 4467.

81. P. J. Hanhela, D. B. Paul, *Aust. J. Chem.*, 1981, **34**, 1669.

82. P. J. Hanhela, D. B. Paul, *Aust. J. Chem.*, 1981, 34, 1687.

83. G. Clauss, W. Reid, *Chem. Ber.*, 1975, **108**, 528.

84. D. P. Lydon, L.Porrés, A. Beeby, T. B. Marder, P. J. Low, *New J. Chem.*, 2005, **29**, 972.

85. C. Wang, A. S. Batsanov, M. R. Bryce, G. J. Ashwell, B. Urasinska, I. Grace, C. J. Lambert, *Nanotechnology*, 2007, **18**, 044005.

86. G. J. Ashwell, B. Urasinska, C. Wang, M. R. Bryce, I. Grace, C. J. Lambert, *Chem. Commun.*, 2006, 4706.

87. C. Wang, A. S. Batsanov, M. R. Bryce, I. Sage, *Org. Lett.*, 2004, **6**, 2181.

88. J. Launay, *Chem. Soc. Rev.*, 2001, **30**, 386.

89. B. C. Brunschwig, C. Creutz, N. Sutin, *Chem. Soc. Rev.*, 2002, **31**, 168.

90. N. Sutin, C. Creutz, *Adv. Chem. Ser.*, 1978, **168**, 1.

91. K. D. Demadis, C. M. Hartshorn, T. J. Meyer, *Chem. Rev.*, 2001, **101**, 2655.

92. C. Creutz, H. Taube, *J. Am. Chem. Soc.*, 1969, **91**, 3988.

93. C. Creutz, H. Taube, *J. Am. Chem. Soc.*, 1973, **95**, 1086.

94. J. E. McGrady, T. Lovell, R. Stranger, M. G. Humphrey, *Organometallics*, 1997, **16**, 4004.

95. C. –Y. Wong, C. –M. Che, M. C. W. Chan, J. Han, K. –H. Leung, D. L. Phillips, K. –Y. Wong, N. Zhu, *J. Am. Chem. Soc.*, 2005, **127**, 13997.

96. P. Mathur, A. K. Ghosh, S. Mukhopadhyay, C. Srivinasu, S. M. Mobin, *J. Organomet. Chem.*, 2003, **678**, 142.

97. D. L. Lichtenberger, S. K. Renshaw, R. M. Bullock, *J. Am. Chem. Soc.*, 1993, **115**, 3276.

98. N. Chawdhury, A. Köhler, R. H. Friend, W. Y. Wong, J. Lewis, M. Younus, P. R. Raithby, T. C. Corcoran, M. R. A. Al-Mandhary, M. S. Khan, *J. Chem. Phys.* , 1999, **10**, 4963.

99. R. P. Kingsborough, T. M. Swager, *Prog. Inorg. Chem.*, 1999, **48**, 123.

100. M. J. Irwin, J. J. Vittal, R. J. Pudephatt, *Organometallics*, 1997, **16**, 3541.

101. G. Frapper, M. Kertesz, *Inorg. Chem.*, 1993, **32**, 732.

102. C. W. Faulkner, S. L. Ingham, M. S. Khan, J. Lewis, N. J. Long, P. R. Raithby, *J. Organomet. Chem.*, 1994, **482**, 139.

103. D. Bloor, *Chem. Ber.*, 1995, **31**, 385.

104. A. A. Dembek, R. R. Burch, A. E. Feiring, *J. Am. Chem. Soc.*, 1993, **115**, 2087.

105. M. Altmann, V. Enkelmann, G. Lieser, U. H. F. Bunz, *Adv. Mater.*, 1995, **7**, 726.

106. I. R. Whittal, A. M. McDonagh, M. G. Humphrey, *Adv. Organomet. Chem.*, 1998, **42**, 291.

107. W. J. Yang, C. H. Kim, M. –Y. Jeong, S. K. Lee, M. J. Piao, S. –J. Jeon, B. R. Cho, *Chem. Mater.*, 2004, **16**, 2783.

108. G. T. Crisp, P. D. Turner, *Tetrahedron*, 2000, **56**, 8335.

109. O. Lavastre, J. Plass, P. Bachmann, S. Guesmi, C. Moinet, P. H. Dixneuf, *Organometallics*, 1997, **16**, 184.

110. C. Joachim, J. K. Gimzewski, A. Aviram, *Nature*, 2000, **408**, 541.

111. J. M. Tour, *Acc. Chem. Res.*, 2000, **33**, 791.

112. M. D. Ward, *J. Chem. Educ.*, 2001, **78**, 321.

113. J. Lewis, M. S. Khan, A. K. Kakkar, B. F. G. Johnson, T.B. Marder, H. B. Fyfe, F. Whittmann, R. H. Friend, A. E. Dray, *J. Organomet. Chem.*, 1992, **425**, 165.

114. M. S. Khan, A. K. Kakkar, N. J. Long, J. Lewis, P. Raithby, P. Nguyen, T. B. Marder, F. Whittmann, R. H. Friend, *J. Mater. Chem.*, 1994, **4**, 1227.

115. F. de Montigny, G. Argouarch, K. Costuas, J. –F. Halet, T. Roisnel, L. Toupet, C. Lapinte, *Organometallics*, 2005, **24**, 4558.

116. T. Weyland, K. Costuas, A.Mari, J. –F. Halet, C. Lapinte, *Organometallics*, 1998, **17**, 5569.

117. S. Le Stang, L. Toupet, C. Lapinte, *C. R. Chimie*, 2003, **6**, 353.

118. P. J. Low, R. L. Roberts, R. L. Cordiner, F. Hartl, *J. Solid State Electrochem.*, 2005, **9**, 717.

119. W. Y. Wong, *J. Inorg. Organomet. Polym. Mater.*, 2005, **15**, 197.

120. M. S. Khan, A. K. Kakkar, S. L. Ingham, P. R. Raithby, J. Lewis, B. Spencer, F. whittmann, R. H. Friend, *J. Organomet. Chem.*, 1994, **472**, 247.

121. J. Vicente, M. Chicote, M. Abrisqueta, *Organometallics*, 1997, **16**, 5628.

122. R. H. Crabtree, *The Organometallic Chemistry of the Transition Metals*, John Wiley & Sons, Inc. 2001.

123. E. Band, E. L. Mutterties, *Chem. Rev.*, 1978, **78**, 639.

124. R. D. Adams, T. Barnard, A. Rawlett, J. M. Tour, *Eur. J. Inorg. Chem.*, 1998, 429.

125. J. R. Shapely, S. I. Richter, M. Tachikawa, J. B. Keister, *J. Organomet. Chem.*, 1975, **94**, C43.

126. M. Akita, A. Sakurai, M. –C. Chung, Y.Moro-oka, *J. Organomet. Chem.*, 2003, **670**, 2.

127. M. I. Bruce, P. J. Low, *Adv. Organomet. Chem.*, 2004, **50**, 179.

128. M. I. Bruce, B. W. skleton, A. H. White, N. N. Zaitseva, *J. Chem. Soc., Dalton Trans.*, 1999, 1445.

129. M. I. Bruce, P. J. Low, N. N. Zaitseva, S. Kahlal, J. –F. Halet, B. W. Skelton, A. H. White, *Dalton Trans.*, 2000, 2939.

130. G. Ferguson, J. Gallagher, A. –M. Kelleher, T. R. Spalding, F. T. Deeney, *J. Organomet. Chem.*, 2005, **690**, 2888.

131. R. Hoffmann, *Angew. Chem. Int.Ed.*, 1982, **21**, 711.

132. M. I. Bruce, P. A. Humphrey, E. Horn, E. R. T. Tiekink, B. W. Skelton, A. H. White, *J. Organomet. Chem.*, 1992, **429**, 207.

133. M. I. Bruce, N. N. Zaitseva, B. W. Skelton, A. H. White, *J. Organomet. Chem.*, 2005, **690**, 3268.

Chapter 2. 'Syntheses and Characterisation of Conjugated Oligo-phenylene ethynylenes As Ligands'

2.1. Introduction

Long 'rigid-rod' organic molecules with extended π-conjugated systems are of considerable interest within the fields of both molecular materials for electronics and also molecular electronics, [1] due to their numerous potential applications as components within electrical circuits. These applications include not only use as molecular wires and switches, taking advantage of the extended linear π-conjugated framework, but also as emitting components within light-emitting devices and as lumophores in sensors, particularly in the case of molecular materials containing aromatic moieties with the extended π-framework, due to the efficient photo-excitation and luminescent decay often associated with such systems. [2-7] Although much of the work with "wire-like" molecules described to date has been concerned with materials derived from 1,4-bis(phenylethynyl)benzene, [8-18] there is a rapidly growing body of work associated with longer phenylene ethynylene derivatives which are suitably functionalised to allow the assembly of multi-nanometre long molecules onto metallic or semi conducting surfaces. [19-23] These very long, chemically well defined species, the associated metal-molecule-metal test structures that can be constructed from them and the measurements of "through-molecule" conductivity (i.e. molecular wire-like properties) represent the cutting-edge of molecular electronics research.

Before being classified as "molecular wires" candidate molecules must meet the same requirements needed to act as a wire at the macroscopic level. In other words, whilst molecular wires can in principle be sub-classified as either electron-conducting or hole-conducting, the essential criterion is that the molecular framework is able to carry a current through the circuit. Thus the wire provides a pathway for transport of electrons (or holes) from one reservoir to another that is more efficient than electron transport through space. [14,24-28] For purely practical reasons, many workers have chosen to impose other critical requirements on

molecular wire candidates. These include demands that the candidate molecules must be linear and of a known, finite and specified length in order to facilitate fabrication of test devices in which the candidate molecules span a well-defined gap between two components in the circuit. Issues of how the molecular wire candidate will be attached to interfaces with the macroscopic world, usually a metallic or semi-conducting surface, must also be addressed.

Whilst numerous and diverse molecular scaffolds have been designed, synthesised and tested in a variety of contexts as molecular wires, [4,7,19,21,29-30] including those which can be considered as possessing an integrated insulating sheath. [31,32] Arguably the most prototypical examples all posses a delocalised π-electron system based on linear carbon-rich strings comprised of alternating single and double or triple carbon-carbon bonds. [19,33-37]

However, for synthetic simplicity instead of using conjugated linear carbon chains for the construction of the wires, chains of various aromatic rings linked by acetylene units, for example oligo(1,4-phenylene ethynylene) derivatives, [38-41] have been perhaps the most widely studied systems. These studies of generic arylene ethynylene based molecular wires have provided the incentive for the preparation and study of more elaborate molecules of nanometre proportions in what amounts to a synthetic tour de force of acetylene chemistry. [22,23,42]

In order to ensure that molecular wires can be attached to the metal surfaces, so-called 'molecular alligator clips' are often introduced to each end of the molecular wire. [43-46] The most common example of these molecular alligator clips are thiols, which form gold-thiolates on exposure to gold surfaces. [47-48] This chemical attachment of the wire to the metal surface, the nature of which is still not fully understood, nevertheless does provide a dramatic increase in "through molecule" conductivity. [49-52] However thiols are oxidatively unstable and the optimal method of assembling thiols onto gold surfaces is likely to be *via* an *in-situ* deprotection approach. [53-55] Research into other methods of molecule-metal attachment has also been carried out. [56] Very recently, Langmuir-Blodgett assembled films of 1,4-

bis(phenylene ethynylene) derivatives featuring carboxylic acid, nitrile and amine surface binding groups have attracted attention. [57,58] Common to all of the "alligator clips" is the desire to allow the molecular wire to be more or less firmly attached to two electrodes so that a current can be passed efficiently. This is then allows the direct measurement of the conductivity of a molecular wire, which has become possible with the development of methods involving the use of the Scanning Tunnelling Microscope (STM), [19,59-63] break-junctions [64-67] and nano-pore assemblies. [68-72]

Before discussion of the results contained in this thesis, it is important to summarise the key synthetic methodologies that underpin the preparation of oligo(phenylene ethynylene) based molecular materials. Whilst there are many synthetic methods available for the preparation of acetylenes, [73-75] including oligo(phenylene ethynylene) derivatives, the most common approach used at the present time involves the Sonogashira Pd^0/Cu^I catalysed cross-coupling reaction. Phenylene ethynylene oligomers are often prepared from iodo- or bromo arenes and the terminal acetylenes by application of the Sonogashira cross-coupling protocol. [9,74,76-79] However, the introduction of different acetylenic substituents around a single aromatic core can involve tedious, often multi-step synthetic strategies based on the use of an excess of dihalo arene, necessitating chromatographic separation of the product from the unreacted reagent, (**Scheme 2.1**) [80] or chemospecific reaction sequences of iodobromobenzenes, for an exaples is shown in **Scheme 2.2.** [34,54,81-85]

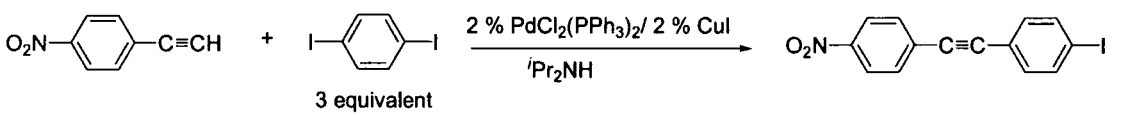

Scheme 2.1. The use of excess dihaloarene often involves tedious chromatographic separations. [80]

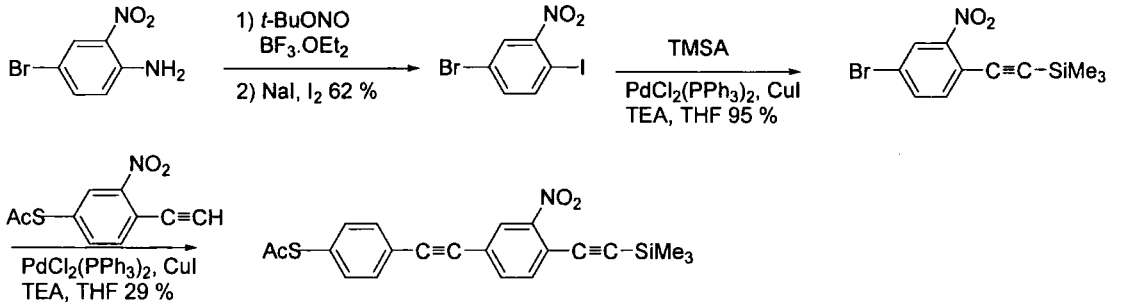

Scheme 2.2. Synthesis of mononitro compound which involving regiospecific reaction sequence of iodobromobenzene. [81]

Alternatively, a linear synthetic route requiring functional group inter-conversions to give halide (preferably iodide) derivatives for further cross-coupling reactions can be employed as shown in **Scheme 2.3**. [34]

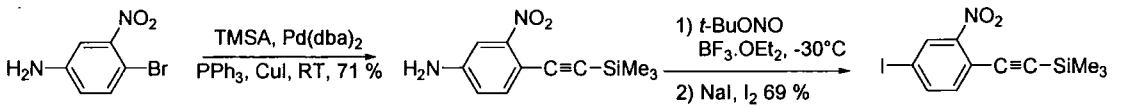

Scheme 2.3. An example of synthetic route to the conversion of the amine group to the iodide. [34]

Fortunately, there is an alternative way of preparing series of compounds which make use of the electrophilicity of carbonyl carbon centres in quinones. [97-99] The protocol is believed to be simple and cost effective, and is readily adapted to the preparation of both symmetric and differentially substituted materials. The addition of diones, naphthaquinone and anthraquinone to tow molar equivalent of trimethylsilylacetylide readily afforded the corresponding enediols which obtaines as a mixture of syn and anti in an approximately 1:2 ratio. Both isomers are readily reduce by tin(II) chloride followed by reduction as shown in the **Scheme 2.4**. [86]

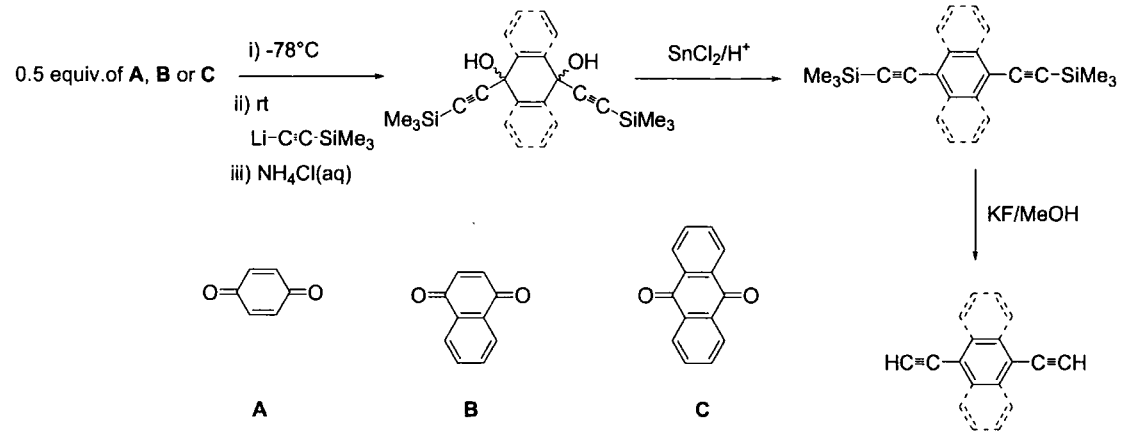

Scheme 2.4. The synthesis of diethynyl aromatic compounds from the aromatic diones **A**, **B**, and **C**. [86]

Another unique characteristics of this sequence is introduced by the sequential reaction of the lithiated acetylides that allows the rapid assembly of the carbon skeleton of differentially substituted 1,4-bis(ethynyl)diols in one-pot, with subsequent reduction affording the dialkynyl aromatics.

This method of synthesis of phenylene ethynylenes, has proven to give better yield result than the typical Sonogashira Pd/Cu cross-coupling reaction. For an example, the subsequential reaction of 1,4-benzoquinone with lithium phenylacetylide followed by lithium trimethylsilylacetylide gave trimethylsilyl ethynyl tolan in 61 % overall yield. [86] In contrast as the sequence of Sonogashira Pd/Cu reactions with 1-bromo-4-iodobenzene only managed to obtain 53 % overall yield. [44]

In this thesis, the syntheses of phenylene-ethynylene oligomer were prepared by Sonogashira Pd/Cu cross-coupling reactios via the nucleophilic attack of the benzoquinone by lithialated anions, and subsequent reduction of the intermediate diols formed has been undertaken.

One of the general aims of this project was to investigate the propagation of electronic effects from a donor or acceptor group located at one end of an oligomeric (phenylene ethynylene) based structure to an organometallic group located at the

remote terminus. This Chapter describes the synthesis and characterisation of the 1,2-diphenyl acetylene [tolan] and 1,4-bis(phenylethynyl) benzene [BPEB] derivatives that underpin the synthetic work in this Thesis.

2.2. Result and Discussion

2.2.1. Syntheses

The trimethylsilyl-protected ethynyl tolan derivative **1** is available *via* a simple synthetic route involving the sequential reaction of lithium tolylacetylide and lithium trimethylsilylacetylide with benzoquinone and reduction by $SnCl_2$ of the mixture of *meso* and *anti* diols thus formed. Compound **1** was obtained as cream-coloured solid in 63 % yield (**Scheme 2.5**).

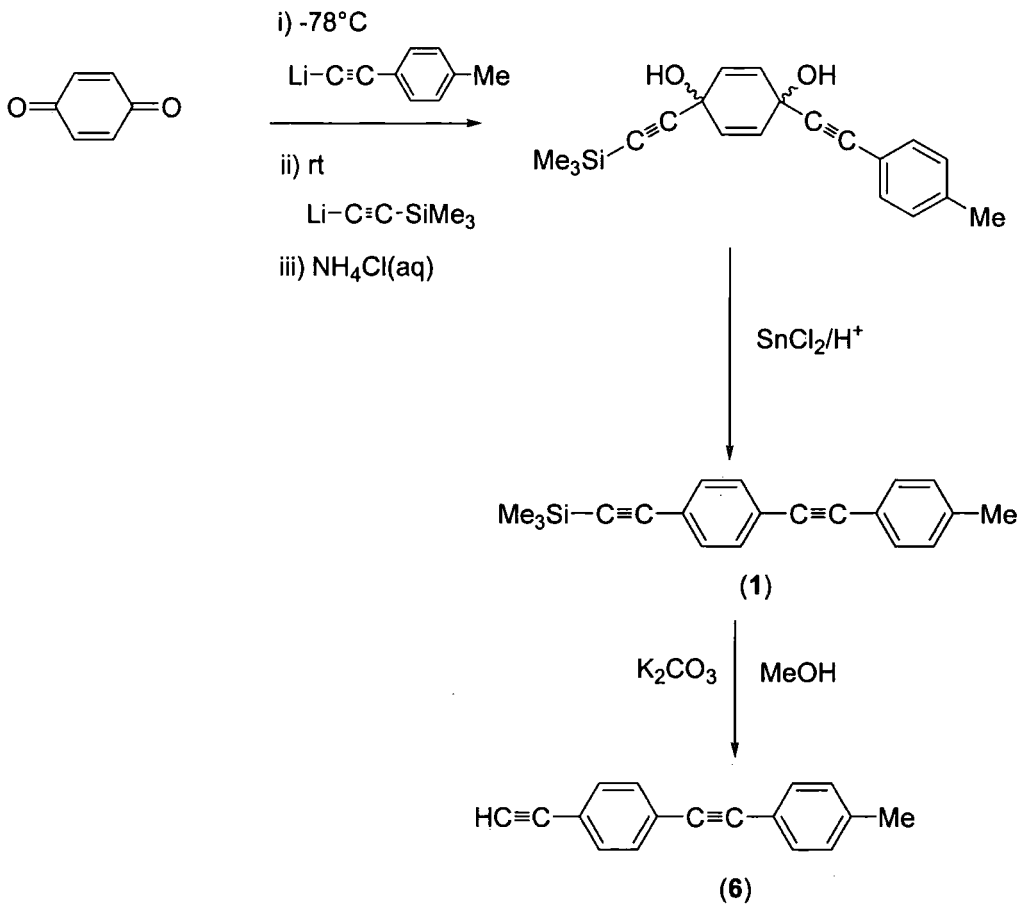

Scheme 2.5. Synthesis of compound **1** *via* benzoquinone nucleophilic attack followed by desilyation to afford terminal alkyne **6**.

However, following the development of conditions that permit the multi-gram scale preparation of 4-(trimethylsilyl ethynyl)phenyl acetylene, [34,87,88] it proved possible and expeditious to utilise this compound as a key building block in the assembly of other ethynyl tolans **2-5** (**Scheme 2.6**). The $PdCl_2(PPh_3)_2$/CuI catalysed cross-coupling reaction of 1-trimethylsilylethynyl-4-ethynylbenzene with a range of aryl halides carried out in refluxing NEt_3 afforded ethynyl tolans featuring substituents with various electron withdrawing (CO_2Me, NO_2, CN) or donating (OMe) properties. In each case the progress of the reaction was monitored by spot TLC and when judged complete, the reaction mixtures were purified by conventional or flash chromatography on silica and/or recrystallisation from hot toluene. The yellow compounds **2-5** were obtained in 50-90 % isolated yields.

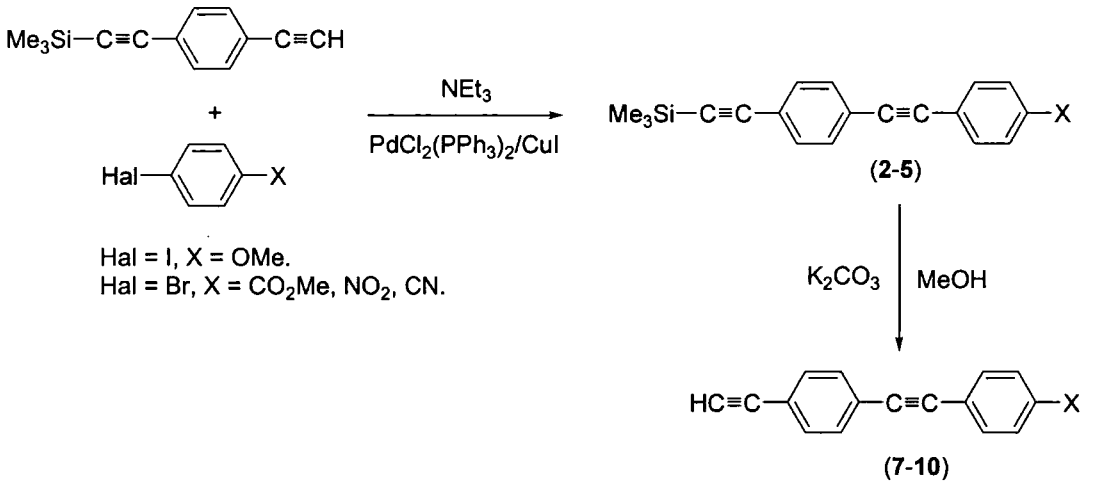

Scheme 2.6. Syntheses of compounds **2-5** *via* Pd/Cu Sonogashira cross-coupling reaction followed by desilyation to afford terminal alkynes **7-10**.

Compounds **1-5** were desilylated at room temperature by reaction with K_2CO_3 in MeOH. The reaction mixture was partitioned between H_2O/diethylether and dried over $MgSO_4$ to afford terminal alkynes **6-10** as cream and yellow solid in 50-90% yield.

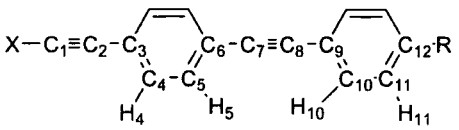

X = $SiMe_3$, R = Me (**1**) X = H, R = Me (**6**)
= $SiMe_3$, R = OMe (**2**) = H, R = OMe (**7**)
= $SiMe_3$, R = CO_2Me (**3**) = H, R = CO_2Me (**8**)
= $SiMe_3$, R = NO_2 (**4**) = H, R = NO_2 (**9**)
= $SiMe_3$, R = CN (**5**) = H, R = CN (**10**)

Scheme 2.7. Numbering scheme for NMR spectral assignment of **1-5** and **6-10**.

All the TMS protected (**1-5**) and terminal alkynes tolans (**6-10**) were fully characterised by the usual spectroscopic methods. The numbering scheme for ^1H and ^{13}C NMR spectral assignment is shown in **Scheme 2.7.**

In ^1H NMR spectra of **1-5** the expected TMS resonances can be observed at ca. δ_H 0.26 ppm. In addition, methyl resonance can be observed at δ_H 2.37 ppm for **1** and methoxy and methyl ester resonances at ca. δ_H 3.90 ppm for **2** and **3**. The aromatic protons of **1-5** are often observed as distinctive pseudo-doublet resonances between δ_H 6.9-8.2 ppm but in some cases (**1**, **2** and **5**) only gave rise to unresolved singlet resonances. Unsurprisingly, these characteristics are strongly influenced by the various *p*-substituents groups at the phenyl ring. The spectroscopic properties of the terminal alkyne tolan derivatives (**6-10**) are very similar to those of the precursors **1-5**. The most notable exception is the loss of TMS resonances which have been replaced by the terminal alkyne protons, which can be observed at ca. δ_H 3.2 ppm.

The ^{13}C NMR spectra of the TMS protected tolans, **1-5** and terminal alkyne tolans **6-10**, are, as might be expected, similar, and are consistent with the structures. For example, compounds (**1-6**) contain TMS resonances at ca. δ_C 0.1 ppm. In addition, the spectra of **1** and **6** contain methyl resonances at δ_C 22 ppm, whereas the methoxy and methyl ester carbons in (**2** and **7**) and (**3** and **8**) were observed above δ_C 50 ppm. In addition, the distinctive carbonyl carbon in **4** and **9** were observed near δ_C 167 ppm, whilst in the case of **5** and **10**, the CN carbon was observed at ca. δ_C 122 ppm. The acetylide carbons C_1 and C_2 were observed at ca. δ_C 80 ppm (**Scheme 2.6**).

Another set of acetylenic carbons (C_7 and C_8) can be found at ca. δ_C 90 ppm. The aromatic carbons of the tolan fragment $C_3 - C_6$ and $C_9 - C_{10}$ are all clearly observed and assigned on the basis of comparisons within the series of compounds **1-5** and **6-10**. Thus, C_3 can be found between δ_C 115-130 ppm, with C_4 and C_5 falling at higher chemical shift ca. δ_C 132 ppm; C_6 and C_9 are found at ca. δ_C 120 ppm. The C_{10} resonances are observed near δ_C 130 ppm, whilst C_{11} and C_{12} can be found between δ_C 114-132 ppm and δ_C 112-160 ppm, respectively. The IR spectra of **1-5** and terminal alkynes **2-10** were recorded as Nujol mulls, and show one ν(C≡C) band at ca. 2150 cm^{-1} and another near 2200 cm^{-1}, the latter likely being attributable to the terminal acetylene moiety.

The positive ion electron-impact mass spectra $[EI\text{-}MS]^+$ of **1-5** contained M^+ at *m/z* 288 and $[M\text{-}Me]^+$ at *m/z* 273 for **1**, for **2** M^+ at *m/z* 304, $[M\text{-}OMe]^+$ at *m/z* 274 and $[M\text{-}Me]^+$ at *m/z* 201. Meanwhile, for **3**, contained M^+ at *m/z* 332, $[M\text{-}Me]^+$ at *m/z* 317 and $[M\text{-}OMe]^+$ at 301. For **4** and **5** only M^+ found at *m/z* 319 and *m/z* 299 respectively. The $[EI\text{-}MS]^+$ compounds **6-10** were also recorded showing M^+ at *m/z* 216 for **6**, M^+ at *m/z* 232 and $[M\text{-}Me]^+$ at *m/z* 217 for **7.** For **8**, M^+ at m/z 260 and $[M\text{-}OMe]^+$ at *m/z* 229. M^+ at *m/z* 247 and a simple protonated species of $[M\text{-}NO_2H]^+$ for **9**. Another protonated species was found for **10** showing $[M+H]^+$ at *m/z* 228, M^+ at *m/z* 277 and another fragment of $[M\text{-}C{\equiv}N]^+$ at *m/z* 201.

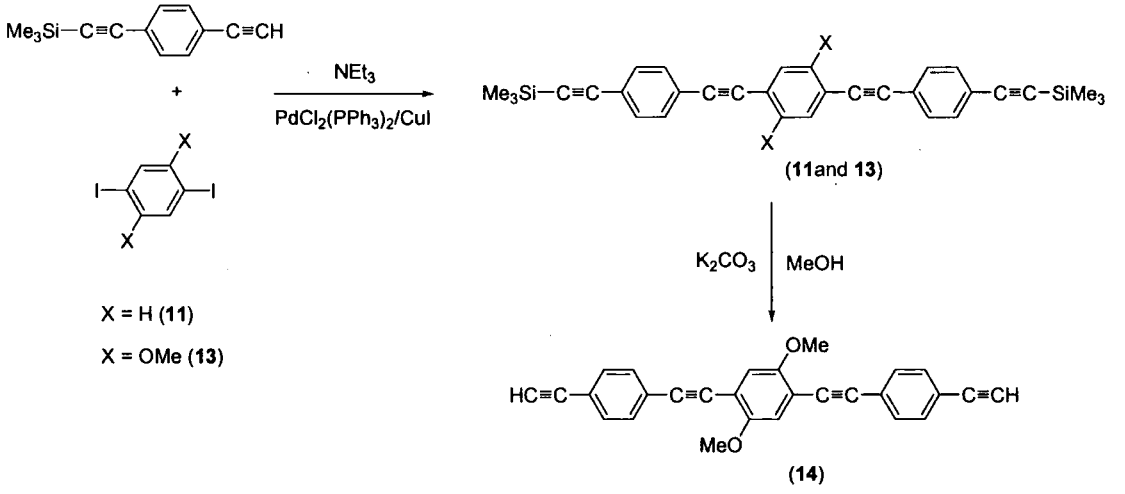

Scheme 2.8. Syntheses of compound **11** and **13** *via* Pd/Cu Sonogashira cross-coupling reaction followed by desilyation of **13** to afford terminal alkyne **14**.

Sonogashira cross-coupling protocols were also used to prepare the extended three rings system **11** and **13** with *ca.* 69 % yield (**Scheme 2.8**). Desilylation of **11** afforded $HC{\equiv}CC_6H_4C{\equiv}CC_6H_4C{\equiv}CC_6H_4C{\equiv}CH$, **12** [89] which was insoluble in methanol. The introduction of the two methoxy groups to the middle ring of the similar system, **13**, gives increased the solubility in most organic solvents. Desilylation of **13** afforded **14** in a high yield (95 %).

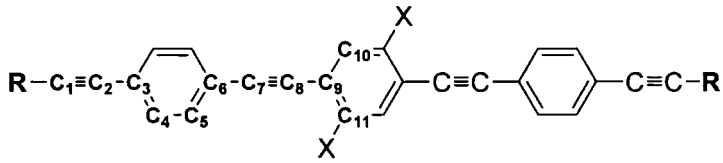

R = $SiMe_3$, X = H (**11**) R = H, X = H (**12**)

R = $SiMe_3$, X = OMe (**13**) R = H, X = OMe (**14**)

Scheme 2.9. Numbering scheme for NMR spectral assignment of **11-12** and terminal alkynes **13** and **14**.

Compounds **11**, **13** and terminal alkyne **14** were fully characterised by the usual spectroscopic methods. The numbering scheme for ^1H and ^{13}C NMR spectral assignment are shown in **Scheme 2.9**.

The ^{1}NMR spectra of **11** and **13** are consistent with the proposed structures, the TMS moieties being observed at ca. δ_H 0.25 ppm. In the aromatic region, two unresolved singlet resonances at δ_H 7.45 ppm and δ_H 7.50 ppm can be observed for **11**. For **13**, a singlet methoxy resonance can be observed at δ_H 3.90 ppm. In the aromatic region, singlet resonance can be observed at δ_H 7.01 ppm which corresponds to two aromatic protons in the middle ring. In addition, a distinctive two pseudo-doublets resonances can be observed at δ_H 7.45 ppm (J_{HH} = 8.8 Hz) and δ_H 7.51 ppm (J_{HH} = 8.8 Hz).

The desilylation of **13** afforded **14**, evidenced by the lost of the TMS peak in the ^1H NMR spectrum, which was replaced by terminal acetylene peaks at δ_H 3.18 ppm. Like the parent compound **13**, a methoxy resonance also can be observed at δ_H 3.90. In the aromatic region, a singlet resonance can be observed at δ_H 7.03 ppm which

corresponds to two aromatic protons in the middle ring. Two sets of pseudo-doublet resonances can be observed at δ_H 7.48 ppm (J_{HH} = 8 Hz) and δ_H 7.53 ppm (J_{HH} = 8Hz).

Unsurprisingly, the ^{13}C NMR spectra for compounds **11**, **13** and the desilylated compound **14** are very similar. Both compounds **11** and **13** contain TMS resonances at ca. δ_C 0.1 ppm. The methoxy resonance in **13** and **14** can be observed at ca. δ_C 57 ppm. The acetylide carbons C_1 and C_2 and C_7 and C_8 are identified and observed between δ_C 90-100 ppm (**Scheme 2.8**). For the aromatic carbons, there are six identifiable resonances for **11** and seven in the case of **13** and **14** as expected on the basis of symmetry. Thus, C_3 and C_6 can be found at ca. δ_C 123 ppm, with C_4 and C_5 falling at higher chemical shift ca. δ_C 132 ppm; for C_9, the resonance is found in between δ_C 114-123 ppm. The C_{10} resonances are observed between δ_C 116-132 ppm, whilst the resonance for carbon C_{11} in **13** and **14** can be found at higher chemical shift, δ_C 154 ppm.

The electro-spray $[MS\text{-}ES]^+$ mass spectrum for **11** and MALDI-TOF(+)-MS spectrum for **13** and **14** all show isotopic envelopes corresponding to molecular ions $[M]^+$ at *m/z* 470 for **11**, for **13** M^+ at *m/z* 530 and M^+ at *m/z* 386 for **14**. In addition, all compounds also exhibit ions arising from the simple protonated species $[M+H]^+$ at *m/z* 471 for **11**, at *m/z* 531for **13** and at *m/z* 387 for **14**.

2.2.2. Molecular Structural Analysis of 14

The molecular structure of **14**, has been determined by single crystal X-ray diffraction. Crystallographic data, selected bond lengths and angles are listed in **Table 2.1** and **Table 2.2.** The crystallographic work has been carried out by Dr D. S. Yufit.

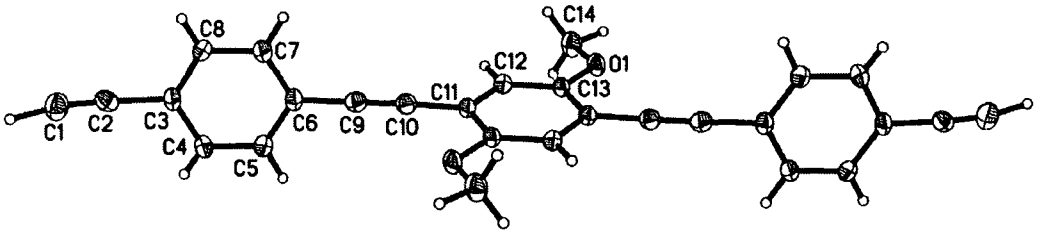

Figure 2.1. A plot of molecule of **14**, illustrating the atom numbering scheme.

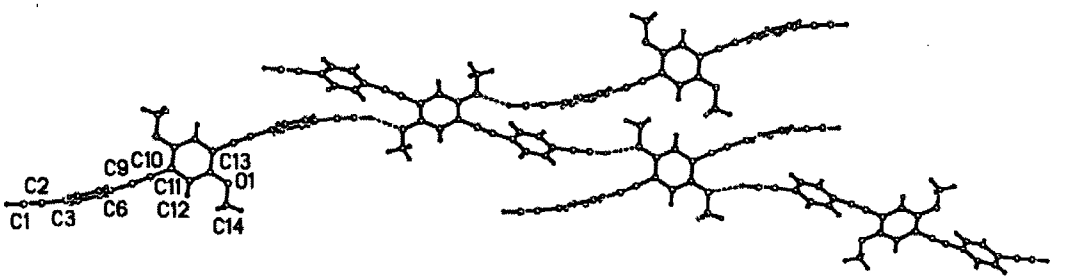

Figure 2.2. Representative Packing diagram of **14** revealing intermolecular O...H interactions.

There are several structurally characterised 1-4-bis(phenylethynylbenzene) derivatives. [18,90-93] However, none of these feature terminal C≡CH units. In fact, the only 4,4"-diethynyl-1-4-bis(phenylethynylbenzene) derivative and structurally characterised to date is that prepared and characterised by Luo [94] (**Figure 2.3**). The terminal acetylenes in **14** are unusually short when compared with "normal" acetylenic bond lengths [C(1)-C(2) and C(9)-C(10) 1.327(19) and 1.1759(18) Å]. The structure is essentially linear with C(1)-C(2)-C(3) and C(6)-C(9)-C(10) [175.51(15) and 175.85(14)°], and comparable with the structure reported by Xue [C(1)-C(2)-C(3) and C(6)-C(9)-C(10) 177.8(6) and 176.8(6)°].

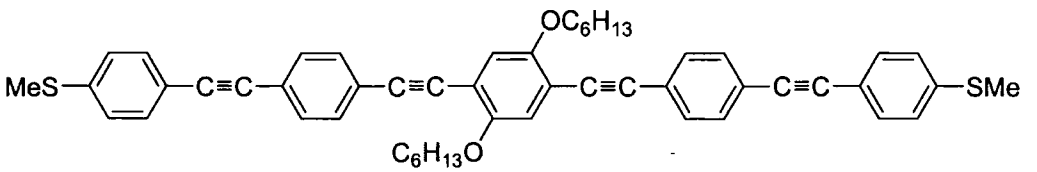

Figure 2.3.: Structure no. *9* synthesised by Xue and Luo. [94]

Table 2.1. Crystal data for and parameters of refinement of the structure **14***.

	14
Molecular formula	$C_{28}H_{18}O_2$
Formula WeightM / g mol^{-1}	386.42
Crystal system	Monoclinic
a / Å	12.0449(3)
b / Å	7.1061(2)
c / Å	12.6949(3)
α / °	90
β / °	115.26(1)
γ / °	90
V / Å^3	982.70(4)
Space group	$P2_1/c$
Z	2
D_{calc} / (Mg/m^3)	1.306
Crystal size / mm	0.24×0.22×0.10
Crystal habit	plate
F (000)	404
Radiation	Mo(K_α)
Wavelength / Å	0.71073
μ / mm^{-1}	0.081
Temperature / K	120(2)
Data collection range / °	1.87-27.99
Reflections measured	12310
Data, restraints, parameters	2380, 0, 172
R_1, wR_2 (all data)	0.0538, 0.1405
Goodness-of-fit on F^2 (all data)	1.064
peak, hole / eÅ^{-3}	0.476, -0.197

* Symmetry transformations used to generate equivalent atoms: #1 –x+1, -y+1, -z+1.

Table 2.2. Selected bond lengths *(Å)* and angles(°) for **14**

	14
C(1)-C(2)-C(3)	175.51(16)
C(6)-C(9)-C(10)	175.85(14)
C(9)-C(10)-C(11)	178.72(14)
	14
C(1)-C(2)	1.1327(19)
C(2)-C(3)	1.4810(17)
C(3)-C(4, 8)	1.4132(18), 1.4150(18)
C(4)-C(5),C(7)-C(8)	1.3895(16), 1.3796(17)
C(6)-C(5, 7)	1.3986(18), 1.4000(18)
C(6)-C(9)	1.4549(17)
C(9)-C(10)	1.1759(18)
C(10)-C(11)	1.4435(16)
C(11)-C(12)	1.4000(17)
C(12)-C(13),	1.3920(16)

2.2.3. Photophysical Properties

The electronic absorption properties of the tolans (**1-5** and **6**), and the extended "three-ring" system **11**, and selected luminescent properties, have been investigated and fully described in the **Chapter 5** (**'Photophysical and Electrochemical Properties of Triruthenium Carbonyl Clusters Featuring Phenylene Ethynylene Ligands'**). These data provide opportunity for comparisons with the triruthenium carbonyl acetylide clusters (**36-43**) along with the mononuclear gold(**15-19**) and bis-gold (**23**) acetylide complexes described later in this Thesis.

2.3. Conclusions

The targeted oligo-phenylene ethynylene ligands precursors were prepared via Sonogashira Pd/Cu cross-coupling reactions or *via* nucleophilic attack of benzoquinones by lithiated acetylide anions and subsequent reduction in good yields. These TMS protected tolans contain donor (Me, OMe) and acceptor groups (CO_2Me,

NO_2, CN). These tolans were desilylated in methanolic solution containing K_2CO_3 to afford the terminal alkynes **6-10**, also in good yields. A simple Sonogashira cross-coupling reaction was employed in the preparation of the symmetric phenylene ethynylene oligomers **11** and **13**. Desilylation of **11** afforded $HC{\equiv}CC_6H_4C{\equiv}CC_6H_4C{\equiv}CC_6H_4C{\equiv}CH$ (**12**), which was insoluble in methanol. The introduction of the two methoxy groups to the middle ring (i.e. **13**) gives increased solubility. Desilylation of **13** afforded **14** in a high yield (95 %). All these ligands precursors were fully characterised spectroscopically and show little differences in the data obtained. In addition, the molecular structural of **14** was also determined by X-ray analysis; the structure is essentially linear and the crystal packing shows there is intermolecular O...H interaction in the solid state. The terminal acetylenes in **14** are unusually short when compared with "normal" acetylenic bond lengths and the first of the 1-4-bis(phenylethynylbenzene) derivatives with C≡CH units ever to have been structurally determined.

2.4. Experimental Details

2.4.1. General Condition

All reactions were carried out under an atmosphere of nitrogen using standard Schlenk techniques. Reaction solvents were purified and dried using an Innovative Technology SPS-400, and degassed before use. No special precautions were taken to exclude air or moisture during work-up. The compounds $PdCl_2(PPh_3)_2$, [95] and 1-trimethylsilylethynyl-4-ethynylbenzene [87] were prepared by literature routes. Other reagents were purchased and used as received.

The NMR spectra were recorded on a Bruker Avance (^1H 400.13 MHz, ^{13}C 100.61 MHz, spectrometer from $CDCl_3$ solutions and referenced against solvent resonances (^1H, ^{13}C). The IR spectra were recorded using a Nicolet Avatar spectrometer from nujoll mull suspended between NaCl plates. Mass spectra were recorded using Thermo Quest Finnigan Trace MS-Trace GC or Thermo Electron Finnigan LTQ FT mass spectrometers or or Matrix-Assisted Laser Desorption/Ionisation-Time-of-Flight (Mass Spectrometry) (MALDI-TOF MS) ABI Voyager STR.

Diffraction data for **14** were collected at 120K on a Bruker SMART 6000 CCD three-circle diffractometers, using graphite-monochromated Mo-K_α radiation. The diffracrometer were equipped with Cryostream (Oxford Cryosystems) low-temperature nitrogen cooling devices. The structures were solved by direct-methods and refined by full matrix least-squares against F^2 of all data using *SHELXTL* software. [97] All non-hydrogen atoms where refined in anisotropic approximation except the disordered ones, H atoms were placed into the calculated positions and refined in "riding" mode. The crystallographic data and parameters of the refinements are listed in **Table 2.1** and **Table 2.2**.

2.4.2. Experimental

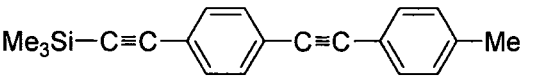

2.4.2.1. Preparation of $Me_3SiC{\equiv}CC_6H_4C{\equiv}CC_6H_4Me$ (1)

A solution of n-butyllithium (17.8 ml, 1.6 M in hexane, 25.8 mmol) was added slowly to a solution of 4-tolylacetylene (3.00 g, 25.8 mmol) in THF (20 mL) at –78 °C. The reaction mixture was allowed to come to 0 °C and stirred for 45 mins, before being cooled again to –78 °C and added dropwise to a solution of benzoquinone in THF (20 mL) (3.08 g, 25.8 mmol), also at –78 °C. The reaction mixture was stirred for 1 h at -78 °C, then a solution of lithium trimethylsilylacetylide [prepared by addition of n-butyllithium (17.8 ml, 1.6 M in hexanes, 25.8 mmol) to trimethylsilylacetylene (2.77 g, 25.8 mmol) in THF (20 mL) at –78 °C and stirred for 45 mins before warming to 0 °C] was added, also at –78 °C. The reaction mixture was allowed to come to room temperature overnight before being quenched (0 °C) with aqueous NH_4Cl and extracted into ethyl acetate (2 x 100 mL). The organic extracts were passed through a silica pad with ethyl acetate and dried *in vacuo* to afford a mixture of *meso* and *anti* diols as a dark caramel-coloured solid, which was not purified further. The crude mixture of diols (8.24 g) was dissolved in 30 mL of EtOH and treated with a solution of $SnCl_2$ (5.27 g, 0.278 mmol) in 15 ml acetic acid / 15 ml water, and the mixture heated at 45 °C for 45 mins. The reaction mixture was filtered, and the filtrate purified by column chromatography (silica/hexane), the solvent was removed *in-vacuo* to give a white solid of **1** (4.70 g, 63 %). IR(nujol): ν(C≡C) 2202, 2151 cm^{-1}. ^1H NMR($CDCl_3$, 400.13 MHz): δ 0.26 (s, 9H, $SiMe_3$); 2.37 (s, 3H, Me); 7.16 (pseudo-d, J_{HH} = 8 Hz, 2H, C_6H_4); 7.42 (pseudo-d, J_{HH} = 8 Hz, 2H, C_6H_4); 7.40 (s, 4H, C_6H_4). ^{13}C NMR ($CDCl_3$, 100.61 MHz): δ 0.00 (s, $SiMe_3$); 21.6 (s, Me); 88.5, 91.6, 96.2, 104.8 (4 × s, 4 × C≡C); 119.9, 121.7, 124.0, 129.2, 131.4, 131.5, 132.0, 138.7 (8 × s, Ar). EI^+-MS(m/z): 288, M^+; 273, $[M\text{-}Me]^+$. Found: C 83.41, H 6.86 %. $C_{20}H_{20}Si$ requires: C, 83.30; H, 6.94 %.

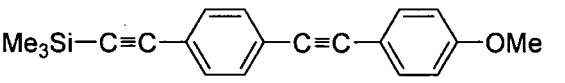

2.4.2.2. Preparation of $Me_3SiC{\equiv}CC_6H_4C{\equiv}CC_6H_4OMe$ (2)

A 500 ml Schlenk flask was charged with 1-iodo-4-methoxybenzene (2.34 g, 10 mmol), 1-trimethylsilylethynyl-4-ethynylbenzene (2.18 g, 11 mmol), $PdCl_2(PPh_3)_2$ (0.70 g, 0.1 mmol) and CuI (0.19 g, 0.1 mmol), and was evacuated and purged with nitrogen 3 times. Triethylamine (ca. 250 ml) was transferred to the reaction flask *via* cannula under nitrogen. The reaction mixture was heated to reflux for 2 h. The solvent was removed *in vacuo* and the residue passed through a silica pad with hexane and CH_2Cl_2. The solvent was removed *in-vacuo* to give a yellow solid of the title product (**2**) which was recrystallised from hexane and CH_2Cl_2 (1.90 g, 63%). IR(nujol): ν(C≡C) 2215, 2158 cm^{-1}. ^1H NMR ($CDCl_3$, 400.13 MHz): δ 0.25 (s, 9H; $SiMe_3$), 3.83 (s, 3H; OMe), 6.88 (pseudo-d, J_{HH} = 8.6 Hz, 2H; C_6H_4), 7.43 (s, 4H; C_6H_4), 7.46 (pseudo-d, J_{HH} = 8.6 Hz, 2H; C_6H_4).^{13}C NMR ($CDCl_3$, 100.61 MHz): δ 0.13 (s, $SiMe_3$), 55.3 (OMe), 85.7, 91.4, 96.0, 104.8 (4 x s, C≡C), 114.1, 115.1, 122.5, 123.7, 131.2, 131.8, 133.1, 159.8 (8 x s, Ar). EI^+-MS(m/z): 304, M^+; 274, $[M\text{-}OMe]^+$; 201, $[M\text{-}SiMe_3]^+$. Found: C, 78.24; H, 6.58 %. $C_{20}H_{20}OSi$ requires: C, 78.90; H, 7.11 %.

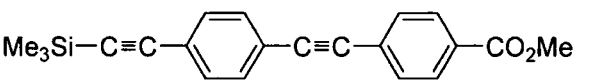

2.4.2.3. Preparation of $Me_3SiC{\equiv}CC_6H_4C{\equiv}CC_6H_4CO_2Me$ (3)

A 500 ml Schlenk flask was charged with 4-bromo-benzoic acid methyl ester (2.14 g, 10 mmol), 1-trimethylsilylethynyl-4-ethynyl benzene (2.18 g, 11 mmol), $PdCl_2(PPh_3)_2$ (0.70 g, 0.1 mmol) and CuI (0.19 g, 0.1 mmol) and was evacuated and purged with nitrogen 3 times. Triethylamine (ca. 250 ml) was transferred to the reaction flask via cannula under nitrogen. The reaction mixture was heated to reflux for 20 h. The solvent was removed and the residue passed through a silica pad eluting with cold toluene and then with hot toluene. The solvent was removed *in-vacuo* to give a yellow solid of the title product (**3**) which was recrystallised from hot toluene (1.6 g, 49%). IR(nujol): ν(C≡C) 2211, 2155 cm^{-1}. ^1H NMR ($CDCl_3$, 400.13

MHz): δ 0.26 (s, 9H, $SiMe_3$); 3.93 (s, 3H, OMe); 7.47 (pseudo-d, J_{HH} = 2 Hz, 4H, C_6H_4); 7.59 (pseudo-d, J_{HH} = 8.4 Hz, 2H, C_6H_4); 8.03 (pseudo-d, J_{HH} = 8.4 Hz, 2H, C_6H_4). ^{13}C NMR ($CDCl_3$, 100.61 MHz): δ 0.13 (s, $SiMe_3$), 52.3 (OMe), 90.5, 91.8, 96.7, 104.5 (4 x s, C≡C), 122.7, 123.8, 127.8, 129.7, 129.7, 131.5, 131.9, 132.1 (8 x s, Ar), 166.5 (s, C=O). EI^+-MS(m/z): 332, M^+; 317, $[M-Me]^+$; 301, $[M-OMe]^+$. Found: C, 75.85; H 5.95 %. $C_{21}H_{20}O_2Si$ requires: C, 75.86; H, 6.05 %.

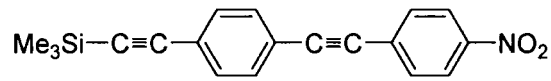

2.4.2.4. Preparation of $Me_3SiC{\equiv}CC_6H_4C{\equiv}CC_6H_4NO_2$ (4)

Triethylamine (200 ml) was degassed by three freeze-pump-thaw sequences before 1-bromo-4-nitrobenzene (2.00 g, 9.90 mmol), 1-trimethylsilylethynyl-4-ethynylbenzene (1.96 g, 9.90 mmol), CuI (38 mg, 0.2 mmol) and $PdCl_2(PPh_3)_2$ (140 mg, 0.2 mmol) were added. The mixture was allowed to stir overnight overnight (ca. 12 h) at reflux. The solvent was removed and the residue purified by column chromatography (silica, hexane: CH_2Cl_2 70:30) to afford a yellow band of compound **4**. (2.43 g, 84 %). IR(nujol): ν(C≡C) 2209, 2149 cm^{-1}. ^1H NMR ($CDCl_3$, 400.13 MHz): δ 0.26 (s, 9H, $SiMe_3$); 7.48 (pseudo-d, J_{HH} = 2 Hz, 4H, C_6H_4); 7.65 (pseudo-d, J_{HH} = 9.2 Hz, 2H, C_6H_4); 8.22 (pseudo-d, J_{HH} = 9.2 Hz, 2H. ^{13}C NMR ($CDCl_3$, 100.61 MHz): δ 0.13 (s, $SiMe_3$); 79.8, 83.2, 89.6, 94.2 (4 × s, 4 x C≡C); 122.7, 123.3, 123.9, 130.1, 131.9, 132.0, 132.5, 147.4 (8 × s, Ar). EI^+-MS(m/z): 319, M^+. Found: C, 71.44; H 4.62; N, 4.94 %. $C_{19}H_{17}NO_2Si$ requires: C 71.47; H 5.33; N 4.39 %.

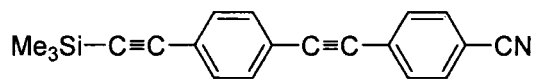

2.4.2.5. Preparation of $Me_3SiC{\equiv}CC_6H_4C{\equiv}CC_6H_4CN$ (5)

Triethylamine (200 ml) was degassed by three freeze-pump-thaw sequences before 1-bromo-4-cyanobenzene (2.00 g, 11.0 mmol), 1-trimethylsilylethynyl-4-ethynylbenzene (2.18 g, 11.0 mmol), CuI (42 mg, 0.22 mmol) and $PdCl_2(PPh_3)_2$ (154 mg, 0.22 mmol) were added. The mixture was allowed to stir overnight overnight (ca. 12 h) at reflux. The solvent was removed and the residue purified by column

chromatography (silica, hexane: CH_2Cl_2 60:40) to afford a yellow band of compound **5**. (3.00 g, 91 %). IR(nujol): ν(C≡C) 2209, 2149 cm^{-1}. ^1H NMR ($CDCl_3$, 400.13 MHz): δ 0.26 (s, 9H, $SiMe_3$); 7.47 (s, 4H, C_6H_4); 7.60 (pseudo-d, J_{HH} = 8 Hz, 2H, C_6H_4); 7.65 (pseudo-d, J_{HH} = 8 Hz, 2H, C_6H_4). ^{13}C NMR ($CDCl_3$, 100.61 MHz): δ 0.0 (s, $SiMe_3$); 89.6, 93.4, 97.1, 104.5 (4 × s, 4 x C≡C); 111.9, 118.6, 122.5, 124.0, 131.7, 131.9, 132.2, 132.2 (8 × s, Ar); 121.7 (s, CN). EI^+-MS(m/z): 299, M^+. Found: C, 79.90; H, 5.63; N, 4.23 %. $C_{20}H_{17}NSi$ requires : C, 80.22; H, 5.72; N, 4.68 %.

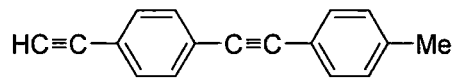

2.4.2.6. Preparation of $HC{\equiv}CC_6H_4C{\equiv}CC_6H_4Me$ (6)

A solution of **1** (780 mg, 2.71 mmol) and K_2CO_3 (370 mg, 2.71 mmol) in MeOH (70 ml) was stirred under nitrogen at room temperature for ca. 48 hours. The reaction mixture was partitioned between Et_2O (100 ml) and H_2O (100 ml), the organic layer collected, dried over $MgSO_4$, and finally dried *in vacuo* to afford **6** as a cream solid (473 mg, 81 %). IR(nujol): ν(C≡C) 2212, 2103 cm^{-1}. ^1H NMR($CDCl_3$, 400.13 MHz): δ 2.38 (s, 3H, Me); 3.17 (s, 1H, C≡CH); 7.16 (pseudo-d, J_{HH} = 8 Hz, 2H, C_6H_4); 7.42 (pseudo-d, J_{HH} = 8 Hz, 2H, C_6H_4); 7.45 (s, 4H, C_6H_4). ^{13}C NMR ($CDCl_3$, 100.61 MHz): δ 21.5 (s, Me); 78.7, 83.3, 88.2, 91.6 (4 x s, 4 x C≡C); 119.9, 121.7, 124.0, 129.2, 131.4, 131.5, 132.0, 138.7 (8 × s, Ar). EI^+-MS(m/z): 216, M^+. Found: C, 94.32; H, 5.62%. $C_{17}H_{12}$ requires: C, 94.40; H, 5.59 %.

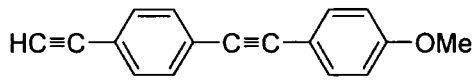

2.4.2.7. Preparation of $HC{\equiv}CC_6H_4C{\equiv}CC_6H_4OMe$ (7)

A solution of **2** (150 mg, 0.49 mmol) and K_2CO_3 (270 mg, 1.97 mmol) in MeOH (30 ml) was stirred under nitrogen at room temperature overnight (ca. 12 h). The reaction mixture was partitioned between Et_2O (50 ml) and H_2O (50 ml), the organic layer collected, dried over $MgSO_4$, and finally dried *in vacuo* to afford **7** as a yellow solid (102 mg, 89 %). IR(nujol): ν(C≡C) 2214, 2028 cm^{-1}. ^1H NMR ($CDCl_3$, 400.13 MHz): δ 3.16 (s, 1H, C≡CH); 3.83 (s, OMe); 6.90 (pseudo-d, J_{HH} = 8.6 Hz, 2H, C_6H_4); 7.48 (pseudo-d, J_{HH} = 8.6 Hz, 6H, C_6H_4). ^{13}C NMR ($CDCl_3$, 100.61 MHz): δ

55.3 (s, OMe); 78.7, 83.3, 87.6, 91.5 (4 x s, 4 x C≡C); 114.1, 115.1, 121.5, 124.2, 131.3, 132.0, 133.1, 159.9 (8 × s, Ar). EI^+-MS(m/z): 232, M^+; 217, $[M\text{-}Me]^+$. Found: C, 87.24; H, 5.05 %. $C_{17}H_{12}O$ requires: C, 87.93; H, 5.17 %.

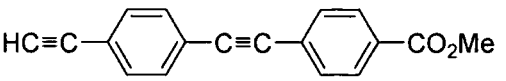

2.4.2.8. Preparation of $HC{\equiv}CC_6H_4C{\equiv}CC_6H_4CO_2Me$ (8)

A solution of **3** (300 mg, 0.90 mmol) and K_2CO_3 (120 mg, 0.90 mmol) in MeOH (70 ml) was stirred under nitrogen at room temperature overnight overnight (ca. 12 h). The reaction mixture was partitioned between Et_2O (25 ml) and H_2O (25 ml), the organic layer collected, dried over $MgSO_4$, and finally dried *in vacuo* to afford **8** as a yellow solid (200 mg, 85 %). IR(nujol): ν(C≡C) 2211, 2101 cm^{-1}. ^1H NMR ($CDCl_3$, 400.13 MHz): δ 3.19 (s, 1H, C≡CH); 3.93 (s, OMe); 7.49 (s, 4H, C_6H_4); 7.60 (pseudo-d, J_{HH} = 8.4 Hz, 2H, C_6H_4); 8.04 (pseudo-d, J_{HH} = 8.4 Hz, 2H, C_6H_4). ^{13}C NMR ($CDCl_3$, 100.61 MHz): δ 52.5 (s, OMe); 79.5, 83.4, 90.7, 91.9 (4 x s, 4 x C≡C); 122.6, 123.4, 127.8, 129.8, 129.9, 131.7, 131.8, 132.4 (8 × s, Ar); 166.7 (s, C=O). EI^+-MS(m/z): 260, M^+; 229, $[M\text{-}OMe]^+$. Found: C, 81.37; H, 4.59 %. $C_{18}H_{12}O_2$ requires: C, 83.08; H, 4.62 %.

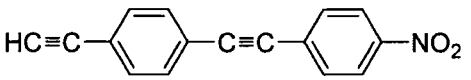

2.4.2.9. Preparation of $HC{\equiv}CC_6H_4C{\equiv}CC_6H_4NO_2$ (9)

A solution of **4** (1.2 g, 3.76 mmol) and K_2CO_3 (2.08 g, 15.1 mmol) in MeOH (50 ml) was stirred under nitrogen at room temperature overnight overnight (ca. 12 h). The reaction mixture was partitioned between Et_2O (75 ml) and H_2O (75 ml), the organic layer collected, dried over $MgSO_4$, and finally dried *in vacuo* to afford **9** as a yellow solid (825 mg, 89 %). IR(nujol): ν(C≡C) 2210, 2101 cm^{-1}. ^1H NMR ($CDCl_3$, 400.13 MHz): δ 3.21 (s, 1H, C≡CH); 7.51 (s, 4H, C_6H_4); 7.60 (pseudo-d, J_{HH} = 9.2 Hz, 2H, C_6H_4); 8.24 (pseudo-d, J_{HH} = 9.2 Hz, 2H, C_6H_4). ^{13}C NMR ($CDCl_3$, 100.61 MHz): δ 79.6, 83.0, 89.3, 93.9 (4 x s, C≡C); 122.5, 123.1, 123.7, 129.9, 131.7, 132.2, 132.3, 147.2 (8 x s, Ar). EI^+-MS(m/z): 247, M^+; 200 $[M\text{-}NO_2H]^+$. Found: C, 77.72; H, 3.89; N, 5.31 %. $C_{16}H_9NO_2$ requires: C, 77.73; H, 3.64; N 5.67 %.

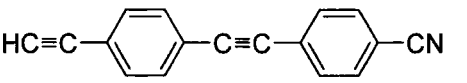

2.4.2.10. Preparation of $HC{\equiv}CC_6H_4C{\equiv}CC_6H_4CN$ (10)

A solution of **5** (1.5 g, 5.02 mmol) and K_2CO_3 (2.77 g, 20.0 mmol) in MeOH (70 ml) was stirred under nitrogen at room temperature overnight overnight (ca. 12 h). The reaction mixture was partitioned between Et_2O (100 ml) and H_2O (100 ml), the organic layer collected, dried over $MgSO_4$, and finally dried *in vacuo* to afford **10** as a yellow solid (707 mg, 51 %). IR(nujol): ν(C≡C) 2209, 2100 cm^{-1}. ^1H NMR ($CDCl_3$, 400.13 MHz): δ 3.21 (s, 1H, C≡CH); 7.49 (s, 4H, C_6H_4); 7.61 (pseudo-d, J_{HH} = 8.8 Hz, 2H, C_6H_4); 7.66 (pseudo-d, J_{HH} = 8.8 Hz, 2H, C_6H_4). ^{13}C NMR ($CDCl_3$, 100.61 MHz): δ 79.5, 83.0, 89.5, 93.1 (4 x s, C≡C); 111.8, 118.4, 122.9, 122.9, 131.7, 132.1, 132.1, 132.2 (8 × s, Ar); 121.9 (s, CN). EI^+-MS(m/z): 228, $[M+H]^+$; 227, M^+; 201, $[M-C{\equiv}N]^+$. Found: C, 89.43; H, 3.98; N, 5.74 %. $C_{17}H_9N$ requires: C, 89.87; H, 3.96; N 6.17 %.

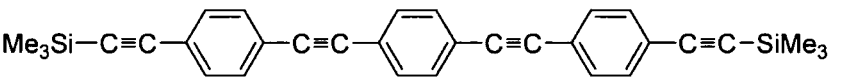

2.4.2.11. Preparation of $Me_3SiC{\equiv}CC_6H_4C{\equiv}CC_6H_4C{\equiv}CC_6H_4C{\equiv}CSiMe_3$ (11)

Triethylamine (150 ml) was degassed by three freeze-pump-thaw sequences before 1,4-diiodobenzene (2.00 g, 5.06 mmol), 1-trimethylsilylethynyl-4-ethynylbenzene (2.40 g, 12.10 mmol), CuI (19 mg, 0.10 mmol) and $PdCl_2(PPh_3)_2$ (71 mg, 0.10 mmol) were added. The mixture was allowed to stir overnight (ca. 15 h) at room temperature. The solvent was removed and the residue purified by column chromatography (silica, hexane: CH_2Cl_2 60:40) to afford a pale yellow band containing compound **11** which was recrystallised from hexane (2.45 g, 69 %). IR(nujol): ν(C≡C) 2152 cm^{-1}. ^1H NMR ($CDCl_3$, 400.13 MHz): δ 0.26 (s, 18H, $SiMe_3$); 7.45 (s, 8H, C_6H_4); 7.50 (s, 4H, C_6H_4). ^{13}C NMR ($CDCl_3$, 100.61 MHz): δ 0.1 (s, $SiMe_3$); 91.2, 91.3, 96.7, 104.8 (4 × s, 4 x C≡C); 123.2, 123.4, 123.4, 131.6, 131.8, 132.2 (6 × s, Ar). ES^+-MS(m/z): 470, M^+, 471 $[M+H]^+$ Found: C 81.88; H 6.24 %. $C_{32}H_{30}Si_2$ requires: C 81.70; H 6.38 %.

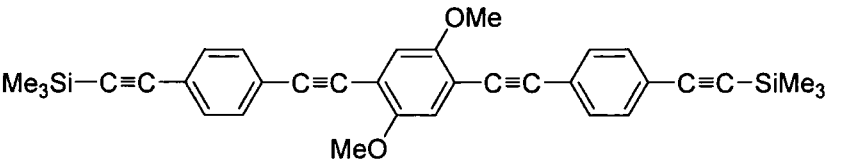

2.4.2.12. Preparation of $Me_3SiC{\equiv}CC_6H_4C{\equiv}CC_6H_2(OMe)_2C{\equiv}CC_6H_4C{\equiv}CSiMe_3$ (13)

Triethylamine (220 ml) was degassed by three freeze-pump-thaw sequences before 1,4-diiodo-2,5-bismethoxybenzene (2.00 g, 5.13 mmol), 1-trimethylsilylethynyl-4-ethynylbenzene (2.13 g, 11.00 mmol), CuI (20 mg, 0.10 mmol) and $PdCl_2(PPh_3)_2$ (72 mg, 0.10 mmol) were added. The mixture was allowed to stir overnight (ca. 15 h) under nitrogen. The solvent was removed and the residue purified by column chromatography (silica, hexane: ethyl acetate 80:20) to afford a yellow band containing compound **13**. (1.85 g, 68 %). IR(nujol): ν(C≡C) 2155, 2027 cm^{-1}. ^1H NMR ($CDCl_3$, 400.13 MHz): δ 0.25 (s, 18H, $SiMe_3$); 3.90 (s, 6H, OMe); 7.01 (s, 2H, $C_6H_2(OMe)_2$); 7.45 (pseudo-d, J_{HH} = 8.8 Hz, 4H, C_6H_4); 7.51 (pseudo-d, J_{HH} = 8.8 Hz, 4H, C_6H_4). ^{13}C NMR ($CDCl_3$, 125.7 MHz): δ 0.2 (s, $SiMe_3$); 56.7 (s, OMe); 87.8, 95.1, 96.6, 104.9 (4 × s, 8 x C≡C); 113.6, 115.8, 123.3, 123.5, 131.7, 132.2, 154.2 (7× s, 18 x Ar). TOF^+-MALDI(m/z): 530, $M^{+\cdot}$ 531, $[M+H]^+$. Found: C 76.25; H 6.26 %; $C_{34}H_{34}O_2Si_2$ requires : C 76.87; H 6.41 %.

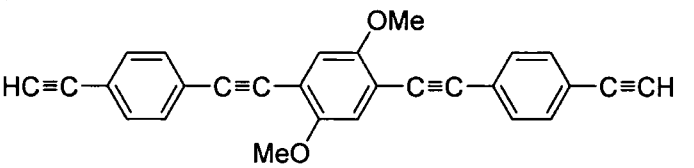

2.4.2.13. Preparation of $HC{\equiv}CC_6H_4C{\equiv}CC_6H_2(OMe)_2C{\equiv}CC_6H_4C{\equiv}CH$ (14)

A solution **12** (250 mg, 0.47 mmol) and K_2CO_3 (522 mg, 3.78 mmol) in MeOH (70 ml) was stirred under nitrogen at room temperature for ca. 48 h. The reaction mixture was partitioned between Et_2O (100 ml) and H_2O (100 ml), the organic layer collected, dried over $MgSO_4$, and dried *in vacuo* followed by recrystallisation from $CHCl_3$ to afford **14** as a yellow crystals (172 mg, 95 %). IR(nujol): ν(C≡C) 2101, 2017 cm^{-1}. ^1H NMR ($CDCl_3$, 400.13 MHz): δ 3.18(s, 2H, C≡CH); 3.91(s, 6H, OMe); 7.03(s, 2H, ($C_6H_2(OMe)_2$); 7.48(pseudo-d, J_{HH} = 8 Hz, 4H, C_6H_4); 7.53 (pseudo-d, J_{HH} = 8 Hz, 4H, C_6H_4). ^{13}C NMR ($CDCl_3$, 125.7 MHz): δ 56.7 (s, OMe); 79.3, 83.5, 87.98, 94.8 (4 x s, 8 x C≡C); 113.5, 115.8, 122.3, 123.9, 131.8, 132.3, 154.2 (7 × s,

18 x Ar). TOF$^+$-MALDI(m/z): 386, $M^{+\cdot}$ 387, $[M+H]^+$. Found: C 87.03; H 4.53 %; $C_{28}H_{18}O_2$ requires: C 87.02; H 4.69 %.

2.5. References

1. M. C. Petty, M. R. Bryce, D. Bloor (Eds.), *Introduction to Molecular Electronics*, 1995, Edward Arnold, London.
2. F. Maya, S. H. Chanteau, L. Cheng, M. P. Steward, J. M. Tour, *Chem. Mater.*, 2005, **17**, 1331.
3. S. A. Jenekhe, M. M. Alam, Y. Zhu, S. Jiang, A. B. Shevade, *Adv. Mater.*, 2007, **19**, 536.
4. M. D. Ward, *J. Chem. Educ.*, 2001, **78**, 321.
5. F. R. Fan, J. Yang, L. Cai, D. W. Price, S. M. Dirk, D. V. Kosynkin, Y. Yao, A. M. Rawlett, J. M. Tour, A. J. Bard, *J. Am. Chem., Soc.*, 2002, **124**, 5550.
6. A. K. Flatt, S. M. Dirk, J. C. Henderson, D. E. Shen, J. Su, M. A. Reed, J. M. Tour, *Tetrahedron*, 2003, **59**, 8555.
7. K. Müllen, G. Wegner (Eds.), *Electronic Materials: The Oligomer Approach, 1998,* Wiley-VCH, Weinheim, **1998**.
8. J. He, B. Chen, A. K. Flatt, J. J. Stephenson, C. D. Doyle, J. M. Tour, *Nature*, 2006, **5**, 63.
9. E. Negishi, L. Anastasia, *Chem. Rev.*, 2003, **103**, 1979.
10. P. F. H. Schwab, M. D. Levin, J. Michl, *Chem. Rev.*, 1999, **99**, 1863.
11. U. H. F. Bunz, *Chem. Rev.*, 2000, **100**, 4, 1605.
12. A. Beeby, K. Findlay, P. J. Low, T. B. Marder, *J. Am. Chem. Soc.*, 2002, **124**, 8280.
13. U. H. F. Bunz, *Acc. Chem. Res.*, 2001, **34**, 998.
14. L. A. Bumm, J. J. Arnold, M. T. Cygan, T. D. Dunbar, T. P. Burgin, L. Jones, D. L. Allara, J. M. Tour, P. S. Weiss, *Science*, 1996, **271**, 1705.
15. J. M. Seminario, A. G. Zacarias, J. M. Tour, *J. Am. Chem. Soc.*, 1998, **120**, 3970.
16. Z. J. Donhauser, B. A. Mantooth, T. P. Pearl, K. F. Kelly, S. U. Nanayakkara, P. S. Weiss, *Jpn. J. Appl. Phys. 1*, 2002, **41**, 4871.
17. J. Cornil, Y. Karzazi, J. L. Bredas, *J. Am. Chem. Soc.*, 2002, **124**, 3516.
18. C. Dai, P. Nguyen, T. B. Marder, A. J. Scott, W. Clegg, C. Viney, *Chem. Commun.*, 1999, 2493.

19. J. M. Tour, *Acc. Chem. Res.* 2000, **33**, 791.
20. G. Maruccio, R. Cingolani, R. Rinaldi, *J. Mater. Chem.*, 2004, **14**, 542.
21. N. Robertson, C. A. McGowan, *Chem. Soc. Rev.* 2003, **32**, 96.
22. C. Wang, A. S. Batsanov, M. R. Bryce, G. J. Ashwell, B. Urasinska, I. Grace, C. J. Lambert, *Nanotechnology*, 2007, **18**, 044005.
23. G. J. Ashwell, B. Urasinska, C. Wang, M. R. Bryce, I. Grace, C. J. Lambert, *Chem. Commun.*, 2006, 4706.
24. L. Cai, Y. Yao, D. W. Price Jr., J. M. Tour, *Chem. Mater.*, 2002, **14**, 2905.
25. X. Yin, H. Liu, J. Zhao, *J. Chem. Phys.*, 2006, **125**, 094711.
26. J. M. Tour, L. Jones II, D. L. Pearson, J. J. S. Lamba, T. P. Burgin, G. M. Whitesides, D. L. Allara, A. N. Parikh, S. V. Atre, *J. Am. Chem. Soc.,* 1995, **117**, 9529.
27. M. P. Samanta, W. Tian, S. Datta, J. I. Henderson, and C. P. Kubiak, *Phys. Rev. B*, 1996, **53**, 7626.
28. M. Magoga, C. Joachim, *Phys. Rev. B*, 1997, **56**, 4722.
29. I. Willner, B. Basnar, B. Willner, *Adv. Funct. Mater.*, 2007, **17**, 702.
30. S. M. Dirk, D. W. Price Jr., S. Chanteau, D. V. Kosynkin, J. M. Tour, *Tetrahedron*, 2001, **57**, 5109.
31. H. L. Anderson, M. J. Frampton, *Angew. Chem., Int. Ed.*, 2007, **46**, 1028.
32. R. van Noorden, *Chem. World*, 2007, **4**, 7, 27.
33. C. Xue, Z. Chen, Y. Wen, F. –T. Luo, J. Chen, H. Liu, *Langmuir*, 2005, **21**, 7860.
34. F. Maya, A. K. Flatt, M. P. Stewart, D. E. Shen, J. M. Tour, *Chem. Mater.*, 2004, **16**, 2987.
35. J. Chen, W. Wang, M. A. Reed, A. M. Rawlett, D. W. Price, J. M. Tour, *Appl. Phys. Lett.*, 2000, **77**, 8, 1224.
36. A. M. Boldi, J. Anthony, V. Gramlich, C. B. Knobler, C. Boudon, J. Gisselbrecht, M. Gross, F. Diederich, *Helv. Chim. Acta*, 1995, **78**, 779.
37. R. Dembinski, T. Bartik, B. Bartik, M. Jaeger, J. A. Gladysz, *J. Am. Chem., Soc.*, 2000, **122**, 810.
38. F. –R. F. Fan, J Yang, S. M. Dirk, D. W. Price, D. Kosynkin, J. M. Tour, A. J. Bard, *J. Am. Chem. Soc.*, 2001, **123**, 2454.

39. S. Huang, J. M. Tour, *J. Org. Chem.*, 1999, **64**, 8898.

40. L Jones II, J. S. Schumm, J. M. Tour, *J. Org. Chem.*, 1997, **62**, 1388.

41. M. A. Reed, J. Chen, A. M. Rawlett, D. W. Price, J. M. Tour, *Appl. Phys. Lett.*, 2001, **78**, 23, 3735.

42. C. Wang, A. S. Batsanov, M. R. Bryce, *J. Organic Chem.*, 2006, **71**, 108.

43. D. W. Price, S. M. Dirk, F. Maya, J. M. Tour, *Tetrahedron*, 2003, **59**, 2497.

44. (a) S. M. Dirk, J. M. Tour, *Tetrahedron*, 2003, **59**, 287. (b) J. J. Hwang, J. M. Tour, *Tetrahedron*, 2002, **58**, 10387.

45. J. M. Tour, A. M. Rawlett, M. Kozaki, Y. X. Yao, R. C. Jagessar, S. M. Dirk, D. W. Price, M. A. Reed, C. W. Zhou, J. Chen, W. Y. Wang, I. Campbell, *Chem. Eur. J.*, 2001, **7**, 23, 5118.

46. W. A. Reinerth, L. Jones, T. P. Burgin, C. W. Zhou, C. J. Muller, M. R. Deshpande, M. A. Reed, J. M. Tour, *Nanotechnology*, 1998, **9**, 3, 246.

47. T. R. Lee, P. E. Laibinis, J. P. Folkers, G. M. Whitesides, *Pure & Appl. Chem.*, 1991, **63**, 6, 821.

48. G. M. Whitesides, P. E. Laibinis, *Langmuir*, 1990, **6**, 81.

49. J. –P. Choi, M. M. Coble, M. R. Branham, J. M. DeSimone, R. W. Murray, *J. Phys. Chem. B*, 2007, **111**, 3778.

50. (a) C. Chu, J. –S. Na, G. N. Parsons, *J. Am. Chem. Soc.*, 2007, **129**, 2287, (b) R. J. Tseng, C. O. Baker, B. Shedd, J. Huang, R. B. Kaner, J. Ouyang, Y. Yang, *Appl. Phys. Lett.*, 2007, **90**, 053101.

51. B. Vercelli, G. Zotti, A. Berlin, *Chem. Mater.*, 2007, **19**, 443.

52. G. R. Wang, L. Wang, Q. Rendeng, J. Wang, J. Luo, C. –J. Zhong, *J. Mater. Chem.*, 2007, **17**, 457.

53. D. L. Pearson, J. M. Tour, *J. Org. Chem.*, 1997, **62**, 1376.

54. L. Jones II, J. S. Schumm, J. M. Tour, *J. Org. Chem.*, 1997, **62**, 1388.

55. G. J. Ashwell, W. D. Tyrrell, B. Urasinska, C. Wang, M. R. Bryce, *Chem. Commun.*, 2006, 1640.

56. V. A. L. Roy, Y. –G. Zhi, Z. –X. Xu, S. –C. Yu, P. W. H. Chan, C. –M. Che, *Adv. Mater.*, 2005, **17**, 1258.

57. G. Pera, A. Villares, M. C. López, P. Cea, D. P. Lydon, P. J. Low, *Chem. Mater.*, 2007, **19**, 857.

58. A. Villares, D. P. Lydon, L. Porrès, A. Beeby, P. J. Low, P. Cea, F. M. Royo, *J. Phys. Chem. B*, 2007, **111**, 7201.

59. J. J. Stapleton, T. A. Daniel, S. Uppili, O. M. Cabarcos, J. Naciri, R. Shashidhar, D. L. Allara, *Langmuir*, 2005, **21**, 11061.

60. D. Takajo, Y. Okawa, T. Hasegawa, M. Aono, *Langmuir*, 2007, **23**, 5247.

61. P. A. Lewis, C. E. Inman, F. Maya, J. M. Tour, J. E. Hutchison, P. S. Weiss, *J. Am. Chem. Soc.*, 2005, **127**, 17421.

62. A. S. Blum, J. C. Yang, R. Shashidhar, B. Ratna, *Appl. Phys. Lett.*, 2003, **82**, 3322.

63. G. P. Lopinski, D. D. M. Wayner, R. A. Wolkow, *Nature*, 2000, **406**, 6791.

64. S. Tanibayashi, T. Tada, S. Watanabe, H. Sekino, *Chem. Phys. Lett.*, 2006, **428**, 367.

65. X. Li, J. He, J. Hihath, B. Xu, S. M. Lindsay, N. Tao, *J. Am. Chem. Soc.*, 2006, **128**, 2135.

66. G. K. Ramachandran, M. D. Edelstein, D. L. Blackburn, J. S. Suehle, E. M. Vogel, C. A. Richter, *Naotechnology*, 2005, **16**, 1294.

67. P. A. Derosa, J. M. Seminario, *J. Phys. Chem. B*, 2001, **105**, 471.

68. M. Lee, M. –H. Park, N. –K. Oh, W. –C. Zin, H. –T. Jung, D. –K. Yoon, *Angew. Chem. Int. Ed.*, 2004, **43**, 6466.

69. U. Mueller, M. Schubert, F. Teich, H. Puetter, K. Schierle-Arndt, J. Pastré, *J. Mater. Chem.*, 2006, **16**, 626.

70. H. Alem, F. Blondeau, K. Glinel, S. Demoustier-Champagne, A. M. Jonas, *Macromolecules*, 2007, **40**, 3366.

71. E. Gultepe, D. Nagesha, L. Menon, A. Busnaina, S. Sridhar, *Appl. Phys. Lett.*, 2007, **90**, 163119.

72. J. Reguera, A. Fahmi, P. Moriarty, A. Girotti, J.C. Rodríguez-Cabello, *J. Am. Chem.Soc.*, 2004, **126**, 13212.

73. P. Cadiot, W. Chodkiewicz, *Chemistry of Acetylenes*, H. G. Viehe (ed.), 1969, Marcel Dekker, New York.

74. L. Brandsma, *Preparative Acetylenic Chemistry*, 2nd edn., Elsevier, 1988, Elsevier Science Publishers B. V., Amsterdam, The Netherlands.

75. F. Diederich, P. J. Stang, *Metal-catalysed Cross-Coupling Reactions*, 1998, Wiley-VCH, Weinheim Germany.

76. (a) M. C. Venuti, G. A. Jones, R. Alvarez, J. J. Bruno, *J. Med. Chem.*, 1987, **30**, 303, (b) G. T. Crisp, B. L. Flynn, *J. Org. Chem.*, 1993, **58**, 6614.

77. Y. Zhang, J. Wen, *Synthesis*, 1990, 177.

78. D. Gelman, S. L. Buchwald, *Angew. Chem. Int. Ed.*, 2003, **42**, 5990.

79. A. Kollhofer, T. Pullman, H. Plenio, *Angew. Chem. Int. Ed.*, 2003, **42**, 9 1056.

80. P. Nguyen, Z. Yuan, L. Agocs, G. Lesley, T. B. Marder, *Inorg. Chim. Acta*, 2004, **220**, 289.

81. A. K. Flatt, Y. Yao, F. Maya, J. M. Tour, *J. Org. Chem.*, 2004, **69**, 1752.

82. S. H. Chanteau, J. M. Tour, *J. Org. Chem.*, 2003, **68**, 8750.

83. C. Hortholary, C. Coudret, *J. Org. Chem.*, 2003, **68**, 2167.

84. L. Jones, J. S. Schumm, J. M. Tour, *J. Org. Chem.* 1997, **62**, 1388.

85. R. G. Heidenreich, K. Köhler, J. G. E. Krauter, J. Pietsch, *Synlett*, 2002, **7**, 1118.

86. D. P. Lydon, L. Porres, A. Beeby, T. B. Marder, P. J. Low, *New. J. Chem.*, 2005, **29**, 972.

87. J. G. Rodríguez, J. L. Tejedor, T. L. Parra, C. Díaz, *Tetrahedron*, 2006, **62**, 3355.

88. J. C. Collings, University of Durham, personal communication.

89. M. S. Khan, A. K. Kakkar, N. J. Long, J. Lewis, P. Raithby, P. Nguyen, T. B. Marder, F. Wittmann, R. H. Friend, *J. Mater. Chem.*, 1994, **4**, 1227.

90. S. W. Watt, C. Dai, A. J. Scott, J. M. Burke, R. L. Thomas, J. C. Collings, C. Viney, W. Clegg, T. B. Marder, *Angew. Chem. Int. Ed.*, 2004, **43**, 3061.

91. H. Li, D. R. Powell, R. K. Hayashi, R. West, *Macromolecules*, 1998, **31**, 52.

92. H. Li, D. R. Powell, T. K. Firman, R. West, *Macromolecules*, 1998, **31**, 1093.

93. L. Zhao, I. F. Perepichka, F. Türksoy, A. S. Batsanov, A. Beeby, K. S. Findlay, M. R. Bryce, *New J. Chem.*, 2004, **28**, 912.

94. C. Xue, F. –T. Luo, *Tetrahedron*, 2004, **60**, 6285.

95. H. C. Clark, and K. R. Dixon, *J. Am. Chem. Soc.*, 1969, **91**, 596.

96. *SHELXTL, version 6.14,* Bruker AXS, Madison, Wisconsin, USA, 2000.

97. P. J. Hanhela, D. B. Paul, *Aust. J. Chem.*, 1981,**34**,1669.

98. P. J. Hanhela, D. B. Paul, *Aust. J. Chem.*, 1981, **34**, 1687.

99. G. Clauss, W. Reid, *Chem. Ber.*, 1975, **108**, 528.

Chapter 3. 'Synthesis and Structural Characterisation of Gold(I) Oligo(phenylene ethynylene) Complexes'

3.1. Introduction

There is a long standing interest in the preparation and properties of so-called "rigid-rod" compounds. [1,2] These compounds attract interest because of the useful physical properties that can arise from their shape, such as liquid crystalline phases [3-6] and mechanical stability. [7-9] When combined with an extended, delocalised π-system, molecular rigid-rods can also offer a range of potentially technologically valuable electronic and photochemical properties. For example, the extended π-system in 1,4-bis(phenylethynyl) benzene has resulted in the incorporation of this motif in the design of numerous molecular materials for use as molecular wires. [10-20] whilst the intense luminescence from 9,10-bis(phenylethynyl)anthracene has led to the applications in sensors, [21-23] chemiluminesent devices and as the emitting layer in organic light emitting diode (OLED) based displays. [24,25]

In order to tune the physical, electronic and photochemical properties of rigid-rod molecules, and related polymers, many workers have investigated the incorporation of metal centres within the linear rigid-rod framework. For the most part, these studies have sought to extend electronic conjugation along the length of the rod through dπ-pπ bonding, [26-33] or to take advantage of the particular structural properties offered by the metal centre. [31,34-41]

The introduction of gold(I) within rigid-rod systems has recently attracted the attention of many workers. [42-51] The presence of relatively strong aurophilic interactions [52-55] can be used to tailor intricate macromolecular shapes in the solid state. [56-61] However, the introduction of a heavy, third-row transition element also results in significant effects on the photophysical properties of the resulting materials by promoting spin-orbit coupling and increasing the population of triplet states. [62-66] However, as a donor for use in the design of second-order NLO materials, gold(I) phosphines were found to be less effective than metal fragments based on, for

example, ruthenium. [67-69] Gold(I) acetylides are therefore attractive motifs for use in the construction of functionalised molecular materials. The linear –(AuC≡C)- moiety makes systems based on this motif attractive and promising candidates for the design of linear-chain metal-containing materials. [45,70,71]

As indicated above, gold(I) compounds often aggregate in the solid state through aurophillic interactions. Equally, phenylene ethynylene based organic materials display a wide range of π-π, C-H...π and other intermolecular interactions in the solid state. [3,72,73] In this Chapter the preparation, chracterisation and molecular structures of a range of compounds of general type [Au(C≡CC_6H_4C≡CC_6H_4X)L] is described. Selected photophysical and chemical reactivity studies are described in later Chapters of this thesis.

3.2. Result and Discussion

3.2.1. Syntheses

The gold phenylene ethynylene complexes were prepared from the corresponding TMS-terminated ethynyl tolans in the presence of NaOMe. In this manner the complexes Au(C≡CC_6H_4C≡CC_6H_4X)(PL_3) [L = Ph, X = Me (**15**), OMe (**16**), CO_2Me (**17**), NO_2 (**18**), CN (**19**); L = Cy, X = Me (**20**), OMe (**21**), NO_2 (**22**)] were prepared, as shown in **Scheme 3.1**.

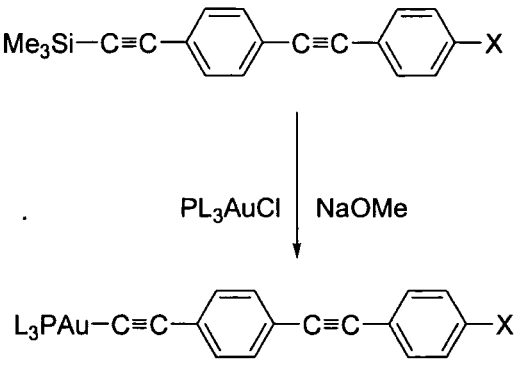

X = Me (**1**), OMe (**2**), CO_2Me (**3**), NO_2 (**4**), CN (**5**)

L = Ph; X= Me (**15**), OMe (**16**), CO_2Me (**17**), NO_2 (**18**), CN (**19**)

L = Cy; X = Me (**20**), OMe (**21**), NO_2 (**22**)

Scheme 3.1. Syntheses of **15-22** from the TMS-protected tolans (**1-5**) as ligands with the presence of NaOMe.

Desilylation of the TMS protected ethynyl tolans by NaOMe at room temperature in the first step of the reaction generates a solution containing the nucleophilic acetylide as shown in **Scheme 3.2**. The addition of $AuCl(PL_3)$ (L = Ph or Cy) to these solutions gives the desired products, which were isolated as precipitates from the reaction mixtures, and purified by recrystallisation from $CHCl_3$/MeOH to afford white to yellow crystals in between 65-84 % yield. Similar reaction conditions are often used in the preparation of gold(I) acetylides. [50, 62-64,74-77]

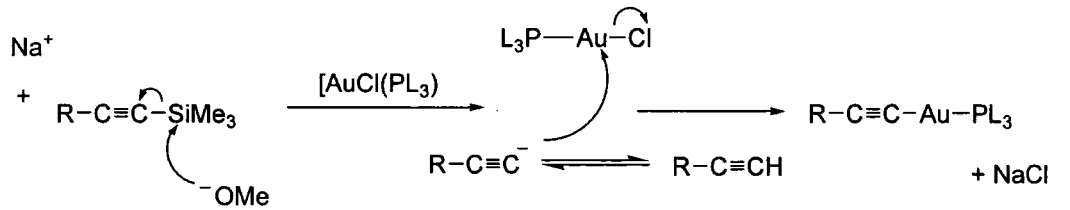

Scheme 3.2. The general mechanism for gold acetylides synthesis. [74]

Each of the complexes **15-22** were characterised by the usual spectroscopic methods. In the case of compound **15**, a singlet at δ_H 2.36 ppm was observed arising from the methyl protons of the tolan moiety. The methoxy and methyl ester moieties in **16** and **17** were observed at ca. δ_H 3.9 ppm. However, the numerous aromatic protons in **15-**

19 were not fully resolved, but were observed as a series of heavily overlapped signals in the range δ_H 6.9-8.2 ppm. The pseudo-doublet resonances from the tolan portion of the molecule were not distinctly observed.

The ^{31}P NMR spectra of **15 – 22** show singlet phosphorus resonances near δ_P 43 ppm in each case, which is shifted downfield from AuCl (PPh_3) (δ_P 33 ppm). [78] The similarities of δ_P in **15-22** indicate a similar electronic environment associated with the phosphine in each case. Clearly, the electronic properties of the tolan substituent are not reflected in the ^{31}P NMR chemical shift of the phosphine moiety.

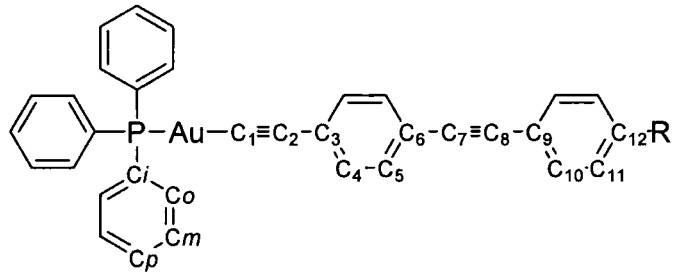

Scheme 3.3. Numbering scheme for NMR spectral assignment of **15-19**

The ^{13}C NMR spectra of **15-19** are, as might be expected, similar, and are consistent with the structures. For example, the spectrum of **15** contains a methyl resonance at δ_C 22 ppm, whereas the methoxy and methyl ester carbons in **16** and **17** were observed above δ_C 50 ppm. In addition, the distinctive carbonyl carbon in **17** was observed near δ_C 167 ppm, whilst in the case of **19**, the CN carbon was observed at δ_C 121 ppm. The acetylide carbons C_1 and C_2 were observed, and identified on the basis of the J_{CP} coupling constants, with a doublet at ca. δ_C 135 ppm with coupling constant $^2J_{CP}$ ~ 142 Hz being assigned to C_1, and another doublet at lower chemical shift (ca. δ_C 104 ppm, $^3J_{CP}$ ~ 27 Hz) assigned to C_2 (**Scheme 3.3**). Similar characteristic resonances have been reported for similar systems. [54,79] It is interesting to note that the C_1 resonances are shifted downfield from that in Au(C≡C^{t}Bu)(PCy_3) (δ_C 120.9 ppm), [80] and this can be attributed to the greater electron-donating ability of the *tert*-butyl group. Another set of acetylenic carbons (C_7 and C_8) can be found at ca. δ_C 90 ppm. The aromatic carbons of the tolan fragment C_3 – C_6 and C_9 – C_{10} are all clearly observed and assigned on the basis of comparisons within the series of

complexes **15-19** and also the analogous ligand precursors. Thus, C_3 can be found between δ_C 116-130 ppm, with C_4 and C_5 falling at higher chemical shift ca. δ_C 132 ppm; C_6 and C_9 are found at ca. δ_C 120 ppm. The C_{10} resonances are observed near δ_C 130 ppm, whilst C_{11} and C_{12} can be found between δ_C 114-132 ppm and δ_C 112-160 ppm, respectively.

The aromatic carbons associated with the triphenyl phosphine ligand are clearly distinguishable from those of the tolan moiety on the basis of the coupling to the phosphorus nucleus, and assigned on the basis of the size of the coupling constant. Thus, C_i is observed as doublet at ca. δ_C 130 ppm ($^1J_{CP}$ ~ 56 Hz), C_o at δ_C 135 ppm ($^2J_{CP}$ ~ 14 Hz), C_m ca. δ_C 129 ppm ($^3J_{CP}$ ~ 11-12 Hz) and C_p δ_C 132 ppm ($^4J_{CP}$ ~ 2 Hz).

The IR spectra of **15-19** were recorded as Nujol mulls, and show one ν(C≡C) band near 2200 cm^{-1}, which is similar to the ν(C≡C) band found in Au(C≡CPh)(PPh_3) [81,82] and other similar systems [45,83] and consequently assigned to the gold-acetylide fragment. Apparently, the local environment of the $C_7{\equiv}C_8$ bond is sufficiently symmetrical that the ν(C≡C) band is very weak in the IR spectrum and not observed.

The electrospray mass spectra $[ES\text{-}MS]^+$ for complexes **15-17** and **19** contain aggregate $[M+AuPPh_3]^+$ ions and the cation $[Au(PPh_3)_2]^+$; similar ions have been observed in many similar systems [84,85] and are believed to be generated during the ionisation process of aggregates present in the solid samples [86,87] although the solid state structures of **15**, **16**, **18** and **19** do not offer strong evidence for Au...Au interactions (see below). In the case of **17**, the aggregate $[M+(AuPPh_3)_2]^+$ was also observed. In the presence of Na^+, either added as a chemical aid to ionisation [88] or abstracted from the glass, ions $[M+Na]^+$ may also be observed. [89] Here, the sodium adduct of the molecular ion was also observed in the spectrum of the OMe derivative **16** and identified by comparison with the calculated isotope pattern ($[M+Na]^+$, *m/z* 713). Compound **18** was not successfully ionised in $[ES\text{-}MS]^+$ mode, and instead the mass spectrum of this compound was obtained using MALDI methods, with $[M+(AuPPh_3)_2]^+$, $[M+AuPPh_3]^+$ and $[Au(PPh_3)_2]^+$ ions all being observed.

The same synthetic procedures as shown in **Scheme 3.1** and **3.2** were followed to synthesise another group of gold acetylides featuring diethynyl tolan derivatives with tricyclohexylphosphine (PCy_3) co-ligands have also been prepared (**20-22**) in 72-84 % yields. Whilst first prepared in 1973, [90] tricyclohexylphosphine supported gold(I) acetylide complexes have been studied in some detail recently, as these systems are highly luminescent due to the fact that there are no low-lying ligand-localised excited states to quench fluorescence. In addition, the bulkiness of the ligand is thought to disfavour metal-metal and π-π oligomerisation processes which can also provide non-luminescent decay mechanism for excited studies. [62-64,91]

The complexes **20-22** were characterised in usual spectroscopic methods. In the case of **20**, singlet methyl peak can be observed at δ_H 2.35 ppm and the methoxy moiety in **21** was observed at δ_H 3.82 ppm arising from the tolan moieties. However, the cyclohexyl (Cy) protons in **20-22** were observed as series of overlapped resonances at δ_H 1.3-2.0 ppm. The expected signals for the aromatic protons arising from the tolan portion were observed as pseudo-doublets in the region δ_H 6.9-8.2 ppm. (**Scheme 3.4**). The ^{31}P NMR spectra show singlet phosphorus resonances near δ_P 57 ppm which is shifted downfield from AuCl (PCy_3) (δ_P 52 ppm) [92] indicating a similar electronic environment associated phosphine in each case.

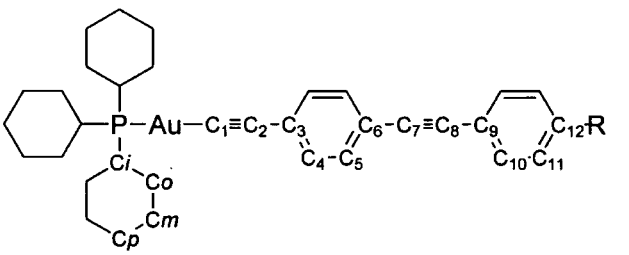

Scheme 3.4. Numbering scheme for NMR spectral assignment of **20-22.**

The ^{13}C NMR of **20-22** are, as might be expected, similar and consistent with the complexes **15-19** and with the ligand precursors. Because of these similarities, the aromatic carbon signals arising from the tolan portions of these complexes are the same and will not be discussed any further. The only distinctive difference is in the replacement of the PPh_3Au with PCy_3Au moieties in the systems.

The acetylide carbons C_1 and C_2 were observed, and identified on the basis of the J_{CP} coupling constants, with a doublet at ca. δ_C 140 ppm with coupling constant $^2J_{CP}$ ~ 140 Hz being assigned to C_1, and another doublet at lower chemical shift (ca. δ_C 104 ppm, $^3J_{CP}$ ~ 25 Hz) assigned to C_2 (**Scheme 3.4**). Similar characteristic resonances have been reported for similar systems. [63,64] The other set of acetylenic carbons (C_7 and C_8) can be found at ca. δ_C 90 ppm.

The aromatic carbons associated with the tricyclohexyl phosphine ligand are clearly distinguishable from those of the tolan moiety on the basis of the coupling to the phosphorus nucleus, and assigned on the basis of the size of the coupling constant. Thus, C_i is observed as doublet at ca. δ_C 33 ppm ($^1J_{CP}$ ~ 28 Hz), C_o at δ_C 27 ppm ($^2J_{CP}$ ~ 12 Hz), C_m at δ_C 26 ppm ($^3J_{CP}$ ~ 2 Hz) and C_p arise as singlet at ca. δ_C 30 ppm.

The IR spectra of **20-22** were recorded as Nujol mulls, and show two ν(C≡C) bands near 2200 cm^{-1}, which is similar to the ν(C≡C) band found in $Au(C{\equiv}CPh)(PCy_3)$.[63,64] In addition, a weak ν(C≡C) band can be observed at near 2100 cm^{-1} which correspond to the $C_7{\equiv}C_8$ bond in the tolan moieties.

The electrospray mass spectra $[ES\text{-}MS]^+$ for complexes **20-22** contain aggregate $[M+AuPCy_3]^+$ ions and the cation $[Au(PCy_3)_2]^+$; these complexes do not offer strong evidence for Au...Au interactions in the solid state. Thus, the observation of aggregate ions in the $[ES\text{-}MS]^+$ suggests such aggregates are readily formed in the gas phase. [93]

Protocols similar to those described above for the preparation of **15–22** were applied to prepare the yellow, bis(gold(I)) complexes **23** and **24**, which feature extended "three ring" phenylene ethynylene ligands in 74 % and 82 % yield, respectively (**Scheme 3.5**). In the case of **24**, recrystallisation from chloroform/methanol afforded yellow crystals suitable for crystallography.

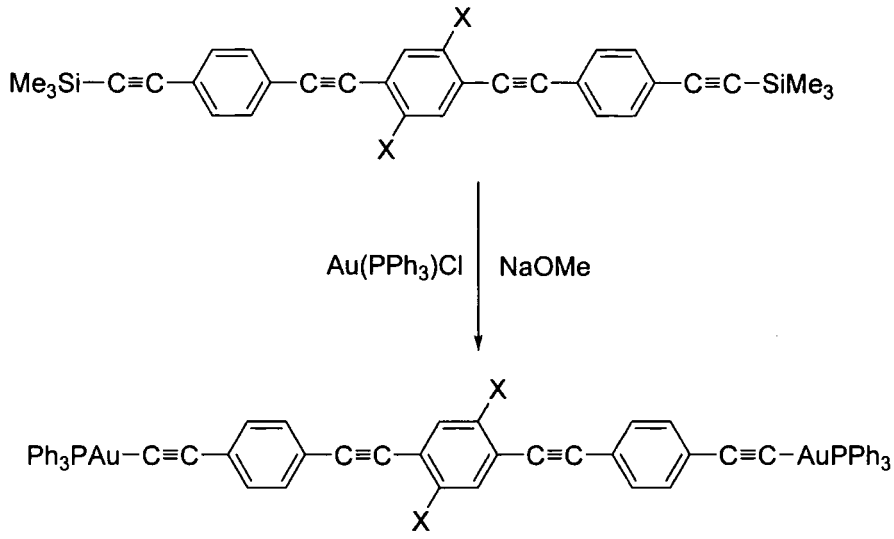

X = H (**23**), OMe (**24**)

Scheme 3.5. The syntheses of **23** and **24** from the TMS-protected tolans with the presence of NaOMe.

Both of the complexes were characterised by the usual spectroscopic methods, which included a methoxy peak at δ_H 3.9 ppm for **24**. The aromatic protons of **23-24** of the bridging ligand were overlapped heavily with those of the triphenylphosphine ligands, although in the case of **24** a singlet at δ_H 7.00 ppm and integrating as 2 protons arising from from the ($C_6H_2(OMe)_2$) protons could be distinguished (**Scheme 3.6**). Only a single ^{31}P NMR resonance was observed near δ_P 43.3 ppm in each case.

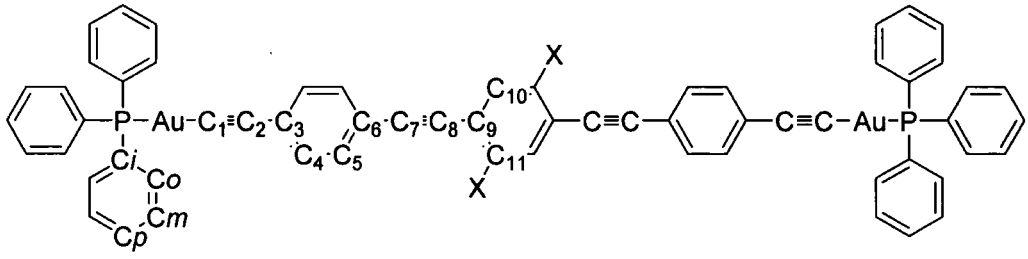

X = H (**23**), OMe (**24**)

Scheme 3.6. Numbering scheme for NMR spectral assignment of **23-24.**

Unsurprisingly, the ^{13}C NMR spectra for both complexes **23** and **24** are very similar with the exception of the methoxy peak at δ_C 57 ppm in **24**. The acetylide carbons C_1 and C_2 are observed as doublets at ca. δ_C 134 ppm ($^2J_{CP}$ ~ 150 Hz) and ca. δ_C 104 ppm ($^3J_{CP}$ ~ 25 Hz) (**Scheme 3.6**). Another set of acetylenic carbons (C_7 and C_8) are

observed at δ_C 90.7 and δ_C 91.7 (**23**), and δ_C 87.1 and δ_C 95.5 ppm (**24**). The assignment of the remaining carbon resonances follow from the magnitude of coupling constants to phosphorus and comparisons with the complexes **15–19** and the ligand precursors, in a manner similar to that described above.

The electro-spray $[MS\text{-}ES]^+$ mass spectrum for **23** and MALDI-TOF(+)-MS spectrum for **24** both show peaks corresponding to aggregate ions $[M+AuPPh_3]^+$ and $[Au(PPh_3)_2]^+$ in addition to M^+ at *m/z* 1243 for **23** and at *m/z* 1301 for **24**.

3.2.3. Molecular Structural Analyses

The molecular structures of **15, 16, 18, 19, 20, 22** and **24** have been determined by single crystal X-ray diffraction as shown in **Figure 3.1** to **Figure 3.8.** Crystallographic data, selected bond lengths and angles are listed in **Table 3.1 - Table 3.6**. The crystallographic work has been carried out by Dr D. S. Yufit and Dr Albesa-Jové.

Molecular Structures of [Au(C≡CC$_6$H$_4$C≡CC$_6$H$_4$R)(PPh$_3$)] [R = Me (15), OMe (16), NO$_2$ (18), CN (19)

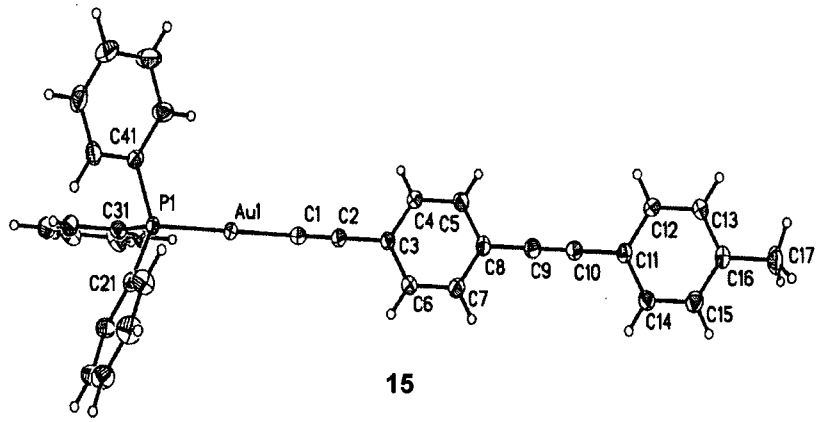

15

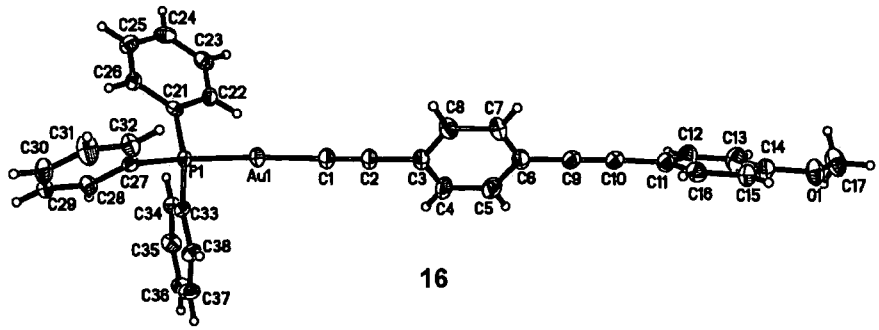

16

Figure 3.1. A plot of molecule of **15** and **16**, illustrating the atom numbering scheme.

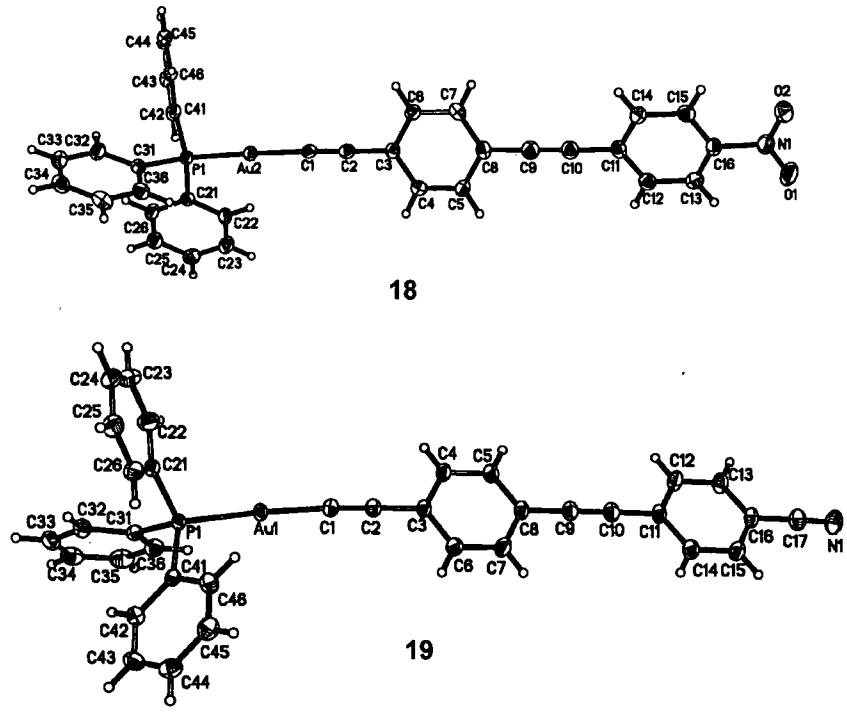

Figure 3.1. A plot of molecule of **18** and **19**, illustrating the atom numbering scheme. (cont.)

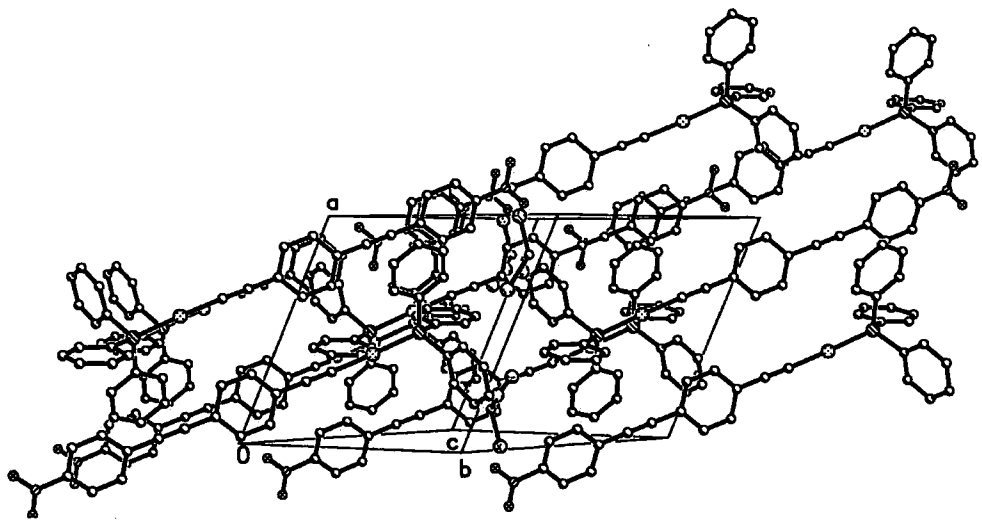

Figure 3.2. Representative molecular packing diagram for **18**.

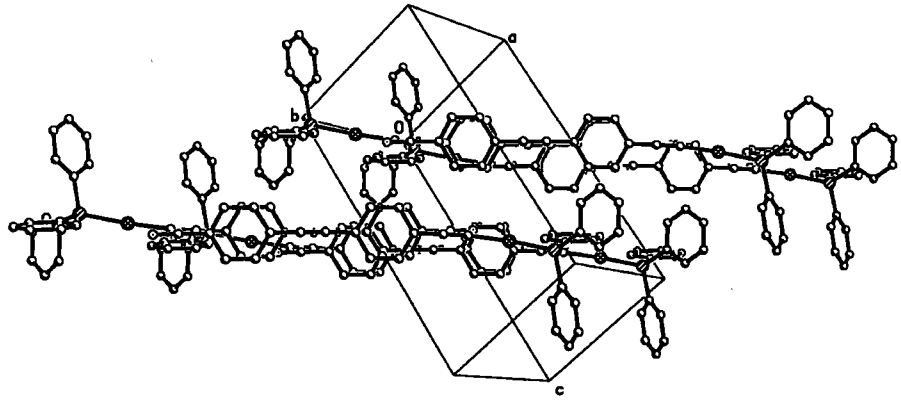

Figure 3.3. Representative molecular packing diagram for **19**.

Table 3.1. Crystal data for **15-16** and **18 -19**.

	15	**16**	**18**	**19**
Molecular formula	$C_{35}H_{26}PAu{\cdot}CHCl_3$	$C_{35}H_{26}OPAu$	$C_{34}H_{23}NO_2PAu$	$C_{35}H_{23}NPAu$
M / g mol^{-1}	793.86	690.46	705.47	685.48
Crystal system	Triclinic	Triclinic	Triclinic	Triclinic
a / Å	7.9229(10)	9.7616(14)	11.750(4)	8.7340(8)
b / Å	12.4445(16)	17.617(3)	11.792(4)	9.8435(9)
c / Å	16.730(2)	18.133(3)	13.058(4)	16.4629(15)
α / °	86.26(1)	110.013(3)	64.418(3)	86.948(2)
β / °	89.92(1)	100.206(3)	76.489(3)	88.443(2)
γ / °	74.97(1)	101.299(3)	68.075(3)	82.302(2)
V / Å^3	1589.5(3)	2770.4(7)	1508.2(9)	1400.3(2)
Space group	P-1	P-1	P-1	P-1
Z	2	4	2	2
D_c / Mg m^3	1.659	1.656	1.553	1.626
Crystal size / mm	0.24×0.22×0.14	0.22×0.12×0.04	0.44×0.40×0.32	0.46x0.10x0.06
Crystal habit	plate	plate	plate	plate
F (000)	776	1352	688	668
Radiation	Mo(K_α)	Mo(K_α)	Mo(K_α)	Mo(K_α)
Wavelength / Å	0.71073	0.71073	0.71073	0.71073
μ / mm^{-1}	4.955	5.394	4.960	5.334
Temperature / K	120(2)	120(2)	120(2)	120(2)
Data collection range / °	1.22 – 30.52	1.24-30.52	1.74-29.88	1.24 - 30.46
Reflections measured	22199	37431	14774	19102
Data, restraints, parameters	9669, 0, 371	16724, 0, 663	7655, 0, 353	8473, 0, 343
R_1, *wR2* (all data)	0.0210, 0.0482	0.0822, 0.1211	0.0309, 0.0567	0.0249, 0.0489
Goodness-of-fit on F^2 (all data)	1.080	0.791	1.065	1.040
peak, hole / eÅ^{-3}	0.977, -0.816	4.315, -1.104	1.772, -1.188	1.129, -1.101

Table 3.2. *S*elected bond lengths *(Å)* and angles (°) for **15-16** and **18-19**.

	15	**16**	**18**	**19**
Au(1)–P(1)	2.2752(5)	2.2652(14)	2.2889(12)	2.2764(5)
Au(1)–C(1)	1.999(2)	2.003(6)	2.023(4)	1.999(2)
C(1)–C(2)	1.204(3)	1.191(8)	1.195(6)	1.204(3)
C(2)–C(3)	1.441(3)	1.447(8)	1.439(6)	1.438(3)
C(9)–C(10)	1.198(3)	1.204(8)	1.207(7)	1.201(3)
P(1)–Au(1)–C(1)	176.4(1)	172(2)	176(1)	176.0(6)
Au(1)–C(1)–C(2)	170.5(2)	168.2(5)	172.8(4)	175.3(2)
C(1)–C(2)–C(3)	174.6(2)	177.3(6)	178.8(5)	178.0(2)
C(8)–C(9)–C(10)	178.8(2)	178.4(7)	178.8(6)	178.7(3)
C(9)–C(10)–C(11)	177.8(2)	177.3(6)	178.2(6)	179.3(3)

Molecular Structural Analyses for 15-19

The molecules of **15-19**, are illustrated in **Figure 3.1** to show the atom labelling scheme. Selected bond lengths and angles are summarised in **Table 3.2**. Within the series **15-19**, the Au-C(1) [1.999(2)-2.023(4) Å] and Au-P(1) [2.2652(14)-2.2752(5) Å] bond lengths are comparable with those of related acetylide complexes, such as Au(C≡CPh)(PPh_3) [Au-C 1.97(2)/2.02(2); Au-P 2.276(5)/2.282(4) Å, for two independent molecules [94] and Au(C≡C$SiMe_3$)(PPh_3) [Au-C 2.000(4); Au-P 2.2786(10) Å]. [80] There is no evidence for significant cumulene/quinoidal character within the phenylene ethynylene portion of the molecule and the C(1)-C(2) [1.191(8)-1.204(3) Å] and C(9)-C(10) [1.198(3)-1.207(7) Å] acetylide bond lengths are the same within the limits of precision of the structure determination. The P-Au-C moiety is essentially linear [171.6(17)-176.4(6)°], but there is a gentle curvature in the molecular backbone, particularly pronounced at C(1) [Au-C(1)-C(2) 168.2(5)-175.32(19)°], brought about by crystal packing effects.

The complexes **15-19** offer an opportunity to examine systems in which Au...Au and $\pi...\pi$ interactions, together with other weak interactions such as CH...π, may work to influence the solid state structures. In this work, no aurophilic interactions were found in the extended solid-state structures, with $\pi...\pi$ interactions between the tolan moieties being more prevalent. In each structure the molecules lie in an anti-parallel arrangement with a number of CH (from various phenyl rings)...π(phenyl or acetylene bond) interactions being evident (**Figure 3.2** and **Figure 3.3**). Stacking $\pi...\pi$ interactions between the phenyl rings of the tolan moieties are observed only in the structures **18** and **19**, which also carry the most strongly electron-withdrawing terminal substituents (X = NO_2 and CN). Whilst in the case of **19** both tolan ring systems are stacked, only the more highly polarised terminal phenyl ring in **18** is involved in this motif. Steric constraints associated with the PPh_3 supporting ligand likely restrict the close approach of the gold centres, and Au...Au interactions are superseded by these various π-hydrocarbons based interactions. [87,95,96]

Molecular Structures of [Au(C≡CC$_6$H$_4$C≡CC$_6$H$_4$R)(PCy$_3$)] [R = Me (20), NO$_2$ (22)

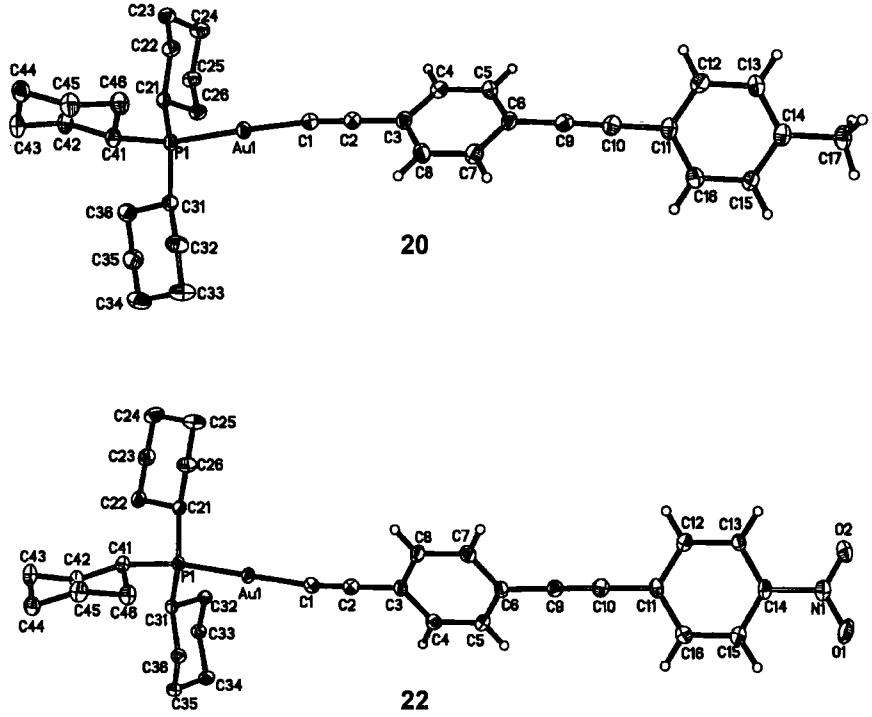

Figure 3.4. A plot of molecule of **20** and **22**, illustrating the atom numbering scheme.

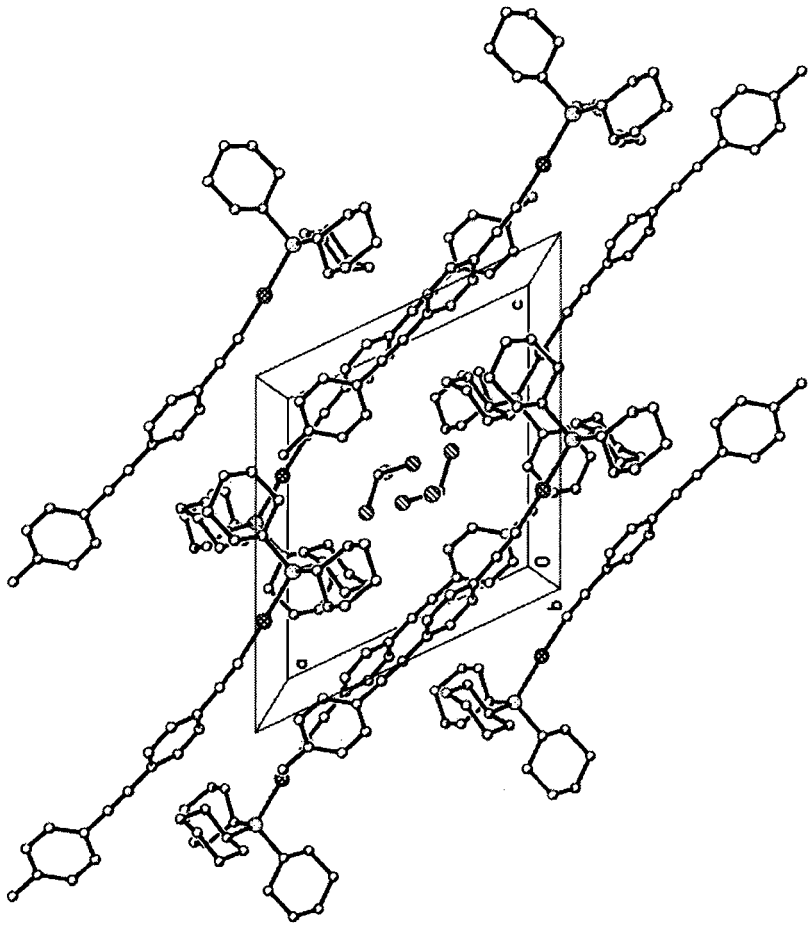

Figure 3.5. Representative packing diagram of **20** revealing that there is no aurophilic interaction due to the steric effect of the supporting ligand attached to gold.

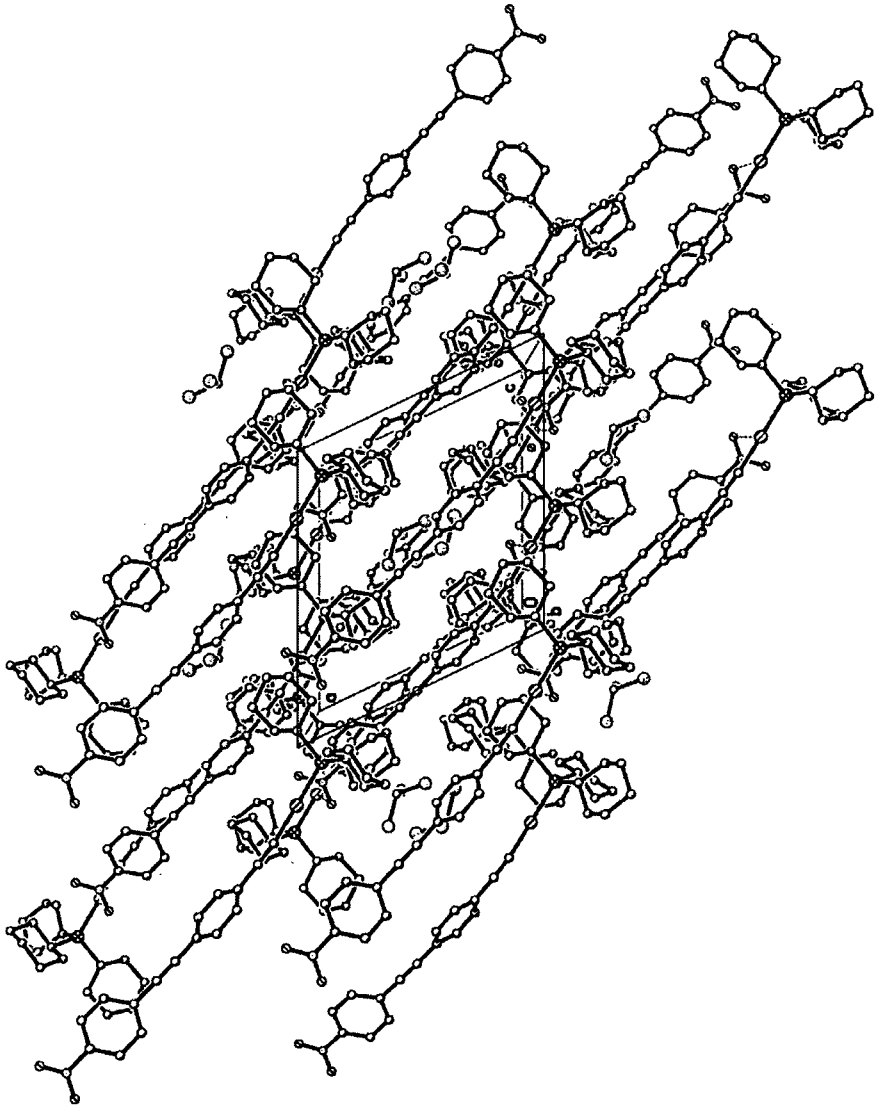

Figure 3.6. Representative packing diagram of **22** revealing that there is no aurophilic interaction due to the steric effect of the supporting ligand attached to gold.

Table 3.3.: Crystal data for **20** and **22**.

	20	**22**
Molecular formula	$C_{35}H_{44}PAu \cdot x\ CHCl_3$	$C_{34}H_{41}NO_2PAu \cdot x\ CHCl_3$
M / g mol^{-1}	812.01	842.98
Crystal system	Monoclinic	Monoclinic
a / Å	12.123(2)	12.0994(3)
b / Å	24.343(5)	23.9198(5)
c / Å	12.807(3)	13.1499(3)
α / °	90	90
β / °	115.40(3)	115.71(1)
γ / °	90	90
V / Å^3	3414.1(12)	3428.98(14)
Space group	P $2_1/c$	P $2_1/c$
Z	4	4
D_c / Mg m^3	1.580	1.633
Crystal size / mm	0.24×0.20×0.08	0.66×0.07×0.06
Crystal habit	plate	plate
F (000)	1624	1680
Radiation	Mo(K_α)	Mo(K_α)
Wavelength / Å	0.71073	0.71073
μ / mm^{-1}	4.955	1.637
Temperature / K	120(2)	120(2)
Data collection range / °	1.67-27.50	1.70-28.00
Reflections measured	20544	38646
Data, restraints, parameters	7728, 0, 386	8267, 0, 400
R_1, *wR2* (all data)	0.0355, 0.0611	0.0242, 0.0453
Goodness-of-fit on F^2 (all data)	0.994	1.038
peak, hole / eÅ^{-3}	0.994, -0.708	0.848, -0.688

Table 3.4. Selected bond lengths *(Å)* and angles(°) for **20** and **22.**

	20	**22**
Au(1)–P(1)	2.2887(9).	2.2891(5)
Au(1)–C(1)	2.004(3)	2.015(2)
C(1)–C(2)	1.209(5)	1.197(3)
C(2)–C(3)	1.437(4)	1.433(3)
C(9)–C(10)	1.203(4)	1.200(3)
P(1)–Au(1)–C(1)	177.88(9)	179.05(7)
Au(1)–C(1)–C(2)	174.1(3)	173.9(2)
C(1)–C(2)–C(3)	176.8(4)	176.7(3)
C(8)–C(9)–C(10)	176.1(3)	175.5(2)
C(9)–C(10)–C(11)	178.3(4)	178.5(2)

Molecular Structural Analyses for 20 and 22

The Au-C(1) [2.004(3) Å] and Au-P(1) [2.289(9) Å] for **20** and Au-C(1) [2.015(2) Å] and Au-P(1) [2.289(5) Å] for **22** bond lengths are comparable with those other similar example that features cyclohexyl groups bound to the phosphine, such as $Au(C{\equiv}CC_6H_4C{\equiv}CC_6H_5)(PCy_3)$ [Au-C(1) 2.007(5) Å, Au-P(1) 2.281(1) Å], $Au(C{\equiv}CC_6H_4C\text{-}CC_6H_5)(PCy_3)$ [Au-C(1) 2.003(7) Å, Au-P(1) 2.291(2) Å]. [63] There is no any evidence for significant cumulene/quinoidal character within the phenylene ethynylene portion of the molecule and the C(1)≡C(2) [1.209(5) Å] and C(9)≡C(10) [1.203(4) Å] **20** and C(1)≡C(2) [1.197(3) Å] and C(9)≡C(10) [1.200(3) Å] **22** acetylide bond lengths are the same within the limits of precision of the structure determination. The P-Au-C moiety is essentially linear [177.88(9)°] (**20**) and [179.05(7)°] (**22**), but there is a gentle curvature in the molecular backbone, particularly pronounced at C(1) [Au-C(1)≡C(2) 174.1(3) °] (**20**) and C(1) [Au-C(1)≡C(2) 173.9(2)°] (**22**), brought about by crystal packing. Like other members of the group, there is no close Au…Au contacts are observed in the extended solid state structure for both complexes. But for **22**, there is Au…O between the Au and the

nitro group of the two complexes due to the crystal packing in the solid state. Other ligands intermolecular interactions also can be observed in similar complexes prepared by Che and co-workers. [62] For an example, there are weak actetylide and proton arising from the phenyl group[C-H...π(C≡C)] interactions between the two complexes of Au(C≡CC_6H_4R)(PCy_3); R = NO_2, CF_3. The two phenyl rings are co-planar and these discrete dimmers are packed into parallel sheets in the crystal lattice.

Molecular Structure of

{Au(PPh_3)}$_2$(μ-C≡CC_6H_4C≡CC_6(OMe)$_2H_2$C≡C_6H_4C≡C) (24)

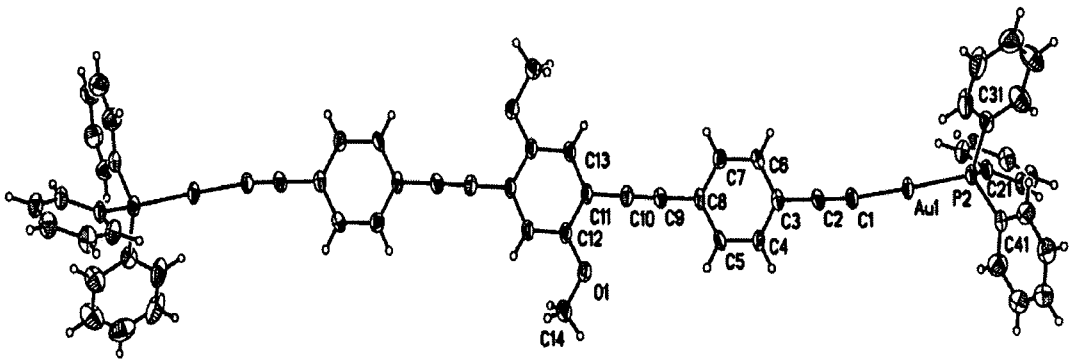

Figure 3.7. A plot of molecule **24**, illustrating the atom numbering scheme.

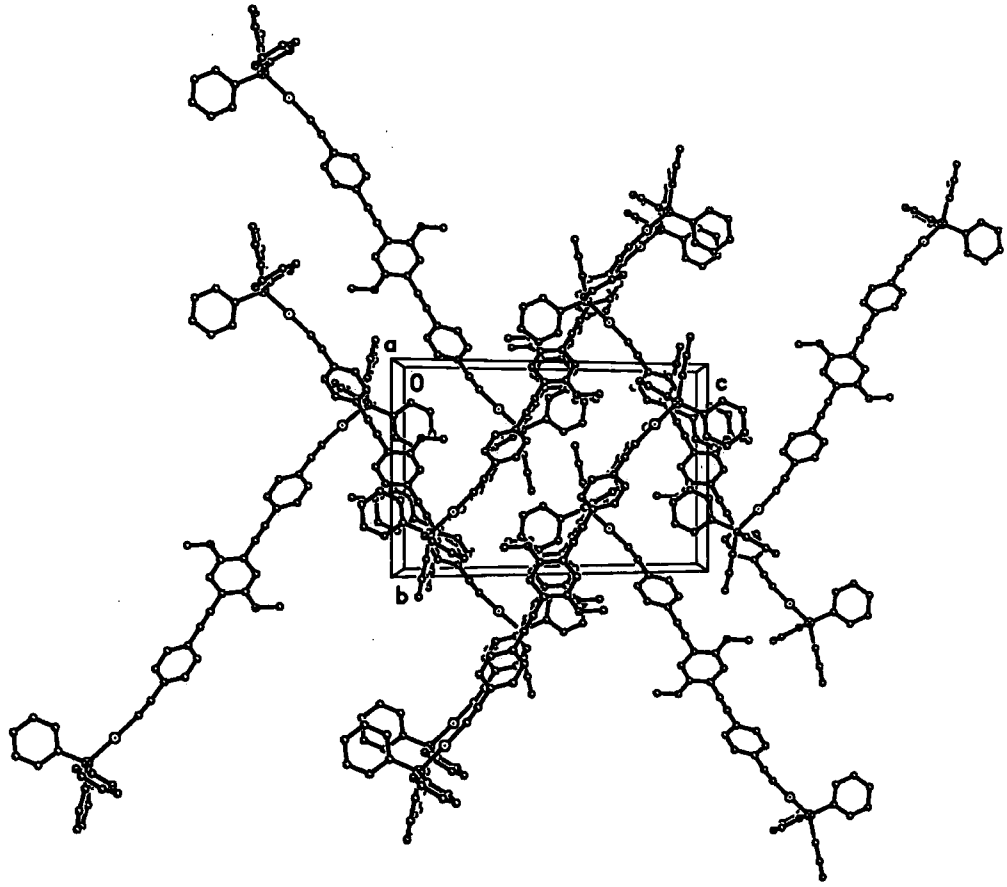

Figure 3.8. Representative Packing diagram of **24**, revealing that there is no aurophilic interaction due to the steric effect of the supporting ligands attached to the gold.

Table 3.5. Crystal data for **24.**

	24
Molecular formula	$C_{64}H_{46}Au_2O_2P_2$
M / g mol^{-1}	1302.89
Crystal system	Monoclinic
a / Å	14.424(2)
b / Å	13.1309(19)
c / Å	21.740(3)
α / °	90
β / °	116.550(7)
γ / °	90
V / Å^3	3683.3(9)
Space group	P2(1)/c
Z	2
D_c / Mg m^3	1.175
Crystal size / mm	0.26×0.20×0.08
Crystal habit	plate
F (000)	1268
Radiation	Mo(K_α)
Wavelength / Å	0.71073
μ / mm^{-1}	4.053
Temperature / K	120(2)
Data collection range / °	1.58-30.52
Reflections measured	29804
Data, restraints, parameters	11140, 0, 317
R_1, *wR2* (all data)	0.0655, 0.1397
Goodness-of-fit on F^2 (all data)	1.031
peak, hole / eÅ^{-3}	2.924, -1.630

Table 3.6.: *S*elected bond lengths *(Å)* and angles(°) for **24.**

	24[a]		**24**[a]
Au(1)–P(1)	2.2687(12)	P(1)–Au(1)–C(1)	178.41(6)
Au(1)–C(1)	2.007(5)	Au(1)–C(1)–C(2)	173.0(5)
C(1)–C(2)	1.197(7)	C(1)–C(2)–C(3)	176.2(6)
C(2)–C(3)	1.442(7)	C(8)–C(9)–C(10)	178.0(2)
C(9)–C(10)	1.207(7)	C(9)–C(10)–C(11)	179.7(7)

[a] for C(6) read C(8)

Molecular Structural Analysis for 24

In general, the structure of **24** is comparable with those of the mono-gold complexes (Au-PPh_3; **15-19**); (Au-PCy_3; **20** and **22**) and the terminal alkyne $HC{\equiv}CC_6H_4C{\equiv}CC_6(OMe)_2(H)_2C{\equiv}C_6H_4C{\equiv}CH$, (**14**). The Au-C(1) [2.007(5) Å] and Au-P(1) [2.269(12) Å] bond lengths are comparable with mono-gold complexes. The addition of the $AuPPh_3$ moieties to the acetylenic carbons does not give any obvious change to the structure, and the P-Au-C moiety is essentially linear [178.41(16)°], which may be compared to the terminal C≡CH ligand (**14**) C(1)-C(2)-C(3) [175.51(16)°]. Like the other examples in the series, there no close Au…Au contacts are observed in the extended solid state structure.

3.2.3. Electrochemical Properties

3.2.3.1. Cyclic Voltammetry

The cyclic voltammograms of the mononuclear gold complexes **15-18** in dichloromethane show totally irreversible anodic [O2, between 0.85-1.15 V vs Fc/Fc^+] and cathodic [R2 < −2.20 V vs Fc/Fc^+] waves close to, or beyond, the limits of the solvent potential window (**Table 3.7**). Indeed, for **15** and **16** which feature electron-donating tolan substituents X = Me and OMe, respectively, the cathodic waves are shifted beyond the limit of the electrochemical window. These irreversible redox processes were not studied in detail. Complex **18** shows an additional cathodic wave R1 at −1.47 V, which is fully reversible and apparently belongs to the reduction of the remote R = NO_2 substituent (**Table 3.4**). The complete thorough discussion of the electrochemical properties regarding these mononuclear gold complexes **15-18** along with the tolan precursors (**1-5**) and the triruthenium carbonyl acetylide clusters (**38-42**) can be obtained in **Chapter 5.**

Table 3.7. Electrochemical properties of the Au-tolan complexes **15-18.**

Compound	$E_{p,c}$ (R2, tolan)	$E_{1/2}$ (R1, NO_2)	$E_{p,a}$ (O2/O3, tolan)
15	*not observed*	--	0.94
16	*not observed*	--	0.88
17	−2.37	--	1.14
18	−2.23	−1.49	1.13

[a] Redox potentials (V vs Fc/Fc^+) were determined from cyclic voltammetric scans. Experimental conditions: Pt disk working microelectrode, v = 100 mV s^{-1}, T = 293 K. E_p denotes peak potential of a chemically irreversible step.

3.2.4. Photophysical Details

The electronic absorption properties of the mononuclear gold(I)acetylide complexes (**15-19**), and the bisnuclear gold(I)acetylide **23,** including the luminescent properties of **15 and 23** also have been investigated and fully discussed in the **Chapter 5 ('Photophysical and Electrochemical Properties of Triruthenium Carbonyl Clusters Featuring Phenylene Ethnylene Ligands')** as a comparison studies with the triruthenium carbonyl acetylide clusters (**36-43**) along with the ligand precursors of the tolans (**1-5** and **6**), and the extended three-ring system featuring $SiMe_3$ protecting groups (**11**).

3.3. Conclusions

In this chapter, gold(I) oligo-phenylene ethynylene complexes were prepared from the tolan ligand precursors and $AuCl(PL_3)$ (L = Ph, Cy) in the presence of NaOMe in a good yields. Molecular structural data for these complexes were also obtained which allow the intermolecular interactions in the solid state to be assessed. In the complexes there are no Au...Au interaction in the solid state due to the steric effect of the phosphine moieties bound to gold but there are some $\pi...\pi$ interactions between the organic ligands. Selected photophysical and chemical reactivity studies of some of the complexes are described in later Chapters of this thesis.

3.4. Experimental Details

3.4.1. General Condition

All reactions were carried out under an atmosphere of nitrogen using standard Schlenk techniques. Reaction solvents were purified and dried using an Innovative Technology SPS-400, and degassed before use. No special precautions were taken to exclude air or moisture during work-up. The compounds $AuCl(PPh_3)$, [78] $AuCl(PCy_3)$ [92] were prepared by literature routes. Other reagents were purchased and used as received.

NMR spectra were recorded on a Bruker Avance (^1H 400.13 MHz, ^{13}C 100.61 MHz, ^{13}C 125.68 MHz, ^{31}P 161.98 MHz) or Varian Mercury (^{31}P 161.91 MHz) spectrometers from $CDCl_3$ solutions and referenced against solvent resonances (^1H, ^{13}C) or external H_3PO_4 (^{31}P) IR spectra were recorded using a Nicolet Avatar spectrometer from nujoll mull suspended between NaCl plates. Mass spectra were recorded using Thermo Quest Finnigan Trace MS-Trace GC or Thermo Electron Finnigan LTQ FT mass spectrometers or Matrix-Assisted Laser Desorption/Ionisation-Time-of-Flight (Mass Spectrometry) (MALDI-TOF MS) ABI Voyager STR.

Diffraction data were collected at 120K on a Bruker SMART 6000 CCD (**15**, **16** and **19**), (**20** and **22**) and (**24**), on Bruker SMART 1K CCD (**18**) (three-circle diffractometers, using graphite-monochromated Mo-K_α radiation. The diffracrometer were equipped with Cryostream (Oxford Cryosystems) low-temperature nitrogen cooling devices. The structures were solved by direct-methods and refined by full matrix least-squares against F^2 of all data using *SHELXTL* software. [97] All non-hydrogen atoms where refined in anisotropic approximation except the disordered ones, H atoms were placed into the calculated positions and refined in "riding" mode. The crystallographic data and parameters of the refinements are listed in **Table 3.1** - **Table 3.3**.

3.4.2. Experimental

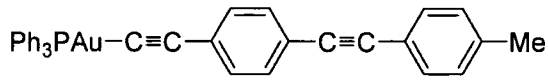

3.4.2.1. Preparation of Au ($C{\equiv}CC_6H_4C{\equiv}CC_6H_4Me)PPh_3$ (15)

A suspension of $Me_3SiC{\equiv}CC_6H_4C{\equiv}CC_6H_4Me$, **1** (64 mg, 0.22 mmol) and NaOH (89 mg, 2.22 mmol) in MeOH (15 ml) was allowed to stir for 30 min, to give a clear solution, which was treated with $AuCl(PPh_3)$ (100 mg, 0.22 mmol) and allowed to stir for a further 3h. The resulting cloudy solution was filtered, the precipitate washed with MeOH (3 ml), diethylether (3 ml) and pentane (3 ml) and dried *in vacuo* followed by recrystallisation from $CHCl_3$/MeOH to afford **15** as pale yellow crystals (93 mg, 68 %). IR (nujol): ν(C≡C) 2213 cm^{-1}. ^1H NMR ($CDCl_3$, 400 MHz): δ 2.36 (s, 3H, Me); 7.13-7.58 (m, 23H, Ar). $^{31}P\{H\}$ NMR ($CDCl_3$, 161.9 MHz): δ (s, 42.1, PPh_3). $^{13}C\{H\}$ NMR ($CDCl_3$, 125.7 MHz): δ 21.5 (s, Me); 89.1, 90.6 (2 x s, 2 x C≡C, C_7 and C_8); 135.2 (d, $^2J_{CP}$ = 142 Hz, Au-C_1≡C); 104.2 (d, $^3J_{CP}$ = 27 Hz, Au-C≡C_2), 121.9, 131.4, 131.7, 120.5, (4 x s, C_3-C_6, Ar); 124.9, 132.5, 129.4, 138.9 (4 x s, C_9-C_{12}, Ar), 129.7 (d, $^1J_{CP}$ = 56 Hz, C*i*), 134.6 (d, $^2J_{CP}$ = 14 Hz, C*o*), 129.4 (d, $^3J_{CP}$ = 12Hz, C*m*), 131.9 (d, $^4J_{CP}$ = 2 Hz, C*p*). (ES)+-MS(m/z): 1133, $[M+AuPPh_3]^+$; 721, $[Au(PPh_3)_2]^+$. Found: C 62.27, H 3.85 %; $C_{35}H_{26}PAu$ requires: C, 62.31; H 3.86 %.

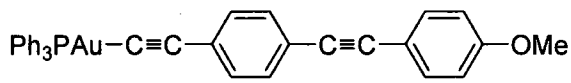

3.4.2.2. Preparation of Au($C{\equiv}CC_6H_4C{\equiv}CC_6H_4OMe)PPh_3$ (16)

A suspension of $Me_3SiC{\equiv}CC_6H_4C{\equiv}CC_6H_4OMe$, **2** (135 mg, 0.44 mmol) and NaOH (162 mg, 4.05 mmol) in MeOH (25 ml) was allowed to stir for 30 min, to give a clear solution, which was treated with $AuCl(PPh_3)$ (200 mg, 0.40 mmol) and allowed to stir for a further 3h. The resulting cloudy solution was filtered, the precipitate washed with MeOH (6 ml), diethylether (6 ml) and pentane (6 ml) and dried *in vacuo* to afford **16** (181 mg, 65 %). IR (nujol): ν(C≡C) 2202 cm^{-1}. ^1H NMR ($CDCl_3$, 400 MHz): δ 3.82 (s, 3H, OMe); 6.88 (pseudo-d, J_{HH} = 8.8 Hz, 2H, C_6H_4); 7.38-7.58 (m, 21H, Ar). $^{31}P\{H\}$ NMR ($CDCl_3$, 80.96 MHz): δ (s, 43.4, PPh_3). $^{13}C\{H\}$ NMR ($CDCl_3$, 125.7 MHz): δ 55.6 (s, OMe); 88.5, 90.8 (2 x s, 2 x C≡C, C_7 and C_8); 134.6

(d, $^2J_{CP}$ = 142 Hz, Au-C_1≡C); 104.3 (d, $^3J_{CP}$ = 27 Hz, Au-C≡C_2), 115.7, 131.3, 132.5, 124.7 (4 x s, C_3-C_6, Ar); 122.0, 133.3, 114.2, 159.8 (4 x s, C_9-C_{12}, Ar), 129.7 (d, $^1J_{CP}$ = 56 Hz, C*i*), 134.6 (d, $^2J_{CP}$ = 14 Hz, C*o*), 129.4 (d, $^3J_{CP}$ = 12Hz, C*m*), 131.9 (d, $^4J_{CP}$ = 2 Hz, C*p*). (ES)+-MS(m/z): 721, $[Au(PPh_3)_2]^+$; 713, $[M+Na]^+$. Found: C, 60.43; H, 3.73%; $C_{35}H_{26}NOPAu$ requires: C, 60.87; H, 3.77 %.

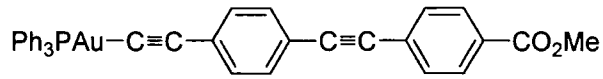

3.4.2.3. Preparation of Au(C≡CC_6H_4C≡C$C_6H_4CO_2$Me)PPh_3 (17)

A suspension of $Me_3SiC{\equiv}CC_6H_4C{\equiv}CC_6H_4CO_2Me$, **3** (300 mg, 0.89 mmol) and NaOH (324 mg, 8.10 mmol) in MeOH (50 ml) was allowed to stir for 30 min, to give a clear solution, which was treated with $AuCl(PPh_3)$ (400 mg, 0.81 mmol) and allowed to stir for a further 3h. The resulting cloudy solution was filtered, the precipitate washed with MeOH (6 ml), diethylether (6 ml) and pentane (6 ml) and dried *in vacuo* followed by recrystallisation from $CHCl_2$/hexane to afford **17** as pale yellow crystals (453 mg, 78 %). IR (nujol): ν(C≡C) 2209 cm^{-1}. ^1H NMR ($CDCl_3$, 400 MHz): δ 3.92 (s, 3H, OMe); 7.28-7.58 (m, 21H, Ar); 8.02 (pseudo-d, J_{HH} = 8.8 Hz, 2H, C_6H_4). $^{31}P\{H\}$ NMR ($CDCl_3$, 80.96 MHz): δ (s, 43.3, PPh_3). $^{13}C\{H\}$ NMR ($CDCl_3$, 125.7 MHz): δ 52.5 (s, OMe); 90.0, 92.9 (2 x s, 2 x C≡C, C_7 and C_8); 135.9 (d, $^2J_{CP}$ = 142 Hz, Au-C_1≡C); 104.2 (d, $^3J_{CP}$ = 27 Hz, Au-C≡C_2), 125.7, 131.6, 132.6, 128.3 (4 x s, C_3-C_6, Ar); 121.0, 129.7, 131.7, 129.8, (4 x s, C_9-C_{12}, Ar), 129.7 (d, $^1J_{CP}$ = 56 Hz, C*i*), 134.6 (d, $^2J_{CP}$ = 14 Hz, C*o*), 129.5 (d, $^3J_{CP}$ = 12 Hz, C*m*), 131.9 (d, $^4J_{CP}$ = 2 Hz, C*p*). 166.8(s, C=OMe). (ES+)-MS(m/z): 1635, $[M+(AuPPh_3)_2]^+$; 1177, $[M+AuPPh_3]^+$; 721, $[Au(PPh_3)_2]^+$. Found: C, 60.31; H, 3.66%; $C_{36}H_{26}O_2PAu$ requires: C, 60.17; H, 3.62.

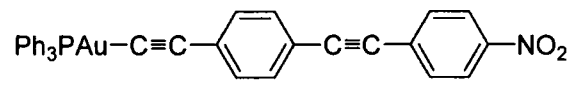

3.4.2.4. Preparation of Au(C≡CC_6H_4C≡C$C_6H_4NO_2$)PPh_3 (18)

A suspension of $Me_3SiC{\equiv}CC_6H_4C{\equiv}CC_6H_4NO_2$, **4** (260 mg, 0.89 mmol) and NaOH (324 mg, 8.10 mmol) in MeOH (50 ml) was allowed to stir for 30 min, to give a clear solution, which was treated with $AuCl(PPh_3)$ (400 mg, 0.81 mmol) and allowed to

stir for a further 3h. The resulting cloudy solution was filtered, the precipitate washed with MeOH (6 ml), diethylether (6 ml) and pentane (6 ml) and dried *in vacuo* followed by recrystallisation from $CHCl_3$/MeOH to afford **18** as orange crystals (393 mg, 69 %). IR (nujol): ν(C≡C) 2209 cm^{-1}. ^1H NMR ($CDCl_3$, 400 MHz): δ 7.43-7.58 (m, 19H, Ar); 7.65 (pseudo-d, J_{HH} = 8.8 Hz, 2H, C_6H_4) 8.22 (pseudo-d, J_{HH} = 8.8 Hz, 2H, C_6H_4). $^{31}P\{H\}$ NMR ($CDCl_3$, 80.96 MHz): δ (s, 43.3, PPh_3). $^{13}C\{H\}$ NMR ($CDCl_3$, 125.7 MHz): δ 88.9, 95.3 (2 x s, 2 x C≡C, C_7 and C_8); 135.1 (d, $^2J_{CP}$ = 142 Hz, Au-C_1≡C); 104.5 (d, $^3J_{CP}$ = 27 Hz, Au-C≡C_2), 130.6, 131.8, 132.4, 123.9 (4 x s, C_3-C_6, Ar); 120.3, 131.8, 123.9, 147.1 (4 x s, C_9-C_{12}, Ar), 129.6 (d, $^1J_{CP}$ = 56 Hz, C*i*), 134.6 (d, $^2J_{CP}$ = 14 Hz, C*o*), 129.5 (d, $^3J_{CP}$ = 12 Hz, C*m*), 131.9 (d, $^4J_{CP}$ = 2 Hz, C*p*). MALDI(+)-TOF(m/z): 1625, $[M+(AuPPh_3)_2]^+$; 1164, $[M+AuPPh_3]^+$; 721, $[Au(PPh_3)_2]^+$. Found: C, 57.46; H, 3.23; N, 1.80 %; $C_{34}H_{23}NO_2PAu$ requires: C, 57.87; H, 3.26; N 1.99 %.

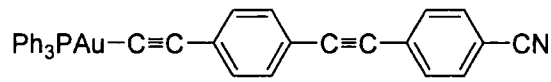

3.4.2.5. Preparation of Au(C≡CC_6H_4C≡CC_6H_4CN)PPh_3 (19)

A suspension of $Me_3SiC{\equiv}CC_6H_4C{\equiv}CC_6H_4CN$, **5** (270 mg, 0.89 mmol) and NaOH (324 mg, 8.10 mmol) in MeOH (50 ml) was allowed to stir for 30 min, to give a clear solution, which was treated with $AuCl(PPh_3)$ (400 mg, 0.81 mmol) and allowed to stir for a further 3h. The resulting cloudy solution was filtered, the precipitate washed with MeOH (6 ml), diethylether (6 ml) and pentane (6 ml) and dried *in vacuo* followed by recrystallisation from $CHCl_3$/MeOH to afford **19** as yellow crystals (393 mg, 71 %). IR (nujol): ν(C≡C) 2207 cm^{-1}. ^1H NMR ($CDCl_3$, 400 MHz): δ 7.41-7.63(m, 23H, Ar). $^{31}P\{H\}$ NMR ($CDCl_3$, 80.96 MHz): δ (s, 43.3, PPh_3). $^{13}C\{H\}$ NMR ($CDCl_3$, 100.6 MHz): δ 89.1, 94.3 (2 x s, 2 x C≡C, C_7 and C_8); 134.2 (d, $^2J_{CP}$ = 142 Hz, Au-C_1≡C); 104.0 (d, $^3J_{CP}$ = 27 Hz, Au-C≡C_2), 120.5, 131.7, 132.2, 118.8 (4 x s, C_3-C_6, Ar); 126.1, 132.6, 132.3, 111.5 (4 x s, C_9-C_{12}, Ar), 129.5 (d, $^1J_{CP}$ = 56 Hz, C*i*), 134.6 (d, $^2J_{CP}$ = 14 Hz, C*o*), 129.4 (d, $^3J_{CP}$ = 12 Hz, C*m*), 131.9 (d, $^4J_{CP}$ = 2 Hz, C*p*), 121.1 (s, C≡N). ES+-MS(m/z): 1144, $[M+AuPPh_3]^+$; 721, $[Au(PPh_3)_2]^+$. Found: C, 61.61; H, 3.33; N, 1.93 %; $C_{35}H_{23}NPAu$ requires: C, 61.31; H, 3.36; N 2.04 %

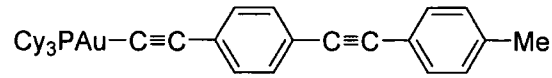

3.4.2.6. Preparation of Au(C≡CC$_6$H$_4$C≡CC$_6$H$_4$Me)PCy$_3$ (20)

A suspension of Me$_3$SiC≡CC$_6$H$_4$C≡CC$_6$H$_4$Me, **1** (124 mg, 0.43 mmol) and NaOH (160 mg, 3.90 mmol) in MeOH (20 ml) was allowed to stir for 30 min, to give a clear solution, which was treated with AuCl(PCy$_3$) (200 mg, 0.39 mmol) and allowed to stir for a further 3h. The resulting cloudy solution was filtered, the precipitate washed with MeOH (3 ml), diethylether (3 ml) and pentane (3 ml) and dried *in vacuo* followed by recrystallisation from CHCl$_3$/MeOH to afford **20** as yellow crystals (193 mg, 72 %). IR (nujol): ν(C≡C) 2210, 2111 cm^{-1}. ^{1}H NMR (CDCl$_3$, 400 MHz): δ 1.27-2.02 (m, 33H, Cy); 2.35 (s, 3H, Me); 7.14 (pseudo-d, J_{HH} = 8 Hz, 2H, C$_6$H$_4$); 7.38 (t, J_{HH} = 8.8 Hz, 4H, C$_6$H$_4$) 7.46 (pseudo-d, J_{HH} = 8 Hz, 2H, C$_6$H$_4$). ^{31}P{H} NMR (CDCl$_3$, 80.96 MHz): δ (s, 57.4, PCy$_3$). ^{13}C{H} NMR (CDCl$_3$, 100.6 MHz): δ 21.5 (s, Me); 33.4 (d, $^1J_{CP}$ = 28 Hz, C*i*); 27.2 (d, $^2J_{CP}$ = 12 Hz, C*o*); 25.9 (d, $^3J_{CP}$ = 2 Hz, C*m*); 30.7 (s, C*p*); 33.4(d, J_{CP} = 28 Hz, Cy); 89.0, 90.5 (2 x s, 4 x C≡C, C$_7$ and C$_8$); 139.6 (d, $^2J_{CP}$ = 131 Hz, AuC$_1$≡C); 103.6 (d, $^3J_{CP}$ = 25 Hz, AuC≡C$_2$), 121.3, 131.1, 131.4, 118.3 (4 x s, C$_3$-C$_6$, Ar); 124.1, 132.2, 129.1, 138.2 (4 x s, C$_9$-C$_{12}$, Ar). (ES)+-MS(m/z): 1169, [M+AuPCy$_3$]$^+$; 757, [Au(PCy$_3$)$_2$]$^+$. Found: C 60.21, H 6.32 %; C$_{35}$H$_{44}$PAu requires: C, 60.69; H 6.36 %.

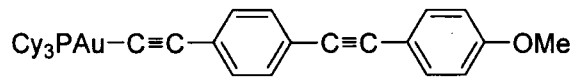

3.4.2.7. Preparation of Au(C≡CC$_6$H$_4$C≡CC$_6$H$_4$OMe)PCy$_3$ (21)

A suspension of Me$_3$SiC≡CC$_6$H$_4$C≡CC$_6$H$_4$OMe, **2** (131 mg, 0.43 mmol) and NaOH (160 mg, 3.90 mmol) in MeOH (20 ml) was allowed to stir for 30 min, to give a clear solution, which was treated with AuCl(PCy$_3$) (200 mg, 0.39 mmol) and allowed to stir for a further 3h. The resulting cloudy solution was filtered, the precipitate washed with MeOH (3 ml), diethylether (3 ml) and pentane (3 ml) and dried *in vacuo* to afford **21** (231 mg, 84 %). IR (nujol): ν(C≡C) 2213, 2107 cm^{-1}. ^{1}H NMR (CDCl$_3$, 400 MHz): δ 1.25-2.00 (m, 33H, Cy); 3.82 (s, 3H, OMe); 6.87 (pseudo-d, J_{HH} = 8.8 Hz, 2H, C$_6$H$_4$); 7.37 (pseudo-d, J_{HH} = 8.8 Hz, 2H, C$_6$H$_4$); 7.45 (pseudo-dd, J_{HH} = 8.6

Hz, 4H, C_6H_4). $^{31}P\{H\}$ NMR ($CDCl_3$, 80.96 MHz): δ (s, 57.4, PCy_3). $^{13}C\{H\}$ NMR ($CDCl_3$, 100.6 MHz): 55.5 (s, OMe); 33.5 (d, $^1J_{CP}$ = 28 Hz, C_i); 27.4 (d, $^2J_{CP}$ = 12 Hz, C*o*); 26.1 (s, C*m*); 31.0 (s, C*p*), 87.5, 94.2 (2 x s, 4 x C≡C, C_7 and C_8); 139.8 (d, $^2J_{CP}$ = 131 Hz, $AuC_1{\equiv}C$); 103.7 (d, $^3J_{CP}$ = 25 Hz, $AuC{\equiv}C_2$); 115.7, 131.2, 132.5, 121.7 (4 x s, C_3-C_6, Ar); 121.7, 133.2, 114.2, 159.8 (4 x s, C_9-C_{12}, Ar). (ES)+-MS(m/z): 1185, $[M+AuPCy_3]^+$; 757, $[Au(PCy_3)_2]^+$. Found: C 60.03, H 6.24 %; $C_{35}H_{44}PAu$ requires: C, 59.32; H, 6.21 %.

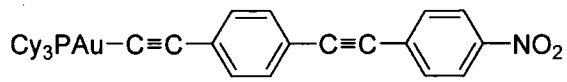

3.4.2.8. Preparation of $Au(C{\equiv}CC_6H_4C{\equiv}CC_6H_4NO_2)PCy_3$ (22)

A suspension of $Me_3SiC{\equiv}CC_6H_4C{\equiv}CC_6H_4NO_2$, **4** (137 mg, 0.43 mmol) and NaOH (160 mg, 3.90 mmol) in MeOH (20 ml) was allowed to stir for 30 min, to give a clear solution, which was treated with $AuCl(PCy_3)$ (150 mg, 0.29 mmol) and allowed to stir for a further 3h. The resulting cloudy solution was filtered, the precipitate washed with MeOH (3 ml), diethylether (3 ml) and pentane (3 ml) and dried *in vacuo* followed by recrystallisation from $CHCl_3$/MeOH to afford **22** as orange crystals (172 mg, 81 %). IR (nujol): ν(C≡C) 2209, 2110 cm^{-1}. ^1H NMR ($CDCl_3$, 400 MHz): δ 1.25-2.01(m, 33H, Cy); 7.42 (pseudo-d, J_{HH} = 8.8 Hz, 2H, C_6H_4); 7.50 (pseudo-d, J_{HH} = 8.4 Hz, 2H, C_6H_4); 7.64 (pseudo-d, J_{HH} = 8.8 Hz, 2H, C_6H_4); 8.22 (pseudo-d, J_{HH} = 8.4 Hz, 2H, C_6H_4). $^{31}P\{H\}$ NMR ($CDCl_3$, 80.96 MHz): δ (s, 57.4, PCy_3). $^{13}C\{H\}$ NMR ($CDCl_3$, 100.6 MHz): δ 32.4 (d, $^1J_{CP}$ = 28 Hz, C_i); 26.2 (d, $^2J_{CP}$ = 12 Hz, C*o*); 24.9 (d, $^3J_{CP}$ = 2 Hz, C*m*); 29.7 (s, C*p*); 87.5, 94.2 (2 x s, 4 x C≡C, C_7 and C_8); 140.2 (d, $^2J_{CP}$ = 131 Hz, $AuC_1{\equiv}C$); 103.5 (d, $^3J_{CP}$ = 25 Hz, $AuC{\equiv}C_2$), 129.4, 131.2, 131.4, 118.8 (4 x s, C_3-C_6, Ar); 125.5, 130.4, 122.6, 145.9 (4 x s, C_9-C_{12}, Ar). (ES)+-MS(m/z): 1200, $[M+AuPCy_3]^+$; 757, $[Au(PCy_3)_2]^+$. Found: C 56.13, H 5.67, N, 1.90 %; $C_{34}H_{41}PNO_2Au$ requires: C, 56.43, H 5.67, N, 1.94 %.

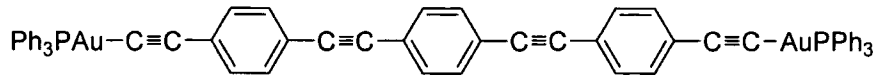

3.4.2.9. Preparation of $\{Au(PPh_3)\}_2(\mu\text{-}C{\equiv}CC_6H_4C{\equiv}CC_6H_4C{\equiv}CC_6H_4C{\equiv}C)$ (23)

A solution of $Me_3SiC{\equiv}CC_6H_4C{\equiv}CC_6H_4C{\equiv}C_6H_4C{\equiv}CSiMe_3$, **11** (52 mg, 0.11 mmol) and NaOH (89 mg, 2.22 mmol) in MeOH (15 ml) was allowed to stir for 40 min, after which time $AuCl(PPh_3)$ (100 mg, 0.20 mmol) was added. The reaction mixture was allowed to stir for a further 3h, after which time a yellow precipitate had formed, which was collected by filtration, washed with MeOH (3 ml), diethylether (3 ml) and pentane (3 ml) and dried to afford **23** as a yellow solid (102 mg, 74%). IR (nujol): ν(C≡C) 2103 cm^{-1}. ^1H NMR ($CDCl_3$, 400 MHz): δ 7.42-7.58 (m, 42H, Ar). $^{31}P\{H\}$ NMR ($CDCl_3$, 80.96 MHz): δ (s, 43.3, PPh_3). $^{13}C\{H\}$ NMR ($CDCl_3$, 100.6 MHz): δ 90.6, 91.7 (2 x s, 2 x C≡C, C_7 and C_8); 134.3 (d, $^2J_{CP}$ = 150 Hz, Au-C_1≡C); 104.2 (d, $^3J_{CP}$ = 25 Hz, Au-C≡C_2), 125.3, 131.5, 131.7, 123.3 (4 x s, C_3-C_6, Ar); 121.4, 132.6 (2 x s, C_9-C_{10}, Ar), 129.7 (d, $^1J_{CP}$ = 56 Hz, C*i*), 134.6 (d, $^2J_{CP}$ = 14 Hz, C*o*), 129.5 (d, $^3J_{CP}$ = 12Hz, C*m*), 131.9 (d, $^4J_{CP}$ = 2 Hz, C*p*). (ES)+-MS(m/z): 1701 $[M+AuPP_3]^+$; 1243, M^+; 721, $[Au(PPh_3)_2]^+$. Found: C, 59.39; H, 3.45 %; $C_{62}H_{42}P_2Au_2$ requires: C, 59.91; H, 3.40 %.

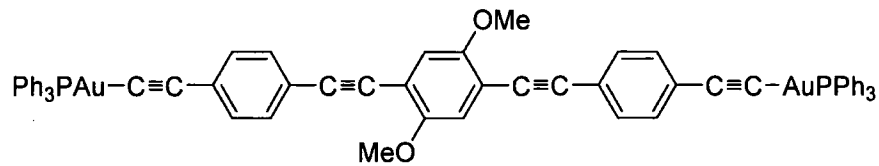

3.4.2.10. Preparation of $\{Au(PPh_3)\}_2(\mu\text{-}C{\equiv}CC_6H_4C{\equiv}CC_6H_2(OMe)_2C{\equiv}CC_6H_4C{\equiv}C)$ (24)

A suspension of $Me_3SiC{\equiv}CC_6H_4C{\equiv}CC_6(OMe)_2(H)_2C{\equiv}C_6H_4C{\equiv}CSiMe_3$, **13** (75 mg, 0.142 mmol) and NaOH (162 mg, 4.05 mmol) in MeOH (25 ml) and dichloromethane (20 ml) was allowed to stir for 30 min, to give a clear yellow solution, which was treated with $AuCl(PPh_3)$ (140 mg, 0.28 mmol) and allowed to stir for a further 14h. The yellow solution was concentrated until the formation of yellow precipitate which was collected by filtration. The filtrate was cooled in the ice-bath to give a second crop of precipitate. The combined precipitates were washed

with MeOH (6 ml), diethylether (6 ml) and pentane (6 ml) and dried *in vacuo* followed by recrystallisation from $CHCl_3$/MeOH to afford **24** as yellow crystals (152 mg, 82 %). IR (nujol): ν(C≡C) 2197, 2109 cm^{-1}. ^1H NMR ($CDCl_3$, 499.8 MHz): δ 3.88 (s, 6H, OMe); 7.00 (s, 2H, ($C_6H_2(OMe)_2$); 7.44-7.57 (m, 38H, Ar). $^{31}P\{H\}$ NMR ($CDCl_3$, 80.96 MHz): δ (s, 43.3, PPh_3). $^{13}C\{H\}$ NMR ($CDCl_3$, 125.67 MHz): δ 56.7 (s, OMe); 87.1, 95.5 (2 x s, 2 x C≡C, C_7 and C_8); 134.1 (d, $^2J_{CP}$ = 142 Hz, Au-C_1≡C); 104.3 (d, $^3J_{CP}$ = 27 Hz, Au-C≡C_2), 125.1, 131.6, 132.5, 121.6 (4 x s, C_3-C_6, Ar); 113.6, 115.8, 154.1 (3 x s, C_9-C_{11}, Ar), 129.7 (d, $^1J_{CP}$ = 56 Hz, C*i*), 134.6 (d, $^2J_{CP}$ = 14 Hz, C*o*), 129.5 (d, $^3J_{CP}$ = 12Hz, C*m*), 131.9 (d, $^4J_{CP}$ = 2 Hz, C*p*). MALDI(+)-TOF(m/z): 1761 $[M+AuPP_3]^+$; 1301, M^+; 721, $[Au(PPh_3)_2]^+$. Found: C, 58.20; H, 3.53 %; $C_{64}H_{46}O_2P_2Au_2$ requires: C, 58.95; H, 3.53 %

3.5. References

1. P. F. H. Schwab, M. D. Levin, J. Michl, *Chem. Rev.*, 1999, **99**, 1863.
2. P. F. H. Schwab, J. R. Smith, J. Michl, *Chem. Rev.*, 2005, **105**, 1197.
3. T. M. Fasina, J. C. Collings, D. P. Lydon, D. Albesa-Jové, A. S. Batsanov, J. A. K. Howard, P. Nguyen, M. Bruce, A. J. Scott, W. Clegg, S. W. Watt, C. Viney, T. B. Marder, *J. Mater. Chem.*, 2004, **14**, 2395.
4. I. Nishiyama, T. Yamamoto, J. Yamamoto, J. W. Goodby, H. Yokoyama, *J. Mater. Chem.*, 2003, **13**, 1868.
5. R. Giménez, M. Piñol, J. L. Serrano, *Chem. Mater.*, 2004, **16**, 1377.
6. L. Oriol, M. Piñol, J. L. Serrano, *Prog. Polym. Sci.*, 1997, **22**, 873.
7. C. Huang, W. Huang, J. Guo, C-. Yang, E-. Kang, *Polymer*, 2001, **42**, 3929.
8. I. K. Spiliopoulos , J. A. Mikroyannidis, *Macromolecules*, 1996, **29**, 5313.
9. J. S. Moore, *Acc. Chem. Res.*, 1997, **30**, 402.
10. M. D. Ward, *J. Chem. Edu.*, 2001, **78**, 321.
11. J. M. Tour, *Acc. Chem. Res.*, 2000, **33**, 791.
12. Z-. Fa, L-., Wang, H. Wang, X-. Cao, H-. Zhang, *Org. Lett.*, 2007, **9**, 4, 595.
13. X. Yin, H. Liu, J. Zhao, *J. Chem. Phys.*, 2006, **125**, 094711.
14. Y. Zhu, N. Gergel, N. Majumdar, L. R. Harriott, J. C. Bean, L. Pu, *Org. Lett.*, 2006, **8**, 3, 355.
15. L. Wang, W. Chen, C. Huang, Z-. Chen, A. T. S. Wee, *J. Phys. Chem. B*, 2006, **110**, 2, 674.
16. P. A. Lewis, C. E. Inman, F. Maya, J. M. Tour, J. E. Hutchison, P. S. Weiss, *J. Am. Chem. Soc.*, 2005, **127**, 17421.
17. F. Maya, A. K. Flatt, M. P. Stewart, D. E. Shen, J. M. Tour, *Chem. Mater.*, 2004, **16**, 2987.
18. L. Cai, Y. Yao, J. Yang, D. W. Price Jr., J. M. Tour, *Chem. Mater.*, 2002, **14**, 2905.
19. N. Robertson, C. A. McGowan, *Chem. Soc. Rev.*, 2003, **32**, 96.
20. S. M. Dirk, D. W. Price Jr., S. Chanteau, D. V. Kosynkin, J. M. Tour, *Tetrahedron*, 2001, **57**, 5109.
21. J. –S. Yang, T. M. Swager, *J. Am. Chem. Soc.*, 1998, **120**, 5321.

22. S. J. Toal, W. C. Trogler, *J. Mater. Chem.*, 2006, **16**, 2871.
23. D. T. McQuade, A. E. Pullen, T. M. Swager, *Chem. Rev.*, 2000, **100**, 2537.
24. T. Kawai, M-. Kim, T. Sasaki, M. Irie, *Optical Materials*, 2002, **21**, 275.
25. S. W. Cha, S-. Choi, K. Kim, J-. Jin, *J. Mater. Chem.*, 2003, **13**, 1900.
26. S. M. Al-Qaisi, K. J. Galat, M. Chai, D. G. Ray III, P. L. Rinaldi, C. A. Tessier, W. J. Youngs, *J. Am. Chem. Soc.*, 1998, **120**, 12149.
27. (a) W. J. Youngs, C. A. Tessier, J. D. Bradshaw, *Chem. Rev.*, 1999, **99**, 3153, (b) A. Y. –Y. Tam, K. M. –C. Wong, G. Wang, V. W. –W. Yam, *Chem. Comm.*, 2007, 2028.
28. G. Frapper, M. Kertesz, *Inorg. Chem.*, 1993, **32**, 732.
29. M. I. Bruce, P. J. Low, *Adv. Organomet. Chem.*, 2004, **50**, 179.
30. N. J. Long, C. K. Williams, *Angew. Chem. Int. Ed.*, 2003, **42**, 2586.
31. W. –Y. Wong, C. –L. Ho, *Coord. Chem. Rev.*, 2006, **250**, 2627.
32. R. R. Tykwinski, P. J. Stang, *Organometallics*, 1994, **13**, 3203.
33. V. W. -W. Yam, K. K. W. Lo, K. M. C. Wong, *J. Organomet. Chem.*, 1999, **578**, 3.
34. J. C. Garrison, M. J. Panzner, P. G. Custer, D. V. Reddy, P. L. Rinaldi, C. A. Tessier, W. J. Youngs, *Chem. Commun.*, 2006, 4644.
35. P. Nguyen, P. Gómez-Elipe, I. Manners, *Chem. Rev.*, 1999, **99**, 1515.
36. A. S. Abd-El-Aziz, *Macromol. Rapid Commun.*, 2002, **23**, 995.
37. Y. –B. Y. Geng, J. –P. Ma, R. –Q. Huang, *Organometallics*, 2006, **25**, 447.
38. Y. W. Chan, A. J. Lough, I. Manners, *Organometallics*, 2007, **26**, 1217.
39. A. Bartole-Scott, A. J. Lough, I. Manners, *Polyhedron*, 2006, **25**, 429.
40. A. Bartole-Scott, C. A. Jaska, I. Manners, *Pure Appl. Chem.*, 2005, **77**, 12, 1991.
41. X. Wang, M. A. Winnik, I. Manners, *Macromolecules*, 2005, **38**, 1928.
42. J. Vicente, M-. Chicote, M-. Abrisqueta, *J. Chem. Soc. Dalton Trans.*, 1995, 497.
43. M. I. Irwin, J. J. Vittal, R. J. Puddephatt, *Organometallics*, 1997, **16**, 3541.
44. W. J. Hunks, M-. MacDonald, M. C. Jennings, R. J. Pudephatt, *Organometallics*, 2000, **19**, 5063.

45. P. Li, B. Ahrens, P. R Raithby, S. J. Teat, M. S. Khan, *Dalton Trans.*, 2005, 874.

46. I. E. Pomestchenko, D. E. Polyansky, F. N. Castellano, *Inorg. Chem.*, 2005, **44**, 3412.

47. P. Alejos, S. Coco, P. Espinet, *New J. Chem.*, 1995, **19**, 799.

48. I. R. Whittall, A. M. McDonagh, M. G. Humphrey, M. Samoc, *Adv. Organomet. Chem.*, 1999, **43**, 349.

49. O. Schuster, H. Schmidbaur, *Inorg. Chim. Acta*, 2006, **359**, 3769.

50. M. I. Bruce, M. Jevric, B. W. Skelton, M. E. Smith, A. H. White, N. N. Zaitseva, *J. Organomet. Chem.*, 2006, **691**, 361.

51. G. Ferguson, J. F. Gallagher, A-. Kelleher, T. R. Spalding, F. T. Deeny, *J. Organomet. Chem.*, 2005, **690**, 2888.

52. C. E. Strasser, S. Cronje, H. Schmidbaur, H. G. Raubenheimer, *J. Organomet. Chem.*, 2006, **691**, 4788.

53. G. –F. Xu, Z. –Q. Liu, H. –B. Zhou, Y. Guo, D. –Z. Liao, *Aust. J. Chem.*, 2006, **59**, 640.

54. O. Schuster, R.-Y. Liau, A. Schier, H. Schmidbaur, *Inorg. Chim. Acta*, 2005, **358**, 1429.

55. O. Schuster, H. Schmidbaur, *Organometallics*, 2005, **24**, 2289.

56. L. Cao, M. C. Jennings, R. J. Puddephatt, *Inorg. Chem.*, 2007, **46**, 1361.

57. M. J. Irwin, G. Jia, N. C. Payne, R. J. Pudephatt, *Organometallics*, 1996, **15**, 51.

58. C. P. McArdle, M. J. Irwin, M. C. Jennings, R. J. Pudephatt, *Angew. Chem. Int. Ed.*, 1999, **38**, 22, 3376.

59. C. A. Wheaton, M. C. Jennings, R. J. Puddephatt, *J. Am. Chem. Soc.*, 2006, **128**, 15370.

60. D. J. Eisler, R. J. Puddephatt, *Inorg. Chem.*, 2006, **45**, 7295.

61. W. J. Hunks, M. C. Jennings, R. J. Puddephatt, *Inorg. Chim. Acta*, 2006, **359**, 3605.

62. W. Lu, N. Zhu, C.,-M. Che, *J. Am. Chem. Soc.*, 2003, **125**, 51, 16081.

63. H-. Chao, W. Lu, Y. Li, M. C. W. Chan, C.,-M. Che, K-. Cheung, N. Zhu. *J. Am. Chem. Soc.*, 2002, **124**, 49, 14696.

64. C.,-M. Che, H-. Chao, V. M. Miskowski, Y. Li, K-. Cheung, , *J. Am. Chem. Soc.*, 2001, 123, **51**, 4985.

65. H. –S. Tang, N. Zhu, V. W. –W Yam, *Organometallics*, 2007, **26,** 22.

66. W-. Wong, Ka-. Choi, G-. Liang, J-. Shi, P-. Lai, S-. Chan, *Organometallics*, 2001, **20**, 5446.

67. S. K. Hurst, N. T. Lucas, M. G. Humphrey, T. Isoshima, K. Wostyn, I. Asselberghs, K. Clays, A. Persoons, M. Samoc, *Inorg. Chim. Acta*, 2003, **350**, 62.

68. S. K. Hurst, M. P. Cifuentes, A. M. McDonagh, M. G. Humphrey, M. Samoc, B. Luther-Davies, I. Asselberghs, A. Persoons, *J. Organomet. Chem.*, 2002, **642**, 259.

69. S. K. Hurst, N. T. Lucas, M. G. Humphrey, I. Asselberghs, A. Persoons, *Aust. J. Chem.*, 2001, **54**, 447.

70. H. de la Riva, M. Nieuwhuyzen, C. M. Fierro, P. R. Raithby, L. Male, M. C. Lagunas, *Inorg. Chem.*, 2006, **45**, 1418.

71. P. Li, B. Ahrens, K. –H. Choi, M. S. Khan, P. R. Raithby, P. J. Wilson, W. –Y. Wong, *Crsyt. Eng. Comm.*, 2002, **4**, 69, 405.

72. A. S. Batsanov, J. C. Collings, R. M. Ward, A. E. Goeta, L. Porrès, A. Beeby, J. A. K. Howard, J. W. Steed, T. B. Marder, *CrystEng Comm.*, 2006, **8**, 622.

73. J. C. Collings, A. S. Batsanov, J. A. K. Howard, D. A. Dickie, J. A. C. Clyburne,H. A. Jenkins, T. B. Marder, *J. Fluorine. Chem.*, 2005, **126**, 515.

74. I. R. Whittall, M. G. Humphrey, S. Houbrechts, J. Maes, A. Persoons, S. Schmid, D. C. R. Hockless, *J. Organomet. Chem*, 1997, **544**, 277.

75. W. J. Hunks, M. C. Jennings, R. J. Puddephatt, *Inorg. Chem.*, 1999, **38**, 5930.

76. G. Jia, R. J. Puddephatt, J. D. Scott, J. J. Vittal, *Organometallics*, 1993, **12**, 3565.

77. T. Kaharu, R. Ishii, T. Adachi, T. Yoshida, S. Takahashi, *J. Mater. Chem.*, 1995, 5, **4**, 687.

78. M. I. Bruce, B. K. Nicholson, and O. bin Shawkataly, *Inorg. Synth.*, 1989, **26**, 325.

79. T. E. Müller, S. W-. Choi, D. M. P. Mingos, D. Murphy, D. J. Williams, V. W.- Yam, J. *Organomet. Chem.*, 1994, **484**, 209.

80. J. Vicente, M. T. Chicote, M. D. Abrisqueta, P.G. Jones, *Organometallics*, 1997, **16**, 5628.

81. R. Cross, M. F. Davidson, A. J. McLennan, *J. Organomet. Chem.*, 1984, **265**, C37.

82. M. I. Bruce, E. Horn, J. G. Matisons, M. R. Snow, *Aust. J. Chem.*, 1984, **37**, 1163.

83. I. R. Whittal, M. G. Humphrey, *Organometallics*, 1996, **15**, 5738.

84. I. R. Whittal, M. G. Humphrey, *Organometallics*, 1996, **15**, 5738.

85. M. C. Gimeno, P. G. Jones, A. Laguna, M. D. Villacampa, *Chem. Ber.*, 1996, **129**, 585.

86. J. D. E. T. Wilton-Ely, A. Schier, N. W. Mitzel, H. Schmidbaur, *Dalton Trans.*, 2001, 1058.

87. K. A. Porter, A. Schier, H. Schmidbaur, α,ω-Bis[(triphenylphosphine)gold(I)] hydrocarbons, Perspective in Organometallic Chemistry, The Royal Society of Chemistry, Cambridge, 2003.

88. A. B. Antonova, M. I. Bruce, P. A. Humphrey, M. Gaudio, B. K. Nicholson, N. Scoleri, B. W. Skelton, A. H. White, N. N. Zaitseva, *J. Organomet. Chem.*, 2006, **691**, 4694.

89. M. I. Bruce, B. C. Hall, B. W. Skelton, M. E. Smith, A. H. White, *Dalton Trans.*, 2002, 995.

90. J. Bailey, *J. Inorg. Nucl. Chem.*, 1973, **35**, 1921.

91. S-. Lai, T-. Lau, W. K. M. Fung, N. Zhu, C.,-M. Che, *Organometallics*, 2003, **22**, 315.

92. A. K. Al-sa'ady, C. A. McAuliffe, R. V. Parish, J. A. Sandbank, *Inorg. Synth.* 1985, **23**, 191.

93. R. A. J. O'Hair, G. N. Khairallah, *J. Cluster. Sci.*, 2004, **15**, 331.

94. M. I. Bruce, D. N. Duffy, *Aust. J. Chem.*, 1986, **39**, 1697.

95. K. Nunokawa, S. Onaka, T. Tatematsu, M. Ito, J. Sakai, *Inorg. Chim. Acta*, 2001, **322**, 56.

96. N. C. Habermehl, M.C. Jennings, C.P. McArdle, F. Mohr, R.J. Pudephatt, *Organometallics*, 2005, **24**, 5004.

97. *SHELXTL, version 6.14,* Bruker AXS, Madison, Wisconsin, USA, 2000.

Chapter 4. 'Synthesis, Structural and Electronic Properties of Half-Sandwich Ruthenium Oligo(Phenylene Ethynylene) Complexes'

4.1. Introduction

Metal complexes containing long unsaturated carbon chains, especially complexes featuring acetylide ligands in the form of the alkynyl, diynyl and polyynyl fragments have been the subjects of many decades of research work. [1-7] While much of the early work was naturally concerned with synthetic and structural issues, there is a considerable and growing body of contemporary interest concerning the electronic, optical, non-linear optical and magnetic properties of these compounds. [8-14] These properties are sensitive to the nature of both of the metal and the acetylide ligand. The comparisons of the properties of half-sandwich of the electron-rich metal centres such as ruthenium acetylides $Ru(C{\equiv}CR)(L_2)(\eta^5\text{-}C_5R_5)$, where L_2 usually represents supporting phosphine ligands, with analogous iron complexes have been carried out, [15,16] from which it can be concluded that iron centres gives rise to much greater metal character in the frontier orbitals, whilst the ruthenium analogues exhibit far greater Ru(d)-acetylide(π) mixing. [17] This greater delocalisation is also found to persist after one-electron oxidation of the ruthenium complexes, and has been used to rationalise the greater chemical reactivity of the 17-electron radical cations $[Ru(C{\equiv}C\text{-}1,4\text{-}C_6H_4X)(dppe)(\eta^5\text{-}C_5Me_5)]^+$ [18,19] when considered alongside the radical cations $[Fe(C{\equiv}CC_6H_4\text{-}X)(dppe)Cp^*]^+$ (X = CN, CF_3, Br, F, Me, ^{t}Bu, OMe, NH_2, NMe_2), which have been isolated as the $[PF_6]^-$ salts. [20] The use of RuL_2Cp' fragments to introduce more acetylide-ligand character to the semi-occupied orbital in $[M(C{\equiv}CR)L_2Cp']^+$ species has prompted consideration of systems containing acetylide ligands with extended π-conjugated structures. Therefore, in this thesis, complexes of the end-capped half-sandwich of $Ru(C{\equiv}CR)(L_2)(\eta^5\text{-}C_5R_5)$ featuring tolan ligands substituented with electron donating (Me and OMe) or withdrawing groups (CO_2Me, NO_2 and CN) have been prepared and fully characterised. These complexes have been prepared with a view to exploring the molecular design parameters that influence the relative contributions of metal and acetylide ligand in

the frontier molecular orbitals of the complexes $[Ru(C{\equiv}CR)(L_2)(\eta^5\text{-}C_5R_5)]^{n+}$ (n = 0, 1).

In addition to the long standing interest in the preparation of the mono metallic acetylide complexes of electron rich metal centres, there is also growing interest in the preparation of the bimetallic ruthenium complexes in which two metal centres are joined by ligands featuring two or more alkynyl groups. [21,22] These complexes display a degree of electronic interaction between metal-based redox groups located at the ligand termini [23] as well as attracting interest from the point of view of their redox-switchable the non-linear optical properties. [10,11,24]

In the most general terms, complexes featuring $[L_xM^{(n)}]$-B-$[M^{(n)}L_x]$ based structures, in which two redox-active metal fragments ML_x each in oxidation state n, are linked by some bridging ligand, are precursors to formally mixed-valence systems $[L_xM^{n}]$-B-$[M^{(n+1)}L_x]$. The classification and properties of mixed-valence complexes continues to provoke thought, with the original class I, II, III based description provided by Robin and Day [25] being gradually refined. [26,27] In light of this ongoing interest in the chemistry and description of mixed-valence systems, compounds $Cp'L_2Ru\text{-}C{\equiv}C\text{-}X\text{-}C{\equiv}C\text{-}RuL_2Cp'$ are worthy of further study, as the role of the bridging ligand itself in the oxidation process needs to be further elucidated.

In this chapter, the preparation, spectroscopic, molecular structural and redox properties of a number of mono- and di-ruthenium acetylide complexes derived from simple phenyl, tolan and oligo(phenylene ethynylene) moieties are described.

4.2. General Synthetic Procedures

Acetylide complexes $[Ru(C{\equiv}CR)(L_2)(\eta^5\text{-}C_5H_5)]$ are conveniently prepared by reactions of the analogous chloride complex $RuCl(L_2)(\eta^5\text{-}C_5H_5)$ with a terminal alkyne, and deprotonation of the resulting vinylidene (**Scheme 4.1**) [28,29]

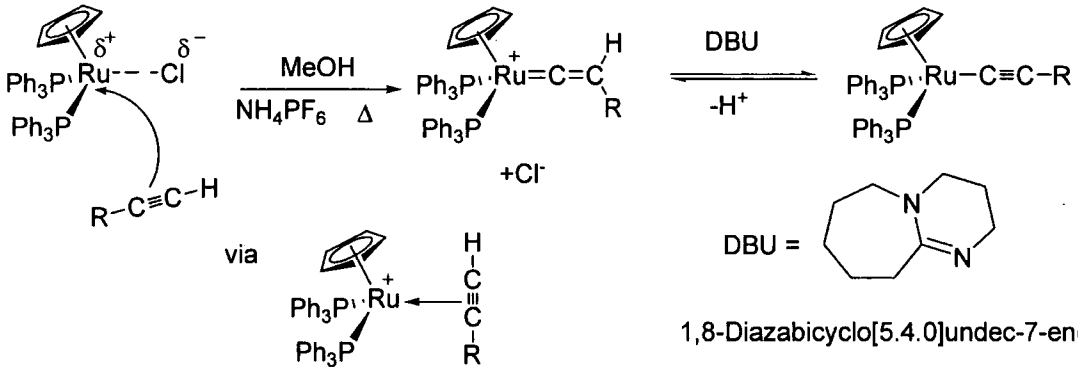

Scheme 4.1. The mechanism for the preparation of ruthenium acetylides from terminal alkynes. [28]

It is also possible to prepare such complexes from trimethylsilyl protected terminal alkynes when the metallation reaction is carried out in the presence of fluoride ions as shown in **Scheme 4.2**. [21] Together, these methods allow the convenient preparation of not only simple phenyl acetylide complexes such as $[Ru(C{\equiv}CPh)(PPh_3)_2Cp]$ [30] and $[Ru(C{\equiv}CPh)(dppe)Cp^*]$, [31] but also substituted derivatives far too numerous to list in detail here. [14, 18, 22, 29, 32-41]

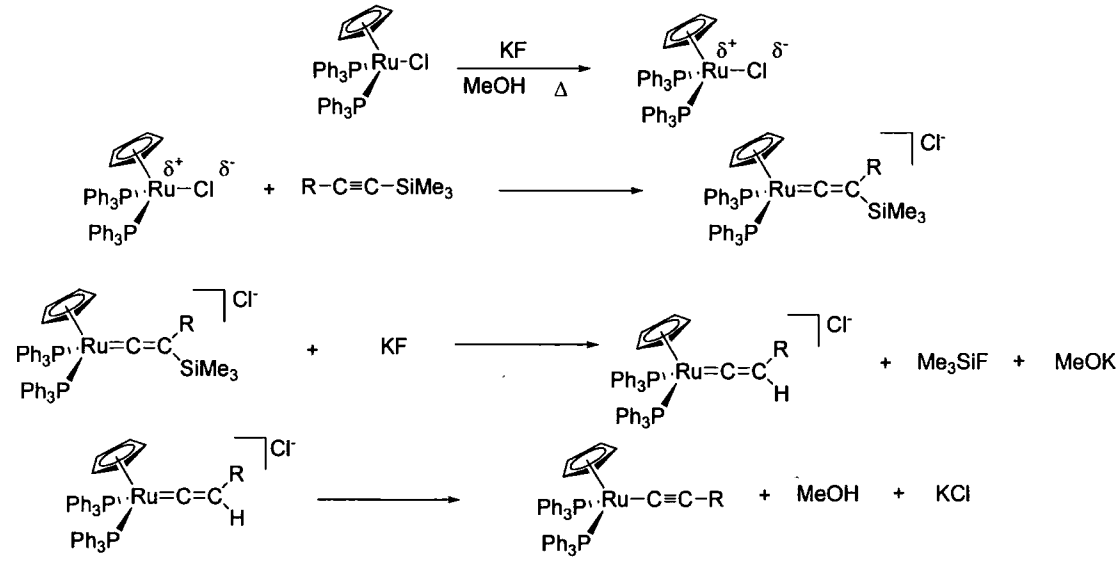

Scheme 4.2. A generalised mechanism for the preparation of ruthenium acetylide complexes from trimethylsilyl protected with the presence of fluoride ions. The precise mechanism for this reaction has not yet been fully elucidated. [21]

The methods described above have been used in the preparations of half-sandwich ruthenium acetylide bearing simple aromatic substituents and tolans derivatives with 49-80 % yields. In addition, the bis-ruthenium complexes featuring a bridging ligand based on diethynyl-1,4-bis(phenylethynyl)benzene has also been prepared by the same route in ca. 70 % yields. The complexes prepared in this study are shown in **Scheme 4.3** and **Scheme 4.4**, whilst a set of important model compounds **Ru1 – Ru4** prepared by Roberts and studied further in the course of the work described in this thesis are illustrated in **Scheme 4.5**.

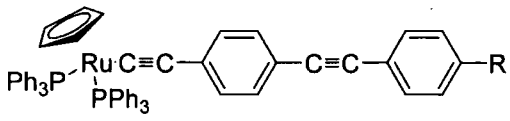

R = Me (**25**), OMe (**26**), CO_2Me (**27**), NO_2 (**28**)

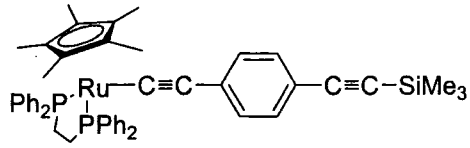

(**29**)

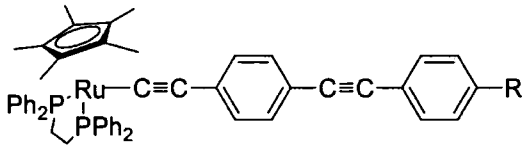

R = Me (**30**), OMe (**31**), CO_2Me (**32**), NO_2 (**33**)

Scheme 4.3. The complexes studied in this work featuring simple phenyl acetylide and bis(ethynylphenyl) derivatives as tolans.

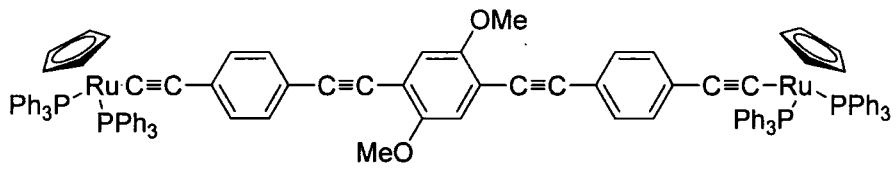

(**34**)

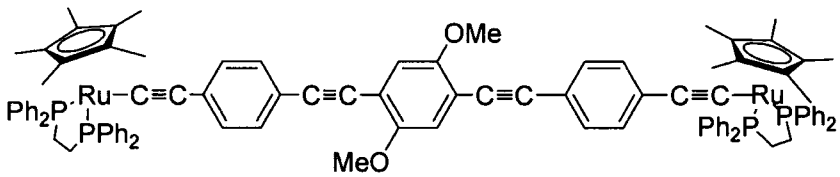

(**35**)

Scheme 4.4. The bis-ruthenium acetylides complexes studied in this work featuring an extended three-rings system as ligands.

4.3. Simple Ruthenium Acetylide Derivatives

The methods described above allow the preparation of half-sandwich ruthenium acetylide complexes bearing simple aromatic substituents (**Ru1 - Ru4**) (**Scheme 4.5**). These complexes were initially synthesised and characterised by Dr R. L. Roberts and have been previously reported. [19] It should be noted that only a small number of related half-sandwich ruthenium acetylide complexes of fused-ring aromatic alkynes, such as ethynyl naphthalimide and ethynyl pyrone, are known. [40,41] The iron analogue of **3b** has recently been reported. [24]

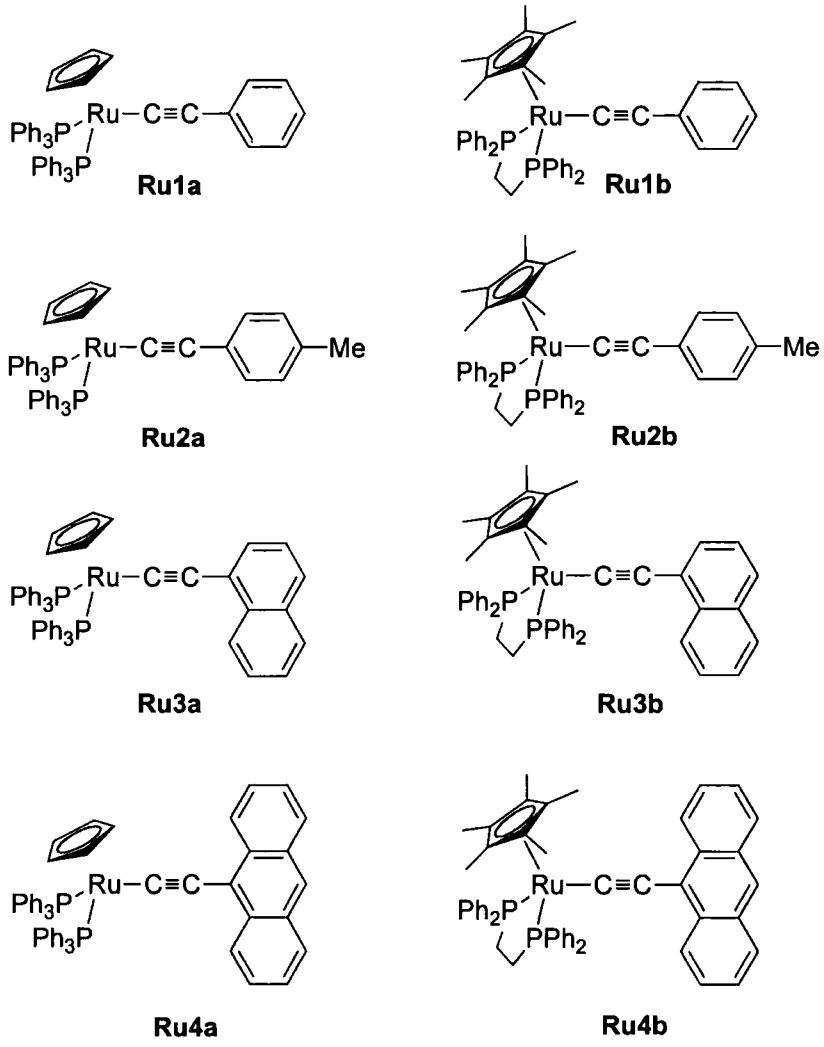

Scheme 4.5. Compounds numbering scheme of simple ruthenium acetylide derivatives.

4.3.1. Syntheses

The IR spectra of complexes **Ru1** - **Ru4** exhibit ν(C≡C) bands for the coordinated acetylide moiety at *ca.* 2070 (**Ru1**, **Ru2**), 2055 (**Ru3**) or 2040 (**Ru4**) cm^{-1}, somewhat lower in energy than the organic alkynes. [42-44] It is interesting to note that whilst these IR bands are remarkably insensitive to the other supporting ligands at the metal centre, the ν(C≡C) frequency is attenuated by the nature of the aromatic acetylide substituent. The carbons of the acetylide moieties were observed in the ^{13}C NMR spectra as triplets (120-130 ppm, C_α, J_{CP} = 25 Hz) and singlets (100 – 110 ppm, C_β).

The Cp and Cp* ligand resonances were found as singlets in the ^{1}H and ^{13}C NMR spectra in the usual regions (Cp / Cp*: δ_H = 4.3 – 4.6 / 1.5 – 1.6 ppm; δ_C = 85-86 / 10.0 – 10.5, 92 – 93 ppm) whilst the supporting phosphine ligands gave rise to singlets in the ^{31}P NMR spectra at ca. δ_P 50.5 – 51.5 (PPh_3) or δ_P 81 - 83 (dppe) ppm.

4.3.2. Electrochemical Characterisation

4.3.2.1. Cyclic Voltammetric Properties

Typically, half-sandwich ruthenium acetylides undergo single electron oxidation in common solvents to give the corresponding radical cations. Their redox potentials and chemical stability are sensitive to both the supporting ligands on the ruthenium centre and the acetylide substituent. [14,18,31,40] In this work the anodic behaviour of [Ru(C≡CC_6H_5)(L_2)Cp'] (**Ru1a**, **Ru1b**), [Ru(C≡CC_6H_4Me-4)(L_2)Cp'] (**Ru2a, Ru2b**), [Ru(C≡C$C_{10}H_7$)(L_2)Cp'] (**Ru3a**, **Ru3b**) and [Ru(C≡C$C_{14}H_9$)(L_2)Cp'] (**Ru4a**, **Ru4b**) has been examined, and provides an important reference point for the discussion of the properties of the tolan based systems which follow.

The cyclic voltammogram of [Ru(C≡CC_6H_5)(PPh_3)$_2$Cp] (**Ru1a**) in dichloromethane is characterised by an oxidation event at 0.59 V (vs. SCE using Fc* / Fc*$^+$ as an internal standard), the chemical reversibility of which improves at lower temperatures (i_{pa} : i_{pc} = 1.7 at -78°C, ν = 100 mV s^{-1}) and at faster scan rates (i_{pa} : i_{pc} = 1.1 at -78°C, ν = 800 mV s^{-1}). At higher potentials, a second anodic wave was also observed, which was completely irreversible (**Table 4.1**). The behaviour of the naphthyl (**Ru3a**) and anthryl (**Ru4a**) substituted derivatives were similar to those described for the phenyl acetylide complex, with the first oxidation event associated with **Ru4a** being rather more thermodynamically favourable (**Table 4.1**). The chemical reversibilities of the naphthyl (**Ru3a**) and anthryl (**Ru4a**) substituted derivatives were poor under all conditions examined.

Table 4.1. Electrochemical data for complexes **Ru1-Ru4**.

	$E_{(1/2)}$[a]	ΔE_p[b]	i_a/i_c	$E(2)_{pa}$[c]
Ru1a[d]	0.59	115	1.7	1.39
Ru2a[e]	0.53	120	1.0	1.40
Ru3a[d]	0.55	85	4.3	1.44
Ru4a[d]	0.42	130	7.7	1.60
Ru1b[e]	0.34	80	1.0	1.19
Ru2b[e]	0.31	90	1.1	1.17
Ru3b[e]	0.36	110	1.1	1.28
Ru4b[e]	0.29	90	1.0	1.07

[a] All E values in Volt vs SCE. Conditions: CH_2Cl_2 solvent, 10^{-1} M NBu_4PF_6 electrolyte, Pt working, counter and pseudo-reference electrodes, ν = 100 mV s^{-1}. The decamethyl ferrocene / decamethyl ferrocenium (Fc* / Fc^{*+}) couple was used as an internal reference for potential measurements (Fc* / Fc^{*+} taken as -0.02 V *vs* SCE in CH_2Cl_2 / 0.1M $[NBu_4]PF_6$ [45]

[b] $\Delta E_p = |E_{pa} - E_{pc}|$. [c] anodic peak potential of a totally irreversible process. [d] -78 °C. [e] 20 °C.

In contrast, the oxidation of the *p*-tolyl compound $[Ru(C{\equiv}CC_6H_4Me)(PPh_3)_2Cp]$ (**Ru2a**) proved to be fully chemically reversible at room temperature (i_{pa} : i_{pc} = 1), with the variation in ΔE_p being no greater than that of the internal decamethyl ferrocene / decamethyl ferrocenium reference couple and independent of scan rate. Plots of i_{pa} vs $\nu^{1/2}$ were also linear for this species. This improved chemical reversibility over the compounds **Ru1a**, **Ru3a** and **Ru4a** suggests the involvement of the ring hydrogen in the position *para* to the metal acetylide fragment in at least one of the chemical pathways responsible for the reactivity of the $[Ru(C{\equiv}CAr)(PPh_3)_2Cp]^+$ systems.

The same trend in electrode potentials as a function of the acetylide substituent observed in the $Ru(PPh_3)_2Cp$ series was also apparent in the Ru(dppe)Cp* complexes, with the anthracene derivative being oxidised at significantly lower potentials than the other members of the series **Ru1b – Ru4b**. The introduction of the bulky and more electron-donating Cp* and dppe ligands around the ruthenium acetylide framework rendered the first oxidation event of the [Ru(C≡CAr)(dppe)Cp*] series ca. 100 - 200 mV more favourable than the analogous $[Ru(C{\equiv}CAr)(PPh_3)_2Cp]$ complexes. These processes are almost completely electrochemically and chemically reversible at room temperature and moderate scan rates (ν = 100 mV s^{-1}), with linear plots of i_{pa} vs $\nu^{1/2}$ being obtained and ΔE_p values of comparable magnitude as the internal reference couple (**Table 4.1**).

4.3.2.2. IR Spectroelectrochemical Studies

The reactivity of $[Ru(C{\equiv}CPh)(PPh_3)_2Cp]^+$ (**Ru1a**) implied by the CV study was briefly investigated by spectroelectrochemical methods with considerable assistance from Dr M.A. Fox, University of Durham and Prof F. Hartl, University of Amsterdam. For this study, and those which are described in more detail below, an air-tight spectroelectrochemical cell fitted with CaF_2 windows to provide transparency across the spectroscopic region of interest was employed. [46] During oxidation of **Ru1a** the ν(C≡C) band at 2074 cm^{-1}, which is characteristic of the 18-electron ruthenium acetylide, shifted to give rise to a transient species with an IR bands at 1937 and 1529 cm^{-1}. By comparison with results obtained from **Ru2a**, and the Ru(dppe)Cp* series **Ru1b** - **Ru4b** these bands are attributed to $[Ru(C{\equiv}CPh)(PPh_3)_2Cp]^+$ ($[\mathbf{Ru1a}]^+$) (*vide infra*). However, $[\mathbf{Ru1a}]^+$ proved to be unstable under the conditions of the spectroelectrochemical experiment, and rapidly converted to a second species with IR bands at 2362, 2173 and 1650 cm^{-1}. Whilst the band at 2173 cm^{-1} is in the appropriate region for an organic alkyne, the nature of the decomposition species was not explored further. However, it should be noted that there is no evidence for the formation of the carbonyl cation $[Ru(CO)(PPh_3)_2Cp]^+$, which gives a characteristic ν(CO) band near 1970 cm^{-1}. [18]

The greater chemical stability of the [Ru(C≡CAr)(dppe)Cp*] series **Ru1b**, **Ru2b**, **Ru3b** and **Ru4b** under the conditions of the cyclic voltammetry experiments prompted more thorough spectroscopic characterisation of the products derived from their one-electron oxidation by spectroelectrochemical means. Oxidation of **Ru1b** was monitored in both the IR and UV-vis-NIR spectroscopic regions. The intensity of the characteristic ν(C≡C) band of **Ru1b** at 2072 cm^{-1} decreased, being replaced by a new band at 1929 cm^{-1} as the oxidation proceeded (**Table 4.2**). In addition, new bands in the aromatic ν(CC) region were also observed (**Table 4.2**). The original spectrum was fully recovered after back-reduction, which confirmed the assignment of the new bands to $[\mathbf{Ru1b}]^+$, and not to some product of an EC process (**Figure 4.1**). This spectroelectrochemical work confirms the tentative assignment of this ν(C≡C) band to $[\mathbf{Ru1b}]^+$ by Paul and co workers from chemically oxidized samples of **Ru1b**. [18] The shift of the ν(C≡C) band by 143 cm^{-1} upon oxidation indicates the appreciable depopulation of an orbital with C≡C bonding character. Similar results were obtained from **Ru2b**, **Ru3b** and **Ru4b**, with oxidation resulting in a shift of the ν(C≡C) band by 145, 137, and 116 cm^{-1}, respectively, and with the original spectra being fully recovered after the back-reduction in the spectroelectrochemical cell.

Table 4.2. IR data (cm^{-1}) for compounds **Ru1b** – **Ru4b** and the corresponding cations.[a]

	Neutral species		Oxidised (cation radical) complex	
	ν(CC)	ν(Aryl)	ν(CC)	ν(Aryl)
Ru1b	2072(s)	1593(w)	1929(s)	1614(m), 1551(s), 1540(s), 1520(m)
Ru2a	2077(s)	1606(vw)	1925(s)	1587(s)
Ru2b	2073(s)	1606(w)	1928(s)	1588(s)
Ru3b	2053(s)	1567(w)	1916(s)	1634(m), 1594(m), 1549(s)
Ru4b	2041(s)	1561(vw)	1925(s)	1610(w), 1597(w), 1588(w), 1534(w)

[a] data from CH_2Cl_2 solutions containing 0.1 M NBu_4BF_4 supporting electrolyte at ambient temperature.

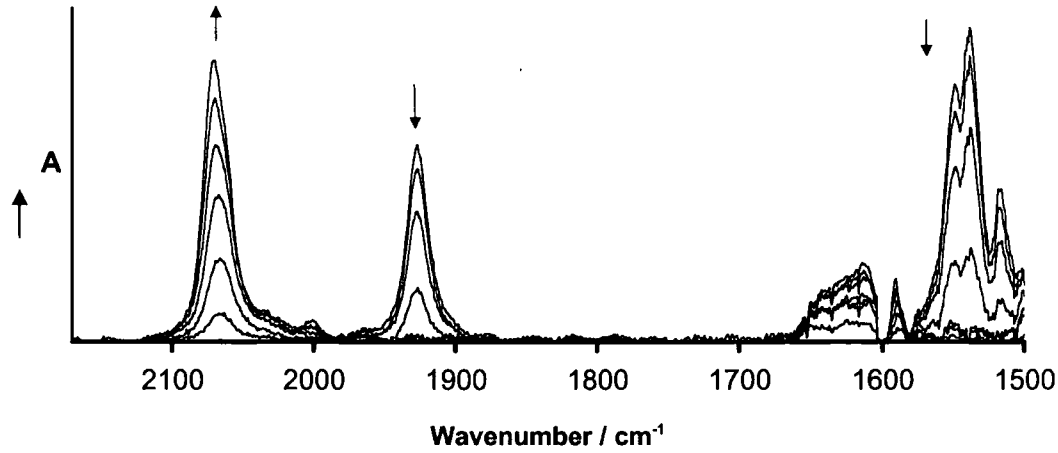

Figure 4.1. IR spectra on back reduction of $[\mathbf{Ru1b}]^+$ to **Ru1b** in a spectroelectrochemical cell (CH_2Cl_2 / 0.1M NBu_4PF_6, ambient temperature).

In the case of the remaining members of the $Ru(PPh_3)_2Cp$ series, we note here that the introduction of the *para*-methyl group in **Ru2a** instills significant chemical stability at room temperature to this simple complex. Upon oxidation of **Ru2a**, the $\nu(C\equiv C)$ band at 2077 cm^{-1} shifts by some 150 cm^{-1} to give a new band at 1925 cm^{-1}, which is assigned to the $\nu(C\equiv C)$ band in $[\mathbf{Ru2a}]^+$. The comparable shift in the spectra of **Ru2a** / $[\mathbf{Ru2a}]^+$ compared with **Ru2b** / $[\mathbf{Ru2b}]^+$ is revealing, and implies similar acetylide bonding character in the radical cations, regardless of the electron-donating ability of the supporting ligands.

4.3.2.3. Electronic Structure Calculations

A theoretical investigation was conducted by Dr M. A. Fox at the DFT level, initially on the model systems $[Ru(C\equiv CC_6H_5)(PH_3)_2Cp]$ (**Ru1-H**) and $[Ru(C\equiv CC_{14}H_9)(PH_3)_2Cp]$ (**Ru4-H**), which were used to mimic complexes **Ru1a** and **Ru1b**, and the corresponding radical cations $[\mathbf{Ru1\text{-}H}]^+$ and $[\mathbf{Ru4\text{-}H}]^+$. The discussion which follows refers to results obtained from calculations at the B3LYP/3-21G* level of theory with no symmetry constraints (**Table 4.3**), as results obtained from other functionals and basis sets are in good general agreement (*vide infra*). There is excellent agreement between the crystallographically determined structures of **Ru1a** [47,48] and **Ru1b** [18] with the DFT optimised geometries determined

here, and also with calculations previously reported. [18] Energies and composition of the frontier orbitals are summarised in **Table 4.4** for **1-H**, **[Ru1-H]$^+$**, **4-H** and **[Ru4-H]$^+$**, while **Scheme 4.6** illustrates the labelling scheme.

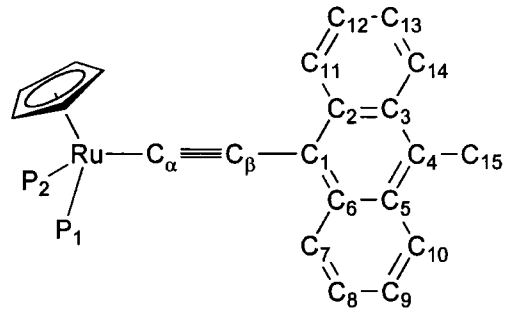

Scheme 4.6. The labelling scheme used in the discussion of the DFT results.

The Ru-C_α, Ru-P, $C_\alpha \equiv C_\beta$ and C_β-C(1) bond lengths in **Ru4-H** are comparable with those found in **Ru1-H**. At the level of theory employed, the aromatic substituents in the neutral systems **Ru1-H** and **Ru4-H** lie in the plane approximately parallel to the Cp ring, although there is a barrier to rotation of the aromatic group around the C(2)-C(3) bond of only ca 0.3 kcal mol^{-1} for **Ru1-H**. In contrast, the plane of the aromatic substituents in the mono-oxidised species **[Ru1-H]$^+$** and **[Ru4-H]$^+$** are found approximately bisecting the P-Ru-P angle. The barrier to rotation of the aromatic group around the C(2)-C(3) bond is considerable at ca 6 kcal mol^{-1} for **[Ru1-H]$^+$**.

Table 4.3. Optimised bond lengths (Å) for **Ru1-H**, **[Ru1-H]$^+$**, **Ru4-H** and **[Ru4-H]$^+$**.

	Ru1-H	**[Ru1-H]$^+$**	**Δ**	**Ru4-H**	**[Ru4-H]$^+$**	**Δ**
Ru-P(1, 2)	2.278	2.324	+0.046	2.280	2.309	+0.029
Ru-C_α	2.018	1.944	-0.074	2.013	1.954	-0.060
$C_\alpha \equiv C_\beta$	1.228	1.247	+0.019	1.230	1.246	+0.016
C_β-C(1)	1.426	1.400	-0.026	1.420	1.385	-0.035
C(1)-C(2, 6)	1.412	1.423	+0.011	1.425	1.448	+0.023
C(2, 6)-C(3, 5)	1.392	1.386	-0.006	1.444	1.437	-0.007
C(3, 5)-C(4)	1.398	1.403	+0.005	1.400	1.407	+0.007

Table 4.4. Energy, occupancy, and composition of frontier orbitals in the model complexes **Ru1-H**, $[\mathbf{Ru1\text{-}H}]^+$, **Ru4-H** and $[\mathbf{Ru4\text{-}H}]^+$ (B3LYP/3-21G*).

Ru1-H									
MO									
	LUMO+3	LUMO+2	LUMO+1	LUMO	HOMO	HOMO-1	HOMO-2	HOMO-3	HOMO-4
ε(eV)	+0.09	-0.03	-0.15	-0.78	-4.91	-5.09	-5.72	-6.46	-6.65
Occ	0	0	0	0	2	2	2	2	2
%Ru	27	53	62	50	30	46	46	0	58
%Cp	2	3	16	24	2	8	26	0	3
$\%PH_3$	12	11	13	27	1	4	14	0	8
$\%C_\alpha$	10	6	8	0	16	10	6	0	4
$\%C_\beta$	1	2	0	0	22	28	1	0	1
%Ph	48	26	0	0	29	4	6	100	27
Ru4-H									
MO									
	LUMO+3	LUMO+2	LUMO+1	LUMO	HOMO	HOMO-1	HOMO-2	HOMO-3	HOMO-4
ε(eV)	-0.08	-0.30	-0.92	-1.38	-4.53	-5.32	-5.68	-6.07	-6.25
Occ	0	0	0	0	2	2	2	2	2
%Ru	75	60	50	2	11	47	49	36	0
%Cp	3	17	24	0	1	8	12	17	0
$\%PH_3$	21	13	27	0	1	4	7	9	0
$\%C_\alpha$	1	9	0	6	11	9	1	8	0
$\%C_\beta$	0	0	0	0	8	25	8	13	0
%Anth	0	0	0	91	67	7	23	18	100

Table 4.4. Energy, occupancy, and composition of frontier orbitals in the model complexes **Ru1-H**, $[\mathbf{Ru1\text{-}H}]^+$, **Ru4-H** and $[\mathbf{Ru4\text{-}H}]^+$ (B3LYP/3-21G*) (cont.)

$[\mathbf{Ru1\text{-}H}]^+$																	
MO																	
	88β	88α	87β	87α	86β	86α	85β	85α	84β	84α	83β	83α	82β	82α	81β	81α	80β	80α
	β-[LUSO+4]	α-[LUSO+3]	β̄-[LUSO+3]	α-[LUSO+2]	β̄-[LUSO+2]	α-[LUSO+1]	β̄-[LUSO+1]	ᾱ-LUSO	β̄-LUSO	ᾱ-HOSO	β̄-HOSO	α-[HOSO-1]	β̄-[HOSO-1]	α-[HOSO-2]	β̄-[HOSO-2]	α-[HOSO-3]	B̄-[HOSO-3]	α-[HOSO-4]
ε (eV)	-3.28	-3.29	-3.67	-4.03	-4.15	-4.26	-4.82	-4.95	-7.27	-9.00	-9.51	-9.67	-9.85	-9.95	-9.92	-10.19	-10.08	-10.41
occ	0	0	0	0	0	0	0	0	0	1	1	1	1	1	1	1	1	1
%Ru	64	64	7	5	55	53	48	47	33	23	51	50	41	39	29	0	0	20
%Cp	2	2	3	1	20	20	26	27	6	7	3	4	29	37	17	0	0	29
$\%PH_3$	33	34	2	2	16	15	26	26	4	4	2	2	10	11	6	0	0	9
$\%C_\alpha$	0	0	16	19	9	10	0	0	10	11	11	11	8	7	11	0	0	6
$\%C_\beta$	0	0	3	7	1	1	0	0	21	16	30	29	3	5	0	0	0	0
%Ph	0	0	70	68	0	0	0	0	26	38	4	3	9	1	37	100	100	35
$[\mathbf{4\text{-}H}]^+$ MO																		
	114β	114α	113β	113α	112β	112α	111β	111α	110β	110α	109β	109α	108β	108α	107β	107α	106β	106α
	β-[LUSO+4]	ᾱ-[LUSO+3]	β̄-[LUSO+3]	ᾱ-[LUSO+2]	β̄-[LUSO+2]	ᾱ-[LUSO+1]	β̄-[LUSO+1]	ᾱ-LUSO	β̄-LUSO	ᾱ-HOSO	β̄-HOSO	ᾱ-[HOSO-1]	β̄-[HOSO-1]	ᾱ-[HOSO-2]	β̄-[HOSO-2]	α-[HOSO-3]	β̄-[HOSO-3]	ᾱ-[HOSO-4]
ε(eV)	-3.13	-3.27	-3.63	-3.71	-4.28	-4.35	-4.73	-5.12	-6.78	-8.08	-8.75	-9.11	-9.03	-9.22	-9.37	-9.43	-9.67	-9.74
occ	0	0	0	0	0	0	0	0	0	1	1	1	1	1	1	1	1	1
%Ru	0	0	56	55	49	48	4	3	17	12	30	55	56	32	43	40	0	0
%Cp	0	0	20	20	26	26	1	1	3	3	8	8	6	14	29	29	0	0
$\%PH_3$	0	0	15	15	25	26	1	1	2	2	4	4	4	6	11	10	0	0
$\%C_\alpha$	0	0	9	9	0	0	8	9	10	8	0	7	7	1	7	8	0	0
$\%C_\beta$	0	0	1	1	0	0	0	0	10	8	11	22	22	11	8	10	0	0
%Anth	100	100	0	0	0	0	87	87	58	67	46	5	4	37	2	2	100	100

The electronic structure of **Ru1-H** has been described before, [18] and only pertinent details will be summarised here. The HOMO and [HOMO-1] are approximately orthogonal and derived from mixing of the metal d and acetylide π-systems, with the HOMO also containing appreciable contributions from the phenyl π-system (**Table 4.4, Figure 4.2**).

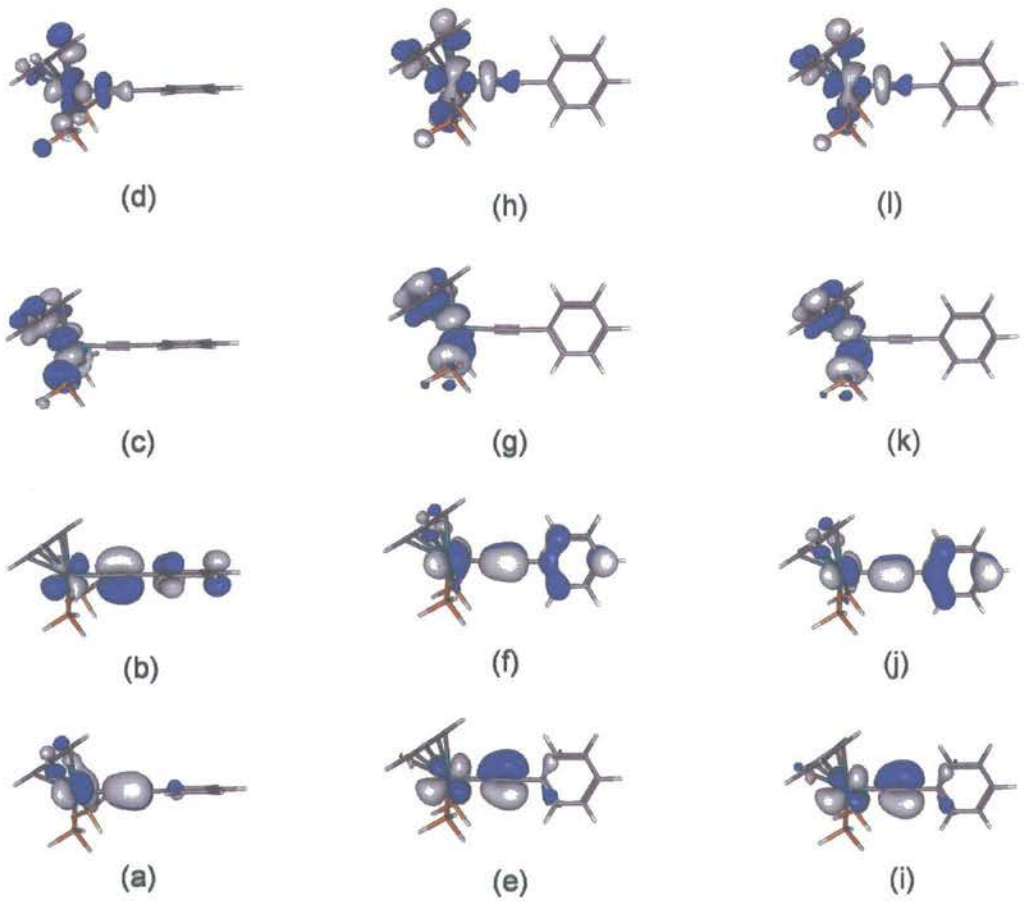

Figure 4.2. The (a) [HOMO-1] (b) HOMO (c) LUMO (d) [LUMO+1] of **Ru1-H** together with (e) β-HOSO (f) β-LUSO (g) β-[LUSO+1] (h) β-[LUSO+2] of [**Ru1-H**]$^+$ and (i) α-[HOSO-1] (j) α-HOSO (k) α-LUSO (l) α -[LUSO+1] of [**Ru1-H**]$^+$ plotted with contour values ±0.04 $(e/bohr^3)^{1/2}$.

Occupied orbitals comprised largely of metal and Cp, metal phosphine and phenyl π-character are found lower in the occupied orbital manifest. The LUMO and [LUMO+1] of **Ru1-H** are largely Ru-Cp anti-bonding in character, with the phenyl

π* system some 1.35 eV higher in energy than the LUMO, and comprising the [LUMO+3] (**Figure 4.3**).

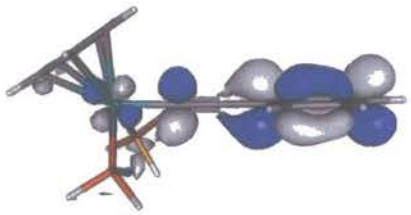

Figure 4.3. The [LUMO+3] of **Ru1-H** plotted with contour values ±0.04 $(e/bohr^3)^{1/2}$.

The frontier orbitals of **Ru4-H** feature important contributions from the anthryl substituent (**Table 4.4**, **Figure 4.4**). Thus, while the HOMO and [HOMO-1] are approximately orthogonal π-type orbitals, the HOMO features a large (67%) contribution from the atoms of the anthryl substitutent and is somewhat removed from the other occupied orbitals. The LUMO is essentially the anthryl π* orbital, which is sufficiently low in energy to lie below the unoccupied Ru-Cp based orbitals that comprise the [LUMO+1] and [LUMO+2].

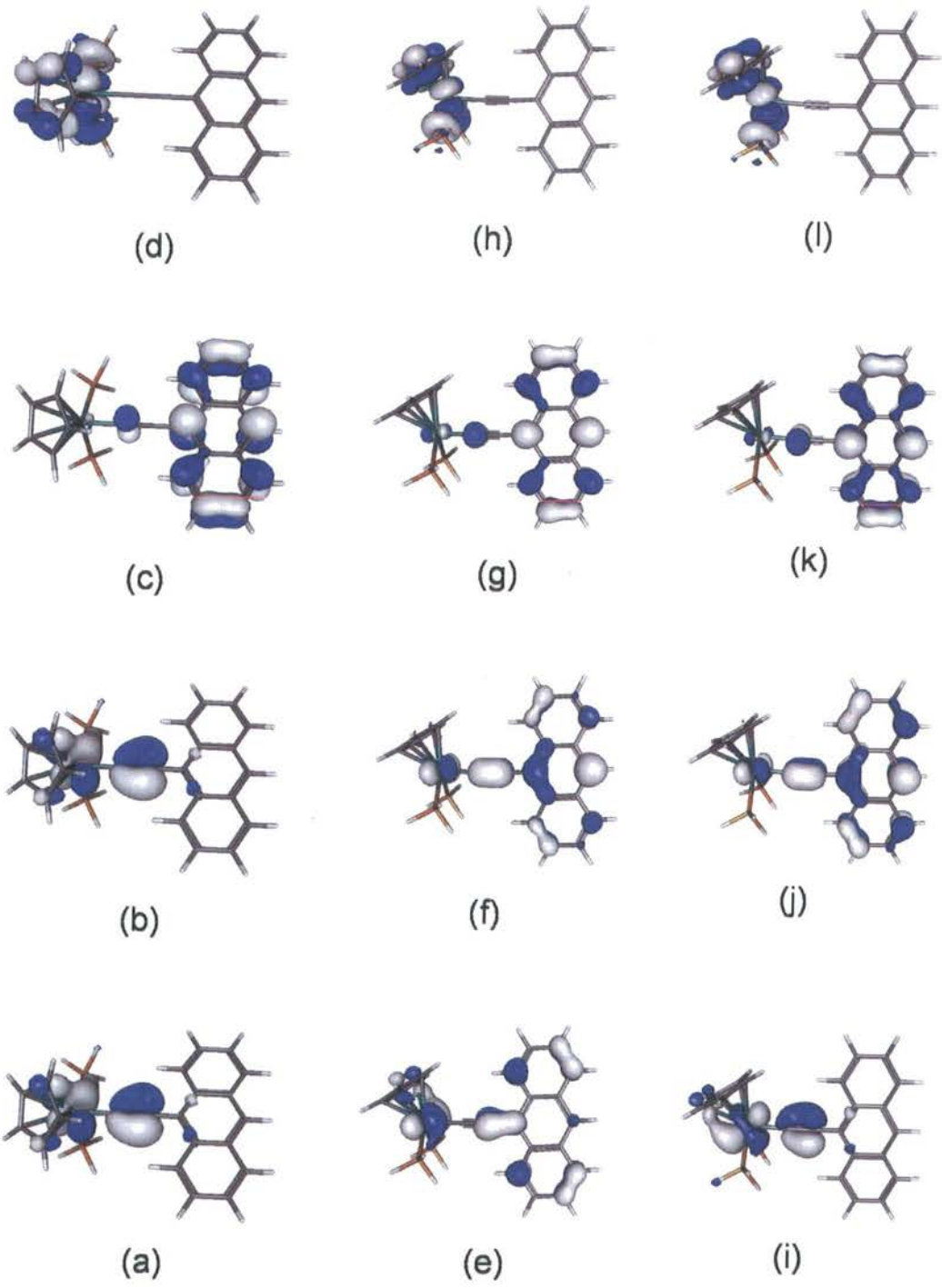

Figure 4.4. The (a) [HOMO-1] (b) HOMO (c) LUMO (d) [LUMO+1] of **Ru4-H** together with (e) β-HOSO (f) β-LUSO (g) β-[LUSO+1] (h) β-[LUSO+2] of [**Ru4-H**]$^+$ and (i) α-[HOSO-1] (j) α-HOSO (k) α-LUSO (l) α-[LUSO+1] of [**Ru4-H**]$^+$ plotted with contour values ± 0.04 $(e/bohr^3)^{1/2}$.

The model radical cation $[\mathbf{Ru1\text{-}H}]^+$ features an Ru-C bond somewhat shorter than **Ru1-H** (**Table 4.3**). The metal-phosphine bond lengths are sensitive to the net electron density available for π-back bonding and as such are elongated in $[\mathbf{Ru1\text{-}H}]^+$ relative to **Ru1-H**. The elongation of the acetylide C≡C bond in $[\mathbf{Ru1\text{-}H}]^+$ when compared with the neutral model system **Ru1-H** is consistent with a decrease in the net acetylide π-bonding character. This is also supported by the calculated ν(C≡C) frequencies of **Ru1-H** (2058 cm^{-1}) and $[\mathbf{Ru1\text{-}H}]^+$ (1938 cm^{-1}). It is known that DFT calculations over estimate the acetylide ν(C≡C) and acetylide ring substituent ν(C=C) frequencies, and a scaling factor of 0.95 has been employed in the data presented in this work. [49,50] The contraction of the C(2)-C(3), C(4)-C(5) and C(7)-C(8) bonds and elongation of the remaining C-C bonds in the phenyl substituent is consistent with the evolution of a degree of cumulenic character in the radical cation. The frontier orbitals of the one-electron oxidation product $[\mathbf{Ru1\text{-}H}]^+$ are similar to those of **Ru1-H**, with the α-HOSO and β-LUSO displaying appreciable Ru(d) and acetylide (π) character and the next highest unoccupied orbitals being largely centred on the $Ru(PH_3)_2Cp$ fragment (**Table 4.4**, **Figure 4.2**).

The optimised geometry of $[\mathbf{Ru4\text{-}H}]^+$ displays elongated Ru-P bond lengths and evidence of an increased cumulenic character in the ethynyl anthryl portion of the molecule when compared with the bond distances in **Ru4-H** (**Table 4.3**). While the trends in the structures and calculated ν(C≡C) frequencies of **[Ru4-H]** [ν(C≡C) = 2038 cm^{-1}] and $[\mathbf{Ru4\text{-}H}]^+$ [ν(C≡C) = 1952 cm^{-1}] follow those observed for **Ru1-H** and $[\mathbf{Ru1\text{-}H}]^+$, it is interesting to compare the pairs of structures **Ru1-H** / $[\mathbf{Ru1\text{-}H}]^+$ and **Ru4-H** / $[\mathbf{Ru4\text{-}H}]^+$ and note the relative differences in the individual bond lengths (**Table 4.3**). Although the magnitude of individual deviations are small (< 0.05 Å) there is a clear trend indicating that the anthryl fragment in $[\mathbf{Ru4\text{-}H}]^+$ experiences a greater relative structural distortion than the phenyl ring in $[\mathbf{Ru1\text{-}H}]^+$. Conversely, the metal ethynyl fragment is more significantly affected in $[\mathbf{Ru1\text{-}H}]^+$ than in $[\mathbf{Ru4\text{-}H}]^+$, which is neatly reflected in the differences between the ν(C≡C) frequencies of the 18- and 17-electron compounds in both the experimental (**Ru1b**/$[\mathbf{Ru1b}]^+$ Δν(C≡C) = 143 cm^{-1}; **Ru4b**/$[\mathbf{Ru4b}]^+$ Δν(C≡C) = 116 cm^{-1}) and

model systems **[Ru1-H/[Ru1-H]**$^+$ $\Delta\nu$(C≡C) = 120 cm^{-1}; **Ru4-H/[Ru4-H]**$^+$ $\Delta\nu$(C≡C) = 86 cm^{-1}.

The frontier orbitals of **[Ru4-H]**$^+$ are similar to those of Ru**4-H**. The α-HOSO and β-LUSO of **[Ru4-H]**$^+$ offer an appreciable anthryl character (α: 67%, 87% respectively). It may therefore be more appropriate to consider species such as **[Ru4b]**$^+$ as metal stabilised anthryl radicals. The optimised geometries of **Ru4-H** and **[Ru4-H]**$^+$ supported this point of view, as do calculated spin densities, with the atoms comprising the anthryl ring system contributing some 60% of the fractional electronic charge in **[Ru4-H]**$^+$ compared with the phenyl ring system contribution of some 25% in **[1-H]**$^+$ (**Table 4.5**).

Table 4.5. Spin densities computed for the model radical cations, **[Ru1-H]**$^+$ and **[Ru4-H]**$^+$.

	[Ru1-H]$^+$	**[Ru4-H]**$^+$	**Δ**
Ru	0.413	0.220	0.193
P	0.000	0.000	0.000
Cp	0.041	0.021	-0.079
C_α	0.043	0.079	-0.036
C_β	0.269	0.114	0.155
$C_6H_5/C_{14}H_9$	0.246	0.598	-0.352

To confirm the results obtained in the electronic structure calculations. The neutral and oxidised states of the model complexes **Ru1-H** and **Ru4-H** at the DFT level have been further discussed in the UV-Vis Spectroelectrochemical Studies. Due to their stability and insensitivity to the atmospheric conditions as shown in the cyclic voltammetric studies, complexes **Ru1b**, **Ru2b**, **Ru3b** and **Ru4b** were chosen to be studied.

4.3.2.4. UV-vis Spectroelectrochemical Studies

Comparison of the electronic absorption spectra of **Ru1b**, **Ru2b**, **Ru3b** and **Ru4b** reveals a strong, and in the case of **Ru4b**, relatively narrow, absorption band between 33000 – 20000 cm^{-1}, which becomes progressively red-shifted as a function of the size of the aromatic substituent and accounts for the colour of these complexes (**Table 4.6**, **Figures 4.5** and **Figure 4.7**). The analogous bands in $Ru(C{\equiv}CC_6H_4X\text{-}4)(dppe)Cp^*$ (X = H, CN, F, OMe, NH_2) have been assigned to MLCT processes by analogy with assignments made for iron. [18] Although electronic structure calculations on $Ru(C{\equiv}CPh)(PH_3)_2Cp$ model systems have been performed on previous occasions, [17,18] only limited use has been made of TD DFT based studies to provide further insight into the nature of the electronic transitions responsible for the characteristic absorption spectra of related systems. [32, 51,52]

Table 4.6. The principal UV-vis absorption bands [ν_{max} / cm^{-1} (ε_{max} / M^{-1} cm^{-1}] observed from CH_2Cl_2 / 10^{-1} M NBu_4PF_6 solutions of $[\mathbf{Ru1b}]^{n+}$, $[\mathbf{Ru2a}]^{n+}$, $[\mathbf{Ru2b}]^{n+}$, $[\mathbf{Ru3b}]^{n+}$ and $[\mathbf{Ru4b}]^{n+}$ (n = 0, 1).

	n	
	0	+1
Ru1b	29500 (9500)	22600 (3900), 21100 (4300), 11200 (5100), 8100 (600)
Ru2a	30700 (7000)	30300 (4500), 19100 (1200), 14300 (1500), 11900 (900), 7500 (100)
Ru2b	33400 (7000)	29800 (4500), 26200 (2700), 16900 (800), 13900 (1800), 8600 (200)
Ru3b	26200 (7000)	20200 (3100), 18600 (2500), 11000 (3900), 7600 (700)
Ru4b	20600 (11600)	27200 (8000), 17900 (14000), 15200 (5900), 10100 (1900), 7800 (600)

On the basis of TD DFT calculations the characteristic absorption band observed in **Ru1b,** and by analogy **Ru2b** and **Ru3b,** can be likened, in the most general terms, to a (d/π) – phenyl π* charge transfer band (HOMO→[LUMO+3]) rather than a purely MLCT band. In the case of **Ru4b** there is a critical distinction and the band at 20600 is better described as an anthryl-centred π-π* transition (HOMO→LUMO). This distinction in assignment is consistent with the different band shapes observed for **Ru1b-Ru3b** on one hand, and **Ru4b** on the other (**Figures 4.5** and **Figure 4.7**).

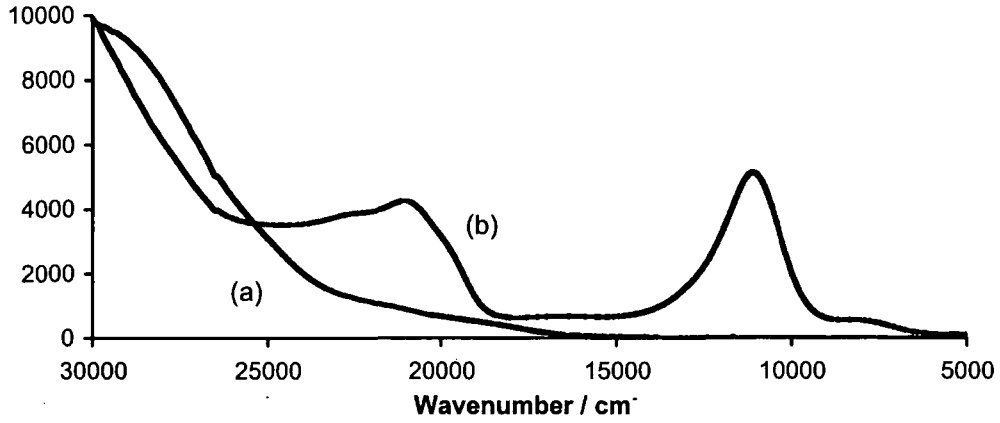

Figure 4.5. The UV-Vis-NIR spectra of (a) **Ru1b** and (b) $[\mathbf{Ru1b}]^+$ (CH_2Cl_2 / 0.1M NBu_4PF_6).

The UV-vis-NIR spectrum of $[\mathbf{Ru1b}]^+$, obtained spectroelectrochemically from **Ru1b**, exhibits strong absorption envelopes centred near 21100 and 11200 cm^{-1}, and a weaker series of bands between 8000 – 4000 nm (**Figure 4.5**). The spectrum of **Ru1b** was fully recovered after back-reduction, which strongly supports the assignment of these characteristic absorption bands to the 17-e species $[\mathbf{Ru1b}]^+$. TD DFT calculations using the $[\mathbf{Ru1\text{-}H}]^+$ model indicate that the highest energy transition can be attributed to charge transfer from the ligand fragment (including the acetylide π-system) to the metal fragment being comprised of electronic transitions from the α-HOSO (highest occupied spin orbital) to the α-[LUSO]. The band centred near 11200 cm^{-1} can be approximated in terms of transitions between occupied orbitals with large amounts of Ru/Cp character (β-[HOSO-1], β-[HOSO-2], (**Table 4.4**, **Figure 4.6**) to the β-LUSO. The presence of low energy (NIR) bands in 17-e cation radicals of the general type $[Ru(C{\equiv}CAr)(dppe)Cp^*]^+$ has been noted by Paul

et al., and attributed to forbidden ligand-field type transitions centred on the Ru(III) centre. [18] The TD DFT calculations carried out in the present study suggest that the lowest energy transition should be attributed to the β-HOSO to β-LUSO transition, with the low intensity of the observed band reproduced by the low calculated oscillator strength and easily explained by the relative, approximately orthogonal orientation of these two orbitals. Other NIR bands of slightly greater intensity and higher energy are attributable to Ru/Cp based β-[HOSO-1] to the β-LUSO.

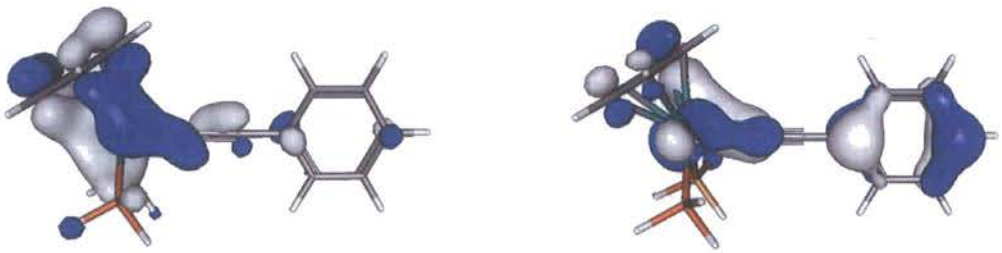

(a) (b)

Figure 4.6. The (a) β-[HOSO-1] and (b) β-[HOSO-2] of [**Ru1-H**]$^+$ plotted with contour values ±0.04 $(e/bohr^3)^{1/2}$.

The tolyl-substituted derivatives [**Ru2a**]$^+$ and [**Ru2b**]$^+$, and the naphthyl derivative [**Ru3b**]$^+$ offer similar electronic spectra to each other, and that of [**Ru1b**]$^+$. Low energy (NIR) bands are observed, together with a more intense band envelope in the visible region, the precise shape and composition of which vary only slightly with the nature of the Cp' and phosphine co-ligands. In the case of [**Ru3b**]$^+$ the characteristic absorption bands are somewhat red-shifted compared with the analogous features in [**Ru1b**]$^+$, [**Ru2a**]$^+$ and [**Ru2b**]$^+$. Given the similar profiles of

these compounds, and the similar chemical behaviour of each member of the series, it is possible to be reasonably confident in attributing these spectroscopic absorption bands to transitions similar to those described for $[\mathbf{Ru1\text{-}H}]^+$.

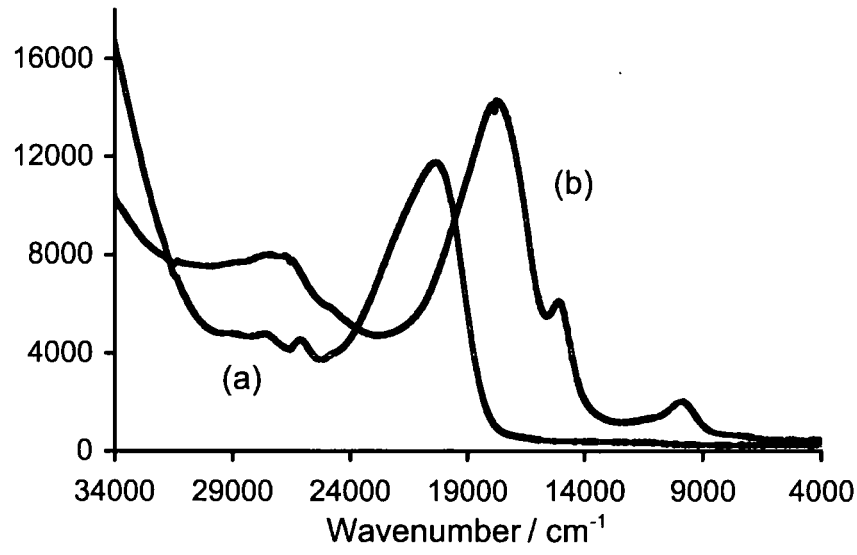

Figure 4.7. The UV-Vis-NIR spectra of (a) **Ru4b** and (b) $[\mathbf{Ru4b}]^+$ (CH_2Cl_2 / 0.1M NBu_4PF_6).

The anthryl derivative $[\mathbf{Ru4b}]^+$ offers four principal absorption bands near 27000, 18200, 15000 and 10000 cm^{-1}, together with weaker bands tailing further into the NIR region (**Figure 4.7**). On the basis of TD DFT calculations using $[\mathbf{Ru4\text{-}H}]^+$ as a model, the highest-energy band observed in the UV-vis-NIR spectrum of $[\mathbf{Ru4b}]^+$ is due to electronic excitations from the largely metal/ethynyl based β-HOSO and α-[HOSO-2] to the β-[LUSO+1] and α-[LUSO], which are anthracene π^* in character. The intense band at 18200 cm^{-1} is comprised of electronic transitions between α-HOSO and α-LUSO (i.e. the anthryl radical π-π^* transition), and is red-shifted from the analogous band in **Ru4b**. The less intense band at 15200 cm^{-1} is largely associated with electronic excitation from the β-[HOSO-4] to the β-LUSO (**Figure 4.8**), and is approximately an MLCT band.

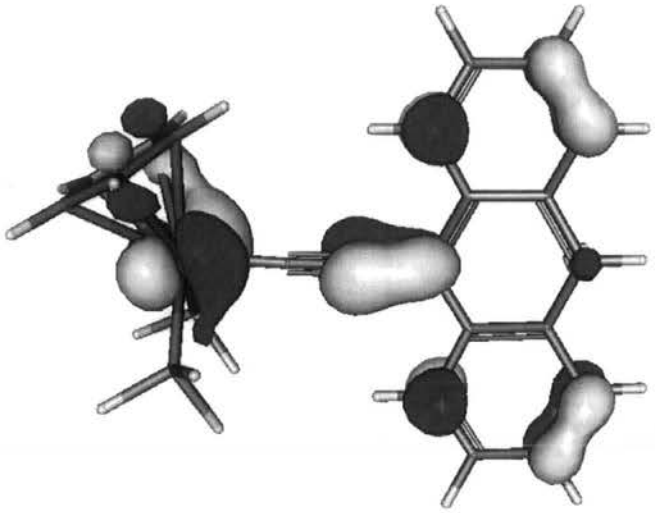

Figure 4.8. The β-[HOSO-4] of [**Ru4-H**]$^+$ plotted with contour values ±0.04 $(e/bohr^3)^{1/2}$.

A relatively intense NIR band (λ_{max} = 10000 cm^{-1}, ε_{max} = 2000 M^{-1} cm^{-1}) is calculated to arise from excitations involving occupied orbitals with the metal-ethynyl-anthryl character (β-HOSO and α-HOSO) and the β-LUSO and α-LUSO, which are both rather more heavily centred on the anthryl ring systems (**Figure 4.4**). The very weak NIR bands found at even longer wavelengths are assigned to metal to anthryl charge transfer processes, involving excitations largely between the β-[HOSO-1] and β-LUSO (**Figure 4.9**). The critical distinction between the assignments of the optical transitions in compounds modelled by [**Ru1-H**]$^+$ and [**Ru4-H**]$^+$ is the greater localisation of the β-LUSO and α-HOSO on the aromatic ring in the anthracene derivative.

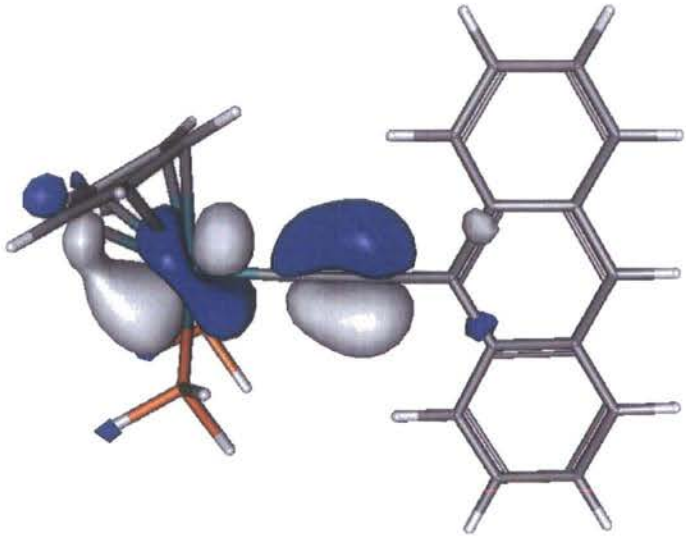

Figure 4.9. The β-[HOSO-1] of [**4-H**]$^+$ plotted with contour values ±0.04 (e/bohr^3)$^{1/2}$

As a test of the reliability of the B3LYP/3-21G* calculations presented above, the geometry optimisation, frequency calculations and TD DFT calculations on the models [**Ru1-H**] and [**Ru1-H**]$^+$ were repeated using a range of other functionals and basis sets (**Table 4.7**). There is little significant variation in the optimised geometries with computational method. The electronic structures calculated from these various methods are largely consistent, with perhaps the most notable feature being the relative order of the predominantly metal centred orbitals lying below the β-HOSO in [**Ru1-H**]$^+$.

Time-dependent density functional theory calculations of the first vertical transition energies of both the neutral and monocationic models are particularly revealing. Whilst the energy of electronic transitions computed using the different methods varies significantly, the net assignment of the absorption spectra is the same regardless of the functional or basis set employed. Given the gas-phase nature of the calculation and the use of static model systems, the strong electrolyte solution used

in the spectroelectrochemical measurement of the absorption spectra and the likely low energy barriers to rotation of the aromatic acetylide substituent around the acetylide-aromatic single bond, it is not possible to pass comment on the true precision of the various computational methods. It is clear, however, that the computationally expedient B3LYP/3-21G* calculations are not significantly less accurate than any of the higher level calculations also examined.

As a further test of the reliability of the calculations, the compounds $[\mathbf{Ru1b}]^{n+}$ and $[\mathbf{Ru4b}]^{n+}$ were also studied using B3LYP/3-21G*, the results of which are summarised in **Tables 4.8** and **Table 4.9**, together with the experimental data and that from the models [**1-H**] and [**4-H**] for ease of comparison. The agreement between the data calculated from the systems containing the full ligand sets and those observed experimentally is better than obtained from any of the calculations using the model ligand sets. However, the assignments of the electronic absorption bands in the experimental systems $[\mathbf{Ru1b}]^{n+}$ and $[\mathbf{Ru4b}]^{n+}$ are not significantly changed

Table 4.7. Optimised bond lengths, important vibration frequencies and major electronic excitations for **Ru1-H**, **[Ru1-H]$^+$**, **[Ru1b]** and **[Ru1b]$^+$** determined by TD DFT methods using different functionals and basis sets, with selected experimental data for comparison.

	Expt **[Ru1b]$^{n+}$** [18]	B3LYP/ 3-21G* **[Ru1-H]$^{n+}$**	B3LYP/ Gen **[Ru1-H]$^{n+}$**	B3LYP/ Gen2 **[Ru1-H]$^{n+}$**	PBE1PBE/ 3-21G* **[Ru1-H]$^{n+}$**	PBE1PBE/ Gen **[Ru1-H]$^{n+}$**	BP86/ 3-21G* **[Ru1-H]$^{n+}$**	BP86/ Gen **[Ru1-H]$^{n+}$**	B3LYP/ 3-21G* **[Ru1b]$^{n+}$**
Bond lengths / Å									
n = 0									
Ru-C	2.011(4)	2.018	2.028	2.011	1.999	2.010	2.003	2.012	2.015
C≡C	1.215(5)	1.228	1.229	1.222	1.228	1.229	1.242	1.244	1.231
C-Ph	1.431(5)	1.426	1.428	1.424	1.423	1.425	1.426	1.427	1.425
Ru-P	2.262(1), 2.256(1)	2.278	2.291	2.310	2.250	2.264	2.260	2.273	2.287
n = 1									
Ru-C		1.944	1.946	1.932	1.929	1.929	1.943	1.942	1.957
C≡C		1.246	1.250	1.241	1.248	1.251	1.260	1.263	1.243
C-Ph		1.400	1.403	1.399	1.397	1.400	1.404	1.406	1.411
Ru-P		2.324	2.335	2.356	2.283	2.299	2.294	2.311	2.350
Vibrational frequencies (IR) / cm^{-1} (intensity)									
n = 0									
C≡C	2072(s)	2101 (218)	2084 (248)	2081 (327)	2121 (230)	2108 (256)	2020 (318)	2005 (330)	2077 (374)
Ring	1593(m,w)	1547 (54)	1573 (64)	1556 (76)	1568 (54)	1599 (61)	1494 (71)	1523 (80)	1545 (68)
n = 1									
C≡C	1929(s)	1980 (310)	1965 (209)	1906 (271)	1993 (339)	1983 (210)	1920 (29)	1910 (14)	1952 (520)
Ring	1551(m)	1529 (291)	1551 (290)	1537 (298)	1548 (310)	1574 (309)	1482 (165)	1508 (161)	1496 (91)

Table 4.8. The major electronic excitations for **Ru1-H**, $[\mathbf{Ru1\text{-}H}]^{+}$, **Ru1b** and $[\mathbf{Ru1b}]^{+}$ determined by TD DFT methods using different functionals and basis sets, with selected experimental data for comparison.[a]

	Expt $[\mathbf{Ru1b}]^{n+}$	B3LYP/ 3-21G* $[\mathbf{Ru1\text{-}H}]^{n+}$	B3LYP/ Gen $[\mathbf{Ru1\text{-}H}]^{n+}$	B3LYP/ Gen2 $[\mathbf{Ru1\text{-}H}]^{n+}$	PBE1PBE/ 3-21G* $[\mathbf{Ru1\text{-}H}]^{n+}$	PBE1PBE/ Gen $[\mathbf{Ru1\text{-}H}]^{n+}$	BP86/ 3-21G* $[\mathbf{Ru1\text{-}H}]^{n+}$	BP86/ Gen $[\mathbf{Ru1\text{-}H}]^{n+}$	B3LYP/ 3-21G* $[\mathbf{Ru1b}]^{n+}$
Electronic transitions / cm^{-1} (Molar extinction coefficient / M^{-1} cm^{-1} or intensity)									
n = 0									
HOMO → [LUMO+3]	29500 (9500)	37200 (0.4290)	34600 (0.1740) *HOMO → [LUMO+2]*	33900 (0.2115)	37900 (0.3848) *HOMO → [LUMO+1]*	36500 (0.4345) *[HOMO → LUMO+1]*	31300 (0.4735)	30600 (0.4370)	33900 (0.1103) *[HOMO-1] → [LUMO+9]*
n = 1									
β-HOSO → β-LUSO	8100 (600)	6300 (0.0001)	6000 (0.0001)	5700 (0.0001)	6700 (0.0000)	6300 (0.0000)	6000 (0.0001)	5500 (0.0001)	5200 (0.0010)
β-[HOSO-2] → β-LUSO(β) β-[HOSO-1] → β-LUSO	11200 (5100)	16200 (0.2661)	16200 (0.2610)	16000 (0.2583)	16700 (0.2739)	16700 (0.2540)	16400 (0.2081) *β-[HOSO-3] → β-LUSO*	16400 (0.1992) *β-[HOSO-3] → β-LUSO*	14100 (0.0731)
α-HOSO → α-LUSO	21100 (4300)	22500 (0.0067)	22700 (0.0067)	22500 (0.0074)	24800 (0.0082)	25600 (0.0044)	20400 (0.0038)	20400 (0.0043)	23900 (0.0072)

Table 4.9. Selected IR vibrational frequencies (as wavenumbers), together with major electronic excitations for **[Ru4b]**$^{n+}$ and **[Ru4-H]**$^{n+}$ determined by TD DFT methods using different functionals and basis sets, with selected experimental data for comparison.[a]

	Expt **Ru4b**	Calc **Ru4b**	IR Intensity/ Oscillator strength	Calc **Ru4-H**	IR Intensity/ Oscillator strength
Vibrational frequencies (IR) / cm^{-1} (intensity)					
n = 0					
C≡C	2041(s)	2044	723	2081	385
Ring	1561(vw)	1575	27	1577	18
n = 1					
C≡C	1925(s)	1934	81	1994	628
Ring	1590(w)	1563	12	1551	42
Electronic transitions / cm^{-1} (Molar extinction coefficient / M^{-1} cm^{-1} or intensity)					
n = 0					
HOMO → LUMO	20600 (11600)	474(21100)	0.2147	429(23300)	0.2817
n = 1					
β-[HOSO-1] → β-LUSO	7800 (600)	1536(6500)	0.0035	1097(9100)	0.0021
β-[HOSO] → β-LUSO α-HOSO → α-LUSO	10100 (1900)	1030(9700)	0.1163	878(11400)	0.1248
β-[HOSO-4] → β-LUSO	15200 (5900)	643(15500)*β-[HOSO-3]* → *β-LUSO*	0.0525	504(19800)	0.0442
α-HOSO → α-LUSO	17900 (14000)	605(16500)	0.0998	572(17500)	0.2714

[a] The composition of the orbitals are similar in each case, despite small differences in relative energy (shown in italics).

4.3.2.5. Conclusions from Studies of the Electrochemical Properties and Electronics Structures of Simple Ruthenium Acetylide Derivatives

One-electron oxidation of the half-sandwich bis(phosphine) ruthenium acetylide complexes $Ru(C{\equiv}CAr)(L_2)Cp'$ affords the corresponding radical cations $[Ru(C{\equiv}CAr)(L_2)Cp']^+$. These cations are sensitive to atmospheric conditions, and self-coupling reactions. However, the stability of these species is improved through the use of *p*-tolyl acetylide substituents or the bulky Ru(dppe)Cp* metal end-cap and *in situ* spectroelectrochemical methods may be used to record the infrared and UV-Vis-NIR spectra of these relatively 'reactive' cations. The compounds derived from phenylacetylene, 4-ethynyltoluene and 1-ethynylnapthalene offer frontier orbitals with appreciable metal character, which in the case of the HOMO is also admixed with the ethynyl and aromatic π system. There is a critical distinction in the electronic structure of the compounds based on 9-ethynyl anthracene, which instead feature frontier orbitals largely localised on the anthracene moiety. Thus compounds such as **[Ru4b]**$^+$ which feature larger π-systems on the acetylide substitutents might be better regarded as metal-stabilised anthracene radicals than as radical cations derived from oxidation of the metal centre.

4.3.1. Oligo-Phenylene Ethynylene Ruthenium Complexes

4.4.1. Syntheses

The NMR spectral assignments for all the complexes are quite similar with the simple system which have previously reported. [14,19,64] Each of the complexes **25-28** were characterised by the usual spectroscopic methods. In the case of **25**, a singlet at δ_H 2.36 ppm was observed arising from the methyl protons of the tolan moiety. The methoxy and methyl ester moieties in **26** and **27** were observed at ca. δ_H 3.9 ppm. In addition, singlet Cp resonances can be observed at above δ_H 4 ppm. However, the numerous aromatic protons in **25-28** were not fully resolved, but were observed as series of heavily overlapped δ_H 7.0-8.5 ppm the pseudo-doublet resonances from the tolan portion of the molecules were not distinctly observed.

The ^{31}P NMR spectra show singlet phosphorus resonances near δ_P 51 ppm, which are shifted downfield from $RuCl(PPh_3)_2Cp$ (δ_P 39 ppm), [53] and indicate a similar electronic environment associate with the phosphine in each case. Clearly, the electronic properties of the tolan substituent are not reflected in the ^{31}P NMR chemical shift of the phosphine moiety. This observation is also observed in a simple system of the (R = Ph, Napth. and Anth. substituent, $Ru(C{\equiv}CR)(PPh_3)_2Cp$ (δ_P 51 ppm). [19,64]

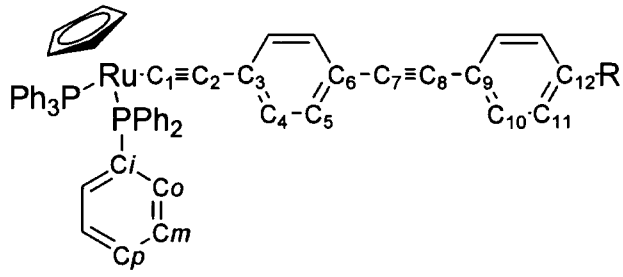

Scheme 4.7. Numbering scheme for ^{13}C NMR peak assignments of **25-28**.

The ^{13}C NMR of **25-28** are similar and consistent with the structures, and with the appropriate spectroscopic properties of the tolan precursors (see **Chapter 2**). For an example, all the spectra show resonances at ca. δ_C 86 ppm arising from the Cp ligand. The spectrum of **25** contains methyl resonance at δ_C 22 ppm, whereas the methoxy and methyl ester carbons in **26** and **27** were observed above δ_C 50 ppm. In addition, the distinctive carbonyl in **27** was observed at δ_C 167 ppm. The acetylide carbons C_1 and C_2 were observed, and identified on the basis of the J_{CP} coupling constant, with a triplet at above δ_C 120 ppm with coupling constant J_{CP} = 25 Hz being assigned to C_1 and singlet at lower chemical shift, at ca. δ_C 115 ppm assigned to C_2. Similar observations have been reported for closely related systems. [14,54] Another set of acetylenic carbons (C_7 and C_8) can be found at ca. δ_C 90 ppm. The aromatic carbons of the tolan fragment C_3-C_6 and C_9-C_{10} are all clearly observed and assigned on the basis of comparisons within the series of complexes **25-28** and also with the gold acetylide complexes (**Chapter 3**) and with the analogous ligand precursors (**Chapter 2**). Thus C_3 and C_4 can be found at between δ_C 114-132 ppm, whereas C_5 falling at higher chemical shift, ca. δ_C 132 ppm; C_6 and C_9 can be observed at ca. δ_C 116 ppm and at ca. δ_C 132 ppm respectively. For C_{10} the

resonances can be observed at δ_C 131 ppm; whereas C_{11} and C_{12} can be observed in between δ_C 124-131 ppm and δ_C 131-160 ppm, respectively.

The aromatic carbons associated with the triphenyl phosphine ligand are clearly distinguishable from those of the tolan moieties on the basis of the coupling to the phosphorus nucleus, and are assigned on the basis of the magnitude of the coupling constants. Thus, C_i is observed as doublet-of-doublet (dd) at ca. δ_C 139 ppm ($^1J_{CP}/^4J_{CP}$ ~ 11 Hz), C_o at δ_C 134 ppm ($^2J_{CP}/^5J_{CP}$ ~ 5Hz), C_m at ca. δ_C 128 ppm ($^2J_{CP}/^6J_{CP}$ ~ 5Hz) and C_p arises as singlet at δ_C 128 ppm. The ^{13}C numbering scheme for complexes 25-28 is shown in **Scheme 4.7** above.

The IR spectra of complexes **25-28** were recorded as Nujol mulls, and show strong ν(C≡C) bands near 2060 cm^{-1} somewhat lower in energy than the organic alkynes; ca. 2150 cm^{-1} (see syntheses section in **Chapter 2**) and also with other similar organic alkynes. [42-44] Another weak ν(C≡C) bands in the complexes was observed at ca. 2200 cm^{-1}. In addition to the acetylenic bands, the IR spectrum of **27** contains strong ν (C=O) band near 1724 cm^{-1}.

The electrospray mass spectra $[ES\text{-}MS]^+$ for complexes **25-28** contain the molecular ion M^+ and show fragmentation of the tolan portions at *m/z* 691. In the case of **26**, the presence of an adduct containing Na^+, which is believed abstracted from the glass in the preparation of the complex, is also observed in the spectrum along with the protonated molecular ion $[M+H]^+$. Such ions are commonly observed in the $[ES\text{-}MS]^+$ of acetylide complexes. [55]

The ^1H NMR spectra of [Ru(C≡CR)(dppe)(η^5-C_5Me_5)] of **29-33** are similar and consistent with the structures. The expected Cp* protons can be observed in all complexes at ca. δ_H 1.6 ppm. In addition, the two sets of CH_2 proton resonances from the dppe moieties are clearly distinguishable from the tolans moiety on the basis of the coupling to the phosphorus nucleus, and assigned on the basis of the size of coupling constant, the signal was observed as doublet-of-doublet (dds) at above δ_H 2 ppm ($J_{HP} = J_{HH}$ ~ 6 Hz).

Similarities within the tolan portions also can be observed. A singlet resonance arising from the TMS moiety at δ_H 0.29 ppm in the spectrum of **29** was observed, whilst a singlet resonance at δ_H 3.82 ppm was observed arising from the methyl protons of the tolan moiety in **30**. The methoxy and methyl ester moieties in **31** and **32** were observed at above δ_H 3 ppm. However, the numerous aromatic protons from the dppe moieties in **29-33** were not fully resolved, which were instead observed as series of overlapped δ_H 7.2-7.8 ppm. However, the pseudo-doublet resonances arising from the tolan portion of the molecules were observed at δ_H 6.7-8.2 ppm. The ^{13}C numbering scheme for complexes **29-33** is shown in **Scheme 4.8** below.

The ^{31}P NMR spectra show singlet phosphorus resonances near δ_P 81 ppm which indicate a similar electronic environment associated with the phosphine in each case. The chemical shifts of the resonances are expected in the ruthenium acetylide complexes featuring dppe as supporting ligands. [18] Clearly, as was the case with **Ru1 – Ru4** the electronic environment of the acetyleneic (tolan) substituent is not reflected in the ^{31}P NMR chemical shift of the phsophine moiety.

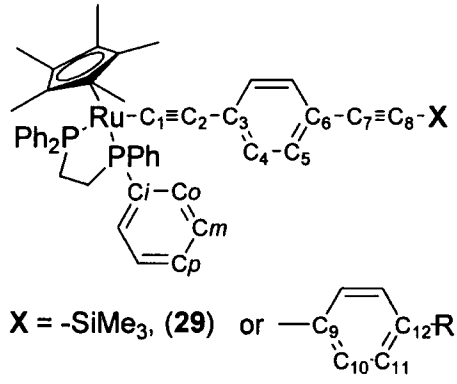

R = Me (**30**), OMe (**31**), CO_2Me (**32**), NO_2 (**33**)

Scheme 4.8. Numbering scheme for ^{13}C NMR spectral assignment of **29-33**.

The ^{13}C spectra of **29-33** are, as might expected, similar, and are consistent with the structures. The spectrum of **30** contains a methyl peak at δ_C 22 ppm, whereas the methoxy and methyl ester carbons in **31** and **32** were observed above δ_C 50 ppm. In addition, the distinctive carbonyl carbon in **33** was observed near δ_C 167 ppm. The acetylide carbons C_1 and C_2 were observed, and identified on the basis of the J_{CP}

coupling constants with a triplet at around δ_C 133-138 ppm with coupling constant J_{CP} = 25 Hz being assigned to C_1, and a singlet above δ_C 100 ppm assigned to C_2 (**Scheme 4.8**). Similar resonances have been reported for similar systems. [18] Another set of acetylenic carbons (C_7 and C_8) were observed at ca. δ_C 90 ppm. The aromatic carbons of the tolan fragment in this series are very similar with the **25-28** and comparable with the tolan precursors (see **Chapter 2**). In addition, the spectra of **29-33** also show singlet resonances of methyl at Cp at ca. δ_C 10 ppm and Cp resonances at ca. δ_C 93 ppm.

The aromatic carbons associated with the diphenylphosphine ethane (dppe) ligand are clearly distinguishable from those of the tolan moiety on the basis of the coupling to the phosphorus nucleus, and assigned on the basis of the size of the coupling constant. Thus, C*i* is observed as a multiplet (dds) at δ_C 138.4 and δ_C 138.7 ppm. For C*o* and C*m*, the resonances were observed as doublet-of-doublet (dds), thus, C*o* at δ_C 133.4 ppm and δ_C 133.1 ppm (C*o,o'*, $J_{CP/CCP}$ ~ 5Hz), C*m* at δ_C 127.0 ppm and 127.3 ppm (C*m*,m' $J_{CP/CCP}$ ~ 5Hz). Whereas the singlet resonances for the C*p* carbon were observed at δ_C 128.7 ppm.

The IR spectra of complexes **29-33** exhibit strong ν(C≡C) bands for the coordinated acetylide moiety at ca. 2060 cm^{-1}, somewhat lower in energy than the organic alkynes; ca. 2150 cm^{-1} (see syntheses section in **Chapter 2**) and other similar organic alkynes. [42-44] Another weak ν(C≡C) bands in the complexes was observed at ca. 2200 cm^{-1} which is from the tolan portion except for **29** at 2149 cm^{-1} which is believed to arise from the TMS moiety of the complex. In addition to the acetylides bands, the strong ν (C=O) band for **32** can be observed 1717 cm^{-1}.The electrospray mass spectra $[ES\text{-}MS]^+$ for complexes **29-33** contain the protonated molecular ions $[M+H]^+$.

Following the same synthetic procedure as shown in **Scheme 4.1**, the disubstituted ruthenium acetylide complexes **34** and **35** featuring the extended three-ring systems have been prepared and characterised by the usual spectroscopic methods. These bimetallic complexes featuring a phenylene ethynylene based bridging ligand offer spectroscopic properties similar to those of the acetylene precursors (**Chapter 2**) and

with the ruthenium acetylides featuring tolans-based ligands (i.e. **25-28** for **34** and **29-33** for **35**).

The aromatic protons associated with the triphenyl phosphine ligand in **34** and the substituent were not fully resolved, but were observed as a series of heavily overlapped δ_H 7.0-7.8 ppm. However, in the case of **35**, the protons of the bridging ligand can be observed as a pseudo-doublet at δ_H 6.71 ppm and a singlet at δ_H 6.97 ppm from the $[C_6H_2(OMe)_2]$ moiety. The two sets of CH_2 proton resonances from the dppe moieties are coupled to the phosphorus nuclei, and observed as doublet-of-doublet (dds) at ca δ_H 2 ppm ($J_{HP} = J_{HH} \sim 6$ Hz). Furthermore, the spectra also show singlet methoxy resonance at ca. δ_H 3.9 ppm arising from the two methoxy substituents in the middle ring; in addition, a singlet from the Cp ligand at δ_H 4.34 ppm for **34**, or a singlet methyl resonances from the Cp* moiety at δ_H 1.56 ppm in **35** can also be observed (**Scheme 4.9**). The ^{31}P NMR spectra show singlet phosphine resonances at usual regions, δ 51.3 ppm for **34** and δ 81.8 ppm for **35**.

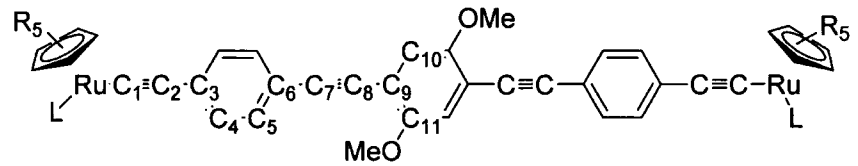

R = H, L = $(PPh_3)_2$ (**34**); Me, L= dppe (**35**)

Scheme 4.9. Numbering scheme for ^{13}C NMR spectral assignment of **34-35**.

In the ^{13}C NMR spectra the carbon C_1 in **34** and **35** was observed and identified on the basis of the J_{CP} coupling constant, as a triplet with coupling constant $J_{CP} = 25$ Hz in each case, found at ca. δ_C 123 ppm for **34** and ca. δ_C 136 ppm for **35**; singlet resonances at lower chemical shift (δ_C 110 ppm) are assigned to C_2. Another set of acetylenic carbons (C_7 and C_8) can be found in between δ_C 81-97 ppm. All the aromatic carbons C_3-C_6 and C_9-C_{11} resonances are similar to those of the ligand precursors (see syntheses section in **Chapter 2**). Thus C_3 and C_4 resonances can be observed above δ_C 110 ppm, whilst C_5 and C_6 can be observed at higher chemical shift, at δ_C 116-131 ppm. For C_9 and C_{10}, the resonances can be observed above δ_C

130 ppm, whilst C_{11} can be observed at higher chemical shift ca. δ_C 154 ppm. In addition, the Cp' resonances for **34** and **35** were observed in the usual region at δ_C 51 ppm and ca. δ_C 82 ppm respectively. In the case of **35**, Cp* resonances can be observed δ_C 10 ppm and the CH_2 carbon of the dppe moiety was observed as a doublet-of-doublet (dd) at ca. δ_C 30 ppm ($J_{CP/CCP}$ ~ 23 Hz).

The aromatic carbons associated with the diphenylphosphine ethane (dppe) ligand in **35** are clearly distinguishable from those of the tolan moiety and are the observation is similar with the tolan ruthenium acetylide complexes (**29-33**). The resonances are observed on the basis of the coupling to the phosphorus nucleus, and assigned on the basis of the size of the coupling constant. Thus, C*i* is observed as a multiplet (dd) at δ_C 137.1 ppm and δ_C 139.0 ppm. For C*o* and C*m*, the resonances were observed as doublet-of-doublet (dds), thus, C*o* at δ_C 133.4 ppm and δ_C 133.9 ppm (C*o,o'*, $J_{CP/CCP}$ ~ 5Hz), C*m* at δ_C 127.2 ppm and 127.4 ppm (C*m*,m' $J_{CP/CCP}$ ~ 5Hz). The singlet resonances for C*p* (C*p*, *p*') were observed at δ_C 128.8 ppm.

Due to the symmetrical nature of the complexes **34** and **35** give rise to two ν(C≡C) bands in the IR spectra. The spectra were recorded as nujol mulls and show strong ν(C≡C) bands for the coordinated acetylide moiety at ca. 2060 cm^{-1}, somewhat lower in energy than the organic alkynes; ca. 2150 cm^{-1} (see syntheses section in **Chapter 2**). Another weak ν(C≡C) bands in the complexes were observed at near ca. 2200 cm^{-1}.

MALDI-TOF(+)-MS spectra for **33** and **34** both show peaks corresponding to the protonated molecular ion $[M+H]^+$ at *m/z* 1767 for **34** and at *m/z* 1654 for **35**.

4.4.2. Molecular Structural Analyses

The molecular structures of **27**, **29** and **30** have been determined by single crystal X-ray diffraction (**Figure 4.10**). Crystallographic data, selected bond lengths and angles are listed in **Table 4.10-Table 4.12**. The crystallographic work has been carried out by Dr D. S. Yufit and Dr D. Albesa-Jové.

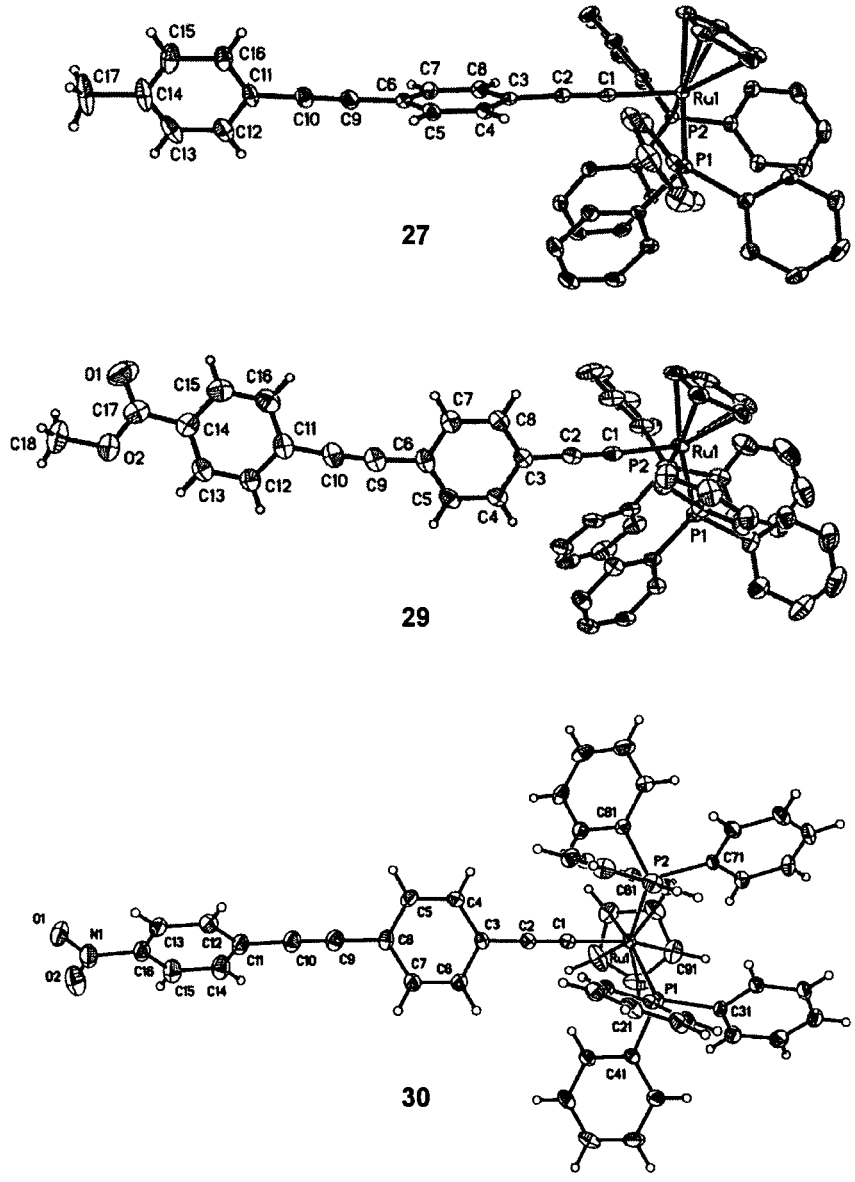

Figure 4.10. A plot of molecule of **27**, **29** and **30**, illustrating the atom numbering scheme.

Table 4.10. Crystal data for **27**, **29**, and **30**.

	27	**29**	**30**
Molecular formula	$C_{58}H_{46}P_2Ru$	$C_{59}H_{46}O_2P_2Ru$	$C_{57}H_{43}NO_2P_2Ru$
M / g mol^{-1}	905.96	949.97	936.93
Crystal system	Monoclinic	Triclinic	Monoclinic
a / Å	9.0871(16)	8.8607(14)	8.9330(11)
b / Å	25.811(4)	16.062(3)	26.063(3)
c / Å	19.291(4)	20.357(3)	18.991(2)
α / °	90	108.503(3)	90
β / °	90.932(4)	99.969(3)	91.754(3)
γ / °	90	95.193(3)	90
V / Å^3	4524.0(14)	2673.0(7)	4419.5(9)
Space group	P2(1)/c	P-1	P2(1)/c
Z	4	2	4
D_c / Mg m^3	1.330	1.180	1.408
Crystal size / mm	0.22 x 0.10 x 0.08	0.24 x 0.12 x 0.04	0.28 x 0.14 x 0.08
Crystal habit	plate	plate	plate
F (000)	1872	980	1928
Radiation	Mo(K_α)	Mo(K_α)	Mo(K_α)
Wavelength / Å	0.71073	0.71073	0.71073
μ / mm^{-1}	0.456	0.391	0.473
Temperature / K	120(2)	120(2)	120(2)
Data collection range / °	1.32 - 30.53	1.08-30.50	2.28-30.51
Reflections measured	37120	30930	36023
Data, restraints, parameters	13679, 0, 551	15670, 0, 578	13273, 0, 568
R_1, *wR2* (all data)	0.0575, 0.0692	0.0757, 0.1160	0.0677, 0.0998
Goodness-of-fit on F^2 (all data)	0.863	0.965	1.029
peak, hole / *e*Å^{-3}	0.521, -0.495	0.793, -0.490	0.943, -0.522

Table 4.11. Selected bond lengths (Å) for **27, 29** and **30**.

	27	**29**	**30**
C(1)-C(2)	1.215(3)	1.217(4)	1.218(3)
C(2)-C(3)	1.429(3)	1.422(4)	1.432(3)
C(3)-C(4, 8)	1.406(2), 1.403(3)	1.393(4), 1.416(4)	1.397(3), 1.407(3)
C(4)-C(5),C(7)-C(8)	1.379(3), 1.382(3)	1.379(4), 1.408(4)	1.382(3), 1.400(3)
C(6)-C(5, 7)	1.397(3), 1.396(3)	1.401(4), 1.375(4)	1.396(3), 1.385(3)
C(6)-C(9)	1.439(3)	1.437(4)	1.445(3)
C(9)-C(10)	1.204(3)	1.195(4)	1.193(3)
C(10)-C(11)	1.436(3)	1.433(4)	1.446(3)
C(11)-C(12, 16)	1.384(3), 1.396(3)	1.403(5), 1.386(4)	1.397(4), 1.390(4)
C(12)-C(13), C(16)-C(15)	1.386(3), 1.383(3)	1.372(5), 1.394(4)	1.393(3), 1.378(4)
C(14)-C(13, 15)	1.375(3), 1.385(3)	1.383(4), 1.389(4)	1.369(4), 1.389(4)
Ru(1)-C(1)	2.0051(19)	2.000(3)	2.009(2)
Ru(1)-P(1)	2.3020(5)	2.2866(7)	2.2894(6)
Ru(1)-P(2)	2.3020(5)	2.2862(7)	2.2976(6)

For C(6) read C(8), for C(16) read C(14)

Table 4.12. Selected bond angles (°) for **27, 29** and **30** (cont.)

	27	**29**	**30**
C(1)-Ru(1)-P(1)	86.04(5)	92.59(7)	92.22(6)
C(1)-Ru(1)-P(2)	89.82(5)	92.59(7)	88.01(6)
Ru(1)-C(1)-C(2)	178.08(15)	174.6(2)	175.88(18)
C(1)-Ru(1)-P(2)	89.82(5)	87.86(7)	88.01(6)
C(1)-C(2)-C(3)	176.82(18)	176.7(2)	177.2(2)
C(6)-C(9)-C(10)	178.2(2)	174.5(3)	175.1(3)
C(9)-C(10)-C(11)	178.9(2)	176.0(4)	174.8(3)

For C(6) read C(8)

The structures of **27**, **29** and **30** reveal the usual pseudo-octahedral geometry about ruthenium, with a P(1)-Ru(1)-P(2) angle of 99.04(2)°. The structures of the ethynyl tolan ligand may be compared with those in the monogold complexes $[Au(C{\equiv}CC_6H_4C{\equiv}CC_6H_4R)(PPh_3)]$ [R = Me (**15**), OMe (**16**), NO_2 (**18**), CN (**19**)]. The Ru(1)-C(1) bond angle in the three complexes are between [2.000(3)-2.009(2) Å] and are comparable with those found in other structurally characterised examples of ruthenium acetylides featuring the $Ru(PPh_3)_2Cp$ moiety. [21,56,57] The C(1)-C(2) triple bond [1.215(3)-1.218(3) Å] is not significantly longer than in **15-16** and **18-19** [1.191(8)-1.204(3) Å]. There is no evidence in the bond lengths associated with the tolan fragment that indicates quinoidal character in the ligand. The only significant difference in the structures of **15-16** and **18-19**, and these complexes (with the nature of the metal fragment excepted) lies in the relative orientation of the C(3)-C(8) and C(11)-C(16) aromatic rings. While in the monogold complexes these are relatively co-planar, it is clear from **Figure 4.10** that in all of these monoruthenium end-caps complexes, the planes containing these rings are almost perpendicular. The structure of tolans has been a subject of some considerable interest in recent times. [58] and it appears likely that these structural differences may be attributed to packing interactions within the crystal lattice, as opposed to any electronic effects.

4.4.3. Electrochemical Characterisation

4.4.3.1 Cyclic Voltammetric Properties

As found with the simple ruthenium acetylide derivatives (**Ru1-Ru4**), the half-sandwich ruthenium complexes featuring tolan based acetylide ligands also undergo a single electron oxidation in common solvents to give the corresponding radical cations, the electrode potential and chemical stability of which are both sensitive to both the supporting ligands on the ruthenium centre and the acetylide substitutent. In this section, we have examined the anodic behaviour of the complexes $Ru(C{\equiv}CC_6H_4C{\equiv}CC_6H_4R)(L_2)Cp'$ [**25-28** and **30-33**], and $Cp'Ru(L_2)(C{\equiv}CC_6H_4C{\equiv}C_6(OMe)_2H_2C{\equiv}CC_6H_4C{\equiv}C)Ru(L_2)Cp'$ [**34** and **35**]. Complexes **31** and **35** were chosen as representative examples for the

spectroelectrochemical studies from this series of complexes, the results of which are discussed in more detail below.

The cyclic voltammogram of [Ru(C≡CC$_6$H$_4$C≡CC$_6$H$_4$Me)(PPh$_3$)$_2$Cp] (**25**) in dichloromethane is characterised by an oxidation event at 0.60 V (vs. Fc / Fc$^+$), which may be described as quasi reversible although the value of i_{pa} : i_{pc} = 0.8 suggest partial insolubility of the cation (**Table 4.13**). The behaviour of two ruthenium tolan acetylides (**26-27**) derivatives were similar to those described for **25**. The CV behaviour of the nitro tolan of **28** differs from tolans **25-27** in that it has a value of i_{pa} : i_{pc} = 1.4 indicating that oxidation is only partly reversible. A reduction wave is also observed for **28** where the nitro group is presumed to accept the electron.

The same trend in electrode potentials as a function of the acetylide tolan substituent observed in the [Ru(C≡CC$_6$H$_4$C≡CC$_6$H$_4$R)(PPh$_3$)$_2$Cp] series was also apparent in the [Ru(C≡CC$_6$H$_4$C≡CC$_6$H$_4$R)(dppe)Cp*] complexes. The introduction of the bulky and more electron-donating Cp* and dppe ligands around the ruthenium acetylide framework rendered the first oxidation event of the Ru(C≡CC$_6$H$_4$C≡CC$_6$H$_4$R)(dppe)Cp* series ca. 100 - 200 mV more favourable than the analogous Ru(C≡CC$_6$H$_4$C≡CC$_6$H$_4$R)(PPh$_3$)$_2$Cp complexes. These processes are completely electrochemically and chemically reversible at room temperature and moderate scan rates (ν = 100 mV s^{-1}), with linear plots of i_{pa} vs $\nu^{1/2}$ being obtained and ΔE_p values of comparable magnitude as the internal reference couple (**Table 4.13**). Again, in this series of Ru(dppe)Cp* based compounds, the CV behaviour of the nitro tolan of **33** exhibits a reduction wave associated with nitro aromatic group.

Table 4.13. Electrochemical data for complexes **25-28, 30-33** and **34-35.**

	$E_{(1/2)oxd}$[a]	ΔE_p[b]	i_a/i_c	$E(2)_{pa}$[c]	$E_{(1/2)red}$[a]
25	0.60	127	0.8	1.38	
26	0.59	113	0.9	1.28	
27	0.63	171	0.8		
28	0.64	156	1.4		-0.85
30	0.37	103	1.1	1.18	
31	0.39	83	1.0	1.23	
32	0.41	135	1.0		
33	0.42	149	1.0	1.27	-0.84
34	0.63	245	2.1		
35	0.43	329	1.1		

[a] All E values in Volt vs SCE. Conditions: CH_2Cl_2 solvent, 10^{-1} M NBu_4PF_6 electrolyte, Pt working, counter and pseudo-reference electrodes, ν = 100 mV s^{-1}. The decamethyl ferrocene / decamethyl ferrocenium (Fc^* / Fc^{*+}) couple was used as an internal reference for potential measurements (Fc^* / Fc^{*+}) taken as -0.02 V *vs* SCE in CH_2Cl_2 / 0.1M $[NBu_4]PF_6$ [45]

[b] $\Delta E_p = |E_{pa} - E_{pc}|$. [c] anodic peak potential of a totally irreversible process. [d] 20 °C.

The extended "three ring" complexes $\{Ru(L_2)Cp'\}2(\mu\text{-}C{\equiv}CC_6H_4C{\equiv}C_6(OMe)_2H_2C{\equiv}CC_6H_4C{\equiv}C)$ (L = $(PPh_3)_2$, dppe; Cp' = Cp, Cp*) of **34** and **35** exhibit only a single oxidation wave, despite the presence of two metal centres. The CV of **34** is characterised by an irreversible oxidation event at 0.63 V (vs. Fc / Fc^+) ($i_{pa} : i_{pc}$ = 2.1) which also may suggest that there is partial insolubility of the dications. The introduction of the bulky and more electron-donating Cp* and dppe ligands in **35** have improved the electrochemical processes. These processes are

completely electrochemically and chemically reversible at room temperature and moderate scan rates (ν = 100 mV s^{-1}).

4.4.3.2. IR Spectroelectrochemical Studies

The greater chemical stability of the [Ru(C≡CAr)(dppe)Cp*] series **Ru1b**, **Ru2b**, **Ru3b** and **Ru4b** under the conditions of the cyclic voltammetry experiments prompted us to consider spectroscopic characterisation of the products derived from their one/two-electron(s) oxidation of tolan derivatives bearing this metal-supporting ligand combination more thoroughly by spectroelectrochemical means. The tolan **31** was selected for study (IR and UV-Vis-NIR); the tolans **25-28**, **30-33** are expected to give similar data. Like the studies dealing with arguably chemically simpler ruthenium complexes (**Ru1a**, and **Ru2-Ru3**), an air-tight spectroelectrochemical cell fitted with CaF_2 windows providing transparency across the spectroscopic region of interest was employed. [46]

The intensity of the characteristic ν(C≡C) band of the metal coordinated acetylide in **31** at 2072 cm^{-1} and which is characteristic of the 18-electron ruthenium acetylide decreased on oxidation, with a transient species **[31]**$^+$ with an IR bands at 1925 and 1576 cm^{-1} being observed as the oxidation proceeded (**Table 4.14**). In the neutral state the ν(C≡C) band of the tolan moiety was also observed at 2207 cm^{-1} (**Table 4.14**) with little change in the band frequency and intensity occurring during oxidation. There is evidence for the carbonyl cation $[Ru(CO)(PPh_3)_2Cp]^+$, present even in the initial sample used for IR spectroelectrochemistry, with the characteristic ν(CO) band being observed near 1975 cm^{-1}. [18] From the spectra, a conclusion can be made that the oxidation (positive charge) is located at the $RuC{\equiv}CC_6H_4$-, moiety with little contribution from the more extended portion of the tolan substituent (**Figure 4.10**).

Table 4.14. IR data (cm^{-1}) for compounds **31** and **35** and the corresponding cations.[a]

	Neutral species		Oxidised [cation(s) radical] complex	
	ν(CC)	ν(Aryl)	ν(CC)	ν(Aryl)
31	2072(s), 2207(s)	1592(w)	1925(s)	1575(s)
35	2061(s), 2196(s)	1591(w)	1924(s)	1575(s)

[a] data from CH_2Cl_2 solutions containing 0.1 M NBu_4BF_4 supporting electrolyte at ambient temperature.

Table 4.15. Selected IR vibrational frequencies (cm^{-1}), together with major electronic excitations for $[\mathbf{31}]^{n+}$ and $[\mathbf{31\text{-}H}]^{n+}$ determined by TD DFT methods.

	Expt **31**	Calc **31-H**
Vibrational frequencies (IR) / cm^{-1} (intensity)		
n = 0		
C≡C	2072(s), 2207(s)	2096(s), 2210(s)
Ring	1576(w)	1563(s)
n = 1		
C≡C	1925(s), 2207(s)	2000(s), 2156(s)
Ring	1577(w)	1558(w)

Electronic transitions / cm^{-1} (Molar extinction coefficient / M^{-1} cm^{-1} or calculated oscillator strength)		
n = 0		
HOMO → LUMO HOMO-1 → LUMO	26 200 (18 000)	28 700 (1.3458) 29 500 (0.3468)
HOMO-2 → LUMO	34 100 (19 900)	34 300 (0.1144) 34 900 (0.1075)
HOMO-4 → LUMO	43 900 (27 900)	43 400 (0.0342)
n = 1		
β-HOSO → β-LUSO	12 600 (1300)	9700 (0.7118)
α-HOSO → α-LUSO	21 800 (1890)	21 900 (0.5202)
β-LUSO → β-LUSO + 2	32 100 (18 700)	26 400(0.3919)
α-HOSO-2 → α-LUSO+4	44 100 (31 800)	43 900 (0.0392)

Table 4.15. Selected IR vibrational frequencies (cm^{-1}), together with major electronic excitations for $[35]^{n+}$ and $[35\text{-}H]^{n+}$ determined by TD DFT methods (cont.).

	Expt **35**	Calc **35-H**
Vibrational frequencies (IR) / cm^{-1} (intensity)		
n = 0		
C≡C	2060 (s), 2196(s)	2091(s), 2208(s)
Ring	1594 (w)	1546(s)
n = 2		
C≡C	1926(s), 2290(s)	1985(s), 2176(s)
Ring	1577(w)	1521(w)

Electronic transitions / cm^{-1} (Molar extinction coefficient / M^{-1} cm^{-1} or calculated oscillator strength)		
n = 0		
HOMO → LUMO	23 600 (48 100)	22 700 (2.9134)
HOMO-5→ LUMO	32 300 (34 100)	33 100 (0.6443)
n = 2		
β-[HOSO] → β-LUSO	7700 (880)	6000 (0.8553)
β-[HOSO-1] → β-LUSO	12 100 (8700)	11 700 (0.6086)
α-HOSO → α-LUSO	25 800 (44 700)	18 000 (0.8318)
β-[HOSO-1] → β-LUSO + 2 α-HOSO-5 → α-LUSO	32 500 (31 400)	28 900 (0.3693) 32 500 (0.1477)

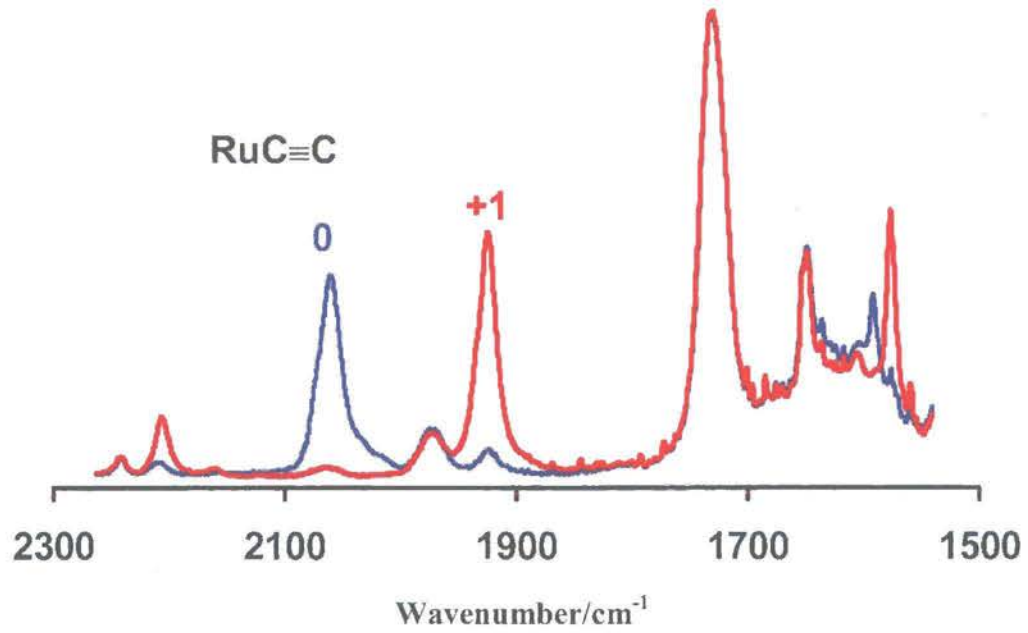

Figure 4.10. IR spectra on oxidation of **31** to $[\mathbf{31}]^{+}$ in a spectroelectrochemical cell (CH_2Cl_2 / 0.1M NBu_4PF_6, ambient temperature).

An IR spectroelectrochemical study on the extended three-ring system of $\{Ru(dppe)Cp^*\}_2(\mu C{\equiv}CC_6H_4C{\equiv}CC_6H_2(OMe)_2C{\equiv}CC_6H_4C{\equiv}C)$, **35**, was also carried out. Like **31**, the ν(C≡C) band of **35** at 2060 cm^{-1}, typical of the 18-electron ruthenium acetylide decreased upon oxidation, with a product species $[\mathbf{35}]^{2+}$ featuring an IR band at 1926 cm^{-1} being formed as the oxidation proceeded (**Table 4.14, Figure 4.11**). In addition, the neutral state ν(C≡C) band of the tolan moiety was also observed at 2196 cm^{-1} (**Table 4.14, Figure 4.11**) and upon oxidation, there is little change on the band shift and intensity. Again, it may be concluded that there is little contribution from the extended π-system of the bridging ligand to the oxidation processes of **35**. The reduction of the dication to neutral is almost fully reversible.

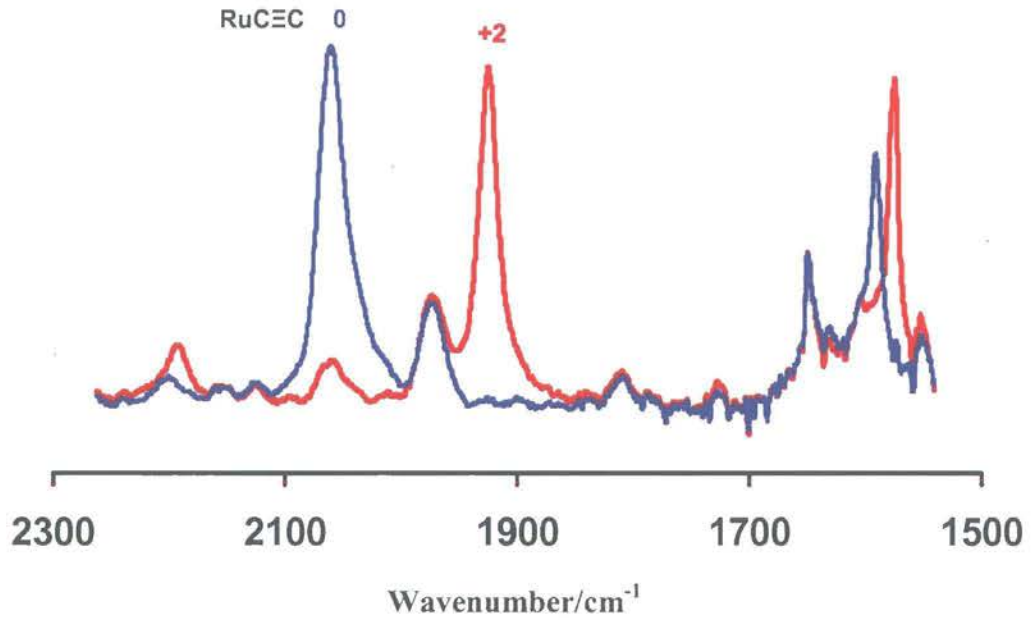

Figure 4.11. IR spectra on oxidation of **35** to $[\mathbf{35}]^{2+}$ in a spectroelectrochemical cell (CH_2Cl_2 / 0.1M NBu_4PF_6, ambient temperature).

4.4.3.3. Electronic Structure Calculations

A theoretical investigation was conducted by Dr M.A. Fox at the DFT level, on the model systems [Ru(C≡CC_6H_4C≡CC_6H_4OMe)$(PH_3)_2$Cp] (**31-H**) and [{Ru$(PH_3)_2$Cp}$_2$ (μ-C≡CC_6H_4C≡$CC_6H_2(OMe)_2$C≡CC_6H_4C≡C)] (**35-H**), which were used to mimic complexes **31** and **35**, and the corresponding radical cations $[\mathbf{31\text{-}H}]^+$ and $[\mathbf{35\text{-}H}]^{2+}$. The latter dication discussed here is high-spin which is computed to be more stable than the low-spin dication. The discussion which follows refers to results obtained from calculations at the B3LYP/3-21G* level of theory with no symmetry constraints (**Table 4.17**), as results obtained from other functionals and basis sets are in good general agreement (*vide infra*). Energies and composition of the frontier orbitals are summarised in **Table 4.18** for **31-H**, $[\mathbf{31\text{-}H}]^{2+}$, **35-H** and $[\mathbf{35\text{-}H}]^{2+}$, whereas **Figure 4.13** show the frontier orbitals of $[\mathbf{31\text{-}H}]^{n+}$ **(n = 0, 1)** and $[\mathbf{35\text{-}H}]^{n+}$ **(n = 0, 2),** while **Scheme 4.10** illustrates the labelling scheme for the electronic calculation studies.

Table 4.17. Optimised bond lengths (Å) for **31-H**, $[\mathbf{31\text{-}H}]^+$, **35-H**, and $[\mathbf{35\text{-}H}]^{2+}$.

	31-H	$[\mathbf{31\text{-}H}]^+$	Δ	**35-H**	$[\mathbf{35\text{-}H}]^{2+}$	Δ
Ru-P(1, 2)	2.280	2.311	-0.031	2.279	2.319	-0.040
Ru-Cα	2.015	1.955	0.060	2.013	1.949	0.064
Cα≡Cβ	1.228	1.244	-0.016	1.229	1.245	-0.016
Cβ-C3	1.414	1.393	0.021	1.420	1.396	0.024
C3-C4	1.422	1.428	-0.006	1.414	1.426	-0.012
C4-C5	1.414	1.376	0.038	1.387	1.379	0.008
C5-C6	1.387	1.425	-0.038	1.412	1.421	0.000
C6-C7	1.421	1.398	0.023	1.418	1.406	0.012
C7≡C8	1.215	1.223	-0.008	1.215	1.218	-0.003
C8-C9	1.421	1.403	0.018	1.415	1.407	0.008
C9-C10	1.401	1.422	-0.021	1.408	1.426	-0.018
C10-C11	1.393	1.377	0.016	1.389	1.389	0.000
C11-C12	1.399	1.412	-0.013	1.408	1.408	0.000
C12-OMe	1.384	1.363	0.021			
C12-C13				1.416	1.426	-0.001
C13-C14				1.389	1.389	0.000

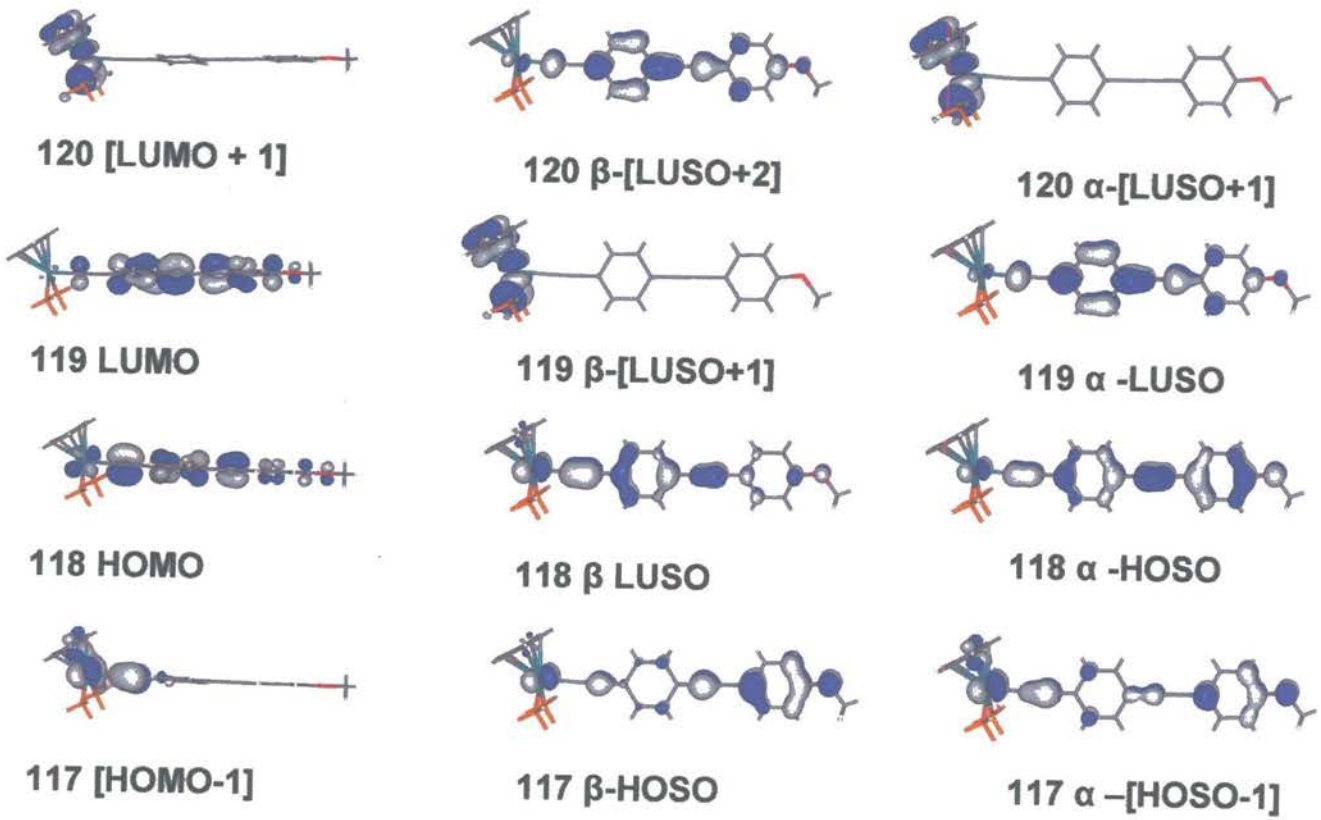

Figure 4.13a. The frontier orbitals of $[31\text{-H}]^{n+}$ **(n = 0, 1)** plotted with contour values ± 0.04 $(e/bohr^3)^{1/2}$.

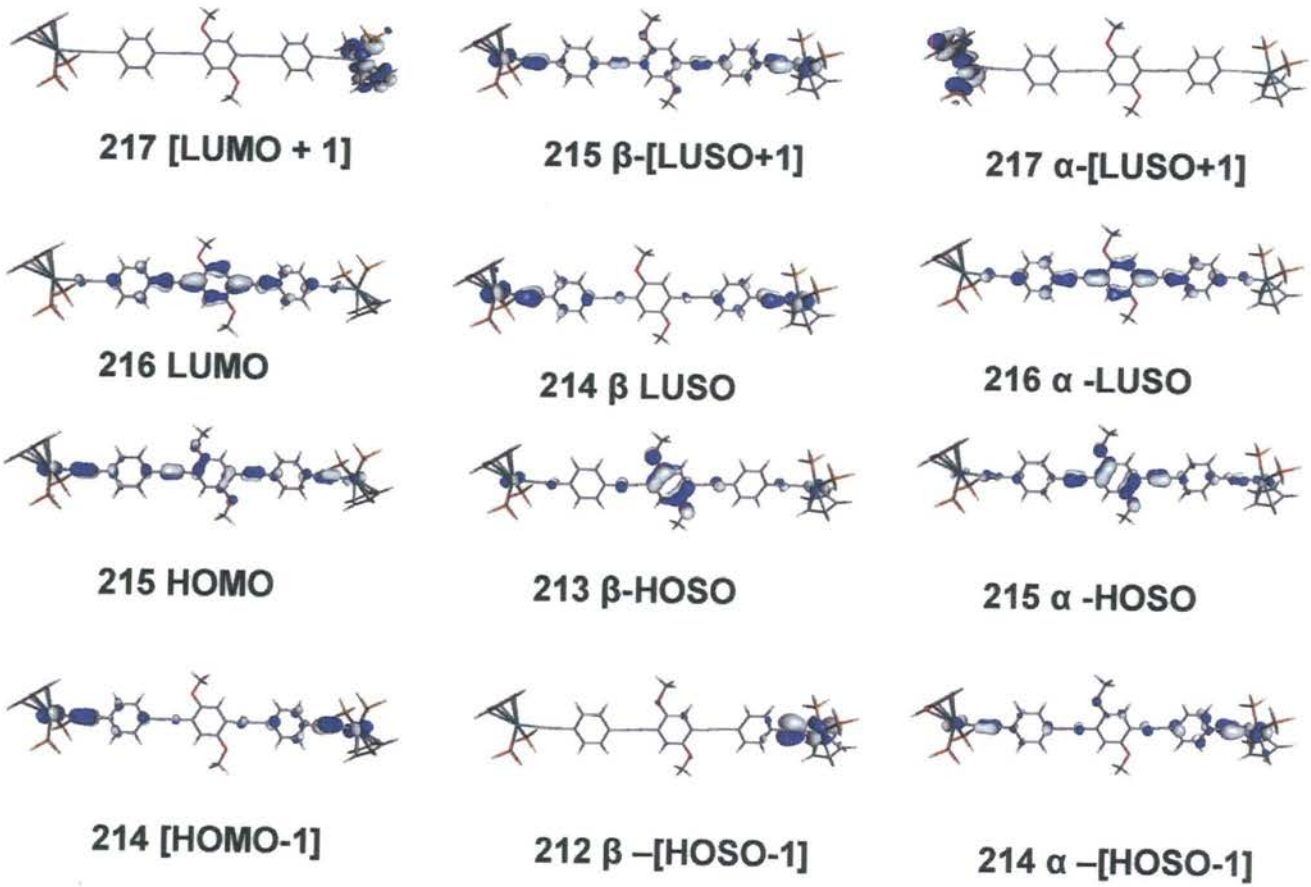

Figure 4.13b. The frontier orbitals of **[35-H]** $^{n+}$ **(n = 0, 2)** plotted with contour values ± 0.04 $(e/bohr^3)^{1/2}$.

Table 4.18. Energy, occupancy, and composition of frontier orbitals in the model complexes **31-H**, $[\mathbf{31\text{-}H}]^{+}$, **35-H** and $[\mathbf{35\text{-}H}]^{2+}$ (B3LYP/3-21G*).

31-H									
	MO								
	LUMO+3	LUMO+2	LUMO+1	LUMO	HOMO	HOMO-1	HOMO-2	HOMO-3	HOMO-4
ε(eV)	-0.04	-0.22	-0.84	-0.91	-4.74	-5.17	-5.56	-5.88	-6.62
occ	0	0	0	0	2	2	2	2	2
%Ru	74	61	50	2	16	46	34	32	0
%Cp	4	17	24	0	1	9	7	20	0
$\%PH_3$	20	13	27	0	0	4	5	10	0
$\%C_\alpha$	1	8	0	7	12	9	1	8	0
$\%C_\beta$	0	1	0	0	12	27	6	6	0
$\%C_6H_{4a}$	0	0	0	41	29	3	5	5	100
$\%C_7$	0	0	0	8	5	0	8	3	0
$\%C_8$	0	0	0	10	8	0	2	0	0
$\%C_6H_{4b}$	1	0	0	28	13	0	23	12	0
OMe	0	0	0	2	3	0	8	5	0

Table 4.18. Energy, occupancy, and composition of frontier orbitals in the model complexes **31-H**, $[\mathbf{31\text{-}H}]^+$, **35-H** and $[\mathbf{35\text{-}H}]^{2+}$ (B3LYP/3-21G*) (cont.)

35-H									
	MO								
	LUMO+3	LUMO+2	LUMO+1	LUMO	HOMO	HOMO-1	HOMO-2	HOMO-3	HOMO-4
ε(eV)	-0.39	-0.76	-0.86	-1.34	-4.41	-4.78	-5.18	-5.27	-5.38
occ	0	0	0	0	2	2	2	2	2
%Ru	2	50	0	1	7	14	22	40	0
%Cp	0	24	0	0	1	3	4	4	0
$\%PH_3$	1	27	0	0	1	1	2	3	0
$\%C_\alpha$	6	0	0	3	5	6	1	0	10
$\%C_\beta$	1	0	0	0	4	10	4	1	24
$\%C_6H_4a$	31	0	0	16	14	12	3	3	0
$\%C_\alpha$	1	0	0	8	4	0	2	1	0
$\%C_\beta$	6	0	0	4	4	3	0	0	0
$\%C_6H_2(OMe)_2$	5	0	0	37	22	3	32	17	1
$\%C_\alpha$	6	0	0	4	4	2	0	0	0
$\%C_\beta$	1	0	0	8	4	0	2	1	0
$\%C_6H_4b$	31	0	0	16	12	13	3	1	2
$\%C_\alpha$	6	0	0	3	5	6	4	7	0
$\%C_\beta$	0	0	0	0	5	10	12	17	0
%Ru	2	0	50	1	6	13	7	3	54
%Cp	1	0	24	0	1	3	2	1	5
$\%PH_3$	1	0	27	0	0	1	1	0	4

Table 4.18. Energy, occupancy, and composition of frontier orbitals in the model complexes **31-H**, $[\mathbf{31\text{-}H}]^{+}$, **35-H** and $[\mathbf{35\text{-}H}]^{2+}$ (B3LYP/3-21G*) (cont.)

$[\mathbf{31\text{-}H}]^{+}$																		
MO																		
	122β	122α	121β	121α	120β	120α	119β	119α	118β	118α	117β	117α	116 β	116α	115β	115α	114 β	113α
	β–[LUSO+4]	α–[LUSO+3]	β–[LUSO+3]	α–[LUSO+2]	β–[LUSO+2]	α–[LUSO+1]	β–[LUSO+1]	α–LUSO	β–LUSO	α–HOSO	β–HOSO	α–[HOSO-1]	β–[HOSO-1]	α–[HOSO-2]	β–[HOSO-2]	α–[HOSO-3]	β–[HOSO-3]	α–[HOSO-4]
ε(eV)	-2.69	-2.7	-3.38	-3.45	-3.95	-4.1	-4.02	-4.2	-6.68	-7.79	-8.05	-8.58	-8.74	-8.8	-9.11	-9.17	-9.27	-9.54
occ	0	0	0	0	0	0	0	0	0	1	1	1	1	1	1	1	1	1
%Ru	69	0	55	55	5	48	48	3	20	8	15	23	55	55	44	41	18	3
%Cp	2	0	19	20	2	26	25	1	4	2	3	7	5	6	29	31	8	3
$\%PH_3$	28	0	15	15	0	26	26	1	2	1	2	4	3	3	11	11	3	1
$\%C_{\alpha}$	0	0	9	9	10	0	0	11	9	6	0	3	9	8	7	8	6	1
$\%C_{\beta}$	0	0	1	1	0	0	0	1	13	5	8	13	26	24	6	8	0	0
$\%C_6H_4$ a	0	100	0	0	45	0	1	51	25	22	10	10	3	3	1	1	24	4
C7	0	0	0	0	4	0	0	5	4	9	11	4	0	0	0	0	1	1
C8	0	0	0	0	12	0	0	11	7	7	1	0	0	0	0	0	9	2
C_6H_4b	0	0	0	0	19	0	0	16	13	30	35	23	0	0	0	0	18	82
OMe	0	0	0	0	2	0	0	2	3	9	14	11	0	0	0	0	13	3

Table 4.18. Energy, occupancy, and composition of frontier orbitals in the model complexes **31-H**, $[\mathbf{31\text{-}H}]^+$, **35-H** and $[\mathbf{35\text{-}H}]^{2+}$ (B3LYP/3-21G*) (cont.)

$[\mathbf{35\text{-}H}]^+$																		
MO																		
	218β	219α	217β	218α	216β	217α	215β	216α	214 β	215α	213β	214α	212 β	213α	211β	212α	210 β	211α
	β–[LUSO +4]	α–[LUSO+3]	β–[LUSO+3]	α–[LUSO+2]	β–[LUSO+2]	α–[LUSO+1]	β–[LUSO+1]	α–LUSO	β–LUSO	α–HOSO	β–HOSO	α–[HOSO-1]	β–[HOSO-1]	α–[HOSO-2]	β–[HOSO-2]	α–[HOSO-3]	β–[HOSO-3]	α–[HOSO-4]
ε(eV)	-5.04	-4.94	-5.22	-5.15	-5.54	-5.33	-7.63	-5.72	-7.96	-8.75	-8.92	-9.34	-9.79	-9.5	-9.82	-9.91	-9.92	-10.05
occ	0	0	0	0	0	0	0	0	0	1	1	1	1	1	1	1	1	1
%Ru	0	2	49	0	2	48	10	1	17	2	6	7	0	10	4	0	53	53
%Cp	0	0	25	0	0	26	2	0	3	1	1	2	0	3	1	0	4	6
$\%PH_3$	0	1	26	0	0	26	1	0	2	0	1	12	0	2	1	0	3	3
$\%C_\alpha$	0	7	0	0	4	0	5	4	3	3	0	5	8	1	2	9	0	0
$\%C_\beta$	0	1	0	0	0	0	8	0	9	2	3	11	24	2	4	25	0	0
$\%C_6H_4a$	0	31	0	0	18	0	10	20	13	10	4	11	0	11	5	0	3	3
C7	0	0	0	0	7	0	2	6	0	6	4	1	0	0	3	0	0	0
C8	0	6	0	0	4	0	3	4	3	4	0	4	1	0	4	0	0	0
$C_6(OMe)_2H_2$	0	5	0	0	32	0	14	30	4	42	59	7	6	52	46	0	0	0
C_α	0	5	0	0	4	0	2	4	3	3	0	3	0	2	3	0	0	0
C_β	0	1	0	0	7	0	3	6	0	6	5	0	1	0	4	0	0	0
C_6H_4	0	31	0	0	32	0	14	18	4	12	59	16	6	2	46	3	0	0
C_α	0	7	0	0	4	0	5	4	3	3	0	5	8	1	2	9	0	0
C_β	0	1	0	0	0	0	8	0	9	2	3	11	24	2	4	25	0	0
Ru	48	2	0	48	2	0	12	1	14	4	7	16	49	3	12	55	0	0
Cp	26	1	0	26	0	0	2	0	3	1	1	5	4	1	2	5	0	0
PH_3	25	0	0	26	0	0	1	0	2	1	1	3	3	1	1	3	0	0

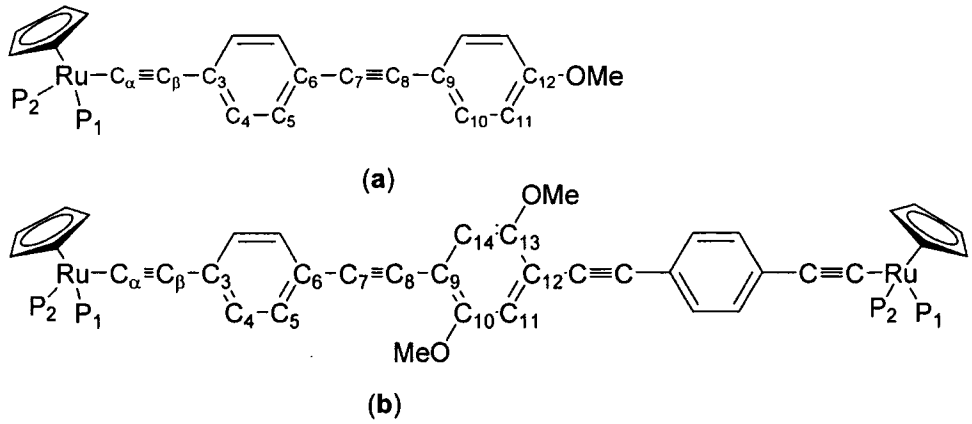

Scheme 4.10. The labelling scheme used in the discussion of the DFT result of (**a**) **31-H** and (**b**) **35-H**.

The Ru-Cα, Ru-P, Cα≡Cβ and Cβ-C(3) bond lengths in **31-H** and **35-H** are comparable with those found the simple ruthenium derivatives of **Ru4-H** and **Ru1-H**. At the level of theory employed, the aromatic substituents of the tolan and the extended three rings derivatives in the neutral systems **31-H** and **35-H** either lie in the plane approximately parallel or perpendicular to the Cp ring. In contrast, the plane of the aromatic substituents in the oxidised species $[\mathbf{31\text{-}H}]^{+}$ and $[\mathbf{35\text{-}H}]^{2+}$ are found approximately bisecting the P-Ru-P angle.

The HOMO and [HOMO-1] of **31-H** are comparable with those of **Ru1-H** being approximately orthogonal and derived from mixing the metal d and acetylide π-systems, with the HOMO also containing appreciable contributions from the tolan system. The characteristic frontier orbitals in **35-H** are similar to those of **31-H** and in both cases feature a significant contribution from the tolan ligand based atoms (**Table 4.18, Figure 4.13a**).

The occupied orbitals comprised largely of metal and Cp, metal phosphine and phenyl π-character are found lower in the occupied orbital manifest. The LUMO and [LUMO+1] of **31-H** are very similar to those of **Ru4-H** (the anthryl substituent) and feature important contributions from the acetylenic ligand, which is in the case of **31-H** is the tolan portion of the molecule. The LUMO is essentially the tolan π* orbital,

which is sufficiently low in energy to lie below the unoccupied Ru-Cp based orbitals that comprise [LUMO + 1] **Figure 4.13a**.

The frontier orbitals of **35-H** feature important contributions from Cα≡Cβ and the ligand substituent **(Table 4.18, Figure 4.13b)**. Thus, while the HOMO and [HOMO-1] are approximately orthogonal π-type orbitals, the HOMO features contribution from the atoms of the ligand substitutent (14% from C_6H_4a), (22 % from $C_6(OMe)_2H_2$) and (12 % from C_6H_4b) and is somewhat removed from the other occupied orbitals. Furthermore, the contribution in [HOMO-1] is largely contributed from the metal and the Cα≡Cβ. The LUMO is essentially the ligand π* orbital, which is sufficiently low in energy to lie below the unoccupied Ru-Cp based orbitals that comprise the [LUMO+1] and [LUMO+2].

The model radical cation $[\mathbf{31\text{-}H}]^+$ and dication $[\mathbf{35\text{-}H}]^{2+}$ feature Ru-C bonds somewhat shorter than **31-H** and **35-H** (**Table 4.17**). The metal-phosphine bond lengths are sensitive to the net electron density available for π-back bonding and as such are elongated in $[\mathbf{31\text{-}H}]^+$/ $[\mathbf{35\text{-}H}]^{2+}$ relative to **31-H/35-H**. The elongation of the acetylide C≡C bond in $[\mathbf{31\text{-}H}]^+$/ $[\mathbf{35\text{-}H}]^{2+}$ when compared with the neutral model system **31-H/35-H** is consistent with a decrease in the net acetylide π-bonding character. The frontier orbitals of the one-electron oxidation product $[\mathbf{31\text{-}H}]^+$/ $[\mathbf{35\text{-}H}]^{2+}$ are similar to those of **31-H/35-H**, with the α-HOSO and β-LUSO displaying appreciable Ru(d) and acetylide (π) character and the next highest unoccupied orbitals being largely centred on the $Ru(PH_3)_2Cp$ fragment (**Table 4.18**, **Figure 4.13**). From the calculations, it may conclude here that there is not much difference between the two complexes of **31-H** and **35-H**.

The spin densities characteristics of the cation $[\mathbf{31\text{-}H}]^+$ and $[\mathbf{35\text{-}H}]^{2+}$ are similar to that found in $[\mathbf{Ru1\text{-}H}]^+$ and $[\mathbf{Ru4\text{-}H}]^+$. **Table 4.19** reveals that the major spin densities are located at Ru (0.251), the Cβ atom and the $-C_6H_4-$ moiety in the case of $[\mathbf{31\text{-}H}]^+$. In the case of $[\mathbf{35\text{-}H}]^{2+}$, the major spin densities also are located at the both Ru (0.686) centres, the Cβ atom and the $-C_6H_4a-$ and also at the middle ring of the system.

Table 4.19. Spin densities for the model radical cations, $[\mathbf{31\text{-}H}]^+$ and $[\mathbf{35\text{-}H}]^{2+}$

	$[\mathbf{31\text{-}H}]^+$	$[\mathbf{35\text{-}H}]^{2+}$	Δ^a	$[\mathbf{Ru1\text{-}H}]^+$	$[\mathbf{Ru4\text{-}H}]^+$
Ru	0.251	0.686	-0.092	0.413	0.220
Cp	0.024	0.027	0.010	0.041	0.021
Cα	0.083	0.080	0.043	0.043	0.079
Cβ	0.148	0.443	-0.074	0.269	0.114
PH_3	-0.010	0.002	-0.011	0.000	0.000
$(C_6H_4)a$/ C_4H_5[b]/$C_{14}H_9$[c]	0.234	0.471	-0.002	0.246	0.598
C7	-0.020	0.062	-0.051		
C8	-0.111	0.063	-0.143		
$(C_6H_4)b/C_6H(OMe)_2H_2$	0.098	0.132	0.032		
OMe	0.006	0.042	-0.015		

[a] $\Delta = [\mathbf{31\text{-}H}]^+ - 0.5[\mathbf{35\text{-}H}]^{2+}$ [b] for $[\mathbf{Ru1\text{-}H}]^+$ [c] for $[\mathbf{Ru4\text{-}H}]^+$

To confirm the results obtained in the electronic structure calculations. The neutral and oxidised states of the model complexes **Ru31-H** and **Ru35-H** at the DFT level have been further discussed in the UV-Vis Spectroelectrochemical Studies. Due to their stability and insensitivity to the atmospheric conditions as shown in the cyclic voltammetric studies, complexes **31** and **35** were chosen to be studied.

4.4.3.4. UV-vis Spectroelectrochemical Studies

Examination of the electronic absorption spectra of **31** reveals strong bands at 26 200 and 43 900 cm^{-1} which are red-shifted but show typical characteristics of the tolan moiety [59,60] (**Table 4.20**, **Figure 4.14**). These characteristics are quite similar with the simple aromatic acetylide derivatives, although they are much more intense.

The UV-vis-NIR spectrum of $[\mathbf{31}]^+$, obtained spectroelectrochemically from **31**, exhibits strong broad absorption envelopes centred near 44 100 cm^{-1} and a weaker bands near 21 100 and 12 600 cm^{-1}, (**Figure 4.14**). The spectrum of **31** was almost fully recovered after back-reduction, which strongly supports the assignment of these characteristic absorption bands to the 17-e species $[\mathbf{31b}]^+$ (**Table 4.15**) TD DFT calculations using the $[\mathbf{31\text{-}H}]^+$ model indicate that the highest energy transition can be attributed to charge transfer from the metal fragment (including the acetylide π-system) to the phenyl (π*) ring being comprised of electronic transitions from the α-HOSO (highest occupied spin orbital) to the α-[LUSO]. The band centred near 21

900 cm^{-1} can be approximated in terms of transitions between occupied orbitals with large amounts of Ru/Cp character (β-[HOSO-1], β-[HOSO-2], to the β-LUSO (**Table 4.20**, **Figure 4.14**). The presence of low energy (NIR) bands in 17-e cation radicals of the general type $[Ru(C{\equiv}CAr)(dppe)Cp^*]^+$ has been noted by Paul *et al.*, and attributed to forbidden ligand-field type transitions centred on the Ru(III) centre. [18] The TD DFT calculations carried out in the present study suggest that the lowest energy transition should be attributed to the β-HOSO to β-LUSO transition, with the low intensity of the observed band reproduced by the low calculated oscillator strength and easily explained by the relative, approximately orthogonal orientation of these two orbitals. Other NIR bands of slightly greater intensity and higher energy are attributable to Ru/Cp based β-[HOSO-1] to the β-LUSO.

Table 4.20. The principal UV-vis absorption bands [ν_{max} / cm^{-1} (ε_{max} / M^{-1} cm^{-1}) observed from CH_2Cl_2 / 10^{-1} M NBu_4PF_6 solutions of $[\mathbf{31}]^{n+}$ and $[\mathbf{35}]^{n+}$ (n = 0, 1, for **31**); n = 0, 2 for **35**).

	n	
	0	+1/+2
31	43 900 (27 900), 34 100 (19 900), 26 200 (18 000)	44 100 (31 800), 32 100 (18 700), 21 800 (1890), 126 00 (1300)
35	32 300 (34 100), 23 600 (48 100)	32 500 (31 400), 25 800 (44 700), 12 100 (8700), 7700 (880)

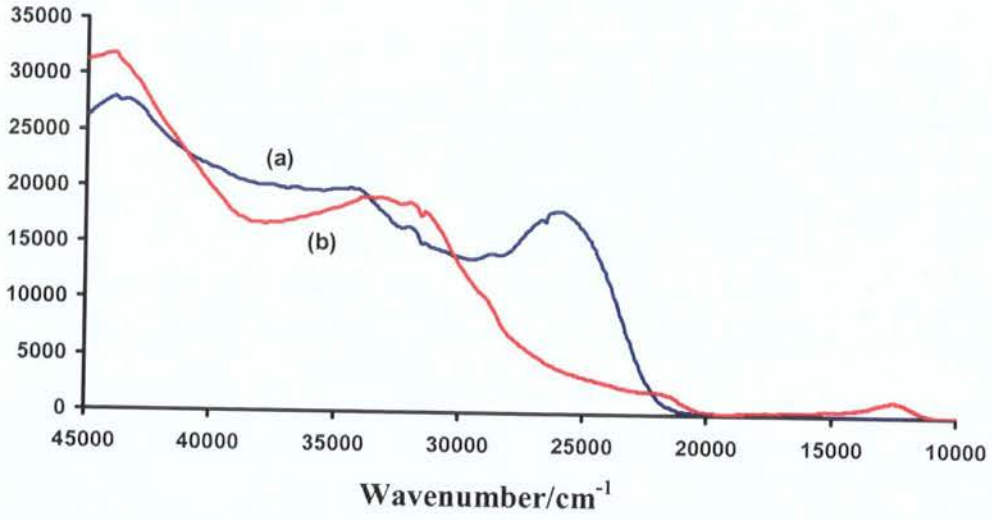

Figure 4.14. The UV-Vis-NIR spectra of (**a**) **31** and (**b**) $[\mathbf{31}]^{+}$ (CH_2Cl_2 / 0.1M NBu_4PF_6).

In the case of **35**, the UV-Vis-NIR spectrum contains strong bands in between 23 600 and 32 300 cm^{-1} which is in the red-shift region due to the conjugated extended three-rings system of the substituent. The extended three-ring derivative $[\mathbf{35}]^{2+}$ offers four principal absorption bands near 7700, 12 100, 25 800 and 31 500 cm^{-1} (**Figure 4.15**). On the basis of TD DFT calculations using $[\mathbf{35\text{-}H}]^{2+}$ as a model, the highest-energy band observed in the UV-vis-NIR spectrum of $[\mathbf{35}]^{2+}$ is due to electronic excitations from the largely middle-ring centred based β-HOSO and delocalised α-[LUSO-2] to bridging-centred α-LUSO.

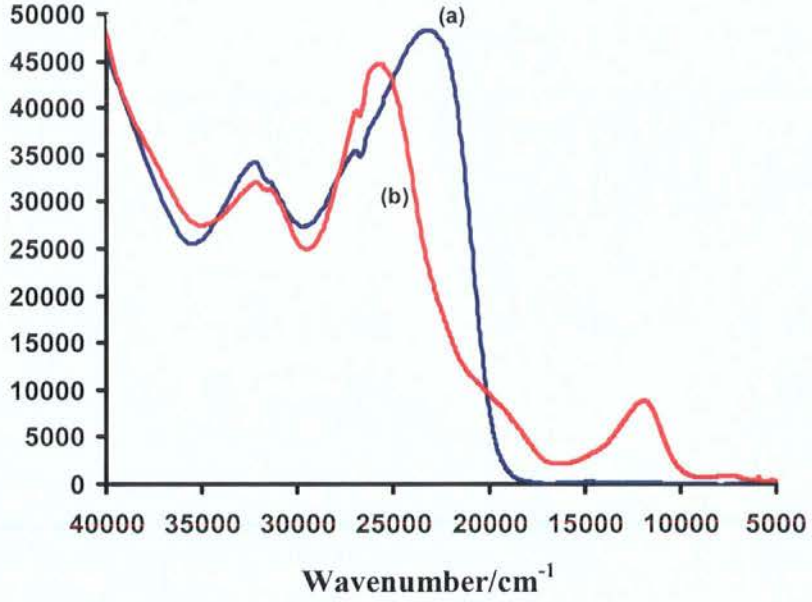

Figure 4.15. The UV-Vis-NIR spectra of (**a**) **35** and (**b**) $[\mathbf{35}]^{2+}$ (CH_2Cl_2 / 0.1M NBu_4PF_6).

4.4.3.5. Conclusions Drawn from the Electrochemical Properties and Electronic Structures of Ruthenium Complexes Featuring Oligo-Phenylene Ethynylene Based Ligands

Oxidation of the half-sandwich bis(phosphine) ruthenium acetylide complexes $Ru(C{\equiv}CC_6H_4C{\equiv}C_6H_4R)(L_2)Cp'$ and $Cp'Ru(L_2)(C{\equiv}CC_6H_4C{\equiv}C_6(OMe)_2H_2C{\equiv}CC_6H_4C{\equiv}C)Ru(L_2)Cp'$ afford the corresponding radical cations $[Ru(C{\equiv}CC_6H_4C{\equiv}C_6H_4R)(L_2)Cp']^+$ and $[\{Cp'Ru(L_2)_2\}(\mu\text{-}C{\equiv}CC_6H_4C{\equiv}C_6(OMe)_2H_2C{\equiv}CC_6H_4C{\equiv}C)]^{2+}$. These cations are sensitive to atmospheric conditions. However, the stability of these species is improved through the use of the bulky Ru(dppe)Cp* metal end-cap and *in situ* spectroelectrochemical methods have been used to record the infrared and UV-Vis-NIR spectra of these relatively 'reactive' cations here. The compounds derived from the tolan and the extended three-rings derivatives offer frontier orbitals with appreciable metal character, which in the case of the HOMO is also admixed with the ethynyl and aromatic π system. There is a critical similarities properties between the tolan ruthenium acetylides (RuCp*) and with the simple phenyl derivatives **Ru1**-**Ru4** complexes. There is little to suggest that the extended phenylene ethynylene system

is a suitable bridging moiety for promoting electronic interactions between metal centres located at the ligand termini.

4.5. Conclusions

The preparation of simple ruthenium acetylide complexes that feature phenyl, tolan and oligo(phenylene ethynylene) moieties were described. These complexes were fully characterised spectroscopically and their electrochemical properties.

One-electron oxidation of the half-sandwich bis(phosphine) ruthenium acetylide complexes $Ru(C{\equiv}CAr)(L_2)Cp'$ [L = $(PPh_3)_2$, dppe; Cp' = Cp, Cp*], (Ar = Ph, *p*-tol, Napth., Anth., $C_6H_4C{\equiv}CC_6H_4R$ and $(-C{\equiv}CC_6H_4C{\equiv}C_6(OMe)_2H_2C{\equiv}CC_6H_4C{\equiv}C-)$ affords the corresponding radical cations $[Ru(C{\equiv}CAr)(L_2)Cp']^{n+}$ (n = 1) and (n = 2) in the case of the extended three rings system. In addition, there is evidence for carbonyl cation $[Ru(CO)(PPh_3)_2Cp]^+$ which proved that these systems are sensitive to atmospheric conditions, and self-coupling reactions. However, the stability of these species is improved through the use of *p*-tolyl acetylide substituents or the bulky Ru(dppe)Cp* metal end-cap.

The result obtained were supported further by the IR shifts calculated by DFT calculations which show very good agreement with observed IR bands. The spectra reveal that the oxidation is occurred at the (Ru-C≡C- The UV-Vis-NIR spectroelectrochemical method was also applied to these complexes and revealed π-π^* arisng from the ethynyl and the substituents for these complexes. On oxidation to the cations which low-energy transition bands were observed which are assigned to ruthenium-ethynyl to ruthenium-ligand character on the basis of TD-DFT computational methods. All the complexes show the appreciable metal character, which in the case of the HOMO is also admixed with the ethynyl and aromatic π system.

There is a critical distinction in the electronic structure of the compounds based on 9-ethynyl anthracene, which instead feature frontier orbitals largely localised on the

anthracene moiety. Thus compounds such as $[\mathbf{Ru4b}]^+$ which feature larger π-systems on the acetylide substitutents might be better regarded as metal-stabilised anthracene radicals than as radical cations derived from oxidation of the metal centre. There is a critical similarities properties between the tolan ruthenium acetylides (RuCp*) and with the simple phenyl derivatives **Ru1-Ru4** complexes.

Conclusion can be made that there is little to suggest that the extended phenylene ethynylene system is a suitable bridging moiety for promoting electronic interactions between metal centres located at the ligand termini.

Molecular structures of **27**, **29** and **30** were obtained, the structures being similar to each other. The structures reveal the usual pseudo-octahedral geometry about ruthenium, with a P(1)-Ru(1)-P(2) angle of 99.04(2)°. There is no evidence in the bond lengths associated with the tolan fragment that indicates quinoidal character in the ligand and the planes containing these rings are almost perpendicular.

4.6. Experimental Details

4.6.1. General Condition

All reactions were carried out under an atmosphere of nitrogen using standard Schlenk techniques. Reaction solvents were purified and dried using an Innovative Technology SPS-400, and degassed before use. No special precautions were taken to exclude air or moisture during work-up. The compounds $RuCl(PPh_3)_2Cp$, [53] $RuCl(dppe)Cp^*$ [61] and $Me_3SiC{\equiv}CC_6H_4C{\equiv}CSiMe_3$ [62] were prepared by literature routes. Other reagents were purchased and used as received. The completed experimental details and characterisation of complexes **Ru1-Ru4** were fully described in the previous occasion. [19]

NMR spectra were recorded on a Bruker Avance (^1H 400.13 MHz, ^{13}C 100.61 MHz, ^{13}C 125.68 MHz, ^{31}P 161.98 MHz) or Varian Mercury (^{31}P 161.91 MHz) spectrometers from $CDCl_3$ solutions and referenced against solvent resonances (^1H, ^{13}C) or external H_3PO_4 (^{31}P). IR spectra were recorded using a Nicolet Avatar spectrometer from nujoll mull suspended between NaCl plates. Electrospray ionisation mass spectra were recorded using Thermo Quest Finnigan Trace MS-Trace GC or WATERS Micromass LCT spectrometers. Samples in dichloromethane (1 mg/mL) were 100 times diluted in either methanol or acetonitrile, and analysed with source and desolvation temperatures of 120 °C, with cone voltage of 30 V. High resolution spectra were recorded using a Thermo Electron Finnigan LTQ FT mass spectrometer with capillary temperature 275 °C and capillary voltage 100 V. MALDI- TOF spectra were recorded using an ABI Voyager STR spectrometer, with a 337 nm desorption laser, linear flight path and 2500 V accelerating voltage and *trans*-2-[3-(4-*tert*-Butylphenyl)-2-methyl-2-propenylidene]malonitrile (DCTB), purchased from Sigma–Aldrich, used as matrix. Samples were prepared from solutions containing 10 mg/ 1 L of the matrix and 1 mg/1 L of the sample and mixed 1:9 sample:matrix. Only 1 μL of the mixtures was used for analyses.

Diffraction data were collected at 120K on a Bruker SMART 6000 CCD (**27** and **29**) and on Bruker Proteum-M CCD (**30**) three-circle diffractometers, using graphite-monochromated Mo-K_α radiation. The diffracrometer was equipped with Cryostream (Oxford Cryosystems) low-temperature nitrogen cooling devices. The structures were solved by direct-methods and refined by full matrix least-squares against F^2 of all data using *SHELXTL* software. [63] All non-hydrogen atoms were refined in anisotropic approximation except the disordered ones, H atoms were placed into the calculated positions and refined in "riding" mode. The crystallographic data and parameters of the refinements are listed in **Table 4.10-Table 4.12**.

4.6.2. Experimental

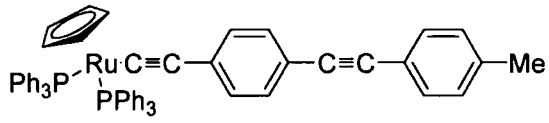

4.6.2.1. Preparation of Ru(C≡CC$_6$H$_4$C≡CC$_6$H$_4$Me)(PPh$_3$)$_2$Cp (25)

A solution of RuCl(PPh$_3$)$_2$Cp (100 mg, 0.14 mmol), Me$_3$SiC≡CC$_6$H$_4$C≡CC$_6$H$_4$Me (**1**) (44 mg, 0.15 mmol) and KF (1.2 mg, 0.021 mmol) in MeOH (10 ml) was heated at reflux for 20 mins to form a bright yellow precipitate, which was collected by filtration, washed with MeOH (3 ml), and air-dried to afford a yellow solid (82 mg, 63 %). Recrystallisation from CH_2Cl_2/MeOH gave bright yellow crystals of **25**. IR(nujol): ν(C≡C) 2063, 2212 cm^{-1}. ^{1}H NMR ($CDCl_3$, 400 MHz): δ 2.36 (s, 3H, Me), 4.33 (s, 5H, Cp), 7.03-7.49 (m, 38H, Ar). ^{13}C{^{1}H} NMR ($CDCl_3$, 100.6 MHz): δ 21.7 (Me), 85.5 (Cp); 89.6, 90.2 (C7, C8); 115.4, 117.4, 121.0 (C2, C6, C3); 123.2 (t, J_{CP} = 25 Hz, C1); 128.8 (C11); 129.3, 130.3, 131.1 (C4, C5, C10); 131.5 (C9); 127.5 (dd, $^3J_{CP}/^6J_{CP}$ ~ 5 Hz, C*m*); 128.7 (C*p*); 134.0 (dd, $^2J_{CP}/^5J_{CP}$ ~ 5 Hz, C*o*); 137.9 (C12); 139.0 (dd, $^1J_{CP}/^4J_{CP}$ ~ 11 Hz C*i*). ^{31}P{^{1}H} NMR ($CDCl_3$, 162 MHz): δ 51.3 (s, PPh$_3$). ES(+)-MS (m/z): 906, M$^+$; 691 [M-$C_{17}H_{11}$]$^+$. [High resolution: calculated for ^{101}RuC$_{58}$H$_{47}$P$_2$ [M+H]$^+$ 907.21910; found 907.22091. Found: C 76.17, H 5.03 %. C$_{58}$H$_{46}$P$_2$Ru requires: C 76.91, H 5.08 %.

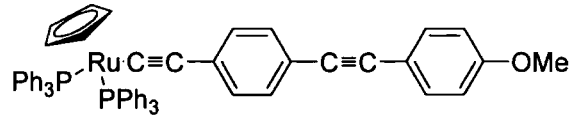

4.6.2.2. Preparation of Ru(C≡CC$_6$H$_4$C≡CC$_6$H$_4$OMe)(PPh$_3$)$_2$Cp (26)

A solution of RuCl(PPh$_3$)$_2$Cp (100 mg, 0.14 mmol), HC≡CC$_6$H$_4$C≡CC$_6$H$_4$OMe (**7**) (44 mg, 0.21 mmol) and NH_4PF_6 (44 mg, 0.14 mmol) in stirring MeOH (10 ml) was heated at reflux for 30 mins to form a bright yellow precipitate in a red-coloured solution, 2-3 drops of DBU was added to form more yellow precipitate which was collected by filtration, washed with cold MeOH (3 ml), and air-dried to afford a yellow solid (101 mg, 80 %). Recrystallisation from $CHCl_3$/hexane gave bright yellow crystals of **26**. IR(nujol): ν(C≡C) 2064, 2215 cm^{-1}.^{1}H NMR ($CDCl_3$, 400 MHz): δ 3.99 (s, 3H, OMe), 4.50 (s, 5H, Cp), 7.03-7.64 (m, 38H, Ar). ^{13}C{1H} NMR ($CDCl_3$, 125.7 MHz): δ 55.5 (OMe), 85.5 (Cp); 89.3, 89.5 (C7, C8); 115.4, 116.3, 117.5 (C2, C6, C3); 122.8 (t, J_{CP} = 25 Hz, C1); 114.2, 130.6, 131.2 (C4, C5, C10); 133.1, 131.3 (C9, C11); 127.5 (dd, $^3J_{CP}/^6J_{CP}$ ~ 5 Hz, C*m*); 128.7 (C*p*); 134.1 (dd, $^2J_{CP}/^5J_{CP}$ ~ 5 Hz, C*o*); 139.0 (dd, $^1J_{CP}/^4J_{CP}$ ~ 11 Hz C*i*); 159.5 (C12). ^{31}P{^{1}H} NMR ($CDCl_3$, 81 MHz): δ 51.3 (s, PPh_3) ES(+)-MS (m/z): 945, $[M+Na]^+$; 923, $[M+H]^+$; 691, $[M-C_{17}H_{11}O]^+$. [High resolution: calculated for $^{101}RuC_{58}H_{47}P_2O$ $[M+H]^+$ 932.21402; found 932.21683.

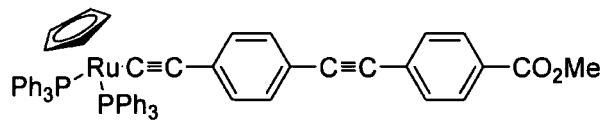

4.6.2.3. Preparation of Ru(C≡CC$_6$H$_4$C≡CC$_6$H$_4$CO$_2$Me)(PPh$_3$)$_2$Cp (27)

A solution of RuCl(PPh$_3$)$_2$Cp (100 mg, 0.14 mmol), HC≡CC$_6$H$_4$C≡CC$_6$H$_4$CO$_2$Me (**8**) (54 mg, 0.21 mmol) and NH_4PF_6 (44 mg, 0.14 mmol) in stirring MeOH (10 ml) was heated at reflux for 30 mins to form a bright yellow precipitate in red-coloured solution, with the addition of 2-3 drops DBU gave more yellow precipitate which was collected by filtration, washed with cold MeOH (3 ml), and air-dried to afford a yellow solid (95 mg, 73 %). Recrystallisation from $CHCl_3$/hexane gave bright yellow crystals of **27**. IR(nujol): ν(C≡C) 2064, 2202; (C≡O) 1724 cm^{-1}. ^{1}H NMR ($CDCl_3$, 400 MHz): δ 3.92 (s, 3H, OMe), 4.33 (s, 5H, Cp), 7.05-8.01 (m, 38H, Ar). ^{13}C{1H}

NMR ($CDCl_3$, 100.6 MHz): δ 52.4 (OMe), 85.5 (Cp); 89.0, 94.3 (C7, C8); 125.1 (t, J_{CP} = 25 Hz, C1); 115.6, 116.5, 132.3 (C2, C6, C3); 129.0(C11), 129.1 129.7, 130.4 (C4, C5, C10); 127.5 (dd, $^3J_{CP}/^6J_{CP}$ ~ 5 Hz, C*m*); 128.8 (C*p*); 131.5 (C9); 131.5 (C12); 134.0 (dd, $^2J_{CP}/^5J_{CP}$ ~ 5 Hz, C*o*); 138.9 (dd, $^1J_{CP}/^4J_{CP}$ ~ 11 Hz C*i*); 166.9 (C=O). $^{31}P\{^1H\}$ NMR ($CDCl_3$, 81 MHz): δ 51.3 (s, PPh_3). ES(+)-MS (m/z): 950, M+; 691, $[M\text{-}C_{18}H_{11}O_2]^+$. [High resolution: calculated for $^{101}RuC_{59}H_{47}P_2O_2$ $[M+H]^+$ 951.20893; found 951.21221.

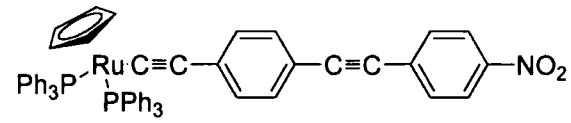

4.6.2.4. Preparation of $Ru(C{\equiv}CC_6H_4C{\equiv}CC_6H_4NO_2)(PPh_3)_2Cp$ (28)

A solution of $RuCl(PPh_3)_2Cp$ (100 mg, 0.14 mmol), $HC{\equiv}CC_6H_4C{\equiv}CC_6H_4NO_2$ (**9**) (51 mg, 0.21 mmol) and NH_4PF_6 (44 mg, 0.14 mmol) in stirring MeOH (10 ml) was heated at reflux for 30 mins to form a bright red precipitate. The addition of 2-3 drops DBU gave more yellow precipitate which was collected by filtration, washed with cold MeOH (3 ml), and air-dried to give a red solid followed by recrystallisation from $CHCl_3$/MeOH to afford bright red crystals of **28** (87 mg, 67 %). IR(nujol): ν(C≡C) 2063, 2200 cm^{-1}. ^1H NMR ($CDCl_3$, 400 MHz): δ 4.34 (s, 5H, Cp), 7.08-8.52 (m, 38H, Ar). $^{13}C\{1H\}$ NMR ($CDCl_3$, 125.7 MHz): δ 85.6 (Cp); 88.2, 97.1 (C7, C8); 115.9, 115.8, 130.8 (C2, C6, C3); 126.9 (t, J_{CP} = 25 Hz, C1); 123.9 (C11), 130.8, 131.7, 132.1 (C4, C5, C10); 127.5 (dd, $^3J_{CP}/^6J_{CP}$ ~ 5 Hz, C*m*); 128.8 (C*p*); 131.3 (C9); 134.1 (dd, $^2J_{CP}/^5J_{CP}$ ~ 5 Hz, C*o*); 138.9 (dd, $^1J_{CP}/^4J_{CP}$ ~ 11 Hz C*i*); 146.7 (C12). $^{31}P\{^1H\}$ NMR ($CDCl_3$, 81 MHz): δ 51.3 (s, PPh_3). ES(+)-MS(m/z): 938, $[M+H]^+$; 691, $[M\text{-}C_{16}H_8NO_2]^+$. [High resolution: calculated for $^{101}RuC_{57}H_{44}P_2O_2N$ $[M+H]^+$ 938.18853; found 938.19064.

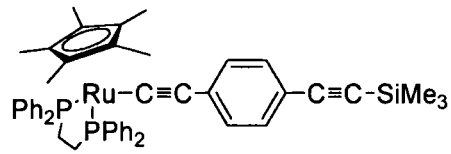

4.6.2.5. Preparation of $Ru(C{\equiv}CC_6H_4SiMe_3)(dppe)Cp^*$ (29)

A suspension of $RuCl(dppe)Cp^*$ (100 mg, 0.15 mmol), $Me_3SiC{\equiv}CC_6H_4C{\equiv}CSiMe_3$ (54 mg, 0.20 mmol), and KF (9.0 mg, 1.72 mmol) in methanol (10 ml) was heated at

reflux for 1 hour under a nitrogen atmosphere. The yellow precipitate formed was collected then washed with MeOH and hexane and dried to give **29** as a yellow powder (95 mg, 76%). IR(nujol): ν(C≡C) 2058, 2149 cm^{-1}. ^1H NMR ($CDCl_3$, 300 MHz): δ 0.29 (s, 9H, $SiMe_3$); 1.62 (s, 15H, Cp*), 2.21(2 x dd, 2H, $J_{HP} = J_{HH} \sim 6$ Hz,), 2.83 (2 x dd, 2H, $J_{HP} = J_{HH} \sim 6$ Hz); 6.65 (pseudo-d, $J_{HH} \sim 8$ Hz, 2H, C_6H_4); 7.10 (pseudo-d, $J_{HH} \sim 8$ Hz, 2H, C_6H_4); 7.18-7.79 (m, Ar 20H). $^{13}C\{1H\}$ NMR ($CDCl_3$, 100.6 MHz): δ 0.14 (s, $SiMe_3$); 10.0 (Me at Cp); 29.4 (dd, $J_{CP}/_{CCP} \sim 23$ Hz, CH_2); 92.7 (Cp); 89.3, 90.6 (C7, C8); 92.6 (Cp); 106.7, 110.9, 116.1(C2, C6, C3); 129.3, 130.3 (C4, C5); 135.6 (t, $J_{CP} = 25$ Hz, C1); 127.0, 127.3 (dds, $J_{CP}/_{CCP} \sim 5$ Hz, C*m*;*m*'); 128.7 (C*p*;*p*'); 133.4, 133.1 (dds, $J_{CP}/_{CCP} \sim 5$ Hz, C*o*;*o*'); 138.4, 138.7 (m, C*i*;*i*') $^{31}P\{^1H\}$ NMR ($CDCl_3$, 121.4 MHz): δ 81.8 (s, dppe). ES(+)-MS(m/z): 833, $[M+H]^+$. [High resolution: calculated for $^{101}RuC_{49}H_{52}P_2Si$ $[M+H]^+$ 833.24298; found 833.24442.

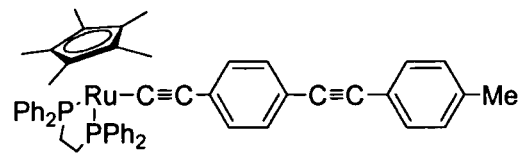

4.6.2.6. Preparation of Ru(C≡CC$_6$H$_4$C≡CC$_6$H$_4$Me)(dppe)Cp* (30)

A solution of RuCl(dppe)Cp* (100 mg, 0.14 mmol), HC≡CC$_6$H$_4$C≡CC$_6$H$_4$Me (**6**) (32 mg, 0.15 mmol) and NH_4PF_6 (24 mg, 0.15 mmol) in stirring MeOH (10 ml) was heated at reflux for 30 mins to form a bright yellow precipitate in red-coloured solution, at which point 2-3 drops of DBU were added to form more yellow precipitate which was collected by filtration, washed with cold MeOH (3 ml), and air-dried to afford **30** as a yellow solid (84 mg, 66 %). IR (nujol). ν(C≡C) 2062, 2206 cm^{-1}. ^1H NMR ($CDCl_3$, 400 MHz): δ 1.56 (s, 15H, Cp*), 2.08 (2 x dd, 2H, $J_{HP} = J_{HH} \sim 6$ Hz,), 2.68 (2 x dd, 2H, $J_{HP} = J_{HH} \sim 6$ Hz); 3.82 (s, 3H, Me); 6.70 (pseudo-d, $J_{HH} =$ 8 Hz, 2H, C_6H_4); 6.86 (pseudo-d, $J_{HH} \sim 9$ Hz, 2H, C_6H_4); 7.16-7.34 (m, 20H Ar); 7.43 (pseudo-d, $J_{HH} \sim 9$ Hz, 2H, C_6H_4); 7.75 (pseudo-d, $J_{HH} \sim 8$ Hz, 2H, C_6H_4). $^{13}C\{1H\}$ NMR ($CDCl_3$, 125.7 MHz): δ 10.3 (Me at Cp); 21.7 (Me); 29.6 (dd, $J_{CP}/_{CCP} \sim 23$ Hz, CH_2); 89.3, 90.4 (C7, C8); 92.9 (Cp); 111.1, 116.7, 121.1 (C2, C6, C3); 129.4 (C11); 129.3, 130.3, 131.1 (C4, C5, C10); 131.5 (C9); 135.6 (t, $J_{CP} = 25$ Hz, C1); 137.9 (C12); 127.7, 127.5 (dds, $J_{CP}/_{CCP} \sim 5$ Hz, C*m*;*m*'); 128.8 (C*p*;*p*'); 133.5, 133.2 (dds, $J_{CP}/_{CCP} \sim 5$ Hz, C*o*;*o*'); 138.4, 138.7 (m, C*i*;*i*') $^{31}P\{^1H\}$ NMR ($CDCl_3$, 81

MHz): δ 81.8 (s, dppe). ES(+)-MS(m/z): 851, $[M+H]^+$. [High resolution: calculated for $^{101}Ru_{53}H_{50}P_2$ $[M+H]^+$ 851.25040; found 851.25213.

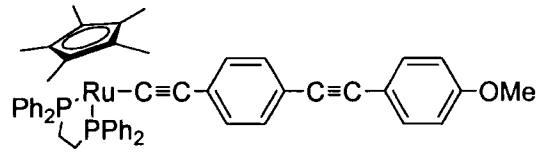

4.6.2.7. Preparation of Ru(C≡CC$_6$H$_4$C≡CC$_6$H$_4$OMe)(dppe)Cp* (31)

A solution of RuCl(dppe)Cp* (100 mg, 0.14 mmol), HC≡CC$_6$H$_4$C≡CC$_6$H$_4$OMe (**7**) (35 mg, 0.15 mmol) and NH_4PF_6 (24 mg, 0.15 mmol) in stirring MeOH (10 ml) was heated at reflux for 30 mins to form a bright yellow precipitate in red-coloured solution, at which point 2-3 drops of DBU were added to form more yellow precipitate which was collected by filtration, washed with cold MeOH (3 ml), and air-dried to afford **31** as a yellow solid (81 mg, 63 %). IR(nujol). ν(C≡C) 2061, 2206 cm^{-1}. ^1H NMR ($CDCl_3$, 400 MHz): δ 1.56 (s, 15H, Cp*), 2.09 (2 x dd, 2H, $J_{HP} = J_{HH}$ ~ 6 Hz,), 2.68 (2 x dd, 2H, $J_{HP} = J_{HH}$ ~ 6 Hz); 3.30 (s, 3H, OMe); 6.68 (pseudo-d, J_{HH} ~ 8 Hz, 2H, C_6H_4); 6.84 (pseudo-d, J_{HH} ~ 9 Hz, 2H, C_6H_4); 7.16 (pseudo-d, J_{HH} ~ 8 Hz, 2H, C_6H_4); 7.41 (pseudo-d, J_{HH} ~ 9 Hz, 2H, C_6H_4); 7.24-7.75 (m, 20H Ar). $^{13}C\{1H\}$ NMR ($CDCl_3$, 125.7 MHz): δ 10.0 (Me at Cp); 29.5 (dd, $J_{CP}/_{CCP}$ ~ 23 Hz, CH_2); 55.5 (s, OMe); 89.1, 89.6 (C7, C8); 92.5 (Cp); 111.0, 114.1, 116.4 (C2, C6, C3); 133.0, 131.4 (C9, C11); 114.2, 130.3, 131.0 (C4, C5, C10); 135.3 (t, J_{CP} = 25 Hz, Cα); 127.7, 127.5 (dds, $J_{CP}/_{CCP}$ ~ 5 Hz, Cm;m'); 128.8 (Cp;p'); 133.8, 133.2 (dds, $J_{CP}/_{CCP}$ ~ 5 Hz, Co;o'); 137.1, 139.0 (m, Ci;i'); 159.4 (C12). $^{31}P\{^1H\}$ NMR ($CDCl_3$, 81.8 MHz): δ 81.8 (s, dppe). ES(+)-MS(m/z): 867, $[M+H]^+$. [High resolution: calculated for $^{101}RuC_{53}H_{50}P_2O$ $[M+H]^+$ 867.24532; found 867.24611.

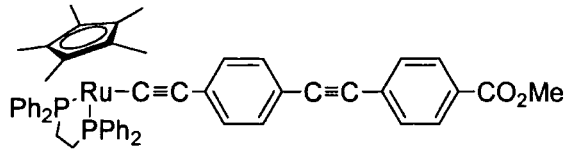

4.6.2.8. Preparation of Ru(C≡CC$_6$H$_4$C≡CC$_6$H$_4$CO$_2$Me)(dppe)Cp* (32)

A solution of RuCl(dppe)Cp* (100 mg, 0.14 mmol), HC≡CC$_6$H$_4$C≡CC$_6$H$_4$CO$_2$Me (**8**) (39 mg, 0.15 mmol) and NH_4PF_6 (24 mg, 0.15 mmol) in stirring MeOH (10 ml) was heated at reflux for 20 mins to form a bright yellow precipitate in red-coloured solution, at which point 2-3 drops of DBU were added to form more yellow precipitate which was collected by filtration, washed with cold MeOH (3 ml), and air-dried to afford **32** as a yellow solid (66 mg, 49 %). IR(nujol): ν(C≡C) 2061, 2208; (C=O) 1717 cm^{-1}. ^{1}H NMR ($CDCl_3$, 400 MHz): δ 1.56 (s, 15H, Cp*), 2.08 (2 x dd, 2H, $J_{HP} = J_{HH} \sim 6$ Hz), 2.68 (2 x dd, 2H, $J_{HP} = J_{HH} \sim 6$ Hz); 3.92 (s, 3H, OMe); 6.70 (pseudo-d, $J_{HH} \sim 8$ Hz, 2H, C_6H_4); 7.19 (pseudo-d, $J_{HH} \sim 8$ Hz, 2H, C_6H_4); 7.21-7.74 (m, 20H Ar); 7.52 (pseudo-d, $J_{HH} \sim 9$ Hz, 2H, C_6H_4); 7.98 (pseudo-d, $J_{HH} \sim 9$ Hz, 2H, C_6H_4. ^{13}C{1H} NMR ($CDCl_3$, 125.7 MHz): δ 10.0 (Me at Cp); 29.5 (dd, $J_{CP}/_{CCP} \sim 23$ Hz, CH_2); 52.4 (s, OMe); 92.5 (Cp); 88.8, 94.6 (C7, C8); 111.4, 115.8, 132.3 (C2, C6, C3); 137.8 (t, $J_{CP} = 25$ Hz, C1); 128.9 (C11), 129.1, 129.7, 130.7 (C4, C5, C10); 127.7, 127.2 (dds, $J_{CP}/_{CCP} \sim 5$ Hz, C*m*;*m*'); 128.8 (C*p*;*p*'); 131.3, 131.4 (C9, C12); 133.8, 133.2 (dds, $J_{CP}/_{CCP} \sim 5$ Hz, C*o*;*o*'); 137.1, 139.0 (m, C*i*;*i*'); 167.0 (C=O). ^{31}P{^{1}H} NMR ($CDCl_3$, 81.8 MHz): δ 81.8 (s, dppe). ES(+)-MS(m/z): 895, $[M+H]^+$. [High resolution: calculated for $^{101}RuC_{54}H_{51}P_2O_2$ $[M+H]^+$ 895.24023; found 895.24303.

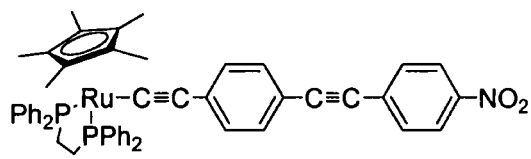

4.6.2.9. Preparation of Ru(C≡CC$_6$H$_4$C≡CC$_6$H$_4$NO$_2$)(dppe)Cp* (33)

A solution of RuCl(dppe)Cp* (100 mg, 0.14 mmol), HC≡CC$_6$H$_4$C≡CC$_6$H$_4$NO$_2$ (**9**) (37 mg, 0.15 mmol) and NH_4PF_6 (24 mg, 0.15 mmol) in stirring MeOH (10 ml) was heated at reflux for 30 mins to form a bright red precipitate, 2-3 drops of DBU were

added to form more red precipitate which was collected by filtration, washed with cold MeOH (3 ml), and air-dried to afford **33** as a red solid (66 mg, 50 %). IR(nujol): ν(C≡C) 2063, 2207 cm^{-1}. ^1H NMR ($CDCl_3$, 400 MHz): δ 1.56 (s, 15H, Cp*), 2.10 (2 x dd, 2H, $J_{HP} = J_{HH} \sim 6$ Hz,), 2.69 (2 x dd, 2H, $J_{HP} = J_{HH} \sim 6$ Hz); 6.72 (pseudo-d, J_{HH} = 8.4 Hz, 2H, C_6H_4); 7.20-7.34 (m, 20H, Ar); 7.60 (pseudo-d, J_{HH} = 8.8 Hz, 2H, C_6H_4); 7.74 (pseudo-d, J_{HH} = 8 Hz, 2H, C_6H_4); 8.20 (pseudo-d, J_{HH} = 8.8 Hz, 2H, C_6H_4). $^{13}C\{1H\}$ NMR ($CDCl_3$, 100.6 MHz): δ 10.0 (Me at Cp); 29.5 (dd, $J_{CP/CCP} \sim$ 23 Hz, CH_2); 87.8, 97.1 (C7, C8); 92.5 (Cp); 111.6, 114.8, 129.8 (C2, C6, C3); 132.7 (t, J_{CP} = 25 Hz, C1); 123.6 (C11); 129.8, 131.3, 131.7 (C4, C5, C10); 131.2 (C9); 127.5, 127.2 (dds, $J_{CP/CCP} \sim$ 5 Hz, C*m*;*m*'); 128.8 (C*p*;*p*'); 133.8, 133.2 (dds, $J_{CP/CCP} \sim$ 5 Hz, C*o*;*o*'); 137.1, 139.0 (m, C*i*;*i*'); 146.4 (C12). $^{31}P\{^1H\}$ NMR ($CDCl_3$, 81.0 MHz): δ. 81.7 (s, dppe). ES(+)-MS(m/z): 882, $[M+H]^+$. [High resolution: calculated for $^{101}RuC_{52}H_{47}P_2O_2N$ $[M+H]^+$ 882.21983; found 882.22115.

4.6.2.10.

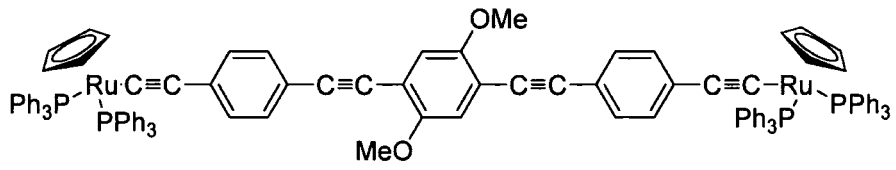

Preparation of {Ru(PPh$_3$)$_2$Cp}$_2$(μC≡CC$_6$H$_4$C≡CC$_6$H$_2$(OMe)$_2$C≡CC$_6$H$_4$C≡C) (34)

A solution of $RuCl(PPh_3)_2Cp$ (200 mg, 0.28 mmol), $HC{\equiv}CC_6H_4C{\equiv}CC_6H_2(OMe)_2C{\equiv}CC_6H_4C{\equiv}CH$ (**14**) (53 mg, 0.14 mmol) and NH_4PF_6 (90 mg, 0.55 mmol) in stirring MeOH (20 ml) was heated at reflux for 20 mins to form a bright yellow precipitate in red-coloured solution, with the addition of 2-3 drops of DBU was gave more yellow precipitate. It was then cooled in the ice-bath which was collected by filtration, washed with cold MeOH (3 ml), and air-dried to give **34** as a yellow solid. (177 mg, 73 %). IR(nujol): ν(C≡C) 2068, 2198 cm^{-1}.^1H NMR ($CDCl_3$, 400 MHz): 3.91 (s, 6H, OMe), 4.34 (s, 10H, Cp), 7.01-7.47 (m, 70H, Ar). $^{13}C\{1H\}$ NMR ($CDCl_3$, 125.7 MHz): δ 56.7 (s, OMe); 85.5 (Cp); 81.6, 86.0 (C7, C8); 115.6, 117.2, 119.9 (C2, C6, C3); 113.6, 130.6, 131.4 (C4, C5, C10); 122.7 (t, J_{CP} = 25 Hz, C1); 127.7 (dds, $J_{CP/CCP} \sim$ 5 Hz, C*m*;*m*'); 128.7 (C*p*;*p*'); 133.2 (C9); 133.8, 134.0 (dds, $J_{CP/CCP} \sim$ 5 Hz, C*o*;*o*'); 138.8, 139.1 (m, C*i*;*i*'); 153.9(C11).

$^{31}P\{^{1}H\}$ NMR ($CDCl_3$, 81 MHz): δ 51.3 (s, PPh_3). MALDI-MS (m/z): 1767, [M+H]. [High resolution: calculated for $^{101}Ru_2C_{110}H_{86}P_4O_2$ $[M]^+$ 1766.37057; found 1766.38675.

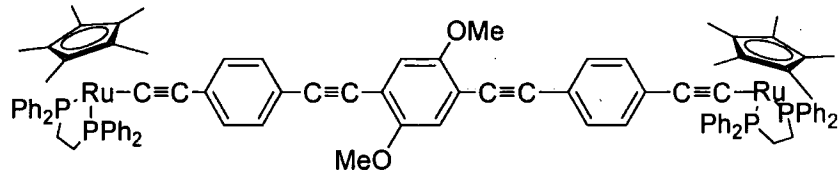

4.6.2.11. Preparation of {Ru(dppe)Cp*}$_2$(μC≡CC$_6$H$_4$C≡CC$_6$H$_2$(OMe)$_2$C≡CC$_6$H$_4$C≡C) (35)

A solution of RuCl(dppe)Cp* (100 mg, 0.15 mmol), HC≡CC$_6$H$_4$C≡CC$_6$H$_2$(OMe)$_2$C≡CC$_6$H$_4$C≡CH (**14**) (29 mg, 0.07 mmol) and NH_4PF_6 (24 mg, 0.15 mmol) in stirring MeOH (15 ml) was heated at reflux for 30 mins to form a bright yellow precipitate in red-coloured solution, with the addition of 2-3 drops of DBU gave more yellow precipitate. It was then cooled in the ice-bath which was collected by filtration, washed with cold MeOH (3 ml) followed by Et_2O (3ml), and air-dried to afford **35** as a yellow solid. (88 mg, 71 %). IR (nujol). ν(C≡C) 2054, 2192; ^{1}H NMR ($CDCl_3$, 400 MHz): δ 1.56(s, 15H, Cp*), 2.07 (2 x dd, 2H, $J_{HP} = J_{HH}$ ~ 6 Hz,), 2.68 (2 x dd, 2H, $J_{HP} = J_{HH}$ ~ 6 Hz); 3.88 , 6H, OMe); 6.71 (pseudo-d, J_{HH} ~ 8 Hz, 2H, C_6H_4); 6.97 (s, 2H, $C_6H_2(OMe)_2$); 7.22-7.76 (m, 46H Ar);. $^{13}C\{1H\}$ NMR ($CDCl_3$, 125.7 MHz): δ 10.3 (Me at Cp); 29.7 (dd, $J_{CP}/_{CCP}$ ~ 23 Hz, CH_2); 92.9 (Cp); 85.8, 96.8 (C7, C8); 111.4, 115.7, 116.5 (C2, C6, C3); 113.7, 130.2, 131.2 (C4, C5, C10); 131.7 (C9); 136.4 (t, J_{CP} = 25 Hz, C1); 127.4, 127.2 (dds, $J_{CP}/_{CCP}$ ~ 5 Hz, C*m*;*m*'); 128.8 (C*p*;*p*'); 133.9, 133.4 (dds, $J_{CP}/_{CCP}$ ~ 5 Hz, C*o*;*o*'); 137.1, 139.0 (m, C*i*;*i*'); 153.9 (C11). $^{31}P\{^{1}H\}$ NMR ($CDCl_3$, 162 MHz): δ 81.8 (s, dppe). MALDI(+)-MS(m/z): 1654, $[M+H]^+$. [High resolution: calculated for $^{101}Ru_2C_{100}H_{94}P_4O_2$ $[M]^+$ 1653.42981; found 1653.44770.

4.7. References

1. N. J. Long, C.K. Williams, *Angew. Chem. Int. Ed.*, 2003, **42**, 2586.
2. U. Belluco, R. Bertani, R.A. Michelin, M. Mozzon, *J. Organomet. Chem.*, 2000, **600**, 37.
3. M. C. Puerta, P. Valerga, *Coord. Chem. Rev.*, 1999, **193-5**, 977.
4. R. Zeissel, M. Hissler, A. El-Ghayoury, A. Harriman, *Coord. Chem. Rev.*, 1998, **178**, 1251.
5. W. Y. Wong, C.L. Ho, *Coord. Chem. Rev.*, 2006, **250**, 2627.
6. T. Ren, *Organometallics*, 2005, **24**, 4854.
7. R. Nast, *Coord. Chem. Rev.*, 1982, **47**, 89.
8. V. W. W. Yam, K.M.C. Wong, *Top. Curr. Chem.*, 2005, **257**, 1.
9. V. W. W. Yam, *Acc. Chem. Res.*, 2002, **35**, 555.
10. M. P. Cifuentes, M. G. Humphrey, *J. Organomet. Chem.*, 2004, **689**, 3968.
11. C. E. Powell, M.G. Humphrey, *Coord. Chem. Rev.*, 2004, **248**, 725.
12. M. Samoc, N. Gauthier, M.P. Cifuentes, F. Paul, C. Lapinte, M.G. Humphrey, *Angew. Chem. Int. Ed.*, 2006, **45**, 7376.
13. K. Costuas, F. Paul, L. Toupet, J.F. Halet, C. Lapinte, *Organometallics*, 2004, **23**, 2053.
14. I. R. Whittall, M. P. Cifuentes, M. G. Humphrey, B. Luther-Davies, M. Samoc, S. Houbrechts, A. Persoons, G. A. Heath, D. C. R. Hockless, *J. Organomet. Chem.*, 1997, **549**, 127.
15. M. I. Bruce, K. Costuas, T. Davin, B.G. Ellis, J. -F. Halet, C. Lapinte, P. J. Low, M. E. Smith, B. W. Skelton, L. Toupet, A. H. White, *Organometallics*, 2005, **24**, 3864.
16. M. I. Bruce, P. J. Low, K. Costuas, J. -F. Halet, S. P. Best, G. A. Heath, *J. Am. Chem. Soc.*, 2000, **122**, 1949.
17. O. F. Koentjoro, R. Rousseau, P.J. Low, *Organometallics*, 2001, **20**, 4502.
18. F. Paul, B. G. Ellis, M. I. Bruce, L. Toupet, T. Roisnel, K. Costuas, J.-F. Halet, C. Lapinte, *Organometallics*, 2006, **25**, 649.
19. M. A. Fox, R. L. Roberts, W. M. Khairul, F. Hartl, P. J. Low, *J.Organomet. Chem.*, 2007, **692**, 3277.

20. F. Paul, L. Toupet, J. Y. Thepot, K. Costuas, J. F. Halet, C. Lapinte, *Organometallics*, 2005, **24**, 5464.

21. M. I. Bruce, B. C. Hall, B. D. Kelly, P. J Low, B. W. Skelton, A. H. White, *J. Chem. Soc., Dalton Trans.*, 1999, 3719.

22. M. I. Bruce, B. C. Hall, P. J. Low, B. W. Skelton, A. H. White, *J. Organomet. Chem.*, 1999, **592**, 74.

23. A. Klein, O. Lavastre, J. Fiedler, *J. Organomet. Chem.*, 2006, **25**, 635.

24. J. A. Shaw-Tarbelet, S. Sinbandhit, T. Roisnel, J. –R. Hamon, C. Lapinte, *Organometallics*, 2006, **25**, 5311.

25. M. B. Robin, P. Day, *Inorg. Chem. Radiochem.*, 1967, **10**, 247.

26. K. D. Demadis, C. M. Hartshorn, T. J. Meyer, *Chem. Rev.*, 2001, **101**, 2655.

27. P. J. Low, R. L. Roberts, R. L Cordiner, F. Hartl, *J. Solid State Electrochem.*, 2005, **9**, 717.

28. M. I. Bruce, *Chem. Rev.*, 1991, **91**, 197.

29. R. L. Cordiner, D. Albesa-Jové, R. L. Roberts, J. D. Farmer, H. Puschmann, D. Corcoran, A. E. Goeta, J. A. K. Howard, P. J. Low, *J. Organomet. Chem.*, 2005, **690**, 4908.

30. M. I. Bruce, R. C. Wallis, *J. Organomet. Chem.*, 1978, **161**, C1.

31. C. Bitcon, M. W. Whitely, *J. Organomet. Chem.*, 1987, **336**, 385.

32. C. E. Powell, M. P. Cifuentes, A. M. McDonoagh, S. K. Hurst, N. T. Lucas, C. D. Delfs, R. Stranger, M. G. Humphrey, S. Houbrechts, I. Asselberghs, A. Persoons, D. C. R. Hockless, *Inorg. Chim. Acta*, 2003, **352**, 9.

33. S. K. Hurst, N. T. Lucas, M. P. Cifuentes, M. G. Humphrey, M. Samoc, B. Luther-Davies, I. Asselberghs, R. Van Boxel, A. Persoons, *J. Organomet, Chem.*, 2001, **633**, 114.

34. N. T. Lucas, M. P. Cifuentes, L. T. Nguyen, M. G. Humphrey, *J. Cluster Sci.*, 2001, **12**, 201.

35. I. R. Whittall, M. G. Humphrey, A. Persoons, S. Houbrechts, *Organometallics*, 1996, **15**, 1935.

36. I. R. Whittall, M. G. Humphrey, D. C. R. Hockless, B. W. Skelton, A. H. White, *Organometallics*, 1995, **14**, 3970.

37. N. J. Long, A. J. Martin, F. Fabrizi de Biani, P. Zanello, *J. Chem. Soc., Dalton Trans.*, 1998, 2017.

38. I.-Y. Wu, J. T. Lin, C.-S. Li, C. Tsai, Y. S. Wen, C.-C. Hsu, F. -F. Yeh, S. Liou, *Organometallics*, 1998, **17**, 2188.

39. I.-Y. Wu, J. T. Lin, J. Luo, S.-S. Sun, C.-S. Li, K. L. Lin, C. Tsai, C.-C. Hsu. J.-L. Lin, *Organometallics*, 1997, **16**, 2038.

40. C. J. McAdam, A.R. Manning, B.H. Robinson, J. Simpson, *Inorg. Chim. Acta*, 2005, **358**, 1673.

41. A. Mishra, D.S. Pandey, K. Mishra, U.C. Agarwala, *Ind. J. Chem. A*, 1990, **29A**, 251.

42. D. L. Lichtenberger, S. K. Renshaw, R. M. Bullock, *J. Am. Chem. Soc.*, 1993, **115**, 3276.

43. J. E. McGrady, T. Lovell, R. Stranger, M. G. Humphrey, *Organometallics*, 1997, **16**, 4004.

44. C. D. Delfs, R. Stranger, M. G. Humphrey, A. M. McDonagh, *J. Organomet. Chem.*, 2000, **607**, 208.

45. G. Connelly, W. E. Geiger, *Chem. Rev.*, 1996, **96**, 877.

46. M. Krejčík, M. Daněk, F. Hartl, *J. Electroanal. Chem.*, 1991, **317**,179.

47. J. M. Wisner, T. J. Bartczak, J. A. Ibers, *Inorg. Chim. Acta*, 1985, **100**, 115.

48. M. I. Bruce, M. G. Humphrey, M. R. Snow, E. R. T. Tiekink, *J. Organomet. Chem.*, 1986, **314**, 213

49. A. P. Scott and L. Radom, *J. Phys. Chem.*, 1996, **100**, 16502.

50. J. C. Roder, F. Meyer, I. Hyla-Kryspin, R.F. Winter, E. Kaifer, *Chem. Eur. J.*, 2003, **9**, 2636.

51. C. E. Powell, M. P. Cifuentes, J. P. Morrall, R. Stranger, M. G. Humphrey, M. Samoc, B. Luther-Davies, G. A. Heath, *J. Am. Chem. Soc.*, 2003, **125**, 602.

52. C. Y. Wong, C. -M. Che, M. C. W. Chan, J. Han, K .H. Leung, D. L. Phillips, K. Y. Wong, N. Y. Zhu, *J. Am. Chem. Soc.*, 2005, **127**, 13997.

53. M. I. Bruce, C. Hamesiter, A. G. Swincer, R. C. Wallis, *Inorg. Synth.*, 1990, **28**, 270.

54. I. R. Whittall, M. G. Humphrey, *Organometallics*, 1995, **14**, 3970.

55. M. I. Bruce, K. Costuas, J. –F. Halet, B. C. Hall, P. J. Low, B. K. Nicholson, B.W. Skelton, A. H. White, *Dalton Trans.*, 2002, 383.

56. R. L. Cordiner, D. Corcoran, D. S. Yufit, A. E. Goeta, J. A. K. Howard, P. J. Low, *Dalton. Trans.*, 2003, 3541.

57. M. I. Bruce, P. Hinterding, E. R. T. Tiekink, B. W. Skelton, A. H. White, J. *Organomet. Chem.*, 1993, **450**, 209.

58. S. W. Watt, C. Dai, A. J. Scott, J. M. Burke, R. L. Thomas, J. C. Collings, C. Viney, W. Clegg, T. B. Marder, *Angew. Chem. Int. Ed.*, 2004, **43**, 3061.

59. W. M. Khairul, L. Porres, D. Albesa-Jove, M. S. Senn, M. Jones, D. P. Lydon, J. A. K. Howard, A. Beeby, T. B. Marder, P. J. Low, *J. Cluster Sci.*, 2006, **17**, 65.

60. M. Biswas, P. Nguyen, T. B. Marder, L. R. Khundkar, *J. Phys. Chem. A,* 1997, **101**, 1689.

61. M. I. Bruce, B. G. Ellis, P. J. Low, B. W. Skelton, A. H. White, *Organometallics*, 2002, **22**, 3184.

62. D. R. Walton, F. Waugh, *J. Organomet. Chem.*, 1972, **27**, 45.

63. *SHELXTL, version 6.14,* Bruker AXS, Madison, Wisconsin, USA, 2000.

64. M. I. Bruce, C. Hameister, A. G. Swincer, R. C. Wallis, *Inorg. Synth.*, 1982, **21**, 78.

Chapter 5 'Photophysical and Electrochemical Properties of Triruthenium Carbonyl Clusters Featuring Phenylene Ethnylene Ligands'

5.1. Introduction

Recent studies have shown that oriented thiol-terminated conjugated rigid-rod molecules have the ability to conduct electrons to and from metallic surfaces. [1-3] This demonstration has led to many studies of such systems with a view to the preparation of viable molecular-based wires for use in future electronic devices. A common approach often employed in the study of the conductivity molecular wires is to attach an organic molecule with an extended, conjugated π-system to metal surface, most frequently the thiol linkage to gold, and to a Scanning Tunneling Microscopy (STM) tip to form the top contact. [4] For single-molecule electronics considerable effort has been invested in the design and the synthesis of the molecules but, the nature of the molecule-surface contact is not clear, nor has the significance of the mode of the attachment in the overall performance of the molecular wire been fully established. [5,6] With a view to expanding the range of available metal-molecule binding groups, and to help establish the role of these groups on the overall performance of single-molecule devices, an increasing number of studies utilising surface-binding groups other than thiols and surfaces other than gold have been conducted.[7-10] For example, long alkyl chains can be covalently linked to silicon surfaces and are particularly appealing "second generation" binding groups. [11-13]

Metal clusters offer an opportunity to study the nature of small-molecule/surface interactions. [14] Although the cluster-surface analogy should not be taken literally, well-defined molecular cluster models have been used to refine current understanding of the preferred binding sites of molecular tethers in numerous computational investigations. [15-17] However, the use of synthetic models systems in this regard is less well established. [18]

While gold is perhaps the most often used metal substrate in molecular electronics, the attributes of ruthenium as an electrode material, such as its ability to form hard

thin films, have recently being highlighted. [5] Metal cluster chemistry is now a mature science, [19] and the extensive chemistry of ruthenium carbonyls and phosphine substituted derivatives suggests these materials are suitable initial model systems for ruthenium surfaces.

Given the ready preparation of ethynyl terminated phenylene ethynylenes, and the rich coordination chemistry of the C≡CH group to clusters, systems of the general type $HC{\equiv}C\{C_6H_4C{\equiv}C\}_nC_6H_4R$ offer an attractive entry point for the further development of the clusters as surface model in molecular electronics. Multimetallic end-caps to phenylene ethynylene moieties, especially those larger than 1,4-diethynyl aromatics, are less common than mononuclear species; examples include those prepared by Adams and co-workers during their investigations of the binding modes of a thiol-terminated 1,4-bis(phenylethynyl)benzene to osmium clusters. [20]

Although reactions of terminal alkynes with carbonyl clusters such as $Ru_3(CO)_{12}$ or the activated derivative $Ru_3(CO)_{10}(NCMe)_2$ usually result in the generation of products derived from cluster fragmentation and alkyne coupling, [21,22] and in some cases, to yield complexes with unusual structures, [23] terminal acetylenes and gold alkynyls $Au(C{\equiv}CR)(PR'_3)$ both react readily with $Ru_3(CO)_{10}(\mu\text{-dppm})$ to give alkynyl clusters $Ru_3(\mu\text{-X})(\mu\text{-}C_2R)(CO)_7(\mu\text{-dppm})$ (X = H, $AuPR'_3$) in high yield. [24] Very recently, the Bruce group have used a combination of these reactions of gold acetylides as part of a strategy to prepare bis(cluster) complexes featuring bridging C_4 ligands. [25]

Several related gold-containing Ru_3 and Os_3 clusters works have been synthesised by [26] while other examples, such as $AuRu_3(\mu_3, \eta^2\text{-}C_2Bu^t)(CO)_9(PPh_3)$ have been obtained from $Ru_3(\mu\text{-H})$ $(\mu_3, \eta^2\text{-}C_2Bu^t)(CO)_9(PPh_3)$ by deprotonation with NaH or K-Selectride followed by reaction of the resulting monoanion with $AuCl(PPh_3)$. [27]

Further examples of mixed-metal gold-ruthenium complexes were prepared by addition of $Au(C_2Ph)(PR_3)$ (R = Ph, tol) to $Ru_3(\mu\text{-dppm})(CO)_{10}$. [24] The likely pathway of this reaction has been mapped through reactions involving Os clusters.

Oxidative addition of $Au(C{\equiv}CPh)(PR_2Ph)$ (R = Me, Ph) to $Os_3(CO)_{10}(NCMe)_2$ afforded $AuOs_3(\mu, \eta^2\text{-}C_2Ph)(CO)_{10}(Pr_2Ph)$ which on heating undergoes decarboxylation to form the μ_3, η-alkynyl complex $AuOs_3(\mu_3, \eta^2\text{-}C_2Ph)(CO)_9(Pr_2Ph)$. [28]

Other examples of the clusters $Ru_3(\mu\text{-}R)(CO)_{10}$ prepared from more exotic extended acetylenes include products from the reaction between $Ru_3(CO)_{10}(NCMe)_2$ with $W(C{\equiv}CC{\equiv}CH)(CO)_3Cp$. The initial product $Ru_3\{\mu_3\text{-}HC_2C{\equiv}C[W(CO)_3Cp]\}(\mu\text{-}CO)(CO)_9$, was readily converted into the corresponding hydrido-alkynyl cluster $Ru_3(\mu\text{-}H)\{\mu_3\text{-}C_2C{\equiv}C[W(CO)_3Cp]\}(CO)_9$ by brief heating in refluxing benzene. [29] Whilst reaction between $Ru_3(\mu\text{-dppm})(CO)_{10}$ with *cis*-$Pt(C{\equiv}CC{\equiv}CH)_2(dppe)$ gave $Ru_3(\mu\text{-}H)\{\mu_3\text{-}\eta^2\text{-}C_2C{\equiv}C[Pt(C{\equiv}CC{\equiv}CH)(dppe)]\}(\mu\text{-dppm})(CO)_7$. [30]

In this report, reactions of terminal acetylene tolan of $HC{\equiv}CC_6H_4C{\equiv}CC_6H_4Me$, **6** and $HC{\equiv}CC_6H_4C{\equiv}CC_6H_4CO_2Me$, **8** with $Ru_3(CO)_{10}(\mu\text{-dppm})$ that afforded products $Ru_3(\mu\text{-}H)(\mu\text{-}C_2C_6H_4C{\equiv}CC_6H_4Me)(CO)_7(\mu\text{-dppm})$ (**36**) and $Ru_3(\mu\text{-}H)(\mu\text{-}C_2C_6H_4C{\equiv}CC_6H_4OMe)(CO)_7(\mu\text{-dppm})$ (**37**), in which the the hydride-bridged clusters 'end-cap' the phenylene ethynylene fragment, are described. The isolobal relationship between H and $(AuPR_3)$ links clusters **36** and **37** with the $AuPPh_3$ bridged clusters **38-42** (**Scheme 5.1**). In addition, the availability of bis(gold)(I) complex, $\{Au(PPh_3)\}_2(\mu\text{-}C{\equiv}CC_6H_4C{\equiv}CC_6H_4C{\equiv}CC_6H_4C{\equiv}C)$, **23**, has led the preparation of bis-cluster **43** (**Scheme 5.3**).The syntheses, molecular structural analyses, electrochemical and photophysical properties of these complexes are fully described and thoroughly discussed in this chapter.

5.2. Result and Discussion

5.2.2. Syntheses

Reactions of the readily synthesised terminal alkynes tolans, $HC{\equiv}CC_6H_4C{\equiv}CC_6H_4R$ [R = Me (**6**); = CO_2Me (**8**) with $Ru_3(CO)_{10}(\mu$-dppm) were carried out in refluxing THF. Purification of the products was carried out by preparative TLC followed by recrystallisation from chlorofom/hexane to give bright yellow $Ru_3(\mu$-H)(μ-$C{\equiv}CC_6H_4C{\equiv}CC_6H_4R(CO)_7(\mu$-dppm) clusters featuring a bridging-hydride ligand[R = Me (**36**); = CO_2Me (**37**) in 41 and 25 % yield respectively (**Scheme 5.1**).

Both of the clusters were characterised by the usual spectroscopic methods. In the ^1H NMR spectra, the hydride ligands were detected as doublets near δ_H -19 ppm (J_{HP} = 33 Hz). In addition, methyl and methyl ester resonances at δ_H 2.38 and δ_H 3.94 ppm in **36** and **37** respectively were also observed. Two sets of doublet-of-triplet (dt) signals were observed at ca. δ_H 3.3 and δ_H 4.3 ppm ($J_{HP} = J_{HH}$ = 11 Hz), arising from the two methylene protons of the dppm moieties. However, the numerous aromatic protons in **36** and **37** were not fully resolved, but were observed as series of heavily overlapped δ_H 6.4-8.1 ppm. The pseudo-doublet resonances from the tolan portion of the molecule were not distinctly observed.

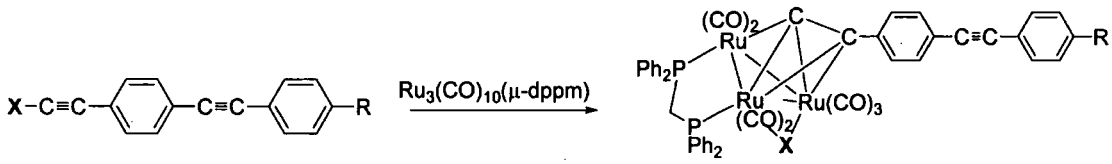

X = H; R = Me (**36**), CO_2Me (**37**)

X = $AuPPh_3$; R = Me (**38**), OMe (**39**), CO_2Me (**40**), NO_2 (**41**), CN (**42**)

Scheme 5.1. Synthesis of clusters **36-42**.

The ^{31}P NMR spectra of **36** and **37** were characterised by a pair of doublets (J_{PP} = 54 Hz), indicating the inequivalence of the phosphorus centres; the resonances near δ_P 34 ppm and δ_P 38 ppm were broadened by unresolved J_{PH} coupling. These

spectroscopic parameters are similar to those of other $Ru_3(\mu\text{-}H)(\mu\text{-}C_2R)(Co)_7(\mu\text{-}dppm)$ species. [31-36]

IR spectra recorded in cyclohexane solutions in a cell fitted with CaF_2 windows showed ν(CO) carbonyl bands of variable intensities between 1940-2064 cm^{-1}. In addition to these bands, both clusters show weak acetylenic bands ν(C≡C) which were observed above 2200 cm^{-1}, and for **37**, an additional strong ν(C=O) band was observed at 1731 cm^{-1}. The electrospray mass spectra [ES-MS]+ showed the aggregate of $[M+K]^+$ ions at *m/z* 1139 (**36**) and at *m/z* 1185 (**37**). The simple protonated species $[M+H]^+$ was also found for **36** as well as the molecular ion M^+ at *m/z* 1146 for **37**.

In a manner similar to that described above, the reaction of the gold complexes $Au(C{\equiv}CC_6H_4C{\equiv}CC_6H_4R)PPh_3$ [R = Me(**15**), OMe (**16**), CO_2Me (**17**), NO_2 (**18**), CN (**19**)] with $Ru_3(CO)_{10}(\mu\text{-dppm})$, in refluxing THF, gave $Ru_3(\mu\text{-}AuPPh_3)(\mu\text{-}C_2C_6H_4C{\equiv}CC_6H_4R)(CO)_7(\mu\text{-dppm})$ [R = Me (**38**), OMe (**39**), CO_2Me (**40**), NO_2 (**41**), CN (**42**) in 12-50 % yield. The hydride ligand in **36** and **37** has been formally substituted by the isolobal $Au(PPh_3)$ fragment (**Scheme 5.1**). Similar species have been obtained from reactions of gold acetylides with triangulo triruthenium clusters. [24,25,37] or through the auration of cluster anions obtained by deprotonation of the corresponding hydride clusters. [26,27]

The ^1H NMR spectra of these clusters show similar characteristics to the hydride-bridging clusters (**36** and **37**) except for the loss of the hydride signal by the replacement of the $(AuPPh_3)$ moiety. The similarities include the methyl resonance can be observed at δ_H 2.37 for **38**. In addition, methoxy and methyl ester resonances of **39** and **40** can be observed above δ_H 2 ppm. Two sets of doublet-of-triplet (dt) signals can be observed at ca. δ_H 3.3 and δ_H 4.3 ppm (J_{HP} = 11-14 Hz, J_{HH} = 10-11 Hz) arising from the methylene protons of the dppm moieties. However, as might be expected, the numerous aromatic protons in **38-42** were not fully resolved, but were observed as series of heavily overlapped δ_H 6.4-8.2 ppm. The pseudo-doublet resonances from the tolan portion of the molecule were not distinctly observed.

The ^{31}P NMR spectra was particularly informative, with the three chemically distinct phosphine centres giving rise to a characteristic pattern in which the resonance from P(2) (for labelling scheme see **Scheme 5.2**) was split into a doublet of doublets at ca. δ_P 41 ppm (J_{PP} = 62 Hz, J_{PP} = 39 Hz) by coupling to both the gold bound phosphine P(1) at ca. δ_P 61 ppm (J_{PP} = 39 Hz) and the dppm phosphorus centre P(3) at ca. δ_P 39 ppm (d, J_{PP} = 62 Hz).

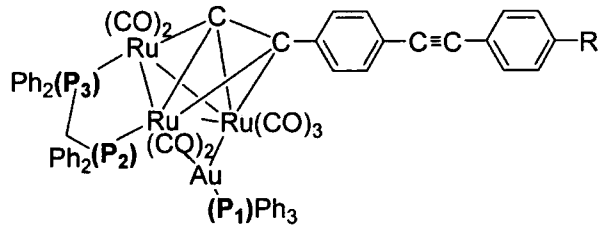

Scheme 5.2. A plot of ($AuPPh_3$) bridging clusters of **38-42** showing the location of three phosphorus centres.

The IR spectra of **38-42** were recorded in cyclohexane solutions in a cell fitted with CaF_2 windows show carbonyl bands of variable intensities in between 1910-2038 cm^{-1}. The ν(CO band pattern is almost the same in each member of the series **38-42** with no apparent systematic shift in frequency that could be attributed to variation in π-back-bonding from the ruthenium centres brought by the electron-donating or –withdrawing properties of the tolan susbtituent. The electronic environment at each cluster core is therefore similar. In addition to these strong ν(CO) bands, weak acetylenic bands ν(C≡C) were observed above 2200 cm^{-1}, and for **40** a strong ν(C=O) band can be seen at 1720 cm^{-1}, while for **42**, a strong nitrile ν(CN) band also can be observed at 2212 cm^{-1}.

The electrospray ionisation mass spectrum $(ES)^+$-(MS) showed the aggregate ion $[M+AuPPh_3]^+$, for **38** at *m/z* 2016 and **42** at *m/z* 2028 and phosphine auration fragmentation $[Au(PPh_3)_2]^+$ at *m/z* 721 for **39-41**. In addition to these fragmentations ions, simple protonated species $[M+H]^+$ also can be observed for all complexes.

The bis(cluster) $\{Ru_3(\mu\text{-}AuPPh_3)(CO)_7(\mu\text{-}dppm)\}_2(\mu\text{-}C_2C_6H_4C{\equiv}CC_6H_4C{\equiv}CC_6H_4C_2)$ (**43**) was obtained in 48% yield from the stoichiometric reaction of the di-gold reagent $\{Au(PPh_3)\}_2(\mu\text{-}C{\equiv}CC_6H_4C{\equiv}CC_6H_4C{\equiv}CC_6H_4C{\equiv}C)$, **23** and $Ru_3(CO)_{10}(\mu\text{-}dppm)$ (**Scheme 5.3**). The complex was isolated as a pure powder following preparative TLC.

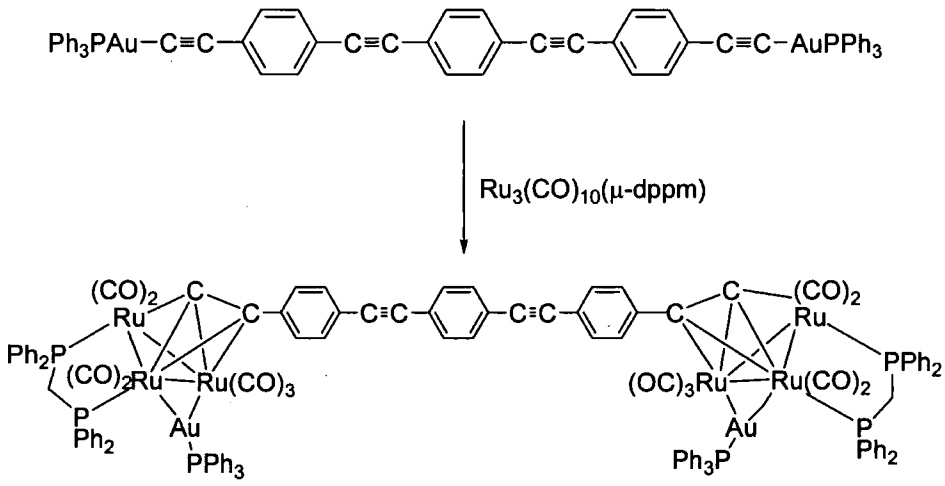

Scheme 5.3. Synthesis of bis-cluster **43**.

In the ^1H NMR spectrum of **43**, the dppm protons are observed as two sets of doublet-of-triplet (dt) signals at ca. δ_H 3.3 and δ_H 4.2 ppm (J_{HP} = 10 Hz, J_{HH} = 14 Hz). As was the case for the monoclusters **36-37** and **38-42**, the numerous aromatic protons in **43** were not fully resolved, but were also observed as series of heavily overlapped δ_H 6.4-8.0 ppm. The pseudo-doublet resonances from the diethynyl -1,4-bis(phenylethynyl)benzene portion of the molecule were not distinctly observed.

The symmetrical nature of the complex was established by the observation of ^{31}P NMR and IR [ν(CO)] spectra essentially identical to those of monoclusters (**38-42**) whereas in the ^{31}P NMR spectrum, the three chemically distinct phosphine centres giving rise to a characteristic pattern in which the resonance from P(2) (for labelling scheme see **Scheme 5.2**) was split into a doublet of doublets at ca. δ_P 41 ppm (J_{PP} = 62 Hz, J_{PP} = 39 Hz) by coupling to both the gold bound phosphine P(1) at ca. δ_P 61 ppm (J_{PP} = 39 Hz) and the dppm phosphorus centre P(3) at ca. δ_P 38 ppm (d, J_{PP} = 62

Hz). The IR spectrum of the carbonyl bands ν(CO) can be observed as variable intensities in between 1907-2032 cm^{-1}

Whilst in the electrospray mass spectrum of **43**, the molecular ion was observed as an isotopic envelope centred at *m/z* 3010, together with adducts of higher mass for which accurate mass measurements suggest formulations of $[M+K]^+$ and $[M+K+NCMe]^{2+}$ as well as $[M+2K]^{2+}$ at m/z 1544.

5.2.3. Molecular Structural Analyses

The molecular structures of **36-42** have been determined by single crystal X-ray diffraction as shown in **Figure 5.1** to **Figure 5.4**. Crystallographic data, selected bond lengths and angles are listed in **Table 5.1**, **Table 5.2** and **Table 5.3** The crystallographic work has been carried out by Dr D. S. Yufit and Dr Albesa-Jové.

Molecular Structure of $Ru_3(\mu\text{-}H)(\mu\text{-}C_2C_6H_4C{\equiv}CC_6H_4R)(CO)_7(\mu\text{-dppm})$ (R = Me (36) and CO_2Me (37)

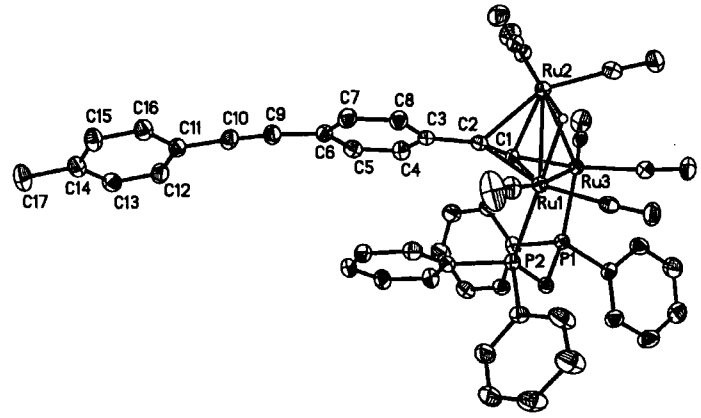

36

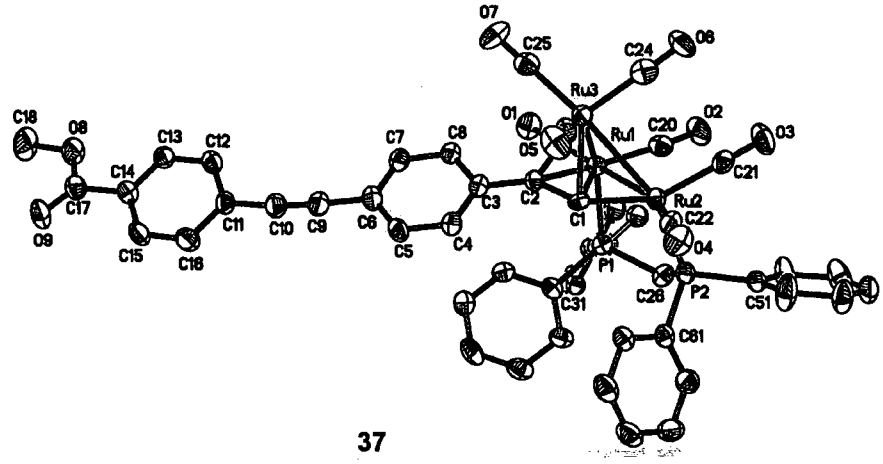

37

Figure 5.1. A plot of a molecule of **36** and **37** illustrating the atom numbering scheme.

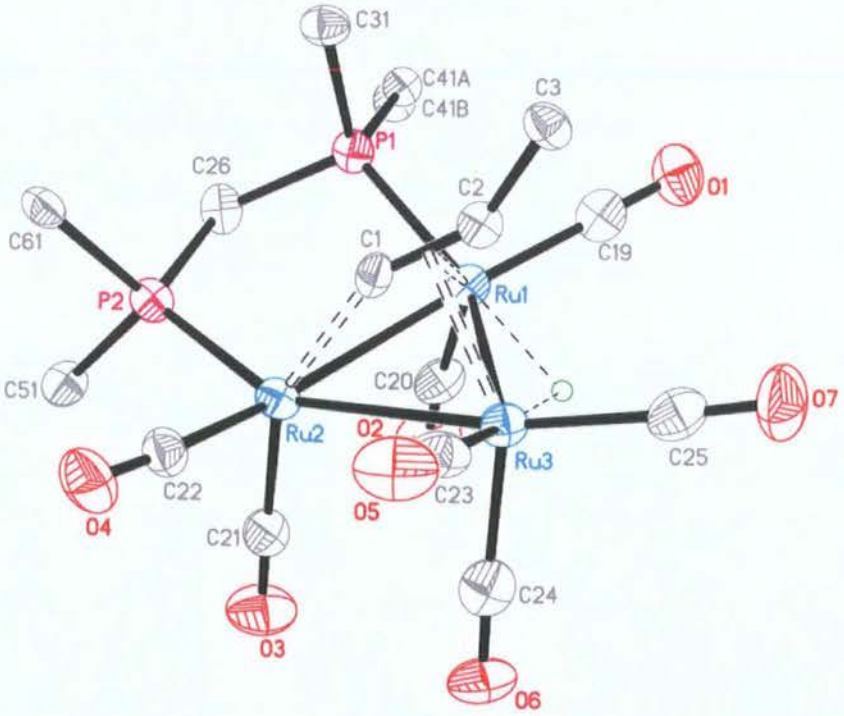

Figure 5.2. The 'core' of the Ru_3-bridging of the molecules **36** and **37**.

Table 5.1. Crystal data for **36** and **37**.

	36	**37**
Molecular formula	$C_{49}H_{34}O_7P_2Ru_3$	$C_{50}H_{34}O_9P_2Ru_3\,xCl_3CH$
M / g mol^{-1}	1099.1	1263.29
Crystal system	Monoclinic	Monoclinic
a / Å	10.6155(7)	14.7618(4)
b / Å	32.425(2)	19.3952(5)
c / Å	13.0009(8)	18.3016(5)
α / °	90	90
β / °	94.43(1)	101.86(1)
γ / °	90	90
V / Å^3	4461.7(5)	5128.1(2)
Space group	P2(1)/n	P 2_1/c
Z	4	4
D_c / Mg m^3	1.637	1.636
Crystal size / mm	0.24×0.18×0.04	0.40×0.12×0.08
Crystal habit	plate	plate
F (000)	2184	2504
Radiation	Mo(K_α)	Mo(K_α)
Wavelength / Å	0.71073	0.71073
μ / mm^{-1}	1.637	1.145
Temperature / K	120(2)	120(2)
Data collection range / °	2.01-26.00	1.55-28.00
Reflections measured	27650	36577
Data, restraints, parameters	8747, 0, 555	8284, 9, 596
R_1, *wR2* (all data)	0.0583, 0.1043	0.0799, 0.1053
Goodness-of-fit on F^2 (all data)	1.052	0.961
peak, hole / eÅ^{-3}	1.553, -0.977	0.851, -0.618

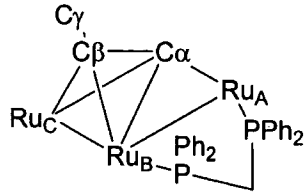

Figure 5.3. The core geometry representative of molecule **36**and **37**.

Table 5.2. Selected bond lengths (Å) for **36** and **37**.

	36	**37**
C(1)-C(2)	1.309(6)	1.315(6)
C(2)-C(3)	1.461(6)	1.460(7)
C(3)-C(4, 8)	1.403(6), 1.400(6)	1.393(7), 1.407(7)
C(4)-C(5),C(7)-C(8)	1.379(6), 1.388(6)	1.387(7), 1.382(7)
C(6)-C(5, 7)	1.399(6), 1.395(7)	1.392(7), 1.399(7)
C(6)-C(9)	1.438(6)	1.433(7)
C(9)-C(10)	1.199(6)	1.182(7)
C(10)-C(11)	1.439(6)	1.436(7)
C(11)-C(12, 16)	1.383(7), 1.392(7)	1.393(7), 1.390(7)
C(12)-C(13), C(16)-C(15)	1.380(6), 1.378(6)	1.375(7), 1.381(8)
C(14)-C(13, 15)	1.399(7), 1.387(7)	1.376(7), 1.391(7)
Ru(1)-C(1)	2.184(4)	2.192(4)
Ru(1)-H(1)	1.80(5)	1.73(5)
Ru(1)-C(2)	2.243(4)	2.246(5)
Ru(2)-C(1)	2.201(4)	1.956(5)
Ru(2)-C(2)	2.263(4)	2.273(4)
Ru(3)-C(1)	1.934(4)	2.223(4)
Ru(1)-P(2)	2.3049(11)	2.3205(14)
Ru(2/3)-P(1/3)	2.3023(11)	2.2920(13)
Ru(1)-Ru(2)	2.7724(5)	2.7966(6)
Ru(1)-Ru(3)	2.8277(5)	2.7935(6)

Ru(2)-Ru(3)	2.8312(5)	2.8035(6)

Table 5.2. Selected bond angles (°) for **36** and **37** (cont.)

	36	**37**
Ru(3)-C(1)-C(2)	156.3(4)	156.7(2)
C(1)-C(2)-C(3)	137.8(4)	145.4(5)
C(6)-C(9)-C(10)	174.9(5)	174.2(6)
C(9)-C(10)-C(11)	176.7(5)	174.9(6)
Ru(1)-Ru(2)-Ru(3)	60.60(1)	59.847(14)
Ru(1)-Ru(3)-Ru(2)	58.67(1)	59.955(14)
Ru(2)-Ru(1)-Ru(3)	60.73(1)	60.199(14)

Molecular Analyses of 36 and 37

There are few, if any, differences within the structures of the H-bridged clusters **36** and **37**, and so discussion of the geometry of **36** may be taken as representative of the molecular structures in this series. The cluster core geometry of Ru_3-bridging of the molecules **36** and **37** is illustrated schematically in **Figure 5.2.** Whereas for the 'bigger picture' of the bond lengths (Å) and angles (°) of the structures, the core geometry representative of molecules **36** and **37** is shown in **Figure 5.3**. Similarly, in the case of the heterometallic complexes, **38** may be used as a reference point for description and discussion.

36: The cluster **36** contains a triangular Ru_3 metal framework with a hydride ligand, which was found in the difference map and refined, bridging the Ru(1)-Ru(2) edge (**Figure 5.1a** and **Figure 5.2**). The Ru(1)-Ru(3) bond is supported by the dppm ligand [Ru(1,3)-P(2,1) 2.3049(11), 2.3023(11) Å], while the C(1)-C(2) moiety caps

one triangular face in the expected μ,η^1,η^2,η^2 mode. As a consequence of the interactions with the metal centres, the C(1)-C(2) bond [1.309 Å] is elongated when compared with that in **15**. The C(9)≡C(10) alkyne bond is normal [1.199(6) Å]. The Ru-Ru bond lengths range from 2.7724(5) Å, for Ru(1)-Ru(2), to 2.8312(5) Å for the non-bridged Ru(2)-Ru(3) bond. There is no evidence for distortion of the phenylene ethynylene structure.

Molecular Structure of $Ru_3(\mu\text{-}AuPPh_3)(\mu\text{-}C_2C_6H_4C{\equiv}CC_6H_4R)(CO)_7(\mu\text{-}dppm)$ [R = Me (38), OMe (39), CO_2Me (40), NO_2 (41) and CN (42)]

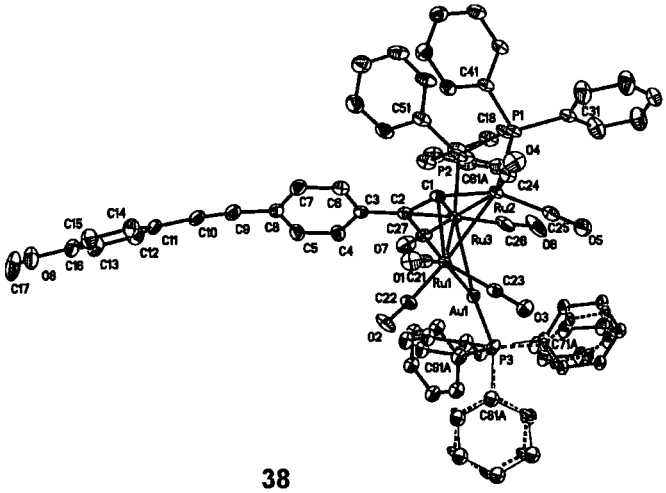

38

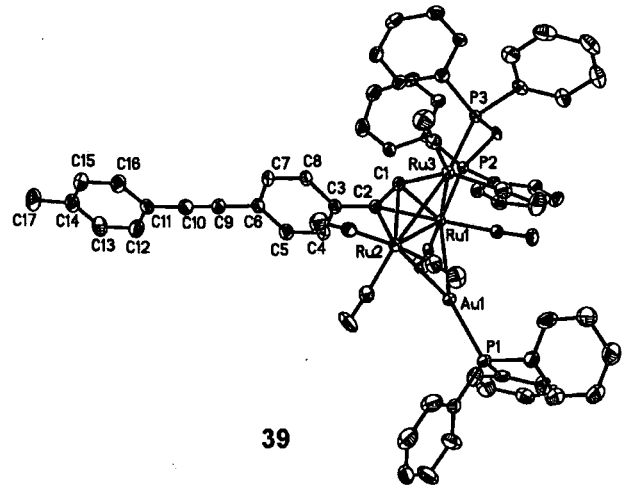

39

Figure 5.4. A plot of molecules of **(a) 38** and **(b) 39** illustrating the atom numbering scheme.

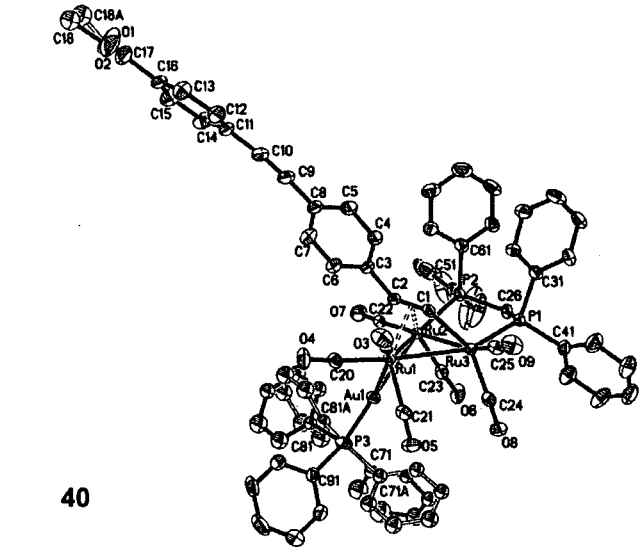

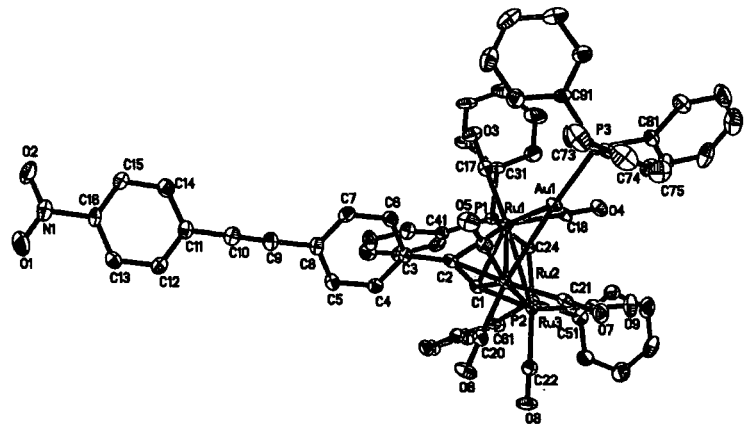

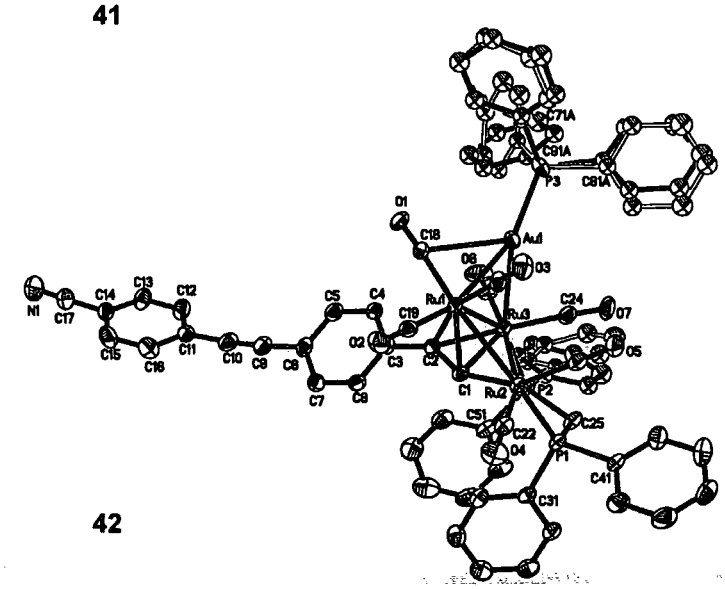

Figure 5.4.(cont.) A plot of molecules of **(c)** 40, **(d) 41, and (e) 42** illustrating the atom numbering scheme.

Table 5.3. Crystal data for **38– 42**.

	38	**39**	**40**	**41**	**42**
Molecular formula	$C_{67}H_{48}O_7P_3Ru_3Au$	$C_{67}H_{48}O_8P_3Ru_3Au$	$C_{69}H_{48}O_9P_3Ru_3Au$ x $CHCl_3$	$C_{67}H_{46}O_9NP_3Ru_3Au$ .Cl_3	$C_{67}H_{45}O_7NP_3Ru_3Au$ x $CHCl_3$
M / g mol^{-1}	1558.14	1574.14	1702.51	1708.48	1688.49
Crystal system	Triclinic	Monoclinic	Monoclinic	Monoclinic	Monoclinic
a / Å	11.1228(5)	11.0042(12)	11.0952(2)	11.1445(18)	11.0569(3)
b / Å	15.3234(7)	27.520(3)	27.417(5)	27.492(4)	27.3570(7)
c / Å	19.8213(9)	20.590(2)	23.226(4)	23.130(16)	20.6694(5)
α / °	89.79(1)	90	90	90	90
β / °	85.77(1)	90.544(3)	115.83(7)	118.255(6)	91.71(1)
γ / °	87.72(1)	90	90	90	90
V / Å^3	3366.5(3)	6234.9(11)	6359.0(2)	6242.3(16)	6249.4(3)
Space group	P-1	P2(1)/n	$P2_1/c$	$P2_1/c$	$P2_1/c$
Z	2	4	4	4	4
D_c / Mg m^3	1.537	1.677	1.797	1.818	1.795
Crystal size / mm	0.20×0.16×0.04	0.34x0.24x0.22	0.20x0.12x0.06	0.10x0.10x0.04	0.26x0.14x0.06
Crystal habit	plate	plate	plate	plate	plate
F (000)	1524	3080	3364	3336	3296

Table 5.3. Crystal data for **38– 42**.(cont.)

Radiation	$Mo(K_\alpha)$	$Mo(K_\alpha)$	$Mo(K_\alpha)$	$Mo(K_\alpha)$	$Mo(K_\alpha)$
Wavelength / Å	0.71073	0.71073	0.71073	0.71073	0.71073
μ / mm^{-1}	2.951	3.189	3.258	3.319	3.312
Temperature / K	120(2)	120(2)	120(2)	120(2)	120(2)
Data collection range / °	1.03-30.53	1.24-30.52	2.59-29.50	2.35-28.30	1.49-31.00
Reflections measured	45893	84736	71159	63851	65628
Data, restraints, parameters	20358, 0, 731	1903, 0, 578	17700, 12, 738	15492, 0, 784	19840, 0, 655
R_1, *wR2* (all data)	0.0654, 0.1008	0.0435, 0.0925	0.0649, 0.0991	0.0572, 0.0865	0.0497, 0.0714
Goodness-of-fit on F^2 (all data)	0.952	1.106	1.006	1.067	1.055
peak, hole / eÅ^{-3}	1.946, -1.969	2.161, -1.461	1.871, -1.359	3.191,-1.796	1.281,-1.213

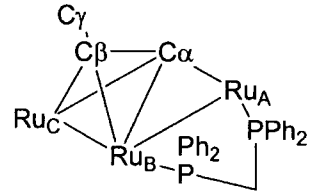

Figure 5.5. The core geometry representative of molecule **38-42**

Table 5.4. Selected bond length (Å) 'core geometry' for **38** to **42**.

	38	**39**	**40**	**41**	**42**
Ru_A-Ru_B	2.7994(4)	2.8394(4)	2.7933(6)	2.7987(5)	2.8353(3)
Ru_A-Ru_C	2.8345(5)	2.7861(4)	2.8451(7)	2.8140(6)	2.7987(3)
Ru_A-C_α	2.198(4)	2.210(3)	2.213(4)	2.186(4)	2.218(2)
Ru_A-C_β	2.217(4)	2.243(3)	2.229(4)	2.229(4)	2.229(3)
Ru_B-Ru_C	2.8330(5)	2.8271(4)	2.8248(6)	2.8321(6)	2.8175(3)
Ru_B-C_α	2.201(4)	1.947(3)	2.191(4)	2.223(4)	1.951(3)
Ru_B-C_β	2.273(4)	2.231(3)	2.238(4)	2.242(4)	2.231(3)
Ru_C-C_α	1.939(4)	2.193(3)	1.944(4)	1.952(4)	2.192(3)
C_α-C_β	1.322(6)	1.324(5)	1.318(6)	1.318(6)	1.322(4)
C_β-C_γ	1.458(5)	1.460(5)	1.460(6)	1.459(6)	1.470(4)

Table 5.4. Selected bond lengths (Å) for **38** to **42** (cont.)

	38	**39**	**40**	**41**	**42**
C(γ)-C(4, 8)	1.394(6),	1.390(5),	1.400(7),	1.398(6),	1.396(4),
	1.402(6)	1.406(5)	1.382(7)	1.397(6)	1.396(4)
C(4)-C(5),C(7)-	1.386(6),	1.391(5),	1.383(6),	1.378(6),	1.383(4),
C(8)	1.374(6)	1.392(6)	1.389(8)	1.399(6)	1.381(4)
C(6)-C(5, 7)	1.386(6),	1.395(5),	1.378(7),	1.403(6),	1.400(4),
	1.395(6)	1.392(5)	1.389(8)	1.373(6)	1.398(4)
C(6)-C(9)	1.442(6)	1.441(5)	1.437(7)	1.432(6)	1.436(4)
C(9)-C(10)	1.198(6)	1.196(5)	1.196(7)	1.201(6)	1.191(5)
C(10)-C(11)	1.429(6)	1.433(5)	1.450(7)	1.432(6)	1.434(5)
C(11)-C(12, 16)	1.396(7),	1.388(6),	1.376(7),	1.383(7),	1.393(4),
	1.389(7)	1.400(5)	1.384(8)	1.391(7)	1.390(5)
C(12)-C(13),	1.391(7),	1.392(6),	1.388(7),	1.383(7),	1.382(5),
C(16)-C(15)	1.398(6)	1.392(6)	1.381(6)	1.379(7)	1.376(5)
C(14)-C(13, 15)	1.390(7),	1.392(5),	1.377(7),	1.377(7),	1.385(5),
	1.378(7)	1.376(5)	1.381(6)	1.377(7)	1.388(5)
Ru(α)-P(β)	2.3173(10)	2.2881(9)	2.3272(11)	2.3164(11)	2.3261(7)
Ru(β/γ)-P(1/3)	2.2881(11)	2.3241(9)	2.2897(11)	2.2925(11)	2.2940(7)
Au(1)-Ru(α)	2.7533(3)	2.7825(3)	2.7889(5)	2.7808(5)	2.7853(2)
Au(1)-Ru(β)	2.7794(4)	2.7920(3)	2.7882(5)	2.7766(5)	2.7836(2)
Au(1)-P(1)	2.2848(10)	2.2924(9)	2.2976(12)	2.2912(11)	2.2974(7)

Table 5.5. Selected bond angles (°) for **38** to **42** (cont.)

	38	**39**	**40**	**41**	**42**
Ru(γ)-C(α)-C(β)	154.8(3)	151.89(2)	154.0(3)	153.1(3)	152.8(2)
C(α)-C(β)-C(γ)	139.4(4)	140.7(3)	142.2(4)	141.6(4)	141.8(3)
C(6)-C(9)-C(10)	177.3(5)	173.8(4)	175.3(6)	176.9(5)	174.8(3)
C(9)-C(10)-C(11)	177.3(6)	176.3(4)	174.0(6)	178.5(5)	173.1(3)
Ru(α)-Au(1)-Ru(β)	60.79(1)	59.972(9)	59.932(13)	60.48(1)	60.338(6)
Ru(α)-Ru(β)-Ru(γ)	60.43(1)	58.901(8)	60.848(16)	59.96(2)	60.006(7)
Ru(α)-Ru(γ)-Ru(β)	59.20(1)	60.768(11)	59.029(11)	59.430(11)	60.643(8)
Ru(β)-Ru(α)-Ru(γ)	60.37(1)	60.330(11)	60.123(15)	60.61(2)	59.351(7)

Molecular Analyses of 38-42

38: The structure of **38** differs from that of **36** by formal replacement of the bridging hydride with the isolobal μ-Au(PPh_3) fragment. The C(1)-C(2) and Ru(1)-P(2) bonds in **38** are longer than in **36**. Conversely, Ru(1)-C(2) is significantly shorter. Metallation of the Ru(1)-Ru(2) bond therefore appears to reduce the amount of electron density available at Ru(1), giving rise to a weaker Ru(1)-P(2) back-bonding interaction and promoting a greater interaction with the acetylide π-system. There is a small expansion of the Ru_3 core in **38** relative to that in **36** brought about by metallation of the Ru(1)-Ru(2) bond. Again, there is no evidence for distortion of the phenylene ethynylene structure.

There are few, if any, differences of note within the structures of **38-42**. Like the hydride-bridging Ru_3 clusters, the cluster core geometry is illustrated schematically in **Figure 5.5**. The selected bond lengths (Å) and angles (°) are summarised in **Table 5.3** and **Table 5.4**. The clusters **38-42** feature a triangular Ru_3 metal framework, with the Au(PPh_3) moiety bridging the Ru_B–Ru_C bond, and the Ru_A–Ru_B bond supported by the bridging dppm ligand. The gold supported metal-metal bond is the shortest of

the three Ru–Ru bonds in the cluster, with the unsupported Ru_A–Ru_C bond generally being the longest. The C(1)–C(2) acetylide ligand caps the triangular face in the expected μ_3-η^1,η^2,η^2 mode. As a consequence of the interaction with the metal centres, this bond is elongated in comparison to typical acetylenic C≡C bond lengths [1.318(6) – 1.324(5) Å]. The tolan C(9)≡C(10) alkyne bond is in the normal range [1.191(5) – 1.201(6) Å].

Planar tolan structures are thought to be more conducting than conformers in which the phenyl ring systems are twisted with respect to one another. [38-40] Thus, whilst the barrier to rotation about the aryl–ethynyl single bond is small in the gas phase and in solution, [41-43] much of the interest in the solid-state structures of tolan and related oligo(phenylene ethynylene) compounds lies in the analysis of the inter-ring torsion angles. In the case of the clusters **38-42**, the dihedral angles between the planes of the tolan phenyl rings range from 33.2-42.8°.

In much the same way as observed in the structures of the parent compounds of $Au(C{\equiv}CC_6H_4C{\equiv}CC_6H_4R)(PPh_3)$ [R = Me **(15)**; OMe **(16)**; CO_2Me **(17)**; NO_2 **(18)**; CN **(19)**] (see **Chapter 3**), the packing of the molecules **38-42** in the crystalline state is also determined by a number of relatively weak C-H...X (X = O, Cl, π) interactions. However, the presence of carbonyl ligands and solvent molecules in these clusters structures result in a much more complicated 3D-network of these interactions than was observed in the structures of parent compounds of the gold(I) acetylides. There are no obvious stacking π...π interactions between tolan ligand fragments in the case of the cluster structures, likely a consequence of the significant steric bulk of the cluster "end-cap".

5.2.4. Electrochemical Properties

Transition metal clusters typically offer closely spaced frontier orbitals with a significant metal character. This can lead to a rich electrochemical response in these systems, and has led to the description of cluster compounds as "electron sinks". [44-46] This potential for redox activity, coupled with the ready spectroscopic probes offered

by both the carbonyl ligands and several of the remote substituents (e.g., the ester and nitro groups) prompted examination of the heterometallic (Ru_3-Au) clusters **38-41** and their mononuclear (phosphine)Au-tolan precursors **15-18** using cyclic voltammetry and, in selected examples, IR spectroelectrochemical methods. Compounds **42** and **19** were not included in the spectro-electrochemical studies. These studies were carried out in collaboration with Dr Frantisek Hartl of the University of Amsterdam.

5.2.4.1. Cyclic Voltammetry

The cyclic voltammograms of the mononuclear gold complexes **15-18** in dichloromethane show totally irreversible anodic [O2, between 0.85-1.15 V vs Fc/Fc^+] and cathodic [R2 < −2.20 V vs Fc/Fc^+] waves close to, or beyond, the limits of the solvent potential window (**Table 5.5**). Indeed, for **15** and **16** which feature electron-donating tolan substituents R = Me and OMe, respectively, the cathodic waves are shifted beyond the limit of the electrochemical window. These irreversible redox processes were not studied in detail. Complex **18** shows an additional cathodic wave R1 at −1.47 V, which is fully reversible and apparently belongs to the reduction of the remote R = NO_2 substituent.

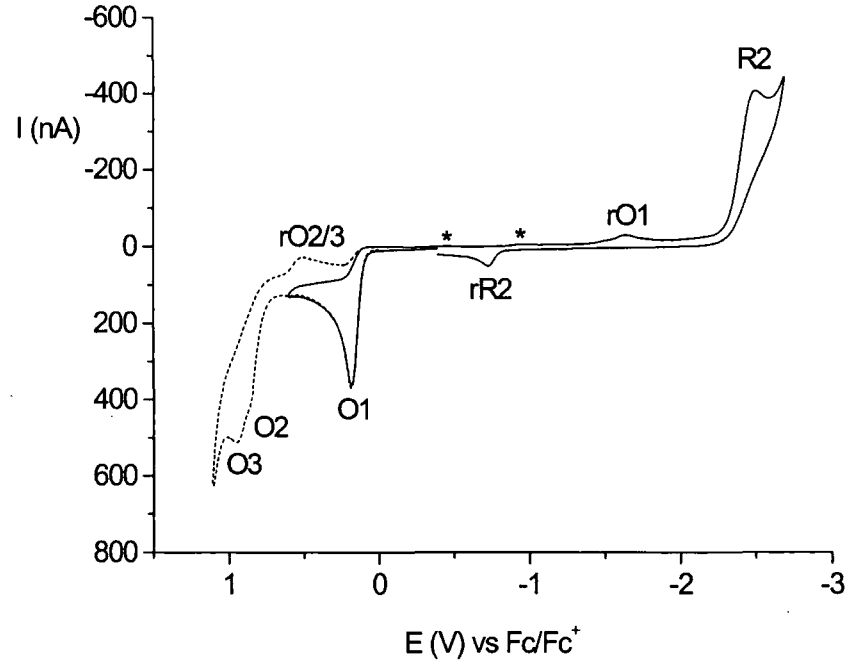

Figure 5.6. Cyclic voltammogram of heterometallic cluster **40** (R = OMe). The asterisks denote two small cathodic peaks observed in addition to rO1 during the reverse cathodic scan triggered beyond O1. Experimental conditions: carefully polished Pt disk microelectrode, dichloromethane containing 10^{-1} M Bu_4NPF_6, v = 100 mV s^{-1} at 293 K.

The cyclic voltammograms of the heterometallic clusters **38-41** exhibit irreversible redox processes at very similar electrode potentials to those observed in the precursors **15-18** (**Table 5.5, Figure 5.6**). The similarity of these electrochemical events point to their localisation at the terminal 1,2-diphenylacetylene moiety, indicating that the tolan chain is not significantly affected by coordination to the triruthenium cluster core through the acetylide moiety. The anodic waves O2 partly overlap with higher-lying irreversible waves O3, which are not observed for **15-18**. The chemically irreversible nature of R2 is further illustrated by the presence of a new anodic wave rR2 arising in the course of the reverse potential scan initiated beyond R2 (**Figure 5.6**). This wave is shifted some 1.7-1.8 V positively relative to R2, and arises from oxidation of an unassigned secondary reduction product.

Table 5.5. Electrochemical properties of the Au-tolan complexes **15-18** and corresponding heterometallic cluster compounds **38-41**.[a]

Compound	$E_{p,c}$ (R2, tolan)	$E_{1/2}$ (R1, NO_2)	$E_{p,a}$ (O1, Ru_3-core)	$E_{p,a}$ (O2/O3, tolan)
15	*not observed*	--	--	0.94
16	*not observed*	--	--	0.88
17	−2.37	--	--	1.14
18	−2.23	−1.49	--	1.13
38	−2.49	--	0.19	0.93/1.02
39	−2.48	--	0.18	0.88/0.95
40[b]	−2.35	--	0.25	1.04/1.16
41	−2.16	−1.47	0.29	1.02/1.15

[a] Redox potentials (V vs Fc/Fc^+) were determined from cyclic voltammetric scans. Experimental conditions: Pt disk working microelectrode, v = 100 mV s^{-1}, T = 293 K. E_p denotes peak potential of a chemically irreversible step. [b] See **Figure 5.6**.

The nitro group in **41** is reduced at essentially the same cathodic potential R1 as that in **18** (**Table 5.5**). At room temperature, the peak-to-peak separation ($\Delta E_p = E_{p,c} - E_{p,a}$) for this redox couple (100 mV) is only slightly larger than the value of 80 mV determined for the Fc/Fc^+ internal standard. At 206 K, however, the ΔE_p value of the nitro reduction increases to 600 mV while that of the internal Fc/Fc^+ standard does not change. The electrochemically quasireversible to irreversible nature of the cathodic step R1 in **41** may reflect some hindered access of the remote NO_2 group to the electrode surface, and in turn sluggish electron transfer kinetics.

The dominant new feature in the cyclic voltammograms of clusters **38-41** is the irreversible two-electron anodic wave O1 (**Table 5.5**, **Figure 5.6**) that corresponds to oxidation of the triruthenium cluster core. The reverse cathodic scan at room temperature reveals the presence of three small cathodic peaks due to reduction of secondary oxidation products, which are shifted significantly more negatively from O1, for example in the case of **38** by 0.63, 1.13 and 1.81 V, respectively. The minor dependence of the anodic potentials O1 on the nature of the electron donating or

withdrawing substituents R, (R = Me, OMe, CO_2Me or NO_2) reflects a rather limited degree of electronic communication between the cluster core and the substituted tolan moiety, in agreement with the conclusions drawn from the IR spectra of the **38-41** series (see below).

5.2.4.2. IR Spectroelectrochemistry

The triruthenium clusters **38** (R = Me), **40** (R = CO_2Me) and **41** (R = NO_2) were selected for IR spectroelectrochemical investigations aimed at obtaining more information about the electronic communication between the cluster core and the remote substituent R on the conjugated tolan chain. These experiments were carried out in dichloromethane solutions containing 10^{-1} M NBu_4PF_6 as supporting electrolyte. For reference purposes, the carbonyl stretching frequencies of the parent compounds are listed in the Experimental section.

One-electron reduction of the nitro group in compound **41** at the electrode potential R1 (**Table 5.5**) led to the expected disappearance of the absorption bands at 1519 and 1344 cm^{-1}, which can be attributed to the $\nu_{as}(NO_2)$ and $\nu_s(NO_2)$ modes, respectively. [47] A new band arose at 1367 cm^{-1}, assigned to $\nu_{as}(NO_2)$. [48] In addition, an absorption band at 1589 cm^{-1} was replaced by a new one at 1568 cm^{-1} that may be due to a nitrobenzene ring ν(C=C) mode. This NO_2-localized reduction also results in a low-frequency shift of the ν(C≡C) band from 2213 to 2186 cm^{-1}. The ν(C≡O) band pattern of the carbonyl-triruthenium fragment was almost unchanged by the reduction, with wavenumbers of individual bands decreasing by only 1-2 cm^{-1}, in agreement with the weak influence of the nitro group on the electronic properties of the metal centres and hence hardly affecting the ruthenium-to-CO π-back-bonding interactions. Apparently, the NO_2 substituent is relatively strongly conjugated with the uncoordinated acetylene moiety of the cluster-anchored tolan ligand, while interactions with the cluster core are more limited.

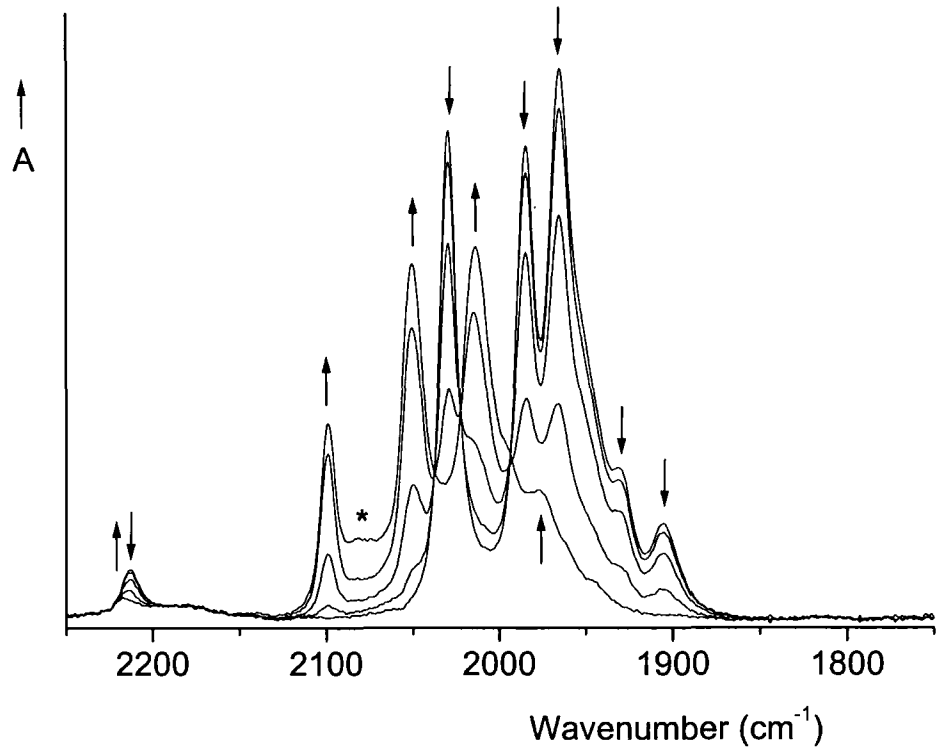

Figure 5.7. IR spectral changes in the C≡C and C≡O stretching region observed during the irreversible oxidation of complex **41** at the anodic wave O1 (**Table 5.5**) in CH_2Cl_2 at 293 K, using an OTTLE cell. The asterisk denotes a product of a slow thermal reaction of the oxidized complex.

The first oxidation event is clearly cluster centred (**Table 5.5**). The $\nu_{as}(NO_2)$ and $\nu_s(NO_2)$ bands shifted by 2 and 1 cm^{-1}, respectively, to higher frequencies when the triruthenium cluster core in **41** was oxidized at the anodic potential O1 (**Table 5.5**). In addition, the oxidation at potential O1 was accompanied by a ν(C≡C) shift to 2217 cm^{-1} (**Figure 5.7**), which is a significantly smaller absolute shift (3 cm^{-1}) than that induced by the NO_2 reduction (27 cm^{-1}). Perhaps surprisingly, the irreversible oxidation of the cluster core largely preserved the ν(C≡O) band pattern, with the oxidation product exhibiting ν(CO) bands at 2100m, 2051s, 2014s, 1997sh, 1977mw, 1962sh and 1947w cm^{-1} (**Figure 5.7**). The shift of the ν(C≡O) bands to higher wavenumbers by 40-70 cm^{-1}, the greatest shift being associated with the fully symmetric all-CO-stretching mode, is consistent with the two-electron nature of the

oxidation wave O1. Whilst it is beyond the scope of this work to determine the structure of the oxidation product, we can, however, state firmly that the irreversible two-electron oxidation of **41** does not induce a rapid CO dissociation reaction and that the geometry of the triruthenium-carbonyl moiety remains largely preserved after this initial oxidation event. The initially observed oxidation product is, however, thermally unstable and slowly converts to another carbonyl cluster species, as judged from a new absorption at 2081 cm^{-1} (**Figure 5.7**).

The oxidation products derived from **38** and **40** were significantly more chemically reactive, with rapid *in situ* electrochemical oxidation of either species resulting directly in a product with a ν(C≡O) band pattern (2083m, 2074sh, 2049m, 2035s, 2024m, 2008s, 1995m-s, 1983m, 1960m-w, 1946sh and 1917w cm^{-1}) quite different from the parent clusters being observed in each case. In line with the very limited electronic communication between the X group and the cluster core, the ν(C=O) band of the ester moiety in **40** was almost unchanged, shifting from 1720 cm^{-1} in **40** to 1722 cm^{-1} in the oxidized species. Interestingly, oxidation of **38** and **40** caused the ν(C≡C) band to completely disappear. This observation is in sharp contrast with the *in situ* electrochemical oxidation of cluster **41**, where the ν(C≡C) band is initially preserved (**Figure 5.7**). We assume that the ethynylene moiety in **38** and **40** features in fast chemical reactions that follow the initial two-electron oxidation. In contrast, the conjugation of the acetylene moiety to the nitro-phenyl-acetylene unit in **41** appears to stabilise the initial oxidation product to such an extent that it can be observed by IR spectroelectrochemical methods at room temperature.

5.2.5. Photophysical Properties

5.2.5.1. UV-Vis Spectroscopy

The electronic absorption spectra of the ligand precursors **1-5**, the mononuclear gold complexes **15-19** and the heterometallic clusters **38-42** were recorded as dilute (1-10 μmol dm^{-3}) solutions in CH_2Cl_2 (**Table 5.6**). The spectra of **1-3** and **5** are characteristic of the tolan (1,2-diphenylacetylene) moiety, exhibiting three relatively

intense transitions between ca. 280 – 350 nm. [18,49] The spectrum of nitro-substituted derivative **4** contains a broad absorption band from the nitrobenzene moiety centred near 340 nm. Substitution of the $SiMe_3$ group for $Au(PPh_3)$ resulted in little change to these spectroscopic profiles. As noted previously, the UV-vis absorption spectra of the cluster derivatives **38-42** exhibit several new features that were not present in the spectra of the precursors **1-5** and **15-19**. The clusters all exhibit an absorption band of low intensity near 450 nm, which is associated with charge transfer transitions from the cluster to the unoccupied orbitals of the tolan moiety. This assignment is supported by the cyclic voltammetric investigations presented above. Two bands between 300 – 400 nm, which were not resolved in all cases (**Table 5.6**) and a higher energy absorption band near 280 nm were also observed. Given their similar energetic positions and intensities as observed for **1-5**, these absorption bands likely contain contributions from tolan-centred transitions.

Table 5.6. The principal UV-vis absorption bands observed from CH_2Cl_2 solutions of **1-5**, **15-19**, **38-42**.

Compound	λ / nm (ε / M^{-1} cm^{-1})		
1	290 (53200)	306 (62300)	326 (59500)
2	[a]	313 (62700)	332 (58300)
3	285 (84200)	314 (59300)	335 (50800)
4	280 (64900)	300sh (41200)	342 (42900)
5	287 (30000)	315 (47300)	336 (45900)
15	297 (41700)	315 (69400)	337 (68300)
16	[b]	320 (65900)	341 (62500)
17	310 (33500)	327 (44900)	348 (39900)
18	284 (42200)	299 (37100)	358 (30300)
19	310 (39500) [c]	328 (55500)	349 (51400)
38		324 (41200)	450 (5500)
39	275 (46600)	329 (22100)	450 (3000)
40	283 (102000)	336 (43000) 376 (32000)	451 (8000)
41	283 (65900)	390 (24500)	463 (9000)
42	285 (84200)	331 (34700) 376 (25600)	440 (5800)

[a] Several unresolved bands were also observed between 250 – 300 nm (ca. 43000 M^{-1} cm^{-1})
[b] Several unresolved bands were also observed between 260 – 300 nm (ca. 28000 – 48000 M^{-1} cm^{-1})
[c] Several unresolved bands were also observed between 260 – 300 nm (ca. 24000–34000 M^{-1} cm^{-1})

The photophysical properties of 1,4-bis(phenylethynyl)benzene have been reported, [42] and the nature of the S_1 excited state examined using time-resolved spectroscopic techniques. [50] The availability of the silyl, Au and cluster capped phenylene ethynylene derivatives **1**, **15**, **36**, **38**, **11**, **23** and **43** prompted consideration of the absorption and luminescent properties of these derivatives. A detailed study of the photophysical properties of $Au(PCy_3)$ substituted phenylene ethynylene derivatives has been reported by Che and colleagues. [51]

For ease of comparison electronic absorption data from various compounds and complexes featuring $SiMe_3$, $Au(PPh_3)$, and cluster end-caps are summarised in **Table 5.7**, and illustrated in **Figure 5.8**. The trimethylsilylethynyl tolan **6** displayed a series of partially resolved absorption bands, the profile of which was consistent with other examples of ethynyl tolans. [52] Substitution of the $SiMe_3$ group for the $Au(PPh_3)$ centre in **15** caused a red-shift in the absorption profile, but no significant change in the profile of the absorption envelope. The 1,4-bis(phenylethynyl)benzene derivatives **11** and **23** each give rise to absorption profiles similar to that of the parent material. [42] The extended conjugation system in **11** results in a red-shift of the lowest energy absorption band relative to that in 1,4-bis(phenylethynyl)benzene, which is modestly accentuated in the gold compound **23**. Consequently the gold centre contributes little to the singlet transitions of these species; similar observations have been made previously by Che and colleagues. [51]

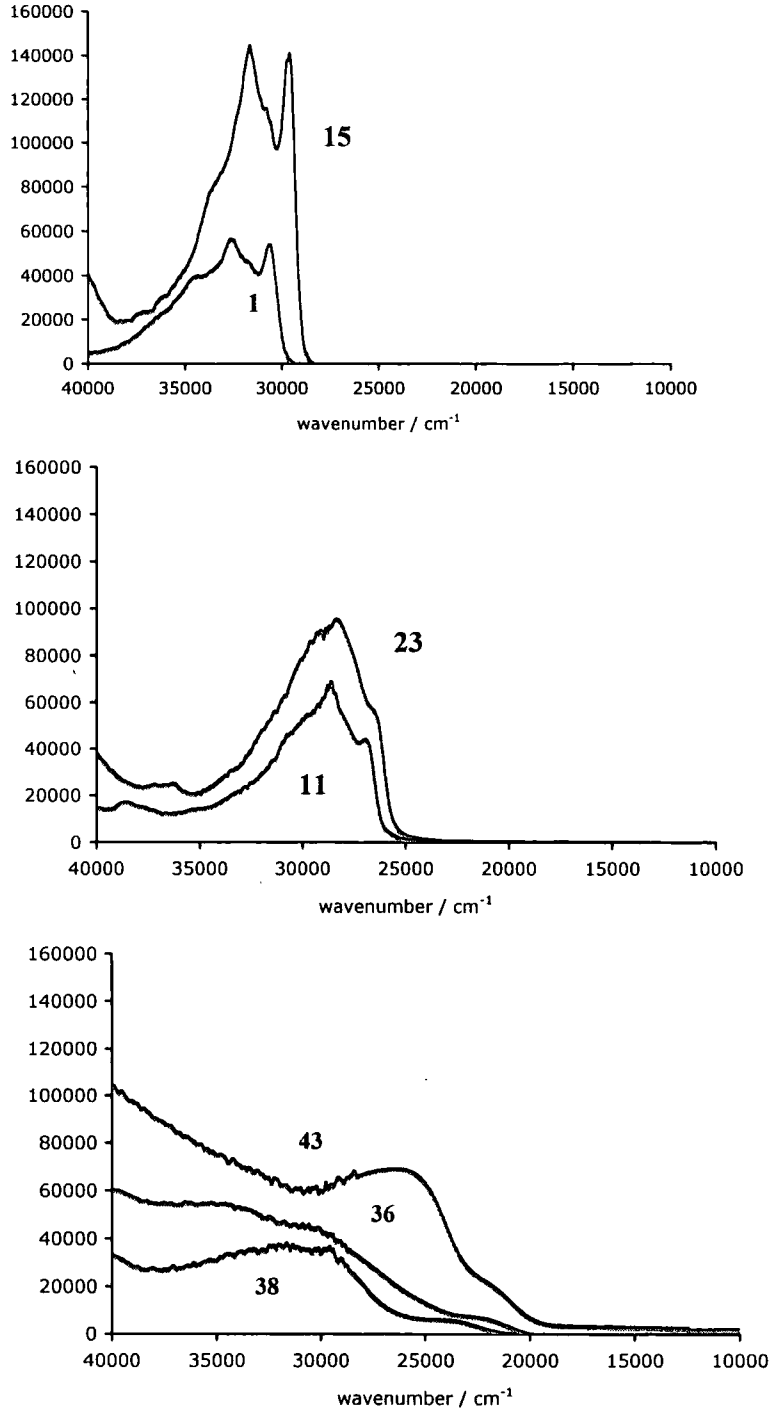

Figure 5.8. The absorption spectra of **1**, **11**, **15**, **23**, **36**, **38** and **43** in CH_2Cl_2.

The cluster derivatives **36**, **38** and **43** give rise to band patterns that are similar to each other, yet significantly different from the silyl and gold phenylene ethynylene derivatives **6**, **15**, **11** and **23**. The UV-Vis absorption spectrum of each cluster

complex was characterised by a low energy band below 25000 cm^{-1} (observed as a shoulder in the case of **43**), and two poorly resolved overlapping transitions at higher energy. There was little clear evidence for the more structured absorption bands associated with the precursors, suggesting the loss of electronic identity associated with the phenylene ethynylene moiety upon introduction of the cluster end-cap.

Table 5.7. The UV-vis spectra of **6**, **11**, **23**, **15**, **36**, **38** and **43** in CH_2Cl_2 solution.

	ν (cm^{-1}) / ε (M^{-1} cm^{-1})
6	30670 / 54000; 31750 / 47000; 32670 / 56580; 34480 / 39500
15	29580 / 140800; 30770 / 115800; 31650 / 144500; 33780 / 78600
36	23750 / 5900; 29760 / 35600; 32000 / 37400
38	22170 / 6750; 30500 / 44400; 32250 / 54000
11	26900 / 43900; 28570 / 68200; 30860 / 44000
23	26450 / 55500; 28330 / 95600; 30000 / 79600
43	21460 / 18100; 25770 / 68300

5.2.5.2. Photoluminescence Properties

These compounds were further probed by luminescence measurements in collaboration with Dr Andrew Beeby of the Department of Chemistry at Durham University, the results of which are summarised in **Table 5.8**, and illustrated in **Figure 5.9**. The tolan based materials **1** and **15** are highly emissive, giving rise to structured emission spectra, similar to that observed from other ethynyl-substituted tolans. [52] The lifetime of the emissive singlet excited state from **1** was measured to be 0.62 ns. In the case of **3** the heavy gold atom promotes population of the triplet state, and in degassed solutions phosphorescent emission is also observed. The extended systems **11** and **23** behave in a comparable fashion, giving rise to bright blue emission, somewhat red-shifted in comparison with that of the tolan derivatives **6** and **15**. A small shoulder on the shorter wavelength side of the fluorescence profile of **23** is thought to be due to photodegradation of the sample. The di(gold) complex **23** is both fluorescent and phosphorescent in degassed CH_2Cl_2 solutions. The modest Stokes shifts observed for this family of phenylene ethynylene derivatives are

indicative of relatively small structural rearrangements in the photo-excited states, as can be observed in other similar systems. [50]

Table 5.8. Selected photophysical properties of **1**, **11**, **15**, **23**, **36**, **38** and **43** in CH_2Cl_2.

Compound	λ_{em} / cm^{-1}	Stokes shift[a] / cm^{-1}	τ^b / ns	$\lambda_{phosphor}{}^c$ / cm^{-1}
1	29760	2800	0.62[d]	
15	29160	2500	0.61	19450
36	28330	4700	0.65	
38	27400	8200	*e*	
11	26740	2700	0.53	
23	25970	2400	*f*	17790
43	*e*			

[a] Stokes shift = $(1/\lambda_{abs} - 1/\lambda_{em})$. [b] Experimental lifetime determined with the time correlated single photon counting (TCSPC) technique (λ_{ex} = 334 nm). [c] In degassed solution. [d] λ_{ex} = 295 nm. [e] fluorescent intensity too low for accurate measurement. [f] Not fitted to a single exponential decay, possibly due to trace amount of a fluorescent impurity or photodegradation.

The cluster **36** was not strongly fluorescent, with emission red-shifted in comparison with that of the tolan precursors **1** and **15**; the lifetimes of all three tolan derived compounds (**1**, **15** and **36**) were similar (**Table 5.8**). Furthermore, the similarities in the emission profiles, including vibrational structure, clearly indicating tolan-centred emission in each case.

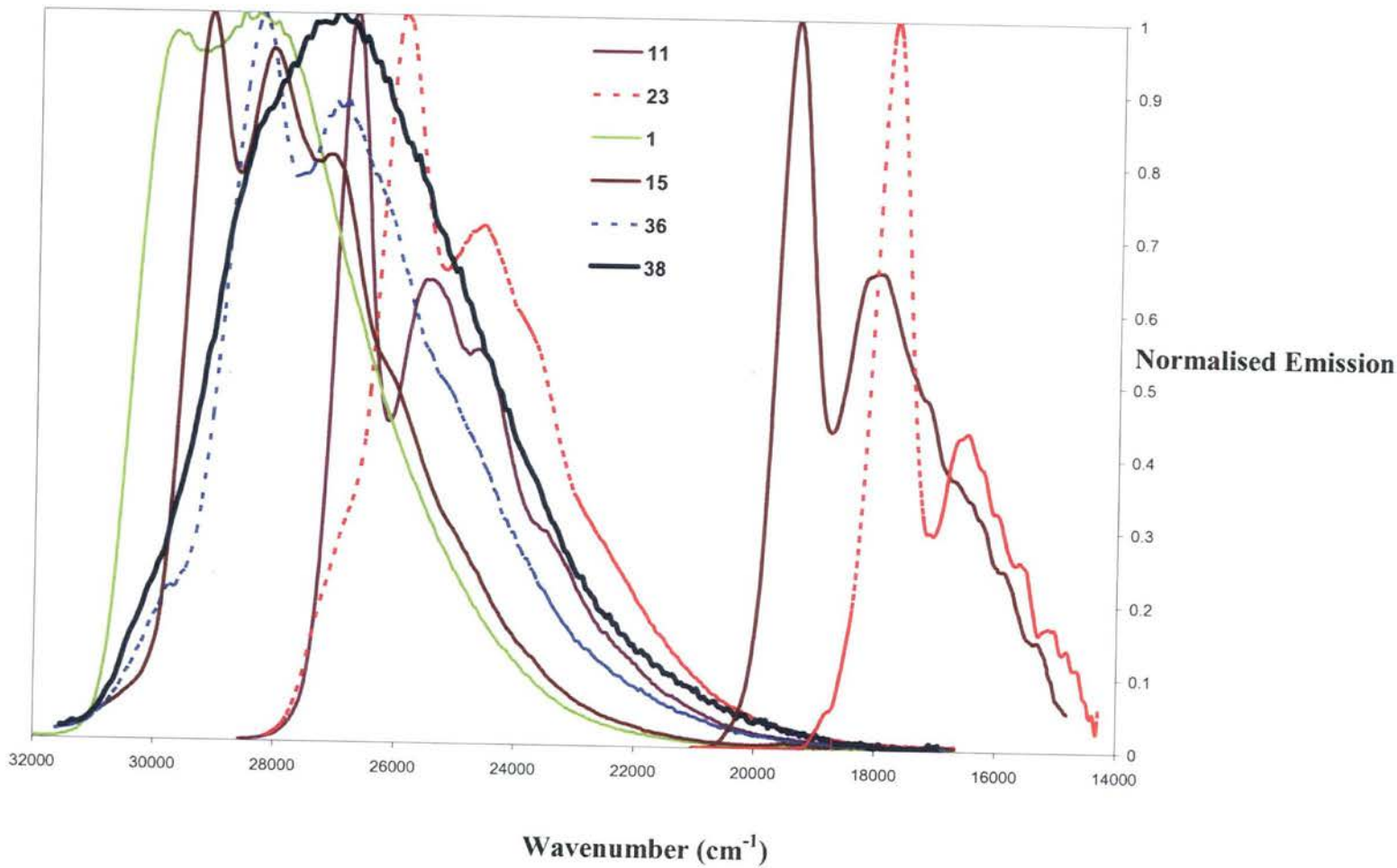

Figure 5.9. The fluorescence and phosphorescence spectra of **1**, **11**, **15**, **23**, **36** and **38** in CH_2Cl_2.

In contrast, the heterometallic cluster **38** displayed only a very weak, broad, structureless emission spectrum. It appears that introduction of the bridging gold centre serves to increase non-radiative decay mechanisms, which is perhaps curious given the intense fluorescence associated with gold acetylide complexes such as **11**.[51] Similarly, and in stark contrast to 1,4-*bis*-(phenylethynyl)benzene and the ethynyl derivatives **11** and **23**, which are all intensely fluorescent, the bis(cluster) **43** was only extremely weakly fluorescent and phosphorescent. Apparently the electronic differences brought about by the cluster end-cap bring about rapid non-radiative decay of the photoexcited state of the oligo(phenylene ethynylene) moiety. The difficulties in determining the lifetime of this weakly emissive sample likely point to the presence of a very small amount of a fluorescent impurity, possibly caused by photodegradation of the sample. This photo-instability may also account for the difficulties in obtaining an accurate microanalysis for this compound.

Taken as a whole, the significantly different absorption profiles of the precursors **6**, **15**, **11**, **23** and the cluster complexes **36**, **38**, **43** points to a perturbation of the ground state electronic structure of the phenylene ethynylene moiety brought about by the cluster, but not the mono-nuclear gold, end-caps. The cluster end-caps provide for non-radiative decay mechanisms that are particularly effective in the case of the $Ru_3(\mu\text{-}AuPPh_3)$ derivatives. Whilst the cluster-surface analogy has largely fallen into disuse over the last decade, the observations reported here support ideas that the electronic structure of a conjugated molecule may be distorted by attachment to a metallic surface, and as such it may be appropriate to consider the use of carefully chosen cluster models in further investigations.

5.3. Conclusions

In this chapter several new gold-containing clusters were prepared *via* the reaction between $Ru_3(CO)_{10}(\mu\text{-dppm})$ with the readily prepared alkynes **6** and **8**, and mono-nuclear gold complexes **11-15**. Cluster complexes featuring bridging hydride (**36** and **37**) and bridging $Au(PPh_3)$ ligands (**38-42**) and bis-clusters with $AuPPh_3$-bridging ligands were synthesised. All the metal complexes exhibited differences in

absorption and emission spectra when the organic precursors, the gold complexes and the clusters were compared, indicating a mixing of electronic states between the cluster and phenylene ethynylene moieties in the photoexcited states. The electronic properties of these clusters show that the cluster carbonyl bands are insensitive to the electronic nature of the tolan substituent, including the NO_2-centred reduction in the case of **41**. Oxidation is centred on the cluster core, and in the case of the most stable system, **41**, IR spectroelectrochemistry reveals the oxidation product to retain the same carbonyl arrangement as the starting material. The tolan group does not act as a particularly efficient conduit for passage of the electronic effect of electron donating or withdrawing groups to the cluster core.

The molecular structures of these clusters were also obtained but the only difference in these structures is the replacement of hydride ligands with the isolobal μ-$Au(PPh_3)$ fragment in **38-42**.

5.4. Experimental Details

5.4.1. General Condition

All reactions were carried out under an atmosphere of nitrogen using standard Schlenk techniques. Reaction solvents were purified and dried using an Innovative Technology SPS-400, and degassed before use. No special precautions were taken to exclude air or moisture during work-up. Preparative TLC was performed on 20 x 20 cm glass plates coated with silica gel (0.5 mm thick, Merck GF-254). The compound $Ru_3(CO)_{10}(\mu\text{-dppm})$ [53] was prepared by literature methods. Other reagents were purchased and used as received, or prepared as described elsewhere in the Thesis. Dichloromethane (Acros Chemicals) for the spectroelectrochemical experiments was freshly distilled from P_2O_5 under an atmosphere of dry nitrogen. Bu_4NPF_6 electrolyte (TBAH; Aldrich) was recrystallized twice from absolute ethanol and dried overnight under vacuum at 80 °C before use. IR spectra of the synthesized complexes were recorded using a Nicolet Avatar spectrometer from cyclohexane solutions in a cell fitted with CaF_2 windows, NMR spectra were obtained with Bruker Avance (^1H 400.13 MHz or ^1H 499.83 MHz) or Varian Mercury (^1H 399.97 MHz), and Varian Mercury (^{31}P 161.91 MHz or ^{31}P 80.96 MHz) spectrometers from $CDCl_3$ solutions and referenced against solvent resonances (^1H, ^{13}C) or external H_3PO_4 (^{31}P). Mass spectra were recorded using Thermo Quest Finnigan Trace MS-Trace GC or Thermo Electron Finnigan LTQ FT mass spectrometers.

Cyclic voltammograms were recorded at υ = 100 mV s^{-1} from solutions of approximately 10^{-4} M in analyte in dichloromethane containing 10^{-1} M Bu_4NPF_6, using a gas-tight single-compartment three-electrode cell equipped with platinum disk working (apparent surface area of 0.42 mm^2), coiled platinum wire auxiliary, and silver wire pseudo-reference electrodes. The working electrode surface was polished between scans with a diamond paste containing 0.25 μm grains (Oberflächentechnologien Ziesmer, Kempen, Germany). The cell was placed in a Faraday cage and connected to a computer-controlled PAR Model 283 potentiostat. All redox potentials are reported against the standard ferrocene/ferrocenium (Fc/Fc+)

redox couple used as an internal reference system. [54,55] Cyclic voltammetric measurements at ca. 210 K were performed with the electrochemical cell immersed into a bath of acetone/dry ice.

IR spectroelectrochemical experiments at room temperature were performed with an air-tight optically transparent thin-layer electrochemical (OTTLE) cell equipped with a Pt minigrid working electrode (32 wires cm^{-1}) and CaF_2 windows. [56] The cell was positioned in the sample compartment of a Bruker Vertex 70 FTIR spectrometer (1 cm^{-1} spectral resolution, 16 scans). The controlled- potential electrolyses were carried out with a PA4 potentiostat (EKOM, Polná, Czech Republic).

Diffraction data were collected at 120K on a Bruker SMART 6000 CCD (**36** and **37**) and (**38**, **39** and **42**), and on Bruker Proteum-M CCD (**40**, **41**) three-circle diffractometers, using graphite-monochromated Mo-K_α radiation. The structures were solved by direct-methods and refined by full matrix least-squares against F^2 of all data using *SHELXTL* software. [57] All non-hydrogen atoms were refined in anisotropic approximation except the disordered ones, H atoms were placed into the calculated positions and refined in "riding" mode. The crystallographic data and parameters of the refinements are listed in **Table 5.1-Table 5.3**.

Fluorescence spectra were measured at room temperature in dilute solutions, with an absorbance of < 0.1, using a Horiba-Jobin-Yvon Fluorolog 3-22 Tau-3 spectrofluorimeter, using conventional 90° geometry. Fluorescence lifetimes were determined with the time correlated single photon counting TCSPC technique using 295 or 334 nm irradiation, as detailed in **Table 5.8**. Phosphorescence spectra were measured using a LS-50B Perkin-Elmer luminescence spectrometer, triplet emission was recorded over 4 ms after 0.3 ms delay time

5.4.2. Experimental

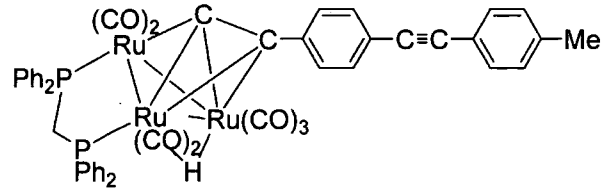

5.4.2.1. Preparation of $Ru_3(\mu\text{-}H)(\mu\text{-}C_2C_6H_4C{\equiv}CC_6H_4Me)(CO)_7(\mu\text{-}dppm)$ (36)

A solution of $Ru_3(CO)_{10}(\mu\text{-}dppm)$ (100 mg, 0.10 mmol) and $HC{\equiv}CC_6H_4C{\equiv}CC_6H_4Me$, **6** (22 mg, 0.10 mmol) in THF (15 ml) was heated at reflux, with the progress of the reaction being monitored by TLC and IR spectroscopy. When adjudged complete (ca. 3h), the solvent was removed and the residue purified by preparative TLC (hexane:acetone 70:30) and the yellow band was collected, and crystallised from ($CHCl_3$/hexane) to afford orange crystals of **36** suitable for X-ray crystallography (49 mg, 41 %). IR(C_6H_{12}): ν(CO) 2064s, 2011s, 2003s, 1994m, 1984m, 1958m, 1940m cm^{-1}; ν(C≡C) 2214w cm^{-1} .^{1}H NMR ($CDCl_3$, 499.83 MHz):δ -19.24 (d, J_{HP} = 33 Hz, 1H, μ-H), 2.38 (s, 3H, Me), 3.32, 4.30 (2 × dt, $J_{HP} = J_{HH}$ = 11 Hz, 2H, dppm), 7.17-7.50 (m, 28H, Ar). $^{31}P\{^1H\}$ NMR ($CDCl_3$, 161.98 MHz): δ 34.7 (d, J_{PP} = 54 Hz); 38.5 (d, J_{PP} = 54 Hz). ES(+)-MS (m/z): 1139, $[M+K]^+$; 1101, $[M+H]^+$. $C_{49}H_{34}O_7P_2Ru_3$ requires: C, 53.51; H, 3.12 % Found: C, 53.34; H, 3.30 %.

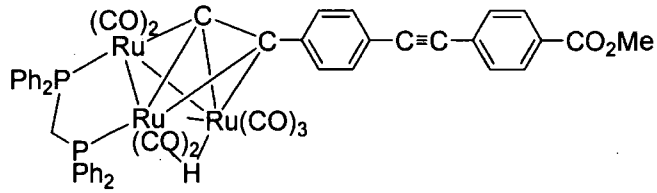

5.4.2.2. Preparation of $Ru_3(\mu\text{-}H)(\mu\text{-}C_2C_6H_4C{\equiv}CC_6H_4CO_2Me)(CO)_7$ (μ-dppm) (37)

In a manner similar to that described above, $Ru_3(CO)_{10}(\mu\text{-}dppm)$ (100 mg, 0.10 mmol) and $HC{\equiv}CC_6H_4C{\equiv}CC_6H_4CO_2Me$, **8** (27 mg, 0.10 mmol) were heated in refluxing THF (15 ml) for 3h. The reaction mixture was purified by preparative TLC (hexane/acetone 70:30) and the yellow band was collected, and crystallised from ($CHCl_3$/hexane) to afford orange crystals of **37** suitable for X-ray crystallography (29 mg, 25 %). IR(C_6H_{12}): ν(CO) 2064s, 2012s, 2003s, 1995m, 1985m, 1959m, 1941m cm^{-1}; ν(C≡C) 2210w cm^{-1}; ν(C=O) 1731s cm^{-1}; ^{1}H NMR ($CDCl_3$, 400.13 MHz): δ -

19.22 (d, J_{HP} = 33 Hz, 1H, μ-H), 3.94 (s, 3H, OMe), 3.33, 4.30 (2 × dt, J_{HP} = J_{HH} = 11 Hz, 2H, dppm), 6.37-8.05 (m, 28H, Ar). $^{31}P\{^{1}H\}$ NMR ($CDCl_3$, 161.98 MHz): δ 34.8(d, J_{PP} = 54 Hz); 38.7 (d, J_{PP} = 54 Hz).). ES(+)-MS (m/z): 1146, M^+; 1185 $[M+K]^+$. $C_{50}H_{34}O_9P_2Ru_3$ requires: C, 52.36; H, 2.97 % Found: C, 51.63; H, 2.92. %.

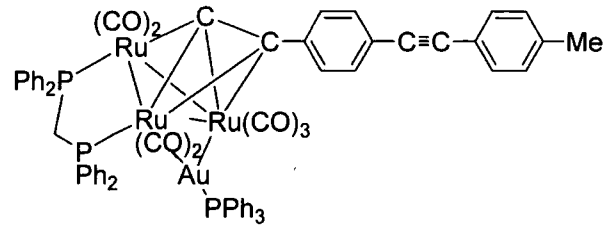

5.4.2.3. Preparation of $Ru_3(\mu\text{-}AuPPh_3)(\mu\text{-}C_2C_6H_4C{\equiv}CC_6H_4Me)(CO)_7(\mu\text{-}dppm)$ (38)

In a manner similar to that described above, $Ru_3(CO)_{10}(\mu\text{-dppm})$ (100 mg, 0.10 mmol) and Au ($C{\equiv}CC_6H_4C{\equiv}CC_6H_4Me)PPh_3$, **15** (70 mg, 0.10 mmol) were heated in refluxing THF (15 ml) for 3 h. Purification by preparative TLC (hexane/CH_2Cl_2: 60:40) afforded a yellow band which was collected, and crystallised from ($CHCl_3$/MeOH) to afford orange crystals of **38** suitable for X-ray crystallography (73 mg, 44 %). IR(C_6H_{12}): ν(CO) 2033s, 1989s, 1970s, 1954m, 1939m, 1910w cm^{-1}; ν(C≡C) 2214w cm^{-1}. ^{1}H NMR ($CDCl_3$, 499.83 MHz): δ 2.37 (s, 3H, Me), 3.33, 4.24 (2 × dt, J_{HP} = 14 Hz, J_{HH} = 11 Hz, 2H, dppm), 6.38-7.93 (m, 43H, Ar). $^{31}P\{^{1}H\}$ NMR ($CDCl_3$, 161.98 MHz): δ 38.3 (d, J_{PP} = 62 Hz); 40.5 (dd, J_{PP} = 62 Hz, J_{PP} = 39 Hz); 60.9 (d, J_{PP} = 39 Hz). ES(+)-MS (m/z) 2016, $[M+AuPPh_3]^+$; 1559, $[M+H]^+$. $C_{67}H_{48}O_7P_3Ru_3Au$ requires: C, 51.64; H, 3.10% Found: C, 51.66; H, 3.28 %.

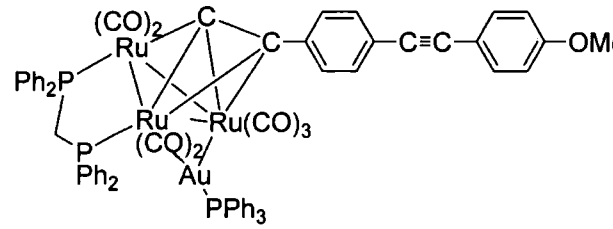

5.4.2.4. Preparation of $Ru_3(\mu\text{-}AuPPh_3)(\mu\text{-}C_2C_6H_4C{\equiv}CC_6H_4OMe)(CO)_7(\mu\text{-}dppm)$ (39)

In a manner similar to that described above, $Ru_3(CO)_{10}(\mu\text{-dppm})$ (100 mg, 0.10 mmol) and Au ($C{\equiv}CC_6H_4C{\equiv}CC_6H_4OMe)PPh_3$, **16** (71 mg, 0.10 mmol) were heated

in refluxing THF (15 ml) for 3 h. Preparative TLC (hexane/CH_2Cl_2: 60:40) gave a yellow band which was crystallised from ($CHCl_3$/hexane) to afford orange crystals of **39** suitable for X-ray crystallography (67 mg, 41 %). IR(C_6H_{12}): ν(CO) 2038s, 1993s, 1972s, 1956m, 1939m, 1909w cm^{-1}; ν(C≡C) 2201w cm^{-1}. ^1H NMR ($CDCl_3$, 499.83 MHz): δ 2.36 (s, 3H, OMe), 3.35, 4.26 (2 × dt, J_{HP} = 12 Hz, J_{HH} = 11 Hz, 2H, dppm), 6.39-7.94 (m, 43H, Ar). $^{31}P\{^1H\}$ NMR ($CDCl_3$, 161.98 MHz): δ 38.5 (d, J_{PP} = 62 Hz); 40.8 (dd, J_{PP} = 62 Hz, J_{PP} = 39 Hz); 61.1 (d, J_{PP} = 39 Hz). ES(+)-MS (m/z) 1575, $[M+H]^+$; 721, $[Au(PPh_3)_2]^+$. $C_{67}H_{48}O_8P_3Ru_3Au$ requires: C, 51.12; H, 3.07 % Found: C, 51.33; H, 3.10 %.

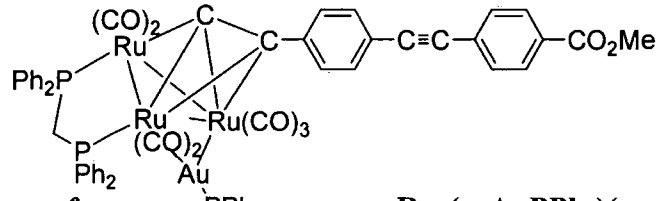

5.4.2.5. Preparation of $Ru_3(\mu\text{-}AuPPh_3)(\mu\text{-}C_2C_6H_4C{\equiv}CC_6H_4CO_2Me)(CO)_7\,\mu\text{-dppm}$ (40)

In a manner similar to that described above, $Ru_3(CO)_{10}$(μ-dppm) (100 mg, 0.10 mmol) and Au ($C{\equiv}CC_6H_4C{\equiv}CC_6H_4CO_2Me$)$PPh_3$, **16** (74 mg, 0.10 mmol) were heated in refluxing THF (15 ml) for 3 h. Preparative TLC (hexane/CH_2Cl_2: 60:40) gave a yellow band which was collected, and crystallised from ($CHCl_3$/MeOH) to afford orange crystals of **40** suitable for X-ray crystallography (20 mg, 12 %). IR(C_6H_{12}): ν(CO) 2034s, 1991s, 1971s, 1959m, 1938m, 1912w cm^{-1}; ν(C≡C) 2210w cm^{-1}; ν(C=O) 1720s cm^{-1};. ^1H NMR ($CDCl_3$, 499.83 MHz): δ 2.64 (s, 3H, OMe), 3.52, 4.26 (2 × dt, J_{HP} = 11 Hz, J_{HH} = 10 Hz, 2H, dppm), 6.38-8.04 (m, 43H, Ar). $^{31}P\{^1H\}$ NMR ($CDCl_3$, 80.96 MHz): δ 38.7 (d, J_{PP} = 62 Hz); 41.3 (dd, J_{PP} = 62 Hz, J_{PP} = 38 Hz); 61.3 (d, J_{PP} = 39 Hz). ES(+)-MS (m/z) 1603, $[M+H]^+$; 721, $[Au(PPh_3)_2]^+$. $C_{68}H_{48}O_9P_3Ru_3Au$ requires: C, 50.97; H, 3.00. Found: C, 50.67; H, 3.34%.

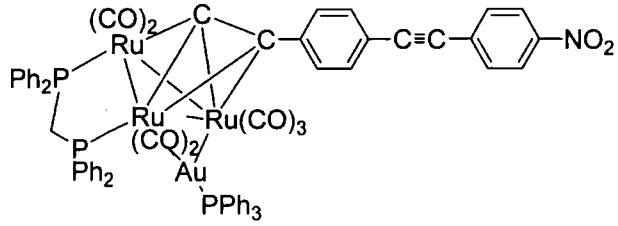

5.4.2.6. Preparation of $Ru_3(\mu\text{-}AuPPh_3)(\mu\text{-}C_2C_6H_4C{\equiv}CC_6H_4NO_2)(CO)_7(\mu\text{-}dppm)$ (41)

In a manner similar to that described above, $Ru_3(CO)_{10}(\mu\text{-}dppm)$ (100 mg, 0.10 mmol) and $Au(C{\equiv}CC_6H_4C{\equiv}CC_6H_4NO_2)PPh_3$, **17** (73 mg, 0.10 mmol) were heated in refluxing THF (15 ml) for 3 h. Purification by preparative TLC (hexane/CH_2Cl_2: 60:40) afforded a yellow band which was crystallised from ($CHCl_3$/MeOH) to give orange crystals of **41** suitable for X-ray crystallography (82 mg, 50 %). IR(C_6H_{12}): ν(CO) 2034s, 1992s, 1971s, 1955m, 1940m, 1910w cm^{-1}; ν(C≡C) 2213w cm^{-1}. ^1H NMR ($CDCl_3$, 399.97 MHz): δ 3.39, 4.30 (2 × dt, J_{HP} = 11 Hz, J_{HH} = 10 Hz, 2H, dppm), 6.38-8.24 (m, 43H, Ar). $^{31}P\{^1H\}$ NMR ($CDCl_3$, 80.96 MHz): δ 38.7 (d, J_{PP} = 62 Hz); 40.6 (dd, J_{PP} = 62 Hz, J_{PP} = 38 Hz); 61.3 (d, J_{PP} = 39 Hz). ES(+)-MS (m/z) 1590, $[M+H]^+$; 721, $[Au(PPh_3)_2]^+$. $C_{66}H_{45}O_9NP_3Ru_3Au$ requires: C, 49.84; H, 2.83; N, 0.88, Found: C, 49.54; H, 2.64; N, 0.78%.

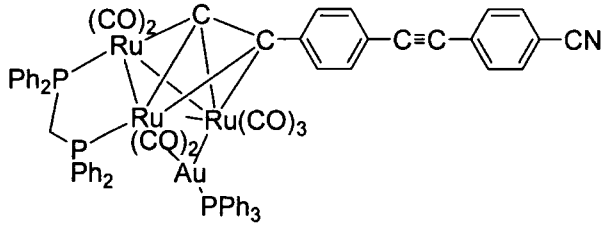

5.4.2.7. Preparation of $Ru_3(\mu\text{-}AuPPh_3)(\mu\text{-}C_2C_6H_4C{\equiv}CC_6H_4CN)(CO)_7(\mu\text{-}dppm)$ (42)

In a manner similar to that described above, $Ru_3(CO)_{10}(\mu\text{-}dppm)$ (100 mg, 0.10 mmol) and $Au(C{\equiv}CC_6H_4C{\equiv}CC_6H_4CN)PPh_3$, **18** (71 mg, 0.10 mmol) were heated in refluxing THF (15 ml) for 3 h. Purification of the reaction mixture by preparative TLC (hexane/CH_2Cl_2: 60:40) gave a yellow band which was collected, and crystallised from ($CHCl_3$/MeOH) to afford orange crystals of **42** suitable for X-ray crystallography (60 mg, 37 %). IR(C_6H_{12}): ν(CO) 2035s, 1991s, 1973s, 1941m, 1918w cm^{-1}; ν(C≡C) 2209w cm^{-1}; ν(C≡N) 2212s cm^{-1}. ^1H NMR ($CDCl_3$, 399.97

MHz): δ 3.37, 4.28 (2 × dt, J_{HP} = 11 Hz, J_{HH} = 10 Hz, 2H, dppm), 6.36-8.06 (m, 43H, Ar). $^{31}P\{^{1}H\}$ NMR ($CDCl_3$, 161.91 MHz): δ 38.5(d, J_{PP} = 62 Hz); 41.0 (dd, J_{PP} = 62 Hz, J_{PP} = 39 Hz); 61.1 (d, J_{PP} = 39 Hz). ES(+)-MS (m/z): 2028, $[M+AuPPh_3]^+$; 1570, $[M+H]^+$. $C_{67}H_{45}O_7NP_3Ru_3Au$ requires: C, 51.24; H, 2.87; N, 0.89, Found: C, 51.08; H, 2.86; N, 0.93%.

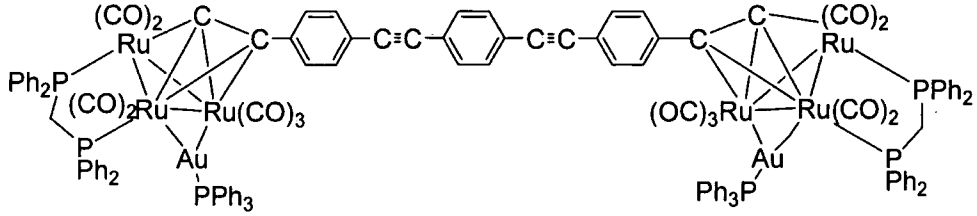

5.4.2.8. Preparation of $\{Ru_3(\mu\text{-dppm})(CO)_7\}_2\{(\mu\text{-AuPPh}_3)\}_2(\mu\text{-C}_2C_6H_4C{\equiv}CC_6H_4C{\equiv}CC_6H_4C_2)$ (43)

In a manner similar to that described above,$Ru_3(CO)_{10}(\mu$-dppm) (50 mg, 0.052 mmol) and $\{Au(PPh_3)\}_2(\mu$-$C{\equiv}CC_6H_4C{\equiv}CC_6H_4C{\equiv}CC_6H_4C{\equiv}C)$, **23** (32 mg, 0.026 mmol) in THF (10 ml) were heated in refluxing THF (10 ml) for 3 h before purification by preparative TLC (hexane/acetone: 60/40). The product (**43**) resisted crystallisation, but was obtained as an orange powder (37 mg, 48%) by precipitation from dropwise addition of the compound dissolved in the minimum volume of CH_2Cl_2 to ca. 10 ml hexane, with stirring. $C_{126}H_{86}O_{14}P_6Ru_6Au_2$ requires: C, 50.27; H, 2.88%. IR(C_6H_{12}): ν(CO) 2032s, 1989s, 1969s, 1955m, 1938m, 1907w cm^{-1}. ^{1}H NMR ($CDCl_3$, 399.97 MHz): δ 3.32, 4.24 (2 × dt, J_{HP} = 10 Hz, J_{HH} = 14 Hz, 2H, dppm), 6.37-7.95 (m, 82H, Ar). $^{31}P\{^{1}H\}$ NMR ($CDCl_3$, 161.91 MHz): δ 38.3 (d, J_{PP} = 62 Hz); 40.6 (dd, J_{PP} = 62 Hz, J_{PP} = 39 Hz); 61.0 (d, J_{PP} = 39 Hz). ES(+)-MS (m/z): 3049, $[M+K]^+$ and $[M+NCMe+K]^{2+}$; 3010, $[M]^+$; 1544, $[M+2K]^{2+}$.The compound, whilst apparently pure by NMR spectroscopic methods, analysed consistently low in carbon.

5.5. References

1. J. M. Tour, L. Jones II, D. L. Pearson, J. S. Lamba, T. Burgin, G. W. Whitesides, D.L. Allara, A. N. Parikh, S. Atre, *J. Am. Chem. Soc.*, 1995, **117**, 9529.
2. A. Dhirani, R. W. Zehner, R. P. Hsung, P. Guyot-Sionnest, L. R. Sita, *J. Am. Chem. Soc.*, 1996, **118**, 3319.
3. L. A. Bumm, J. J. Arnold, M. T. Cygan, T. D. Dunbar, T. P. Burgin, L. Jones II, D. L. Allara, J. M. Tour, P. S. Weiss, *Science*, 1996, **271**, 1705.
4. A. Nitzan, M. A. Ratner, *Science*, 2003, **300**, 1384.
5. G. S. Tulevski, M. B. Myers, M. S. Hybertsen, M. L. Steigerwald, C. Nuckolls, *Science*, 2005, **309**, 591.
6. J. Nara, H. Kino, N. Kobayashi, M. Tsukada, T. Ohno, *Thin Solid Films*, 2003, **438-439**, 221
7. H. Haick, J. Ghabboun, O. Niitsoo, H. Cohen, D. Cohen, A. Vilan, J. Hwang, A. Wan, F. Amy, A. Khan, *J. Phys. Chem. B.*, 2005, **109**, 9622.
8. (a) S. Mankefors, A. Grigoriev, G. Wendin, *Nanotechnology*, 2003, **14**, 849, (b) C. Joachim, J. K. Gimzewski, A. Aviram, *Nature*, 2000, **408**, 541.
9. H. Jian, J. M. Tour, *J. Org. Chem.*, 2003, **68**, 5091.
10. M. S. Doescher, J. M. Tour, A. M. Rawlett, M. L. Myrick, *J. Phys. Chem. B*, 2001, **105**, 105.
11. B. Fabre, D. D. M. Wayner, *Langmuir*, 2003, **19**, 7145.
12. R. Boukherroub, D. D. M. Wayner, *J. Am. Chem. Soc.*, 1999, **121**, 11513.
13. J. T. C. Wojtyk, K. A. Morin, R. Boukherroub, D. D. M. Wayner, *Langmuir*, 2002, **18**, 6081.
14. P. J. Dyson, *Coord. Chem. Rev.*, 2004, **248**, 2443.
15. A. Johansson, S. Stafstrom, *Chem. Phys. Lett.*, 2000, **322**, 301.
16. M. Konopka, R. Rousseau, I. Stich, D. Marx, *J. Am. Chem. Soc.*, 2004, **126**, 12103.
17. D. Kruger, H. Fuchs, R. Rousseau, D. Marx, M. Parrinello, *Phys. Rev. Lett.*, 2002, **89**, 186402-1.

18. W. M. Khairul, L. Porrès, D. Albesa-Jové, M. S. Senn, M. Jones, D. P. Lydon, J. A. K. Howard, A. Beeby, T. B. Marder, P. J. Low, *J. Cluster Sci.*, 2006, **17**, 65.

19. P. Braunstein, L. A. Oro, P. R. Raithby (eds.), *Metal Cluster in Chemistry*, Wiley-VCH, Weinheim, 1999.

20. R. D. Adams, T. Barnard, A. Rawlett, J. M. Tour, *Eur. J. Inorg. Chem.*, 1998, 429.

21. M. I. Bruce, N. N. Zaitseva, B. W. Skelton, A. H. White, *J. Chem. Soc., Dalton Trans.*, 2002, 3879.

22. A. K. Smith, E. W. Abel, F. G. A. Stone, G. Wilkinson (ed.), *Comprehensive Organometallic Chemistry*, 2nd edn., Elsevier, Oxford, 1995, Vol. 7, Ch 13.

23. M. I. Bruce, B. W. Skelton, A. H. White, N. N. Zaitseva, *J. Organomet. Chem.*, 1998, **558**, 197.

24. M. I. Bruce, P. A. Humphrey, E. Horn, E. R. T. Tiekink, B. W. Skleton, A. H. White, *J. Organomet. Chem.*, 1992, **429**, 207.

25. M. I. Bruce, N. N. Zaitseva, B. W. Skelton, A. H. White, *J. Organomet. Chem.*, 2005, **690**, 3268.

26. P. Braunstein, G. Predieri, A. Tiripicchio, E. Sappa, *Inorg. Chim. Acta*, 1982, **63**, 113.

27. M. I. Bruce, E. Horn, O. bin Shawkataly, M. R. Snow, *J. Organomet. Chem.*, 1985, **280**, 289.

28. A. J. Deening, S. Donovan-Mtunzi, K. Hardcastle, *J. Chem. Soc., Dalton Trans.*, 1986, 543.

29. M. I. Bruce, P. J. Low, N. N. Zaitseva, S. Kahlal, J. –F. Halet, B. W. Skleton, A. H. White, J. Chem. Soc., *Dalton Trans.*, 2000, 2939.

30. M. I. Bruce, K. Costuas, J. –F. Halet, B. C. Hall, P. J. Low, B. K. Nicholson, B. W. Skleton, A. H. White, *J. Chem. Soc., Dalton. Trans.*, 2002, 383.

31. M. I. Bruce, B. W. Skelton, A. H. White, N. N. Zaitseva, *J. Organomet. Chem.*, 2002, **650**, 188.

32. M. I. Bruce, P. A. Humphrey, E. Horn, E. R. T. Tiekink, B. W. Skelton, A. H. White, *J. Organomet. Chem.*, 1992, **129**, 207.

33. G. Predieri, A. Tiripicchio, C. Vignali, E. Sappa, *J. Organomet. Chem.*, 1988, **342**, C33.

34. E. Sappa, G. Predieri, A. Tiripicchio, C. Vignali, *J. Organomet. Chem.*, 1989, **378**, 109.

35. G. Gervasio, R. Gobetto, P. J. King, D. Marbello, E. Sappa, *Polyhedron*, 1998, 17, 2937.

36. M. I. Bruce, J. R. Hinchliffe, B. W. Skleton, A. H. White, *J. Organomet. Chem.*, 1995, **195**, 141.

37. A. M. Sheloumov, A. A. Koridze, F. M. Dolgushin, Z. A. Starikova, M. G. Ezernitskaya, P. V. Petrovskii, *Russ. Chem. Bull., Int. Ed.*, 2000, **49**, 1292.

38. Y. Kazazi, J. Cornill, J. L. Bredas, *Nanotechnology*, 2003, **14**, 165.

39. E. E. Nesterov, Z. G. Zhu, T. M. Swager, *J. Am. Chem. Soc.*, 2005, **127**, 10083.

40. L. Venkataraman, J. E. Klare, C. Nuckolls, M. S. Hybertsen, M. L. Steigerwald, *Nature*, 2006, **442**, 9904.

41. S. J. Greaves, E. L. Flynn, E. L. Futcher, E. Wrede, D. P. Lydon, P. J. Low, S. R. Rutter, A. Beeby, *J. Phys. Chem. A*, 2006, **110**, 2114.

42. A. Beeby, K. Findlay, P. J. Low, T. B. Marder, *J. Am. Chem. Soc.*, 2002, **124**, 8280.

43. L. T. Liu, D. Yaron, M. I. Slutch, M. A. Berg, *J. Phys. Chem. B*, 2006, **110**, 18894.

44. P. Zanello, *Struc. Bond.*, 1992, **79**, 101.

45. P. Zanello, *Inorganic Electrochemistry*, Royal Society of Chemistry; Cambridge, 2003.

46. G. Longoni, C. Femoni, M. C. Iapalucci, P. Zanello, in *Metal Clusters in Chemistry*; P. Braunstein, L. A. Oro, P. R. Raithby, Eds. Wiley-VCH: Weinheim, 1999, Vol.2.

47. E. M. Graham, V. M. Miskowski, J. W. Perry, D. R. Coulter, A. E. Stiegman, W. P. Schaefer, R. E. Marsh, *J. Am. Chem. Soc.*, 1989, **111**, 8771.

48. K. Ezumi, H. Miyazaki, T. Kubota, *J. Phys. Chem.*, 1970, **74**, 2397.

49. M. Biswas, P. Nguyen, T. B. Marder, L. R. Khundkar, *J. Phys. Chem. A*, 1997, **101**, 1689.

50. A. Beeby, K. Findlay, P. J. Low, T. B. Marder, P. Matousek, A. W. Parker, S. R. Rutter, M. Towrie, *Chem. Commun.*, 2003, 2406.
51. H. -Y. Chao, W. Lu, Y. Li, M. C. W. Chan, C. -M. Che, K. -K. Cheung, N. Zhu, *J. Am. Chem. Soc.*, 2002, **124**, 14696.
52. A. Beeby, unpublished work.
53. M. I. Bruce, B. K. Nicholson, M. L. Williams, *Inorg. Synth.*, 1989, **26**, 271.
54. G. Gritzner, J. Kůta, *Pure Appl. Chem.*, 1984, **56**, 461.
55. V.V. Pavlishchuk, A.W. Addison, *Inorg. Chim. Acta*, 2000, **298**, 97.
56. M. Krejčík, M. Daněk, F. Hartl, *J. Electroanal. Chem.*, 1991, **317**, 179.
57. *SHELXTL, version 6.14,* Bruker AXS, Madison, Wisconsin, USA, 2000.

Chapter 6. 'Novel Transmetallations From Simple Gold(I) Acetylide Moities'

6.1. Introduction

Transmetallation is a process of increasing importance in the area of transition metals in organic synthesis. The process is defined as exchange of ligands between two metal centres. [1,2] Transmetallation is one of the essential reaction steps in numerous organometallic catalytic cycles and in recent times has been well illustrated in the development of procedures for the simple synthesis of C-C, C-N, C-O bonds. [3-7] Although the process is almost as old as organometallic chemistry itself. For example, in the Sonogashira Pd/Cu cross-coupling reactions discussed in **Chapter 1**, the Pd(II) complex $PdX(Ar)L_n$ formed in the oxidative addition reaction of an aryl halide with the active $Pd(0)L_n$ species undergoes transmetallation with a copper acetylide produced in the copper cycle to produce Pd-acetylide expelling the copper halide, CuX (**Scheme 6.1**). [8-11] In the Stille cross-coupling, transmetallation of the $Pd(II)L_nR^1X$ complex with an organostannane is utilised to form the intermediate complex $Pd(II)L_nR^1R^2$ and expelling SnRX (**Scheme 6.2**). [12-17] Whilst in the Suzuki-Miyaura cross-coupling reactions, the Pd(II) complex produced as a product from the oxidative addition of aryl halide, undergoes transmetallation with the boron-ate complex to from organopalladium species $Pd(II)L_{(n-1)}R_1R_2$ [18-21] and in Negishi cross-coupling reaction, either Ni or Pd complex can undergo transmetallation with ZnRX compound to form organopalladium or organonickel species. [9,11,22-24]

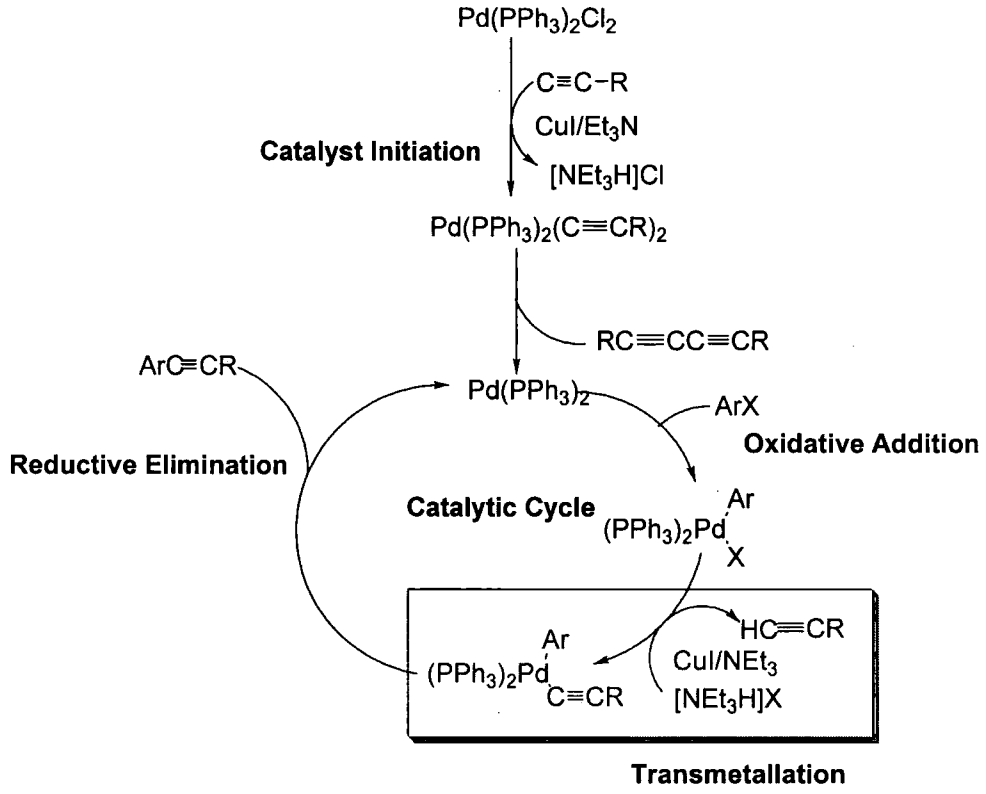

Scheme 6.1. The example of the transmetallation reaction between the active $Pd(0)L_n$ species with a copper acetylide produced in the copper cycle to produce Pd-acetylide expelling the copper halide, CuX in the the Sonogashira cross-coupling reaction using $PdCl_2(PPh_3)_2$/CuI catalysts.

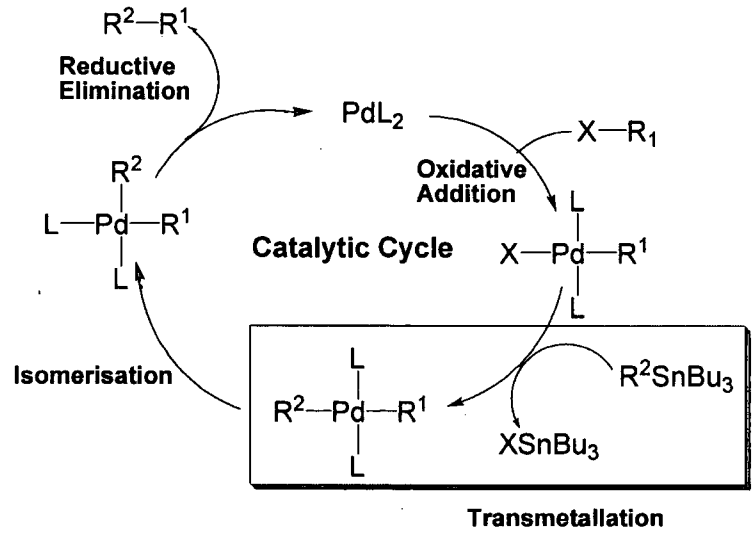

Scheme 6.2. A transmetallation reaction between the active $Pd(II)L_nR^1X$ complex with an organostannane is utilised to form the intermediate complex $Pd(II)L_nR^1R^2$ and expelling SnRX in Stille cross-coupling reaction.

However, and somewhat surprisingly, despite the prevalence of transmetallation reactions involving copper(I) acetylide complexes, and the growing awareness of gold catalysis in general. [25-32] Other known transmetallation reactions include lithiated acetylides, [70,71] and also the use of Grignard reagents. [82]

The examples of transmetallation involving the readily prepared gold(I) species $Au(C{\equiv}CR)(PPh_3)$ are scarce. [33,34,40] Perhaps the work most directly relevant to the topics contained in this thesis is the cross-coupling reaction of $Au(C{\equiv}CR)(PPh_3)$ with halo-carbynes and halo-acetylenes developed by Bruce and co-workers in the last few years. They have developed a simple coupling protocol based upon the formal elimination of $AuX(PR_3)$ during the Pd/Cu catalysed cross-coupling of organometallic halocarbynes with a gold-alkynyl reagent in a manner that resembles the classical Sonogashira synthesis of aromatic acetylenes (**Scheme 6.1**). [35-37]

Other examples of cross-coupling reactions between halo acetylenes and gold(I) acetylides which resemble the Cadiot-Chodkiewicz cross-coupling protocol have also been reported by the same group. [38] These reactions proceed in high yield without any complicating side-reactions, and have been used in the preparation of both even and odd numbered all-carbon ligands, including some of the longest crystallographically characterised examples reported to date. The reaction is carried out at room temperature in ethereal solvents, avoiding the complicating choice of amine solvent or base necessary in the related Sonogashira cross-coupling protocol, and the $AuX(PR_3)$ by-product can be isolated from the reaction mixture and re-cycled (**Scheme 6.3**). [38]

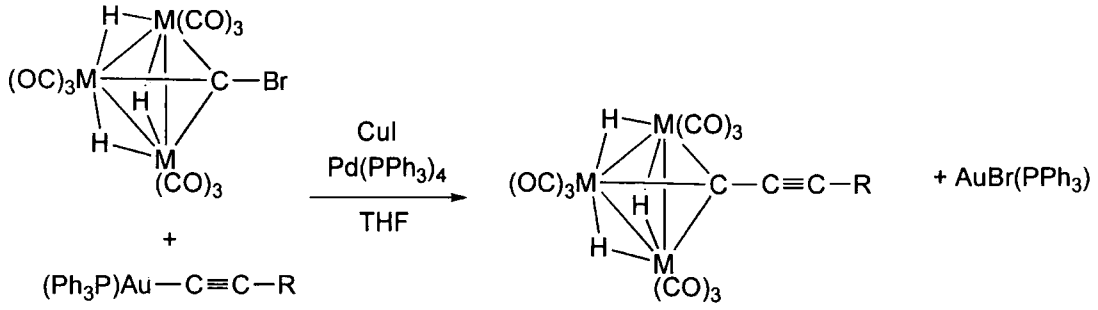

Scheme 6.3. The Pd/Cu catalysed cross-coupling of organometallic halocarbynes with a gold-alkynyl reagent in a manner that resembles the classical Sonogashira synthesis of aromatic acetylenes. [38]

The use of transmetallation reactions of gold(I) acetylide complexes Au(C≡CR)L in preparative scale procedures is not common. To the best of our knowledge, there are few literature examples of the use of this gold-acetylide reagent in their preparation of metal acetylide complexes. Shaw and co-workers have prepared Ni[(μ-dppm)$_2$(C≡CPh)$_2$] complex from the reaction of NiCl$_2$(μ-dppm)$_2$ and two stoichiometric equivalents of Au(C≡CPh)(PPh$_3$) in CH_2Cl_2 at ca. 20°C. [34] Yam and co-workers have prepared the tetranuclear copper (I) alkynyl complexes [Cu$_4$(PR$_3$)$_4$(μ$_3$-η^1, η^1, η^2-C≡CR')$_3$]PF$_6$, (R = Ph, *p*-MeC$_6$H$_4$, *p*-CF$_3$C$_6$H$_4$] and (R' = *p*-MeOC$_6$H$_4$, *p*-EtOC$_6$H$_4$, *p*-*n*BuOC$_6$H$_4$, *p*-*n*HexOC$_6$H$_4$, *p*-*n*HeptoC$_6$H$_4$, *p*-MeC$_6$H$_4$, *p*-*n*BuC$_6$H$_4$, *p*-*n*HexC$_6$H$_4$, *p*-*n*HeptC$_6$H$_4$, *p*-*n*OctC$_6$H$_4$, *p*-PhC$_6$H$_4$, *p*-ClC$_6$H$_4$, *p*C$_4$H$_3$S, and *p*-MeOC$_6$H$_4$) from the transmetallation reaction between [Cu(MeCN)$_4$]PF$_6$ with triaryl phosphine (PR$_3$) and the appropriate gold(I) alkyl polymer. In addition, [Au(PPh$_3$)$_2$]$^+$ was also isolated as a by product from the reaction. (**Scheme 6.4**) [34]

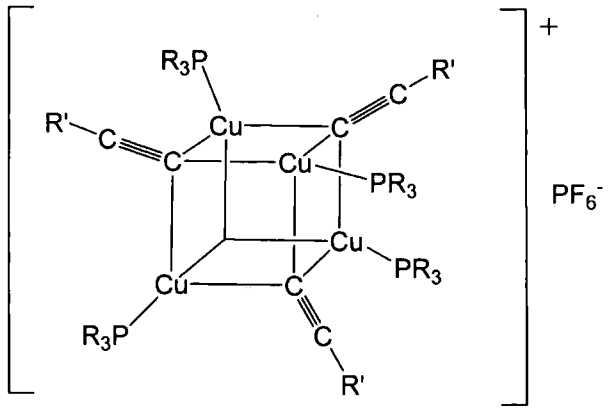

Scheme 6.4. Tetranuclear copper (I) alkynyl "open-cube" complexes prepared by Yam and co-workers. [34]

In this chapter a series of novel, preparative scale, stoichiometric transmetallation reactions involving a gold(I) aceylide complex are presented. Specifically, the readily available complexes $Au(C{\equiv}CR)(PPh_3)$ [R = Ph, C_6H_4Me] have been treated with several inorganic and organometallic compounds MXL_n [M = metal, L_n = supporting ligands, X = halide], to afford the corresponding metal-acetylide complexes $M(C{\equiv}CR)L_n$, (20-80 % yield), with representative examples featuring metals from Groups 8-11. The acetylide products were fully characterised by usual spectroscopic methods including the molecular structural analysis.

6.2. Result and Discussion

6.2.1. Syntheses

6.2.1.1. *Group 8 Complexes*

Metal acetylide complexes $M(C{\equiv}CR)(L_2)Cp'$ (M = Fe, Ru, Os; L = PR_3; Cp' = Cp, Cp*) have been prepared on many previous occasions. [41-45] The synthesis of such species usually takes advantage of the ready isomerisation of 1-alkynes to vinylidenes that takes place in the coordination sphere of the Group 8 metal centre (**Scheme 6.5**). The mechanism of the 1,2-H shift has been the subject of a considerable body of work, and whilst examples of intermediates containing η^2-$HC{\equiv}CR$ ligands have been obtained in the case of the $Ru(PMe_3)_2Cp$ moiety [46-51] a

concerted reaction mechanism is thought to be most prevalent in examples containing bulkier and less-electron donating supporting ligands, such as $Ru(PPh_3)_2Cp$. [52-56]

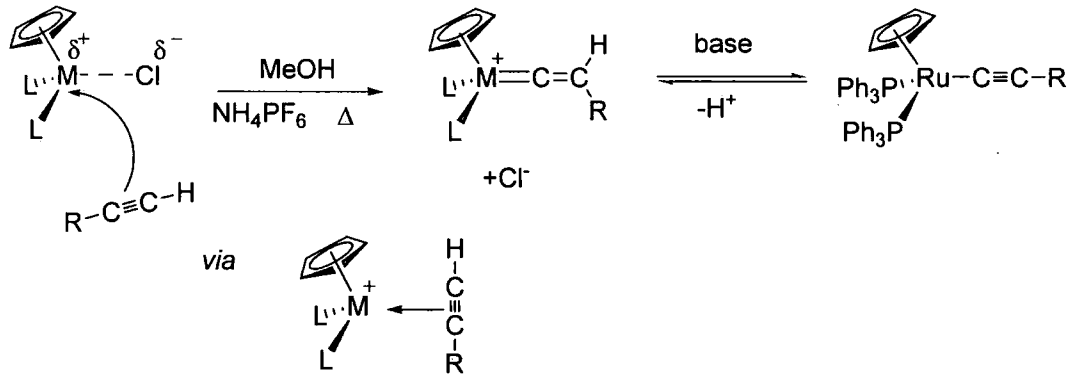

Scheme 6.5. The mechanism of the synthesis of group 8 metal acetylides by the isomerisation of 1-alkynes to vinylidenes.

The cationic vinylidene complexes $[M\{C=C(H)R\}(L_2)Cp']^+$ thus formed are acidic, and deprotonation occurs readily following treatment with bases such as NEt_3, [57-59] NaOMe [60-62] or even on chromatographic Al_2O_3. [63]

Whilst the 1-alkyne/vinylidene/acetylide conversion has proven to be immensely useful in the preparation of metal acetylide complexes of the type $M(C{\equiv}CR)(L_2)Cp'$, it is obviously limited to the use of stable 1-alkynes. Several authors have sought to take advantage of the significant thermal stability of 1-alkynes featuring $SiMe_3$ protecting groups and synthetic routes to metal acetylide complexes from silylalkynes based on desilylation/metallation routes are being developed. [52,64,65] However, whilst silylvinylidenes arising from a 1,2-silyl shift are known on iron, [66] the mechanism of the desilylation/metallation process in the case of ruthenium examples has not been conclusively established.

Complex $Fe(C{\equiv}CPh)(dppe)Cp$ (**44**) was prepared from the reaction between $FeCl(dppe)Cp$ and $Au(C{\equiv}CPh)(PPh_3)$ in the presence of NH_4PF_6 in refluxing MeOH. Treatment of the red solutions formed with DBU and purification of the crude product by extraction with benzene and preparative TLC afforded **44** in 43 % yield (**Scheme 6.6**). In addition another colourless band containing $AuCl(PPh_3)$ was also

collected, characterised from the observation of a singlet resonance in the ^{31}P NMR at δ_P 34 ppm. [67]

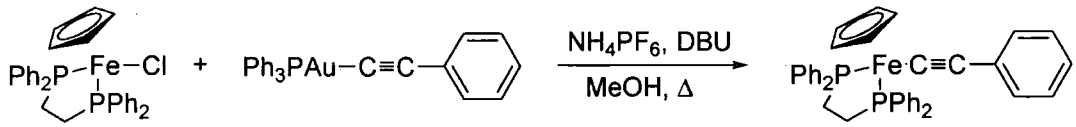

Scheme 6.6. The preparation of **44** through transmetallation from a gold(I) acetylide.

The complex **44** has been prepared in the previously. [68] but only pertinent spectroscopic data of ^{13}C NMR and IR were reported. From this transmetallation procedure, the complex was fully characterised by the usual spectroscopic methods. In the ^{1}H NMR spectrum, the Cp resonance was observed at δ_H 4.25 ppm. The aromatic protons associated with the dppe ligand in **51** and the phenyl acetylide substituent were not fully resolved, but were observed as a series of heavily overlapped resonances between δ_H 6.50-7.94 ppm. The two sets of CH_2 proton resonances from the dppe moieties were clearly observed as doublet-of -doublet (dd) resonances above δ_H 2 ppm ($J_{HP} = J_{HH} \sim 6$ Hz). In addition, in the ^{31}P NMR, complex **51** show a singlet phosphine resonance at δ_P 107.5 ppm.

The ^{13}C spectrum of **44** contains the CH_2 carbon of the dppe moiety resonance was observed as doublet-of-doublet (dd) at δ_C 28 ppm ($J_{CP/CCP} \sim 22$ Hz). The acetylide carbons C_α and C_β were observed, and identified on the basis of the J_{CP} coupling constants with a triplet at δ_C 142.5 ppm with coupling constant J_{CP} = 14 Hz being assigned to C_α, and a singlet at δ_C 123.1 ppm assigned to C_β (**Scheme 6.7**). In addition, the spectrum also shows the resonance of Cp at δ_C 79.3 ppm. The carbon resonances for the phenyl substituent C_1-C_4 were also observed and identified, thus, C_1 and C_2 were observed at δ_C 130.5 ppm and δ_C 129.4 ppm respectively, whereas for C_3 and C_4, the resonances were observed at δ_C 129.0 ppm and δ_C 127.6 ppm.

The aromatic carbons associated with the diphenylphosphine ethane (dppe) ligand are clearly distinguishable from the carbons of the phenyl substituent on the acetylenic moiety on the basis of the coupling to the phosphorus nucleus, and

assigned on the basis of the size of the coupling constant. Thus, C*i* is observed as multiplet (dds) at δ_C 138.1 and δ_C 138.8 ppm. For C*o* and C*m*, the resonances were observed as doublet-of-doublet (dds), thus, C*o* at δ_C 134.0 ppm and δ_C 132.0 ppm (C*o*,*o'*, $J_{CP/CCP}$ ~ 5Hz), C*m* at δ_C 127.0 ppm and 127.8 ppm (C*m*,m' $J_{CP/CCP}$ ~ 5Hz). The singlet resonances for C*p* (C*p*, *p'*) were observed at δ_C 128.1 ppm (**Scheme 6.7**).

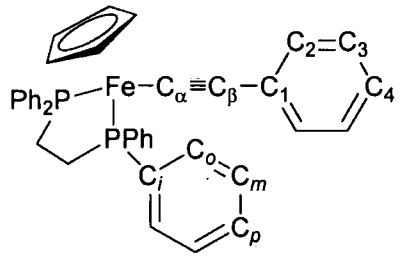

Scheme 6.7. The ^{13}C NMR spectral assignment of **44**.

The IR spectrum of **44** was recorded in CH_2Cl_2 solution in a cell fitted with CaF_2 window, which the spectrum shows one ν(C≡C) band at 2060 cm^{-1} whilst the electrospray mass spectrum $[ES\text{-}MS]^+$ contains the molecular ions $[M]^+$ at *m/z* 620 and the $[M\text{-}C{\equiv}CPh]^+$ at *m/z* 519. The known complex **44** [68] was identified by comparison of the spectroscopic data with the data originally reported (**Experimental Section, 6.4.2.1**).

The reaction between $Au(C{\equiv}CPh)(PPh_3)$ and $RuCl(L_2)(\eta^5\text{-}C_5R_5)$ [L = PPh_3; R = H, L_2 = dppe; R = Me], in the presence of NH_4PF_6 in refluxing methanol resulted in the formation of a red solution presumed to contain a vinylydene intermediate, the deprotonation of which by DBU resulted in the precipitation of the target compounds **45** and **46** as yellow solids in 81% and 53 % yield, respectively (**Scheme 6.8**). As expected, the filtrate recovered from these reactions contained $AuCl(PPh_3)$ as evidence by ^{31}P NMR spectroscopy (δ_P 34 ppm). [67] These known complexes **45**, [69] and **46**, [68] were identified by comparison of the spectroscopic data with the data originally reported (**Experimental Section, 6.4.2.2-6.4.2.3**).

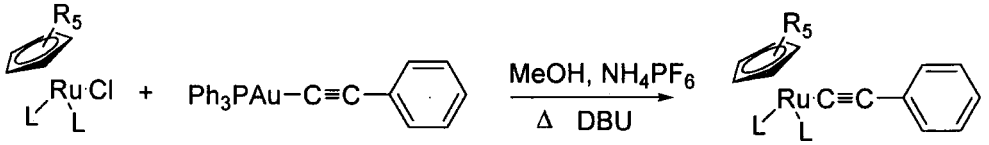

L = PPh_3, R = H; (**45**)
L_2 = dppe, R = Me; (**46**)

Scheme 6.8. The synthetic route of **45** and **46**.

6.2.1.2. *Group 9 Complex*

The alkynyl complex, $Ir(C{\equiv}CR)(CO)(PPh_3)_2$, have been prepared by reactions of Vaska's complex $IrCl(CO)(PPh_3)_2$ with lithiated acetylides [70,71] or from CuI catalysed reactions with terminal acetylenes carried out in amine solvents. Whilst the first method is best described as a simple nucleophilic displacement of chloride the latter method likely involves a Cu(I) acetylide intermediate and could be regarded as a transmetallation reaction. [72-74] For an example, reaction between $IrCl(CO)(PPh_3)_2$ and $CuC{\equiv}CPh$ in refluxing benzene has afforded irregular octahedral cluster of $Cu_4Ir_2(PPh_3)_2(C{\equiv}CPh)_8$ [74] as shown in **Scheme 6.9**.

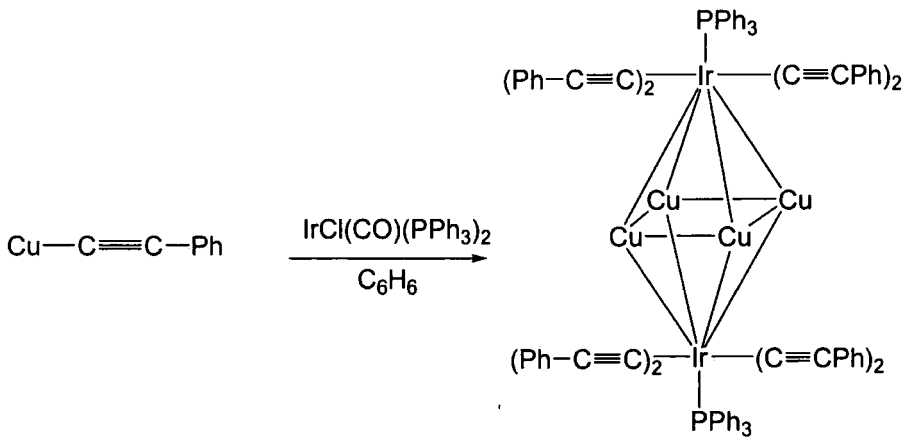

Scheme 6.9. The preparation of $Cu_4Ir_2(PPh_3)_2(C{\equiv}CPh)_8$ from $IrCl(CO)(PPh_3)_2$ and $CuC{\equiv}CPh$. [74]

Here, $Ir(C{\equiv}CC_6H_4Me)(O_2)(CO)(PPh_3)$ (**47**) was prepared by treating $IrCl(CO)(PPh_3)_2$ with $Au(C{\equiv}CC_6H_4Me)(PPh_3)$ in MeOH at room temperature. The gold by-product $AuCl(PPh_3)$ was removed from the crude product by extraction with acetone. Recrystallisation (chloroform/hexane) of the yellow solid that remained after extraction afforded yellow crystals of $Ir(CO)(O_2)(C{\equiv}CC_6H_4Me)(PPh_3)$, **47** (40

%), which were suitable for crystallographic characterisation. Due to the presence of dioxygen during the work-up, and the tendency of the 16-e Ir(I) systems to adopt a further 2 electron-donating ligand, the O_2 adduct obtained in this work is not overly surprising. [75-77] (The route to the formation of dioxygen adduct in **47** is shown in **Scheme 6.10**), although in some cases treatment of the 16 electron Vaska's complex derivatives $Ir(CO)(R)(PPh_3)_2$ [R = alkenyl or alkynyl groups] with a stream of air or O_2 was necessary to obtain complete conversion to the dioxygen adducts. [78-79]

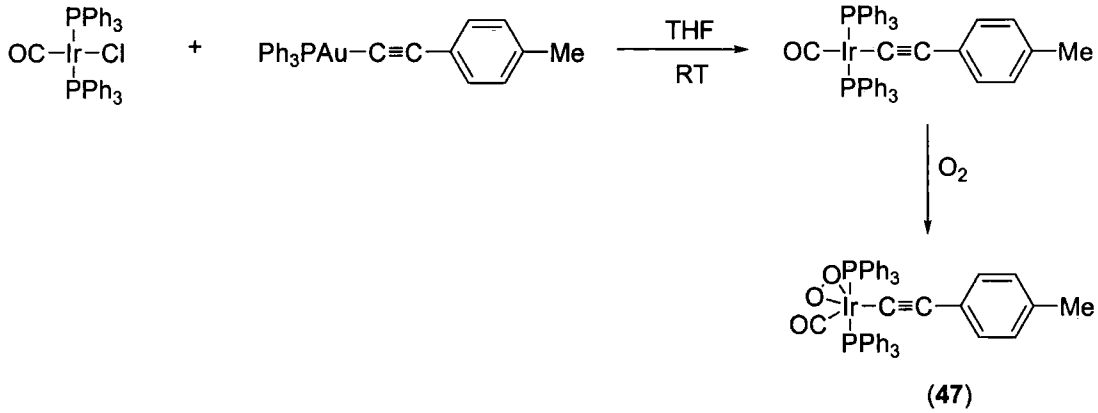

(47)

Scheme 6.10. The preparation of **47** *via* a transmetallation reaction of Vaska's complex, and subsequent reaction with atmospheric dioxygen.

The methyl resonance in **47** was observed at δ_H 2.23 ppm whereas the aromatic protons of the *para*-tolyl substituent can be observed as two sets of pseudo-doublets at δ_H 6.26ppm (J_{HH} = 8 Hz) and 6.82 ppm (J_{HH} = 8 Hz). However, the aromatic protons from the PPh_3 moities in **47** were not fully resolved, but were observed as a series of heavily overlapped resonances between δ_H 7.37-7.64 ppm.

The ^{31}P NMR spectrum of **47** shows a singlet at δ_P 7.36 ppm, which is to the best of our knowledge, the first ^{31}P NMR characterisation has been carried out for this $Ir(O_2)(CO)(C{\equiv}CR)(PPh_3)_2$ complex. In addition, the resonance is slightly shifted to higher field when compared with $Ir(CO)(C{\equiv}CPh)(PPh_3)_2$ (δ_P 4.63 ppm). [80] Whereas the resonance is shifted downfield when compared to the Vaska's complex itself (δ_P 24.8 ppm). [81]

In the ^{13}C NMR spectrum of **47**, the expected methyl resonance can be observed at δ_C 21.4 ppm. The acetylide carbons were observed and identified, thus for Cα, the resonance can be observed at 66.3 ppm and another resonance at δ_C 109.4 ppm was identified as Cβ. The carbon resonances for the *para*-tolyl substituent C_1-C_4 also were observed and identified, thus, C_1 and C_2 were observed at δ_C 125.3 ppm and δ_C 128.7 ppm respectively, whereas for C_3 and C_4 the resonances were observed at δ_C 135.1 ppm and δ_C 131.4 ppm. In addition, the (C≡O) resonance also can be observed at higher chemical shift (δ_C 167.4 ppm).

The aromatic carbons associated with the triphenyl phosphine (PPh_3) ligand are clearly distinguishable from the tolyl moiety on the basis of the coupling to the phosphorus nucleus, and assigned on the basis of the coupling constant. Thus, C_i is observed as doublet-of-doublet (dd) at δ_C 134.9 ppm ($^1J_{CP}/^4J_{CP} \sim 5$ Hz), However, for C_o, arises as singlet resonance at δ_C 131.0 ppm, for C_m the reosonance observed as doublet-of-doublet(dd) at δ_C 128.4 ppm ($^2J_{CP}/^6J_{CP} \sim$ 5Hz) and C_p arises as singlet at δ_C 128.4 ppm. (**Scheme 6.11**)

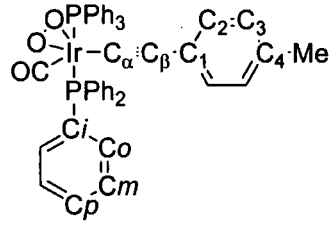

Scheme 6.11. The ^{13}C NMR spectral assignment of **47**.

The IR spectrum of **47** shows one weak ν(C≡C) band at 2128 cm^{-1}. In addition, the strong terminal ν(CO) band was also observed at 1962 cm^{-1}, while the ν(O-O) band can be observed at 834 cm^{-1}. Similar observations have been made previously. [76-80]

The $[ES\text{-}MS]^+$ for complex **47** contains the protonated molecular ion [M+H]+ at *m/z* 893 as well as the MeCN adduct to the molecular ion [M + H + MeCN]+ at *m/z* 934.

6.2.1.3. *Group 10 Complexes*

Group 10 acetylide complexes have been prepared on numerous occasions, being among the earliest metal acetylide complexes prepared and characterised. Whilst, early synthetic routes took advantage of nucleophilic reactions between acetylide anions (as lithium salts or Gringnard reagents) [82] later developments have given rise to more convenient preparations involving CuI catalysed reactions between, for example, $MCl_2(PR_3)_2$ and terminal alkynes. [83-87]

Reaction of $Au(C{\equiv}CPh)(PPh_3)$ with $NiBr(PPh_3)Cp$ in THF resulted formation of a green solution which was purified by preparative TLC and recrystallisation (chloroform/MeOH) afforded $Ni(C{\equiv}CPh)(PPh_3)Cp$ **48**, [88] as green crystals in 53 % yield, (**Scheme 6.12**). In addition a colourless band that contained the expected by product $AuBr(PPh_3)$ was also collected, and characterised by the observation of a singlet resonance in the ^{31}P NMR spectrum (δ_P 34.5 ppm). [89]

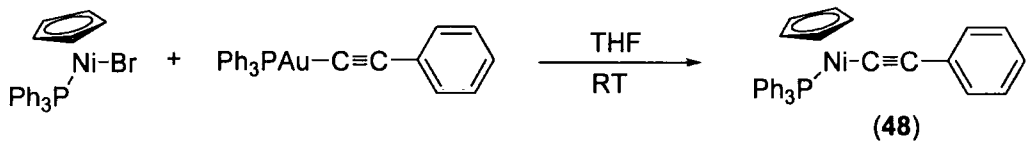

(48)

Scheme 6.12. The synthetic route affording $Ni(C{\equiv}CPh)(PPh_3)Cp$, **48**, *via* transmetallation between Ni(II) and Au(I) centres.

The complex was characterised by usual spectroscopic methods and identified by comparison with the original spectroscopic data and an authentic sample (see **Experimental Section, 6.4.2.5**).

Complexes *trans*-$Pt(C{\equiv}CR)_2(L_2)$ [R = Ph; L = PPh_3 (**49**), R = C_6H_4Me; L = PPh_3 (**50**), R = C_6H_4Me; L = PMe_3 (**51**)] were prepared from room temperature reactions between $PtCl_2(L_2)$ [L = PPh_3, PMe_3] and $Au(C{\equiv}CR)(PPh_3)$ [R = Ph, C_6H_4Me] in methanol affording the targeted products **49-51** as yellow precipitates (**Scheme 6.13**). As expected, the filtrate contains $AuClPPh_3$. Recrystallisation of the yellow solids afforded pale yellow (**49** and **50**) and pale green (**51**) single crystals suitable for X-ray crystallography.

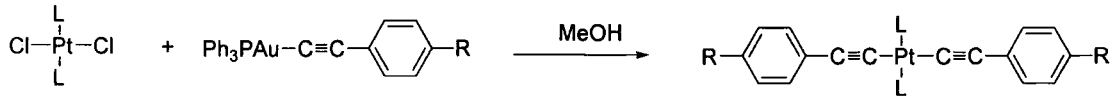

R = H; L = PPh_3 (**49**), R = Me, L = PPh_3 (**50**), R = Me, L = PMe_3 (**51**)

Scheme 6.13. The synthetic route of the preparation of **49-51**.

Each of the complexes **49-51** were characterised by the usual spectroscopic methods. In the case of **49** and **50**, [84] the spectroscopic data of these known complexes were identified by comparison of the spectroscopic data with the data originally reported (**Experimental Section, 6.4.2.5-6.4.2.6**). In the case of compounds **50** and **51**, a singlet at ca. δ_H 2.2 ppm was observed arising from the tolyl substituents. However, the numerous aromatic protons in **49** were not fully resolved, but were observed as a series of heavily overlapped resonances between δ_H 6.3-7.8 ppm. Conversely, the aromatic protons in **51** were observed as pseudo-doublet (J_{HH} ~ 7-8 Hz) resonances in between δ_H 6.2-7.2 ppm which arise from the tolyl portions of the molecule. In addition, in the case of **51**, the resonance of the PMe_3 moiety was observed as doublet at δ_H 1.77 ppm ($^2J_{PH}$, $^4J_{PH}$ ~ 4 Hz). Another doublet was also observed at δ_H 1.80 ppm ($^3J_{Pt\text{-}H}$ ~ 30 Hz) which arise from the coupling of the proton in the PMe_3 moiety to the platinum nucleus.

The ^{31}P NMR spectra contain singlet phosphine resonances, each accompanied by platinum satellites. In the case of **49** and **50**, where as L = PPh_3, the resonances were observed at δ_P 19.7 ppm (s + d, $^1J_{PtP}$ = ca. 2600 Hz, PPh_3), whilst in the case of **51**, where L = PMe_3, exhibit the same characteristics but the resonance was shifted downfield to δ_P -19.3 ppm (s + d, $^1J_{PtP}$ = 2309 Hz, PMe_3).

The ^{13}C NMR spectra of **49** and **50** are similar to each other, with the exception that in **50** addition methyl resonances can be observed at δ_C 22 ppm. Due to the symmetrical nature of the complexes, only two acetylenic carbon were observed with Cα, identified on the basis of the J_{CP} coupling constant, being observed as a triplet (J_{CP} = 16 Hz) at ca δ_C 110, and a singlet resonances at slightly higher chemical shift (ca.δ_C 113 ppm) assigned to C_β.

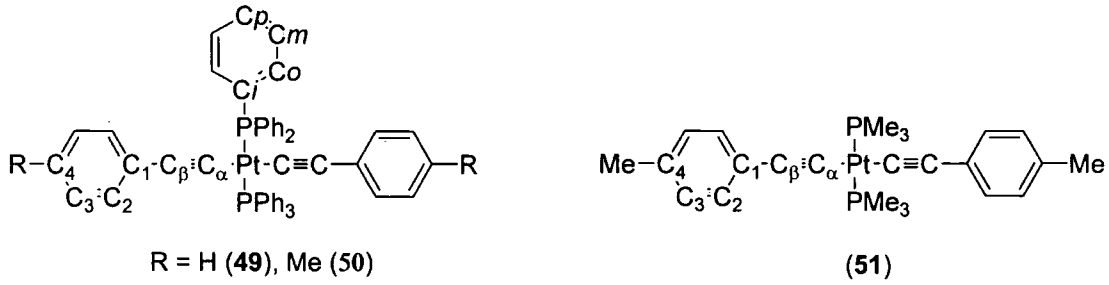

Scheme 6.14. The ^{13}C NMR spectral assignment of (**a**) complexes **49** and **50** and (**b**) **51**.

As with other examples described in this chapter, the aromatic carbons associated with the triphenylphosphine (PPh_3) ligands in **49** and **50** are clearly distinguishable from the substituents moieties on the basis of the coupling to the phosphorus nucleus, and assigned on the basis of the coupling constant. Thus, C*i* is observed as doublet-of-doublet (dd) at ca. δ_C 131 ppm ($^1J_{CP}/^4J_{CP} \sim 29$ Hz). For C*o* and C*m*, the resonances were also observed as doublet-of-doublet (dd), thus, C*o* at ca. δ_C 135 ppm ($^2J_{CP}/^5J_{CP} \sim 5$ Hz), C*m* at ca. δ_C 127 ppm ($^3J_{CP}/^6J_{CP} \sim 5$ Hz). The singlet resonances for C*p* were observed at ca. δ_C 128ppm (**Scheme 6.14a**).

In the ^{13}C spectrum of **51**, the aromatic carbons associated with the trimethylphosphine (PMe_3) ligand are also clearly observed at δ_C 15.7 ppm ($J_{CP} \sim 20$ Hz) as doublet-of-doublet (dd) as result from the coupling of the carbon to the phosphorus nuclei, in addition to satellite resonances arising from the coupling of the carbon nuclei to the platinum nucleus. In addition, methyl resonances can be observed at δ_C 22 ppm (**Scheme 6.14b**). Other carbon nuclei were identified and give rise to resonances similar to those described for **49** and **50**.

Each of the complexes **49-51** give rise to one ν(C≡C) bands in the IR spectra at above 2100 cm^{-1}. The $[ES\text{-}MS]^+$ for complexes **49-51** contain the protonated molecular ion $[M+H]^+$ at *m/z* 922 for **49**, at *m/z* 950 for **50** and at *m/z* 578 for **51**. In the case of **49** the presence of Na^+ which is believed abstracted from the glass used in the preparation of the samples were also observed in the spectrum. In the case of **50**, the protonated molecular ion with the MeOH $[M + H + MeOH]^+$ adduct was also

observed in the spectrum at *m/z* 982. However, in the case of **51**, the dimer ions with the Na^+ $[2M + Na]^+$ was also observed at *m/z* 1177. In addition, the molecular ion with the Na^+ and MeOH adducts was also observed at *m/z* 632.

The room temperature reactions between $PtCl_2(PMe_3)_2$ and $Au(C{\equiv}CC_6H_4Me)(PPh_3)$ with the presence of NH_4PF_6 in methanol resulted in the unexpected formation of $[Au(PMe_3)_2]PF_6$, **53** in 49 % yield as a white crystalline material, which was recrystallised from MeCN/MeOH. The $[ES\text{-}MS]^+$ spectrum of **53** contains the $[M+Na]^+$ at *m/z* 721 and molecular ion M^+ at *m/z* 349. The assignment of the structure is also supported by both high-resolution mass spectrometry and elemental analysis. In addition, the crystal lattice of **53** shows that the PF_6 anion is presence in the packing. Thus it can be concluded that NH_4PF_6 salt in this reaction plays an important role to afford the unexpected product of **53**, but clearly more work remains to be done to elucidate the mechanism of this process, the synthetic route of the preparation of **53** is shown in **Scheme 6.15**.

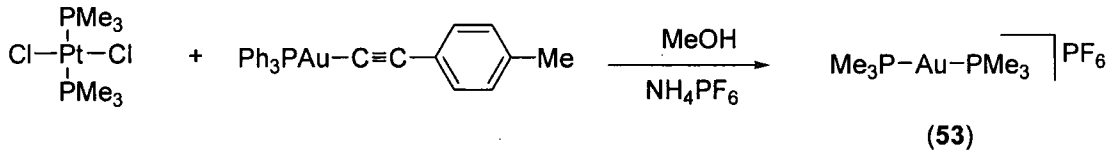

Scheme 6.15. The synthetic route of the formation of **53**.

6.2.1.4. *Group 11 Complex*

The yellow complex $Cu(C{\equiv}CC_6H_4Me)PPh_3$ **52** [90] was prepared by the addition of $Au(C{\equiv}CC_6H_4Me)(PPh_3)$ and CuI in THF. The copper containing product was collected from the reaction mixture by filtration, and as expected $AuI(PPh_3)$ could be recovered from the filtrate as a cream-coloured solids (δ_P 35 ppm). In order to aid characterisation, the $Cu(C{\equiv}CC_6H_4Me)$ obtained was treated with PPh_3 in ethanol/CH_2Cl_2 to give a yellow suspension of **52** in 22 % yield (**Scheme 6.16**). The poor solubility of the $Cu(C{\equiv}CC_6H_4Me)$ is believed the factor that has affecting the low yield of product in this reaction although the reaction was left stirring for ca. 24 hours at room temperature. The complex **52** also has been fully characterised by the

usual spectroscopic methods and the spectroscopic data obtained was compared with the original data. (see **Experimental Section, 6.3.2.9**).

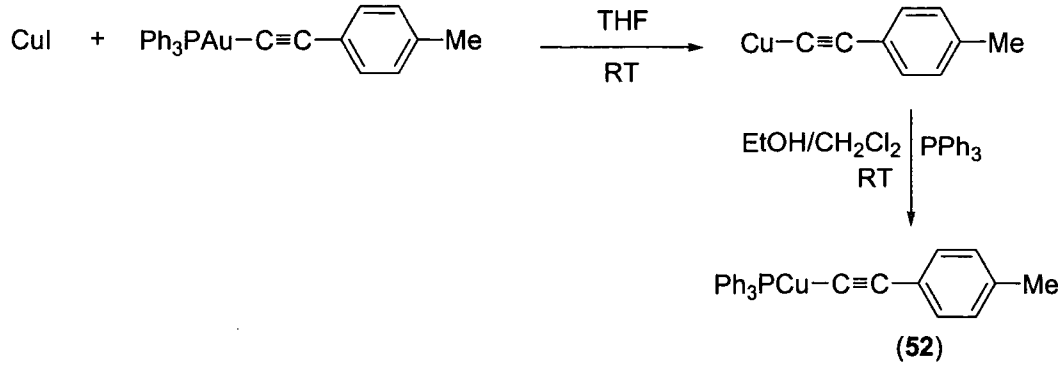

Scheme 6.16. The 'two-steps' reaction of the preparation of **52**.

6.2.2. The Proposed Mechanism

A series of reactions on both preparative and NMR scale were carried out to investigate further the mechanisms of the transmetallation reactions between $[L_n]MX$ [X = Cl, NCMe] with the gold acetylide moieties $Au(C{\equiv}CR)PPh_3$ [R = Ph, C_6H_4Me]. In this context of studies, $RuX(L_2)Cp'$ and $Au(C{\equiv}CC_6H_4Me)PPh_3$ were chosen to represent all the transmetallation reaction in this chapter.

Reaction 1: To investigate the likely role of a vinylidene intermediate and the consequent source of proton in the formation of $Ru(C{\equiv}CC_6H_4Me)(dppe)Cp^*$.

1. $RuCl(dppe)Cp^*$ (100 mg, 0.49 mmol), $Au(C{\equiv}CC_6H_4Me)(PPh_3)$ (86 mg, 0.49 mmol), $NaPF_6$ (25 mg, 0.49 mmol) were added to dry MeOH (12 mL) and the reaction mixture stirred in RT for ca. 3 h resulting in the formation of bright-red solution, presumed to contain the vinylidene $[Ru(C{=}C(H)C_6H_4Me)(dppe)Cp^*]^+$ (see below). The addition of 2-3 drops of DBU caused a yellow precipitate to form, which was collected by filtration and washed with cold MeOH (3 mL) followed by diethyl ether (3 mL) to afford $Ru(C{\equiv}CC_6H_4Me)(dppe)Cp^*$ as a yellow solid, the identity of which was confirmed by the usual spectroscopic methods (^1H, ^{31}P NMR) and MS-ES^+.

2. A similar scale reaction in MeOH was carried out for more than 7 h to follow the course and evolution of the chemical processes involved in the preparation of the acetylide complex. The progress of the reaction was monitored by spot TLC and NMR. After ca. 2 h the reaction mixture had formed a bright orange solution containing both the vinylidene complex $[Ru(C{=}C(H)C_6H_4Me)(dppe)Cp^*]^+$ and the chloride RuCl(dppe)Cp*. After 5 h, a white precipitate was observed. After 7 h, no further change in the reaction mixture was observed. The reaction mixture was filtered to give a white precipitate, which was characterised as $AuCl(PPh_3)$ by ^1H and ^{31}P NMR spectroscopies. The bright-red solution was taken to dryness and recrystallised from diethyl ether to afford a pink solid of the vinylidene $[Ru\{C_2(H)C_6H_4Me\}(dppe)Cp^*]PF_6$, the identity of which was confirmed by ^1H and ^{31}P NMR spectroscopies.

3. Similar scale and procedure of the reaction was carried out but this time, instead of using $Au(C{\equiv}CC_6H_4Me)(PPh_3)$, a stoichiometric amount of the terminal alkyne $HC{\equiv}CC_6H_4Me$ was used. The progress of the reaction was monitored by spot TLC and NMR. After ca. 2 h a bright orange solution was observed. Upon completion, the reaction mixtures were taken to dryness followed by recrystallisation from diethyl ether to afford a pink solid of the vinylidene $[Ru\{C_2(H)C_6H_4Me\}(dppe)Cp^*]$, which was confirmed by ^1H and ^{31}P NMR spectroscopies.

Thus it can be concluded that the cationic vinylidene complex $[Ru\{C_2(H)C_6H_4Me\}(dppe)Cp^*]^+$ was formed as an intermediate in the reaction between RuCl(dppe)Cp* and $Au(C{\equiv}CC_6H_4Me)(PPh_3)$, which can be isolated as a pink solid of the PF_6 salt. The use of $Au(C{\equiv}CC_6H_4Me)(PPh_3)$ as co-reactant also gave PPh_3AuCl as a by-product. Deprotonation of the vinylidene by DBU gave $Ru(C{\equiv}CC_6H_4Me)(dppe)Cp^*$ as a yellow solid. The confirmation of the products were briefly carried out by the simple spectroscopic (NMR and MS-ES+) methods. The source of the proton in these reactions is most likely to be the MeOH solvent.

Reactions conducted in non-protic solvents supported this concept. For example, the reaction of $[Ru(NCMe)(PPh_3)_2Cp][BPh_4]$ and $Au(C{\equiv}C\ C_6H_4Me)PPh_3$ in THF was explored.

The activated ruthenium precursor $[Ru(NCMe)(PPh_3)_2Cp][BPh_4]$ (100 mg, 0.09 mmol) and $Au(C{\equiv}CC_6H_4Me)(PPh_3)$ (55 mg, 0.09 mmol) were added into the dry THF (12 mL) and stirred at RT for ca. 48 h and the progress of the reaction was monitored by spot TLC and ^1H and ^{31}P NMR. After this time the reaction mixture was taken to dryness and ^{31}P NMR spectrum was taken which shows that there was a resonance at δ 51.5 ppm typical of $Ru(C{\equiv}CC_6H_4Me)(PPh_3)Cp$. However, there were also resonances of the starting materials of $[Ru(NCMe)(PPh_3)_2Cp][BPh_4]$ (δ 42.9 ppm) and $Au(C{\equiv}CC_6H_4Me)PPh_3$ (δ 43.6 ppm), and unknown resonances at δ 39.9 ppm and δ 30.5 ppm were also observed. The crude solids also showed the presence of $Ru(C{\equiv}CC_6H_4Me)(PPh_3)Cp$ in MS-ES+, which is the M+ was observed at m/z 806 and [M+Na]+ at m/z 829. These isotopic envelopes were also confirmed by the accurate mass measurement. The unexpected resonances near 40 and 30 ppm could be suggested as arising from an intermediate gold-substituted vinylidene, but such suggestions remain unfounded at present.

To further verify these suggestions, a short series of NMR experiments were also conducted.

Reaction 2: The NMR tube reaction of $[Ru(NCMe)(PPh_3)_2Cp][BPh_4]$ and $Au(C{\equiv}C\ C_6H_4Me)PPh_3$ in $CDCl_3$.

A 1:1 stoichiometric amount of $[Ru(NCMe)(PPh_3)_2Cp][BPh_4]$ and $Au(C{\equiv}C\ C_6H_4Me)PPh_3$ were added to $CDCl_3$ solution in an NMR tube. The progress of the reaction was monitored by ^1H and ^{31}P NMR every 24 h for a week. After 24 h, there was a resonance at δ 51.5 ppm which is a typical signal for $Ru(C{\equiv}CR)(PPh_3)Cp$ (i.e. indicative to $Ru(C{\equiv}CC_6H_4Me)(PPh_3)Cp$]. In addition, there were also resonances of the starting materials of $[Ru(NCMe)(PPh_3)_2Cp][BPh_4]$ (δ 42.9 ppm) and $Au(C{\equiv}C\ C_6H_4Me)PPh_3$ (δ 43.6 ppm) and the unknown resonance at δ 39.9 ppm were also

observed. There were no changes in the chemical shifts of these resonances although the progress of the reaction was monitored daily for 7 days. Apparently the reaction had reached equilibrium.

Reaction 3: The NMR tube reaction of Ru(C≡CPh)(dppe)Cp* and Au(C≡C C_6H_4Me)PPh_3 in $CDCl_3$.

A 1:1 stoichiometric amount of Ru(C≡CPh)(dppe)Cp* and Au(C≡C C_6H_4Me)PPh_3 were added to the $CDCl_3$ solution in an NMR tube. The progress of the reaction was monitored by ^1H and ^{31}P NMR every 24 h for two week. After 3 days, there was no resonance that could be attributed to the expected vinylidene or acetylide products. The only resonances observed were those of the starting materials of Ru(C≡CPh)(dppe)Cp* (δ 81.9 ppm) and Au(C≡C C_6H_4Me)PPh_3 (δ 43.5 ppm). There were no changes in the chemical shifts of these resonances although the progress of the reaction was monitored daily for 3 days. Then, stoichiometrically amount of $AuCl(PPh_3)$ was added on the day 4. After 24 h later, the typical vinylidene resonance was observed at δ 72.8 ppm. However, there were also resonances of both starting materials as well as $AuCl(PPh_3)$ (δ 34.3 ppm). There were no changes in the chemical shifts of these resonances although the progress of the reaction was monitored daily for two weeks.

The absence of any detectable protio-vinylidene in the THF reaction suggests that the transmetallation proceeds perhaps *via* a transient gold vinylidene $[Ru(C{=}C(AuPR_3)R(dppe)Cp^*]^+$ with the position of the equilibrium being solvent / proton dependent. The role of free $AuCl(PPh_3)$ in the reaction is interesting, but clearly more work remains to be done to elucidate the mechanism of this process.

6.2.3. Molecular Structural Analysis

The molecular structures of **47, 49- 51** and **53** have been determined by single crystal X-ray diffraction as shown in **Figure 6.1-Figure 6.6**. Crystallographic data, selected bond lengths and angles are listed in **Table 6.1** to **Table 6.5.** The crystallographic work has been carried out by Dr D. S. Yufit.

Group 9 [Ir(CO)(O_2)(PPh_3)$_2$(C≡CC_6H_4Me)] (47)

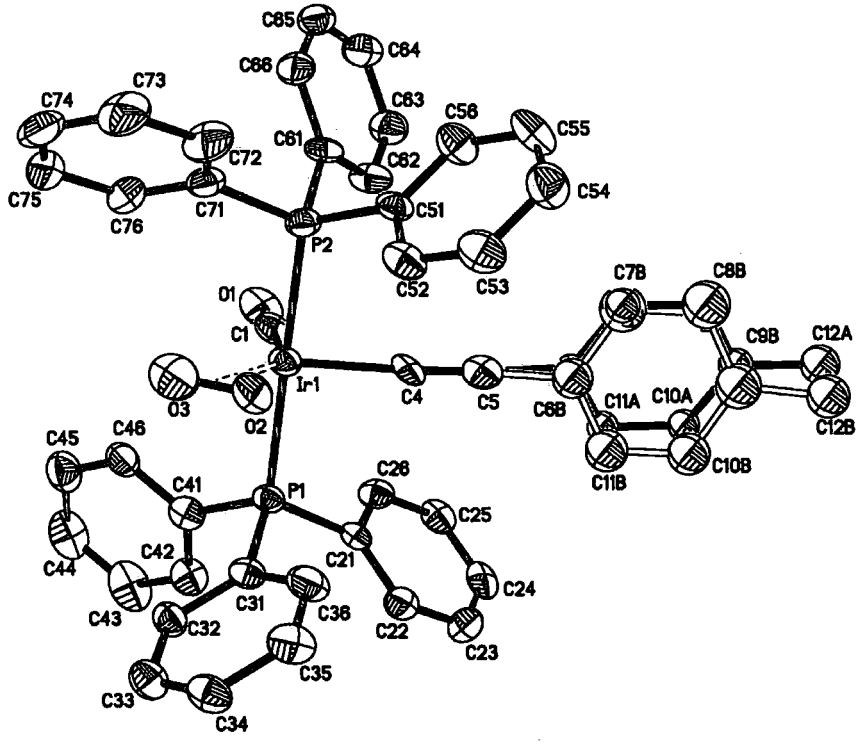

Figure 6.1. A plot of molecules of **47**, illustrating the atom numbering scheme.

Table 6.1. Crystal data for **47.**

	47
Molecular formula	$C_{46}H_{37}P_2O_3Ir$ x $CHCl_3$
M / g mol^{-1}	1011.26
Crystal system	Monoclinic
a / Å	9.8286(3)
b / Å	19.5234(5)
c / Å	22.3040(6)
α / °	90
β / °	98.99(1)
γ / °	90
V / Å^3	4227.3(2)
Space group	P 2_1/c
Z	4
D_c / Mg m^3	1.589
Crystal size / mm	0.12x 0.08 x 0.03
Crystal habit	plate
F (000)	2008
Radiation	Mo(K_α)
Wavelength / Å	0.71073
μ / mm^{-1}	3.465
Temperature / K	120(2)
Data collection range / °	1.39 – 27.50
Reflections measured	46829
Data, restraints, parameters	9712, 6, 401
R_1, *wR2* (all data)	0.1074, 0.1714
Goodness-of-fit on F^2 (all data)	1.064
peak, hole / eÅ^{-3}	2.142, -1.794

Table 6.2. Selected bond lengths (Å) and angles (°) for **47.**

Ir(1)-C(1)	1.900(9)
Ir(1)-C(4)	1.981(9)
Ir(1)-P(1)	2.354(2)
Ir(1)-O(2)	2.057(8)
Ir(1)-O(3)	2.046(8)
Ir(1)-P(2)	2.355(2)
C(1)-O(1)	1.064(11)
C(4)-C(5)	1.203(12)
C(5)-C(6)	1.470(14)
O(2)-O(3)	1.495(11)

P(1)-Ir(1)-C(1)	89.8(3)	P(1)-Ir(1)-O(2)	91.08(19)
P(1)-Ir(1)-C(4)	91.9(2)	Ir(1)-O(2)-O(3)	42.7(3)
P(2)-Ir(1)-C(4)	87.7(2)	C(1)-Ir(1)-C(4)	94.6(4)
P(1)-Ir(1)-P(2)	176.24(8)	C(5)-C(4)-Ir(1)	177.6(7)
P(1)-Ir(1)-O(3)	87.0(2)	C(1)-Ir(1)-O(3)	117.1(4)
P(1)-Ir(1)-O(2)	91.08(19)		

Molecular Analyses of 47

The structure of **47** (**Figure 6.1**) does not differ significantly from those of similar complexes such as $IrCl(O_2)(CO)(PPh_3)_2$, [91] $Ir(CO)(C{\equiv}CPh)(PPh_3)_2$, [80] or from the heteronuclear complex of $\{Cp(OC)_3W\}C{\equiv}CC{\equiv}C\{Ir(CO)(PPh_3)_2(O_2)\}$. [78] Thus, the bond lengths of Ir-CO, Ir-P and Ir-O are 1.900(9), 2.354(2) and 2.355(2), and 2.057(8) and 2.046(8), which is comparable with the $Ir(CO)(PPh_3)_2(O_2)$ fragment in the heteronuclear complex of $\{Cp(OC)_3W\}C{\equiv}CC{\equiv}C\{Ir(CO)(PPh_3)_2(O_2)\}$[2.02(4), 2.35(1) and 2.03(3), 2.08(3). In addition, the bond length of the dioxygen adduct for both complexes is also comparable, 1.495(11) for **47** and 1.36(4) in $\{Cp(OC)_3W\}C{\equiv}CC{\equiv}C\{Ir(CO)(PPh_3)_2(O_2)\}$. These bond lengths are also similar to ranges of 1.882(9)–1.90(1), 2.363(3)–2.370(3) and 2.029(8)–2.084(9) Å, and

1.46(1)–1.477(11) Å for [O(2)-O(3)], respectively, found in $IrCl(O_2)(CO)(PEtPh_2)_2$ [92] and $Ir_2(\mu\text{-dppp})Cl_2(O_2)(CO)_2$. [93]

The ethynyl moiety in the structure of **47** is essentially linear whereas the angle between Ir(1)-C(4)-C(5) is 177.6(7)° where as the angle between P(1)-Ir(1) and P(2) is 176.24(8). These bond angles are comparable with those found in $Ir(CO)(C{\equiv}CPh)(PPh_3)_2$, [80] and in the the $Ir(CO)(PPh_3)_2(O_2)$ fragment in the heteronuclear complex of $\{Cp(OC)_3W\}C{\equiv}CC{\equiv}C\{Ir(CO)(PPh_3)_2(O_2)$, [78] the bond angles found in these structures are Ir(1)-C(4)-C(5) is 174.0(2)° [a little curvature in the heteronuclear complex and found as 154.0(4)°] and the angle between P(1)-Ir(1)-P(2) is in between 173.3 (2)°-174.7(4)°.

Group 10 (*trans*-Pt(C≡CR)$_2$(PL)$_2$)

***trans*-Pt(C≡CPh)$_2$(PPh$_3$)$_2$ (49)**

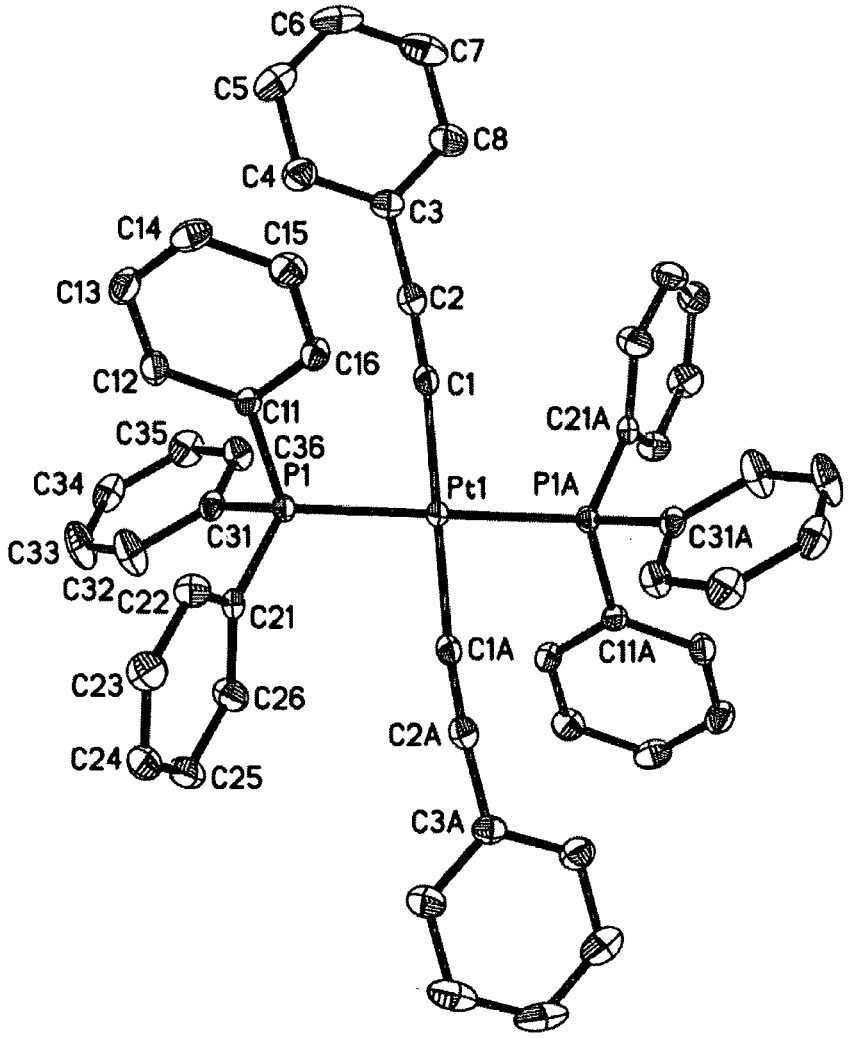

Figure 6.2. A plot of a molecule of **49**, illustrating the atom numbering scheme.

trans-$Pt(C{\equiv}CC_6H_4Me)_2(PPh_3)_2$ **(50)**

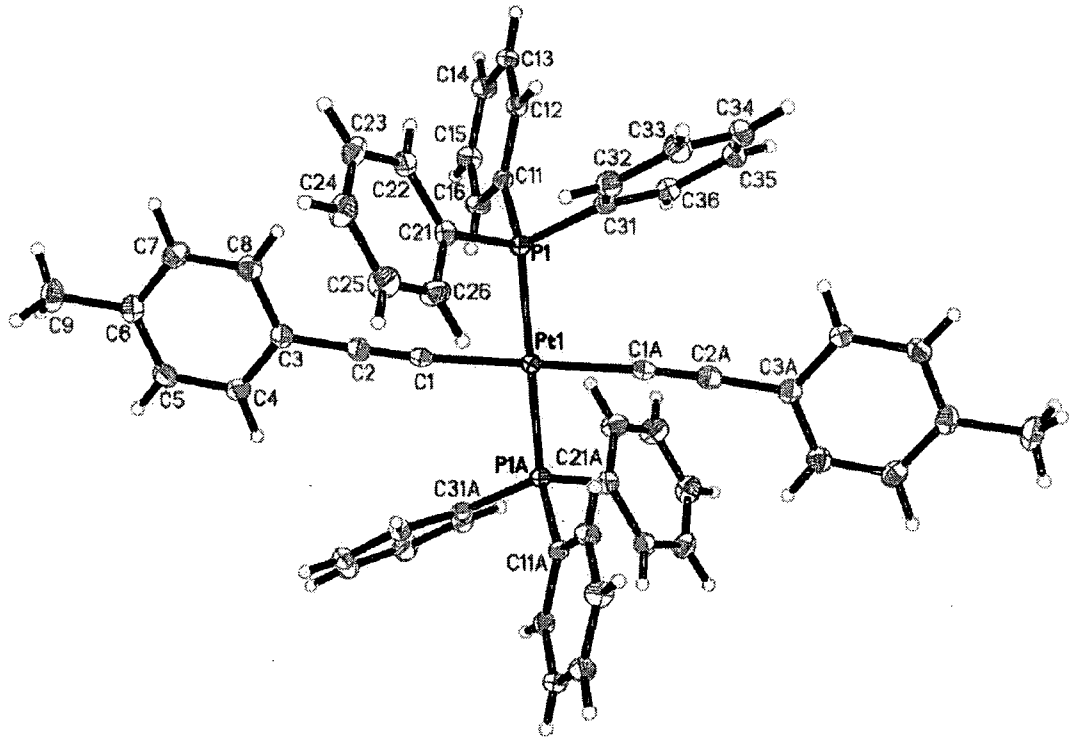

Figure 6.3. A plot of a molecule of **50**, illustrating the atom numbering scheme.

Molecular Analyses of 49 and 50

The structures of complexes **49** and **50** are comparable and similar to each other (**Figure 6.1** and **Figure 6.2**). In both structures, the platinum ion is coordinated by a series of four σ-bonded ligands in a square planar arrangements. The molecular geometry is that normally expected for Pt(II) complexes observed in other acetylide platinum complexes in the this system, [R = C_6H_4SOCMe, $C_6H_4NH_2$, C_6H_4CN, $C_6H_4NO_2$ and $R_1 = C_6H_5$; $R_2 = C_6H_4NO_2$]. [85-87,94,95]

The ethynyl moiety is essentially linear in between the complexes, but there is a gentle curvature in the molecular backbone, being the angles Pt(1)-C(1)-C(2) and C(1)-C(2)-C(3), respectively 172.78(15)-175.88(15)° and 173.27(18)-177.32(18)°, which is brought about by crystal packing. These angles are comparable with those similar structures explained above [174.4(6)-177.5(2) and 173.7(8)-176.0(8)

respectively]. The angles of C(1)-Pt(1)-C(2) is slightly distorted as provided by the value of the *cis* angle 85.90(5)-86.73(5)°. The acetylenic (C≡C) bond lengths are the same within the limit of precision of the structure determination, 1.188(2)-1.207(2) Å. The bond lengths of the Pt(1)-C(1) are also very much similar to each other and are in the typical lengths for this system, 2.0017(17)-2.0252(17)°. The selected bond lengths (Å) and angles (°) of **49** and **50** are shown in the **Table 6.3**.

Table 6.3. Crystal data for **49 -51**

	49	**50**	**51**
Molecular formula	$C_{52}H_{40}P_2Pt$	$C_{54}H_{44}P_2Pt$	$C_{24}H_{32}P_2Pt$
M / g mol^{-1}	921.87	949.92	577.53
Crystal system	Orthorhombic	Monoclinic	Monoclinic
a / Å	17.9771(3)	13.5550(2)	12.3805(5)
b / Å	9.5527(1)	8.5121(1)	5.7372(2)
c / Å	22.9326(3)	18.0271(3)	17.1229(7)
α / °	90	90	90
β / °	90	90.30(1)	105.86(1)
γ / °	90	90	90
V / Å^3	3938.2(1)	2079.97(5)	1169.92(8)
Space group	P b c a	P 2_1/n	P2(1)/c
Z	4	2	2
D_c / Mg m^3	1.555	1.517	1.639
Crystal size / mm	0.34 x 0.18 x 0.08	0.34 x 0.08 x 0.06	0.34 x 0.16 x 0.06
Crystal habit	plate	plate	plate
F (000)	1840	952	568
Radiation	Mo(K_α)	Mo(K_α)	Mo(K_α)
Wavelength / Å	0.71073	0.71073	0.71073
μ / mm^{-1}	3.681	3.487	6.140
Temperature / K	120(2)	120(2)	120(2)
Data collection range / °	2.11 – 30.00	1.88 – 29.00	2.47-29.98
Reflections measured	51715	25528	10382
Data, restraints, parameters	5741, 0, 330	5541, 0, 347	3307, 0, 124
R_1, *wR2* (all data)	0.0296, 0.0508	0.0215, 0.0411	0.0273, 0.0414
Goodness-of-fit on F^2 (all data)	1.053	1.095	1.098
peak, hole / eÅ^{-3}	0.401, -0.785	1.253, -0.378	0.566, -0.851

Table 6.4. Selected bond lengths (Å) and angles (°) for **49** to **51.**

	49	**50**	**51**
C(1)-C(2)	1.207(2)	1.188(2)	1.214(4)
C(2)-C(3)	1.441(2)	1.445(2)	1.437(3)
C(3)-C(4, 8)	1.399(3), 1.395(2)	1.403(2), 1.397(2)	1.404(3), 1.393(3)
C(4)-C(5),C(7)-C(8)	1.392(3) 1.382(3)	1.393(2), 1.387(2)	1.386(4), 1.394(3)
C(6)-C(5, 7)	1.369(3), 1.396(3)	1.388(3) 1.391(2)	1.395(4), 1.392(4)
Pt(1)-C(1)	2.0017(17)	2.0252(17)	2.001(3)
Pt(1)-P(1)	2.3121(4)	2.2887(4)	2.2929(6)
P(1)-C(11)	1.8232(16)	1.8239(16)	1.811(3)
P(1)-C(21,10)	1.8254(16)	1.8181(16)	1.814(3)

	49	**50**	**51**
C(1)-C(2)-C(3)	173.27(18)	177.32(18)	175.3(3)
P(1)-Pt(1)-P(2)	93.27(5)	94.10(5)	90.45(7)
C(3)-C(4)-C(8)	104.15(8)	108.19(7)	117.6(2)
C(1)-Pt(1)-P(1)	86.73(7)	85.90(5)	90.45(7)

trans-$Pt(C{\equiv}CC_6H_4Me)_2(PMe_3)_2$ **(51)**

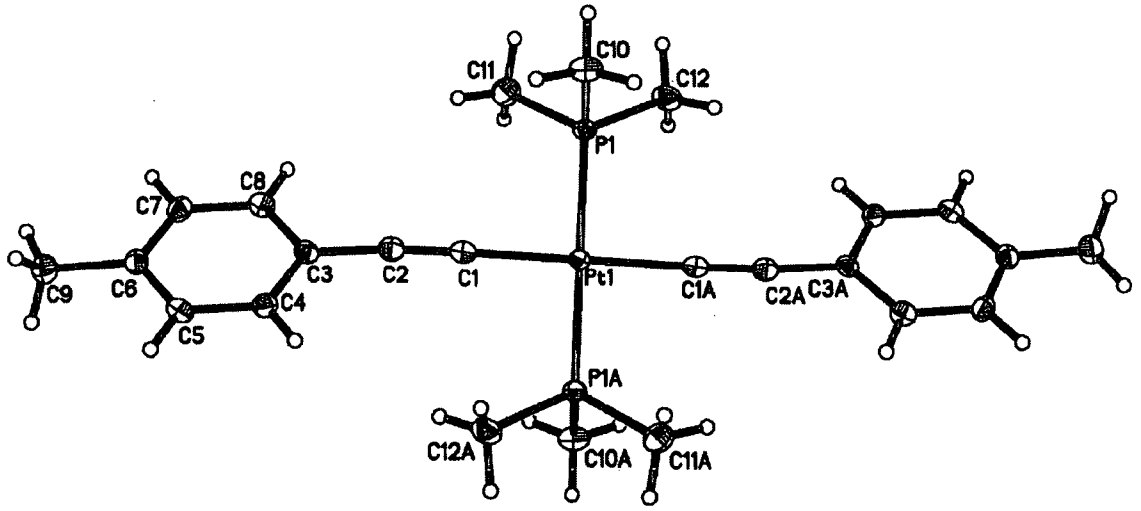

Figure 6.4.: A plot of molecules of **51**, illustrating the atom numbering scheme.

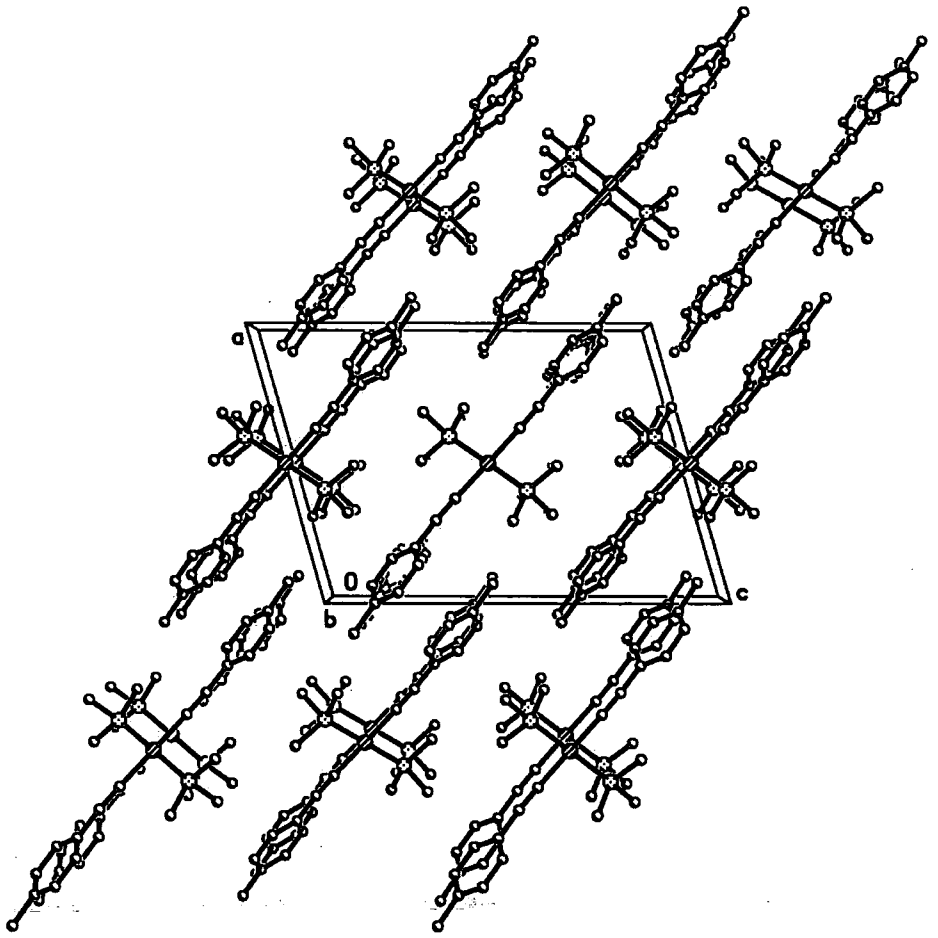

Figure 6.5. Representative packing diagram of **51**.

Molecular Analysis of 51

The structure of complex **51** (**Figure 6.3** and **Figure 6.4**) is quite similar to that of complex **50**, however, the $(PPh_3)_2$ ligands of **50** is replaced by $(PMe_3)_2$ ligands (**Figure 6.3**). Surprisingly, there is no comparable similar structure to complex **51** that features a $(PMe_3)_2$ ligand moiety. However a complex has been reported containing the *cis*-$Pt(C{\equiv}CC_6Me_4)_2(PMe_3)_2$ fragment, the heteronuclear gold complex $[\{Au\{Pt(PMe_3)_2\}_2\}\{\mu\text{–}Ar(C{\equiv}C)_2\}_3]$ reported by Vicente and co-workers (**Figure 6.4**). [96]

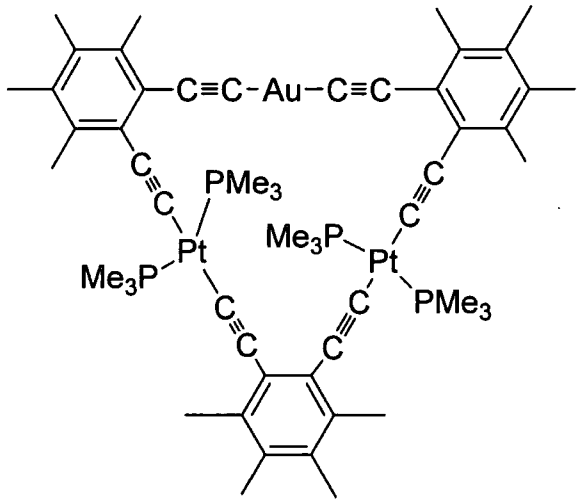

Figure 6.4. The heteronuclear complex of $[\{Au\{Pt(PMe_3)_2\}_2\}\{\mu\text{–}Ar(C{\equiv}C)_2\}_3]$. [96]

The structure of **51** shows the platinum ion to be coordinated in square planar arrangements by two *trans*-PMe_3 groups and two *trans*-acetylene ligands moieties The ethynyl moiety is essentially linear, but there is a gentle curvature in the molecular backbone, resulting from the angles Pt(1)-C(1)-C(2) and C(1)-C(2)-C(3), 178.7(2)° and 175.3(3)°, respectively, which are brought about by crystal packing. These angles are comparable with those similar structures as shown in **Figure 6.4** [177.2(2)° and 174.7(6)° respectively]. The acetylenic (C≡C) bond lengths are also comparable 1.214(4) Å, and in $[\{Au\{Pt(PMe_3)_2\}_2\}\{\mu\text{–}Ar(C{\equiv}C)_2\}_3]$ is 1.215(8) Å. The bond lengths of the Pt(1)-C(1) are also very much similar to each other and are in the typical lengths for this system, 2.001(3) Å [1.994(6) Å]. In addition, the bond length of Pt(1)-P(1) is also comparable which is 2.2929(6) Å [2.2819(18) Å]. The selected bond lengths (Å) and angles (°) of **51** are shown in the **Table 6.3**.

6.2.3.3. *Group 11*

$Au(PMe)_3[PF_6]$ (53)

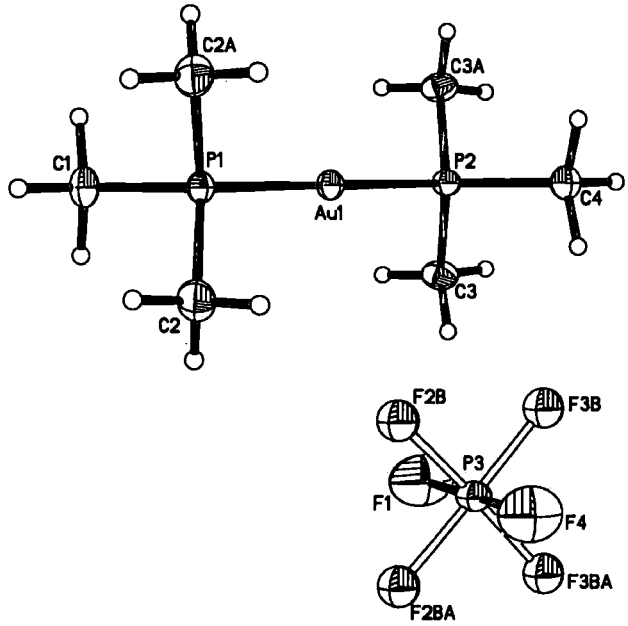

Figure 6.5. A plot of molecules of **53**, illustrating the atom numbering scheme.

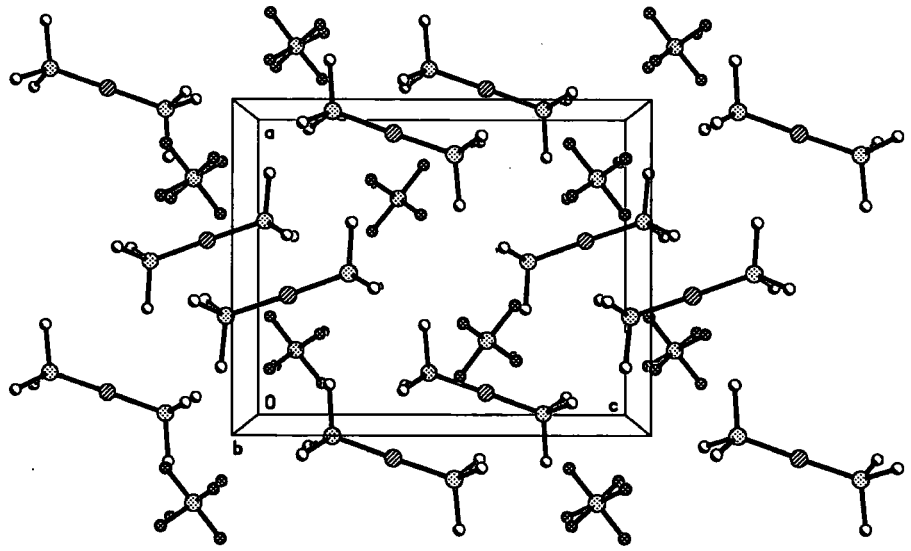

Figure 6.6. Representative packing diagram of **53,** reveals that there is no aurophilic interaction due to the steric effect of the supporting ligand attached to gold as well as the presence of PF_6^- in the lattice.

Table 6.4. Crystal data for **53**.

	53
Molecular formula	$C_6H_{18}P_2xPF_6$
M / g mol^{-1}	494.08
Crystal system	Orthorombic
a / Å	11.5118(2)
b / Å	8.5384(2)
c / Å	14.3292(3)
α / °	90
β / °	90
γ / °	90
V / Å^3	1408.45(5)
Space group	Pn m a
Z	4
D_c / Mg m^3	2.330
Crystal size / mm	0.56 x 0.20 x 0.02
Crystal habit	plate
F (000)	928
Radiation	Mo(K_α)
Wavelength / Å	0.71073
μ / mm^{-1}	0.456
Temperature / K	120(2)
Data collection range / °	2.27-31.50
Reflections measured	19470
Data, restraints, parameters	2477, 4, 106
R_1, *wR2* (all data)	0.0201, 0.0509
Goodness-of-fit on F^2 (all data)	1.054
peak, hole / *e*Å^{-3}	1.280, -1.565

Table 6.5. Selected bond lengths [Å] and angles [°] for **53.**

Au(1)-P(1)	2.3016(8)	P(1)-C(1)	1.813(4)
Au(1)-P(2)	2.3023(8)	P(2)-C(3)	1.803(3)
P(1)-C(2)	1.804(3)	P(2)-C(4)	1.810(4)

P(1)-Au(1)-P(2)	178.90(3)	C(3)#1-P(2)-C(3)	105.20(19)
C(2)#1-P(1)-C(2)	105.7(2)	C(3)-P(2)-C(4)	104.91(12)
C(2)-P(1)-C(1)	104.69(12)	C(3)-P(2)-Au(1)	113.23(9)
C(2)-P(1)-Au(1)	113.74(10)	C(4)-P(2)-Au(1)	114.43(13)
C(1)-P(1)-Au(1)	113.35(13)		

Molecular Analysis of 53

The structure of **53** (**Figure 6.5**) is comparable with the structure of $Au(PMe_3)_2[Cl]$ [97] The P(1)-Au(1)-P(2) coordination is essentially linear, 178.90(3)°, for $Au(PMe_3)_2[Cl]$ is 175.4(1)°. The distance between Au(1)-P(1)/P(2) are 2.3016(8) Å/2.3023(8) Å, which compare with the value of 2,304(1) Å for $Au(PMe_3)_2[Cl]$. From the crystal lattice of **53**, it should be noted that there are no close intermolecular aurophilic interactions perhaps due less to the steric effect of the (PMe_3) ligands and more to Coulombic effects and the presence of PF_6 counter ions that restrain the intermolecular interaction between the molecules.(**Figure 6.6**).

6.3. Conclusions

In this chapter, the series of novel, preparative scale, stoichiometric transmetallation reactions involving a gold(I) acetylide complex are presented. Specifically, the readily available complexes $Au(C{\equiv}CR)(PPh_3)$ [R = Ph, C_6H_4Me] have been treated with several inorganic and organometallic compounds MXL_n [M = metal, L_n = supporting ligands, X = halide], to afford the corresponding metal-acetylide complexes $M(C{\equiv}CR)L_n$, (20-80 % yield). with representative examples featuring metals from Groups 8-11. The acetylide products were fully characterised by usual spectroscopic methods including the molecular structural analysis. A series of both preparative and NMR scale reactions were carried out to investigate further the

mechanisms of the transmetallation reactions between $[L_n]MX$ [X = Cl, NCMe] with the gold acetylide moieties $Au(C{\equiv}CR)PPh_3$ [R = Ph, C_6H_4Me]. In this context of studies, $RuX(L_2)Cp'$ and $Au(C{\equiv}CC_6H_4Me)PPh_3$ were chosen to represent all the transmetallation reaction in this chapter. It can be concluded that the absence of any detectable protio-vinylidene in the THF reaction suggests that the transmetallation proceeds perhaps *via* a transient gold vinylidene $[Ru(C{=}C(AuPR_3)R(dppe)Cp^*]^+$ with the position of the equilibrium being solvent / proton dependent. The role of free $AuCl(PPh_3)$ in the reaction is interesting, but clearly more work remains to be done to elucidate the mechanism of this process.

6.4. Experimental Details

6.4.1. General Condition

All reactions were carried out under an atmosphere of nitrogen using standard Schlenk techniques. Reaction solvents were purified and dried using an Innovative Technology SPS-400, and degassed before use. No special precautions were taken to exclude air or moisture during work-up. Preparative TLC was performed on 20 x 20 cm glass plates coated with silica gel (0.5 mm thick, Merck GF-254). The reagents $NiBr(PPh_3)Cp$, [98] $RuCl(PPh_3)_2Cp$, [99] $RuCl(dppe)Cp^*$ [100] $[Ru(NCMe)(PPh_3)_2Cp][BPh_4]$, [101] *cis*-$PtCl_2(PPh_3)_2$, [102] *trans*-$PtCl_2(PMe_3)_2$, [103] $FeCl(dppe)Cp$, [104] $IrCl(CO)(PPh_3)$, [81] $Au(C{\equiv}CPh)PPh_3$, [105,106] $Au(C{\equiv}CC_6H_4Me)PPh_3$, [105,106] were prepared by literature methods. Authentic samples of $Ni(C{\equiv}CPh)(PPh_3)Cp$, **44**, [43,88,107] $Fe(C{\equiv}CPh)(dppe)Cp$, [68] $Ru(C{\equiv}CPh)(PPh_3)_2$, [69,108] $Ru(C{\equiv}CPh)(dppe)Cp^*$, [68,108] *trans*-$Pt(C{\equiv}CPh)_2(PPh_3)_2$, [84] *trans*-$Pt(C{\equiv}CC_6H_4Me)_2(PPh_3)_2$, [84] $Cu(C{\equiv}CC_6H_4Me)(PPh_3)$, [90] were prepared as described on previous occasions. Other reagents were purchased and used as received. IR spectra of the synthesized complexes were recorded using a Nicolet Avatar spectrometer from dichloromethane solutions in a cell fitted with CaF_2 windows or were recorded using a Nicolet Avatar spectrometer from Nujol mull suspended between NaCl plates. NMR spectra were obtained with Bruker Avance (^1H 400.13 MHz or ^1H 499.83 MHz) or Varian Mercury (^1H 399.97 MHz), and Varian Mercury (^{31}P 161.91 MHz or ^{31}P 80.96 MHz) spectrometers from $CDCl_3$ solutions and referenced against solvent resonances (^1H, ^{13}C) or external H_3PO_4 (^{31}P). Mass spectra were recorded using Thermo Quest Finnigan Trace MS-Trace GC or Thermo Electron Finnigan LTQ FT mass spectrometers.

Diffraction data were collected at 120K on a Bruker SMART 6000 CCD (**49** and **50**) and (**53**), on Bruker SMART 1K CCD (**51**) and on Rigaku R-AXIS Spider IP (**47**), three-circle diffractometers, using graphite-monochromated Mo-K_α radiation. The diffractrometer was equipped with Cryostream (Oxford Cryosystems) low-temperature nitrogen cooling devices. The structures were solved by direct-methods

and refined by full matrix least-squares against F^2 of all data using *SHELXTL* software. [109] All non-hydrogen atoms were refined in anisotropic approximation except the disordered ones, H atoms were placed into the calculated positions and refined in "riding" mode. The crystallographic data and parameters of the refinements are listed in **Table 6.1-Table 6.5**.

6.4.2. Experimental

Group 8

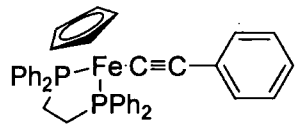

6.4.2.1. Preparation of Fe(C≡CPh)(dppe)Cp (44) [68]

A suspension of FeCl(dppe)Cp (50 mg, 0.09 mmol) and Au(C≡CPh)(PPh_3) (51 mg, 0.09 mmol) and NH_4PF_6 (15 mg, 0.09 mmol) in MeOH (10 ml) was heated at reflux for ca. 1 h under nitrogen, the progress of the reaction being monitored by TLC (hexane: acetone = 7/3). The resulting clear orange solution was treated with 2-3 drops of DBU and the reaction mixture taken to dryness. The crude was extracted with benzene, and the extracts purified by preparative TLC (hexane: acetone = 7/3). The red band was collected and afforded title product. (24 mg, 43 %). IR (CH_2Cl_2): ν(C≡C) 2060 cm^{-1}.^1H NMR ($CDCl_3$, 200): δ 2.23 (2 x dd, 2H, $J_{HP} = J_{HH} \sim 6$ Hz, dppe), 2.63 (2 x dd, 2H, $J_{HP} = J_{HH} \sim 6$ Hz, dppe); 4.25 (s, 5H, Cp), 6.50-7.94 (m, 25H, Ar). $^{31}P\{^1H\}$ NMR ($CDCl_3$, 81 MHz): δ 107.5 (s, dppe). $^{13}C\{^1H\}$ NMR ($CDCl_3$, 125.7 MHz): δ 28.6 (dd, $J_{CP/CCP} \sim 22$ Hz, CH_2); 79.3 (Cp); 123.1 (C_β); 127.6 (C4); 129.0 (C3); 129.4 (C2); 130.5 (C1); 127.8, 127.0 (dds, $J_{CP/CCP} \sim 5$ Hz, $C_{m,m'}$); 128.1 ($C_{p,p'}$); 134.0, 132.0 (dds, $J_{CP/CCP} \sim 5$ Hz, $C_{o,o'}$); 138.1, 138.4 (m, $C_{i,i'}$), 142.5 (t, $J_{CP} = 14$ Hz, C_α). Found: C, 75.15; H, 5.57 %. $C_{39}H_{34}P_2Fe$ requires: C, 75.48; H, 5.48 %. ES+-MS(m/z) : 620, $[M]^+$, 519, $[M\text{-}C{\equiv}CPh]^+$. [High resolution: calculated for $FeC_{39}H_{34}P_2$ $[M]^+$ 620.14797; found 620.14757. Lit. [68]; IR(CH_2Cl_2): ν(C≡C) 2061 cm^{-1}. $^{13}C\{^1H\}$ NMR ($CDCl_3$, 75 MHz): δ 28.4 (CH_2, dppe), 79.2 (Cp), 127.3-142.5 (m, Ar), 140.5 (Cα), 122.8 (Cβ).

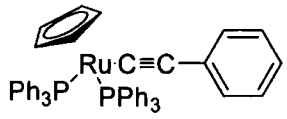

6.4.2.2. Preparation of Ru(C≡CPh)(PPh$_3$)$_2$Cp (45) [69,108]

A suspension of RuCl(PPh$_3$)$_2$Cp (100 mg, 0.14 mmol), Au(C≡CPh)(PPh$_3$) (77 mg, 0.14 mmol) and NH_4PF_6 (22 mg, 0.14 mmol) in MeOH (10 ml) was heated at reflux for 30 mins to form a bright red solution. Addition of 2-3 drops of DBU caused a yellow precipitate to form, which was collected by filtration, washed with cold MeOH (3 ml), and air-dried to afford the title product as a yellow solid (88 mg, 81 %). IR(nujol): ν(C≡C) 2077 cm^{-1}.^{1}H NMR ($CDCl_3$, 400 MHz): δ 4.32 (s, 5H, Cp), 7.08-7.50 (m, 35H, Ar). $^{31}P\{^1H\}$ NMR ($CDCl_3$, 81 MHz): δ 51.5 (s, PPh_3). ^{13}C NMR ($CDCl_3$, 100 MHz): δ 85.2 (Cp); 114.4 (C_β); 116.1 (t, J_{CP} = 25 Hz, C_α); 123.0 (C4), 127.6 (C3); 130.5 (C2); 130.6 (C1); 127.2 (dd, $^3J_{CP/}$ $^6J_{CP}$ ~ 5 Hz, C_m); 128.4 (C_p); 133.9 (dd, $^2J_{CP/}$ $^5J_{CP}$ ~ 5 Hz, C_o); 139.0 (dd, $^1J_{CP/}$ $^4J_{CP}$ ~ 11 Hz C_i). ES+-MS(m/z): 793, $[M+H]^+$; 691$[M-C{\equiv}CC_6H_5]^+$. Lit. [69,108]. ^{13}C NMR ($CDCl_3$, 100 MHz): δ 85.2 (Cp); 114.4 (C_β); 116.1 (t, J_{CP} = 25 Hz, C_α); 123.0 (C4), 127.6 (C3); 130.5 (C2); 130.6 (C1); 127.2 (dd, $^3J_{CP/}$ $^6J_{CP}$ ~ 5 Hz, C_m); 128.4 (C_p); 133.9 (dd, $^2J_{CP/}$ $^5J_{CP}$ ~ 5 Hz, C_o); 139.0 (dd, $^1J_{CP/}$ $^4J_{CP}$ ~ 11 Hz C_i).

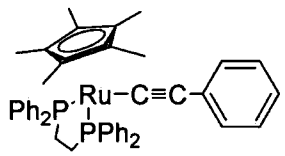

6.4.2.3. Preparation of Ru(C≡CPh)(dppe)Cp* (46) [69,108]

A suspension of RuCl(dppe)Cp* (100 mg, 0.15 mmol), Au(C≡CPh)(PPh$_3$) (84 mg, 0.15 mmol) and NH_4PF_6 (24 mg, 0.15 mmol) in MeOH (10 ml) was heated at reflux for 1 hr to form a bright red solution, which was treated with 2-3 drops of DBU and allowed to stir for a further 1 h at RT. The yellow precipitate that formed over this time was collected by filtration, washed with cold MeOH (3 ml), and air-dried to afford the title product as a yellow solid (56 mg, 51%). IR(nujol): ν(C≡C) 2066 cm^{-1}. ^{1}H NMR ($CDCl_3$, 400 MHz): δ 1.57 (s, 15H, Cp), 2.08 (2 x dd, 2H, $J_{HP} = J_{HH}$ = 6 Hz, dppe), 2.70 (2 x dd, 2H, $J_{HP} = J_{HH}$ = 6 Hz, dppe); 6.78-7.81(m, Ar 25H). $^{31}P\{^1H\}$ NMR ($CDCl_3$, 162 MHz): δ 81.1 (s, dppe). ^{13}C NMR ($CDCl_3$, 100 MHz): δ 10.0 (Me); 92.5 (Cp); 109.6 (C_β); 128.8 (t, J_{CP} = 25 Hz, C_α); 122.4 (C4), 127.4 (C3);

130.2 (C2); 131.3 (C1); 127.1, 127.4 (dd, $^{3}J_{CP/}$ $^{6}J_{CP}$ ~ 5 Hz, $C_{m,m'}$); 128.8, 128.8 ($C_{p,p'}$); 133.2, 133.7 (dd, $^{2}J_{CP/}$ $^{5}J_{CP}$ ~ 5 Hz, $C_{o,o'}$); 136.9, 138.9 (m, $C_{i,i'}$). ES(+)-MS (m/z):635, $[M\text{-}C{\equiv}CC_6H_5]^+$; 737, $[M+H]^+$. Lit. [69,108] IR(CH_2Cl_2): ν(C≡C) 2071 cm^{-1}. ^{1}H NMR (C_6D_6, 300 MHz): δ 1.69 (s, 15H, Cp), 1.92 (br, 2H, dppe), 2.70 (br, 2H, dppe), dppe); 7.22-7.98 (m, Ar 25H). $^{31}P\{^{1}H\}$ NMR ($CDCl_3$, 162 MHz): δ 81.0 (s, dppe). ^{13}C NMR ($CDCl_3$, 100 MHz): δ 10.0 (Me); 92.5 (Cp); 109.6 (C_β); 128.8 (t, J_{CP} = 25 Hz, C_α); 122.4 (C4), 127.4 (C3); 130.2 (C2); 131.3 (C1); 127.1, 127.4 (dd, $^{3}J_{CP/}$ $^{6}J_{CP}$ ~ 5 Hz, $C_{m,m'}$); 128.8, 128.8 ($C_{p,p'}$); 133.2, 133.7 (dd, $^{2}J_{CP/}$ $^{5}J_{CP}$ ~ 5 Hz, $C_{o,o'}$); 136.9, 138.9 (m, $C_{i,i'}$).

Group 9

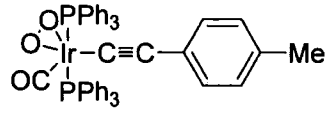

6.4.2.4. Preparation of $Ir(CO)(O_2)(PPh_3)_2(C{\equiv}CC_6H_4Me)$ (47)

A suspension of $IrCl(CO)(PPh_3)$ (100 mg, 0.13 mmol) and $Au(C{\equiv}CC_6H_4Me)(PPh_3)$ (74 mg, 0.13 mmol) were stirred at RT in THF (12 ml) for ca. 6 h to give an orange solution. The progress of the reaction was monitored by TLC and when adjudged complete the solvent was removed to give a greenish-yellow solid. Acetone (5 ml) was added to the crude product and the mixture stirred for 10 mins followed by filtration to give a yellow solid which was recrystallised ($CHCl_3$/hexane) to afford yellow crystals of the title product (46 mg, 40 %). IR (CH_2Cl_2): ν(C≡C) 2128; ν(C≡O) 1962, ν(O-O) 834 cm^{-1}.^{1}H NMR ($CDCl_3$, 400 MHz) δ 2.23 (s, 3H, Me), 6.26 (pseudo-d, J_{HH} = 8 Hz, C_6H_4), 6.82 (pseudo-d, J_{HH} = 8 Hz, C_6H_4), 7.37-7.64 (m, 30H, PPh_3). $^{31}P\{^{1}H\}$ NMR ($CDCl_3$, 161.98 MHz): δ 7.36 (s, PPh_3). $^{13}C\{^{1}H\}$ NMR ($CDCl_3$, 125.7 MHz): δ 21.4 (s, Me); 66.3 (s, Ir-Cα≡C); 109.4 (s, Ir-C≡C_β); 125.3 (C1); 128.7 (C2), 135.1 (C3); 131.4 (C4); 128.4 (dd, $^{3}J_{CP/}$ $^{6}J_{CP}$ ~ 5 Hz, C_m); 128.4 (C_p); 131.0 (C_o); 134.9 (dd, $^{1}J_{CP/}$ $^{4}J_{CP}$ ~ 5 Hz C_i); 167.4 (s, C≡O). Found: C, 61.52; H, 4.10 %. $C_{46}H_{37}P_2O_3Ir$ requires: C, 61.94; H, 4.18. %.ES+-MS(m/z): 893, $[M+H]^+$, 934, $[M+H+MeCN]^+$. [High resolution: calculated for $IrC_{46}H_{38}O_3P_2$ $[M+H]^+$ 893.19199; found 893.19242.

Group 10

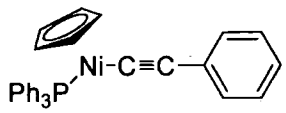

6.4.2.5. Preparation of Ni(C≡CPh)(PPh$_3$)Cp (48) [43,88,107]

To a stirred solution of NiBr(PPh$_3$)Cp (100 mg, 0.21 mmol) in dry THF (10 ml) under nitrogen Au(C≡CPh)(PPh$_3$) (120 mg, 0.21 mmol) was added and the mixture allowed to stir at room temperature, the progress of the reaction being monitored by TLC (hexane/acetone, 8:2). The solution colour become pale brown after 1 hr. After 4h at room temperature, the solution was distinctly green . After stirring for 6 hrs, the reaction was adjudged complete and the mixture was taken to dryness followed by purification on preparative TLC. A green band was isolated which was recrystallised (chloroform/MeOH) to afford the title product as green crystals. (55 mg, 53 %). ^{1}H NMR: (500 MHz, $CDCl_3$): δ 5.25 (s, 5H, CpH), 6.64-6.65(m, 2H, ≡CPh-H), 6.91-6.94 (m, 3H, ≡CPh-H), 7.34-7.47(m, 9H, PPh$_3$-H), 7.72-7.77(m, 6H, PPh$_3$-H); ^{13}C NMR: (125.67 MHz, $CDCl_3$) δ 85.90 (d, J_{PC} = 50 Hz), 92.84 (s, CpC), 120.00 (s, C≡CNi), 124.81-134.52(m, ArC); ^{31}P NMR: (80.96 MHz, $CDCl_3$) δ 41.8 (s, PPh$_3$); IR (CH_2Cl_2): ν (C≡C) 2097 cm^{-1}. ES+-MS(m/z) : 995, $[2M + Na]^+$, 509, $[M + Na]^+$, 486, $[M]^+$, 385, $[M\text{-}C{\equiv}CPh]^+$. Lit. [43,88,107]: IR (KBr pellet): ν (C≡C) 2098 cm^{-1}. ^{1}H NMR: (270 MHz, $CDCl_3$): δ 5.25 (s, 5H, CpH), 6.65-6.62(m, 2H, ≡CPh-H), 6.88-6.93 (m, 3H, ≡CPh-H), 7.25-7.42(m, 9H, PPh$_3$-H), 7.70-7.78(m, 6H, PPh$_3$-H); ^{13}C NMR: (67.8 MHz, $CDCl_3$) δ 85.77 (d, J_{PC} = 49 Hz), 92.58 (s, CpC), 119.73 (s, C≡CNi), 124.53-134.44(m, ArC); ^{31}P NMR: (162 MHz, $CDCl_3$) δ 41.3 (s, PPh$_3$);.

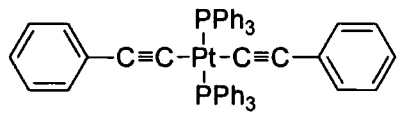

6.4.2.6. Preparation of *trans*-Pt(C≡CPh)$_2$(PPh$_3$)$_2$ (49) [84]

To a stirred aliquot of MeOH (15 ml), *cis*-$PtCl_2(PPh_3)_2$ (141 mg, 0.18 mmol) and Au(C≡CPh)(PPh$_3$)$_2$ (200 mg, 0.36 mmol) were added under nitrogen to form pale yellow suspension, and gradually forming to pale green precipitate. The reaction mixture was allowed to stir at RT for ca. 15 h, after which time it was filtered and the

precipitate collected and washed with acetone to give a yellow solid which recrystallised (CH_2Cl_2/hexane) to afford pale yellow crystals of the title product. (86 mg, 59 %). IR (nujol) ν(C≡C) 2107 cm^{-1}.^1H NMR ($CDCl_3$, 400 MHz): δ 6.26-7.83 (m, 40H, Ar). $^1P\{^1H\}$ NMR ($CDCl_3$, 80.96 MHz): δ 19.7 (s + d, $^1J_{PtP}$ = 2642 Hz, PPh_3). $^{13}C\{^1H\}$ NMR ($CDCl_3$, 125.7 MHz): δ 111.0 (t, J_{CP} ~ 16 Hz, C_α); 113.5 (C_β);128.8 (C1); 124.8 (C2), 131.1 (C3); 130.4 (C4); 127.3 (dd, $^3J_{CP/}$ $^6J_{CP}$ ~ 5 Hz, C_m); 128.1 (C_p); 131.7 (dd, $^1J_{CP/}$ $^4J_{CP}$ ~ 5 Hz C_i); 135.4 (dd, $^2J_{CP/}$ $^5J_{CP}$ ~ 29 Hz, C_o). Found: C, 68.03; H, 4.44 %. $C_{52}H_{40}P_2Pt$ requires: C, 67.75; H, 4.37 %. ES+-MS(m/z): 922, $[M+H]^+$; 944, $[M+Na]^+$; [High resolution: calculated for $PtC_{52}H_{41}P_2$ $[M+H]^+$ 922.23257; found 922.23318, $PtC_{52}H_{40}P_2Na$ $[M+Na]^+$ 944.21452; found 944.21662. Lit. [84] : IR (nujol) ν(C≡C) 2110 cm^{-1}.

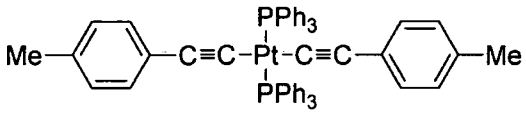

6.4.2.7. Preparation of *trans*-$Pt(C{\equiv}CC_6H_4Me)_2(PPh_3)_2$ (50) [84]

To a stirred aliquot of MeOH (40 ml), *cis*-$PtCl_2(PPh_3)_2$ (200 mg, 0.25 mmol) and $Au(C{\equiv}CC_6H_4Me)(PPh_3)$ (291 mg, 0.51 mmol) were added under nitrogen to form pale yellow suspension, which gradually evolved to pale green precipitate. The reaction mixture was allowed to stir at RT for ca. 15 h which was filtered and the solid collected washed with acetone to give a pale yellow precipitate solid which was recrystallised (CH_2Cl_2/MeOH) to afford pale yellow crystals of the title product. (73 mg, 30 %). IR (nujol) ν(C≡C) 2106 cm^{-1}. ^1H NMR ($CDCl_3$, 400 MHz): δ 2.21 (s, 6H, Me), 6.19 (pseudo-d, J_{HH} ~ 7 Hz, C_6H_4), 6.73 (pseudo-d, J_{HH} ~ 7 Hz, C_6H_4), 7.15-7.83 (m, 30H, PPh_3). $^1P\{^1H\}$ NMR ($CDCl_3$, 80.98 MHz): δ 19.7 (s + d, $^1J_{PtP}$ = 2658 Hz, PPh_3). $^{13}C\{^1H\}$ NMR ($CDCl_3$, 125.7 MHz): δ 22.4 (Me), 111.8 (t, J_{CP} ~ 16 Hz, C_α); 113.1 (C_β);128.3 (C1); 123.8 (C2), 131.7 (C3); 131.2 (C4); 127.4 (dd, $^3J_{CP/}$ $^6J_{CP}$ ~ 5 Hz, C_m); 128.3 (C_p); 130.9 (dd, $^2J_{CP/}$ $^5J_{CP}$ ~ 29 Hz, C_o); 135.2 (dd, $^1J_{CP/}$ $^4J_{CP}$ ~ 5 Hz C_i). Found: C, 68.76; H, 4.55 %. $C_{54}H_{44}P_2Pt$ requires: C, 68.27; H, 4.67 %. ES+-MS(m/z): 950, $[M+H]^+$, 972, $[M + Na]^+$, 982, $[M + H + MeOH]^+$. [High resolution: calculated for $^{194}PtC_{54}H_{45}P_2$ $[M+H]^+$ 949.26178; found 949.26252. Lit. [84]: IR (nujol) ν(C≡C) 2106 cm^{-1}.

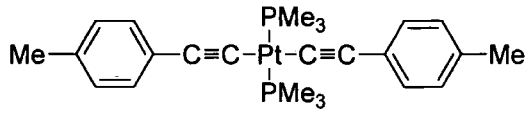

6.4.2.8. Preparation of *trans*-$Pt(C{\equiv}CC_6H_4Me)_2(PMe_3)_2$ (51)

To a stirred aliquot of MeOH (15 ml), *trans*-$PtCl_2(PMe_3)_2$ (100 mg, 0.24 mmol) and $Ph_3Au(C{\equiv}CC_6H_4Me)(PPh_3)$ (275 mg, 0.48 mmol) were added under nitrogen to afford a pale green suspension, which was stirred at RT for ca. 15 h, filtered and washed with cold MeOH (3 ml) and hexane (3 ml), and recrystallised ($CHCl_3$/MeOH) to afford pale green crystals of the title product (93 mg, 67 %). IR (nujol): ν(C≡C) 2108 cm^{-1}. ^1H NMR ($CDCl_3$, 500 MHz): δ 1.77 (dd, $^2J_{PH}$, $^4J_{PH}$ ~ 4 Hz, PMe_3), 1.80 (dd, $^3J_{Pt\text{-}H}$ ~ 30 Hz), 2.29 (s, 6H, Me), 7.03 (pseudo-d, J_{HH} = 8 Hz, C_6H_4); 7.23 (pseudo-d, J_{HH} = 8 Hz, C_6H_4). $^{31}P\{^1H\}$ NMR ($CDCl_3$, 80.98 MHz): δ -19.4 (s + d, $^1J_{PtP}$ = 2309 Hz, PMe_3). $^{13}C\{^1H\}$ NMR ($CDCl_3$, 125.7 MHz): δ 15.7 (dd, J_{CP} ~ 20 Hz, PMe_3), 16.0 (d, $J_{Pt\text{-}C}$ ~ 83 Hz), 21.6 (s, Me,, 106.3 (t, J_{CP} = 15 Hz, C_α); 108.7 (C_β); 125.5 (C1); 128.9 (C2), 131.2 (C3); 135.3 (C4). Found: C, 49.26; H, 5.56 %. $C_{24}H_{32}P_2Pt$ requires: C, 49.91; H, 5.58 %. ES+-MS(m/z): 1177, $[2M + Na]^+$; 632, $[M + Na + MeOH]^+$; 578, $[M + H]^+$; [High resolution: calculated for $PtP_2C_{24}H_{33}$ $[M+H]^+$ 578.16997; found 578.17067.

Group 11

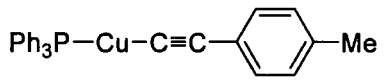

6.4.2.9. Preparation of $Cu(C{\equiv}CC_6H_4Me)(PPh_3)$ (52) [90]

An aliquot of THF (60 ml) was rapidly stirred and treated with CuI (200 mg, 1.05 mmol) and $Au(C{\equiv}CC_6H_4Me)(PPh_3)$ (600 mg, 1.05 mmol) under nitrogen to form a white suspension which gradually changed to yellow after ca. 2 h. The reaction was left stirring for ca. 24 hours at room temperature. The yellow suspension was filtered and the solid collected washed with hexane (5 ml) to give an orange solid (175 mg, 94 %) assumed to be $Cu(C{\equiv}CC_6H_4Me)$ [IR (nujol): 2064 cm^{-1}]. Removal of the solvent from the filtrate afforded $AuI(PPh_3)$. A sample of $Cu(C{\equiv}CC_6H_4Me)$ so

prepared (100 mg, 0.56 mmol) in EtOH (30 ml) and CH_2Cl_2 (5 ml) was treated with triphenylphosphine (147 mg, 0.56 mmol) to give a yellow suspension. The mixture was allowed to stir for ca. 12 hr before being filtered and the solid collected washed with a small volume of cold EtOH to give the title product, **52** as a yellow solid (100 mg, 22 %). IR (nujol) ν(C≡C) 2016 cm^{-1}; ^1H NMR (400 MHz, $CDCl_3$) δ 2.07 (s, 3H, Me), 5.83 (pseudo-doublet, 2H, C_6H_4, J ~ 8 Hz), 6.39 (pseudo-doublet, 2H, C_6H_4, J_{HH} ~ 8 Hz), 6.78-7.56 (m, 15H, C_6H_5); $^{13}C\{1H\}$ NMR (125.7 MHz, C_6D_6) 2.12 (s, Me), 77.2, 97.6 (s, C≡C), 125-136 (Ar). Lit. [90]: IR (KBr) ν(C≡C) 2014 cm^{-1}; ^1H NMR (CD_2Cl_2): δ 2.1 (s, 3H, Me), 5.9 (d, 2H, C_6H_4, J = 8 Hz), 6.4 (d, 2H, C_6H_4, J = 8 Hz), 6.9-7.8 (m, 15H, C_6H_5); $^{13}C\{1H\}$ NMR (C_6D_6): 2.12 (s, Me), 77.1, 97.5 (s, C≡C), 124-136 (Ar).

$Me_3P-Au-PMe_3]PF_6$

6.4.2.10. Preparation of $Au(PMe_3)_2[PF_6]$ (53)

The suspension of $Pt(Cl_2)(PMe_3)_2$ (200 mg, 0.48 mmol) and $Ph_3PAuC{\equiv}CPh$ (130 mg, 0.23 mmol) and NH_4PF_6 (78 mg, 0.48 mmol) in MeOH (15 mL) was allowed to stir at RT for ca. 8 hrs to give a white precipitate which then filtered, washed with a small qunatity of cold MeOH (3 ml) followed by hexane (3 ml) and the white solid was then dried in-vacuo. Crystallisation from MeCN/MeOH gave white crystals of the title product. (41 mg, 49 %). ES+-MS(m/z) : 721, $[M + Na]^+$; 349, $[M]^+$; [High resolution: calculated for $C_6H_{18}AuP_2$ $[M]^+$ 349.05439; found 349.05424.

6.5. References

1. S. L. Hegedus, *Transition Metals in the Synthesis of Complex Organic Molecules*, 1994, University Science Books, Mill Valley, California.
2. C. Elschenbroich, *Organometallics 3rd edn.*, 2006, Wiley-VCH, Weinheim, Germany.
3. M. S. Betson, A. Bracegirdle, J. Clayden, M. Helliwell, A. Lund, M. Pickworth, T. J. Snape, C. P. Worrall, *Chem. Commun.*, 2007, 754.
4. K. Godula, D. Sames, *Science,* 2006, **312**, 67.
5. B. D. Dangel, K. Godula, S. W. Youn, B. Sezen, D. Sames, *J. Am. Chem. Soc.*, 2002, **124**, 11856.
6. I. P. Beletskaya, A. V. Cheprakov, *Coord. Chem. Rev.*, 2004, **248**, 2337.
7. L. Kürti, B. Czakó, *Strategic Applications of Named Reactions in Organic Synthesis, Background and Detailed Mechanisms*, Elsevier Academic Press, 2005.
8. K. Sonogashira, Y. Tohda, N. Hagihara, *Tetrahedron Lett.*, 1975, 4467.
9. F. Diederich, P. J. Stang, *Metal-Catalysed Cross-Coupling Reactions*, 1998, Wiley-VCH Verlag GmbH, Weinheim Germany.
10. F. Chinchilla, C. Nájera, *Chem. Rev.*, **107**, 3, 874.
11. E. –I. Negishi, A. De Meijere, *Handbook of Organopalladium Chemistry for Organic Synthesis*; 2002, Wiley, New York.
12. D. Milstein, J. K. Stille, *J. Am. Chem. Soc.*, 1979, **101**, 4992.
13. (a) W. Shi, C. Liu, Z. Yu, A. Lei, *Chem. Commun.,* 2007, 2342, (b) J. Louie, J. F. Hartwig, *J. Am. Chem. Soc.*, 1995, **117**, 11598.
14. A. L. Casado, P. Espinet, *J. Am. Chem. Soc.*, 1998, **120**, 8978.
15. A. L. Casado, P. Espinet, A. M. Gallego, *J. Am. Chem. Soc.*, 2000, **122**, 11771.
16. A. L. Casado, P. Espinet, A. M. Gallego, J. M. Martinez-Ilarduya, *Chem. Commun.*, 2001, 339.
17. A. L. Casado, P. Espinet, *J. Am. Chem. Soc.*, 1998, **120**, 8978.
18. N. Miyaura, A., Suzuki, *J. Chem. Soc., Chem. Commun.*, 1979, 866.
19. N. Miyaura, A., Suzuki, *Chem. Rev.*, 1995, **95**, 2457.

20. S. Kotha, K. Lahiri, D. Kashinath, *Tetrahedron*, 2002, **58**, 9633.
21. M. Miura, *Angew. Chem., Int. Ed. Engl.*, 2004, 1851.
22. E. Negishi, S. Baba, *Chem. Commun.*, 1976, 596.
23. S. Baba, E. Negishi, *J. Am. Chem. Soc.*, 1976, **98**, 6729.
24. I. Sapountzis, H. Dube, P. Knochel, *Adv. Synth. Catal.*, 2004, **346**, 709.
25. E. Jiménez-Núñez, A. M. Echavarren, *Chem. Commun.* **2007**, 333.
26. N. D. Shapiro, F. D. Toste, *J. Am. Chem. Soc.*, 2007, **129**, 4160.
27. E. Jiménez-Núñez, C. K. Claverie, C. Nieto-Oberhuber, A. M. Echavarren, *Angew. Chem., Int. Ed.*, 2006, **45**, 5452.
28. M. Haruta, *Nature*, 2005, **437**, 1098.
29. M. R. Luzung, J. P. Markham, F. D. Toste,. *J. Am. Chem. Soc.* 2004, **126**, 10858.
30. A. S. K. Hashmi, G. J. Hutchings, *Angew. Chem. Int. Ed.*, 2006, **45**, 7896.
31. R. A. Widenhoefer, X. Han, *Eur. J. Org. Chem.*, 2006, 4555.
32. A. S. K. Hashmi, *Angew. Chem., Int. Ed.*, 2005, **44**, 6990.
33. M. Ferrer, L. Rodríguez, O. Russell, J. C. Lima, P. Gómez-Sal, A. Martín, *Organometallics,* 2004, **23**, 5096.
34. C. –L. Chan, K. –L. Cheung, W. H. Lam, E. C. –C. Cheng, N. Zhu, S. W. –K. Choi, V. W. –W. Yam, *Chem. Asian J.*, 2006, **1-2**, 273.
35. M. I. Bruce, B. W. Skelton, A. H. White, N. N. Zaitseva, *J. Organomet. Chem.*, 2003, **683**, 398.
36 M. I. Bruce, M. E. Smith, N. N. Zaitseva, B. W. Skelton, A. H. White, *J. Organomet. Chem.*, 2003, **670**, 170.
37. M. I. Bruce, P. A. Humphrey, G. Melino, B. W. Skelton, A. H. White, N. N. Zaitseva, *Inorg. Chim. Acta*, 2005, **358**, 1453.
38. A. B. Antonova, M. I. Bruce, B. G. Ellis, M. Gaudio, P. A. Humphrey, M. Jevric, G. Melino, B. K. Nicholson, G. J. Perkins, B. W. Skelton, B. Stapleton, A. H. White, N. N. Zaitseva, *Chem. Commun.*, 2004, 960.
39. X. L. R. Fontaine, S. J. Higgins, C. R. Langrick, B. L. Shaw, *J. Chem. Soc., Dalton Trans.*, 1987, 777.
40. R. J. Cross, M. F. Davidson, *Inorg. Chim. Acta,* 1985, **97**, 2, L35.
41. C. E. Powell, M. G. Humphrey, *Coord. Chem. Rev.*, 2004, **248**, 725.

42. R. Nast, *Coord. Chem. Rev.*, 1982, **47**, 89.

43. M. I. Bruce, M. G. Humphrey, J. G. Matisons, S. K. Roy, A. G. Swincer, *Aust. J. Chem.*, 1984, **37**, 1955.

44. N. J. Long, C. K. Williams, *Angew. Chem. Int. Ed.*, 2003, **42**, 2586.

45. M. P. Cifuentes, M. G. Humphrey, *J. Organomet. Chem.*, 2004, **689**, 3968.

46. R. M. Bullocks, *J. Chem. Soc., Chem. Commun.*, 1989, 165.

47. J. P. Selegue, *Coord. Chem. Rev.*, 2004, **248**, 1543.

48. J. P. Selegue, *Organometallics*, 1982, **1**, 217.

49. J. R. Lomprey, J. P. Selegue, *J. Am. Chem. Soc.*, 1992, **114**, 5518.

50. I. de los Ríos, M. J. Tenorio, M. C. Puerta, *J. Am. Chem. Soc.*, 1997, **119**, 6529.

51. I. de los Ríos, M. J. Tenorio, M. C. Puerta, *J. Chem. Soc. Chem. Commun.*, 1995, 1757.

52. M. I. Bruce, *Chem. Rev.*, 1991, **91**, 197.

53. M. C. Puerta, P. Valerga, *Coord. Chem. Rev.*, 1999, **193-195**, 977.

54. M. Baya, P. Crochet, M. A. Esteruelas, A. M. López, J. Modrego, E. Oñate, *Organometallics*, 2001, **20**, 4291.

55. Y. Wakatsuki, N. Koga, H. Yamazaki, K. Morokuma, *J. Am. Chem. Soc.*, 1994, **116**, 8105.

56. R. Stegmann, G. Frenking, *Organometallics*, 1998, **17**, 2089.

57. M. I. Bruce, P. J. Low, F. Hartl, P. A. Humphrey, F. de Montigny, M. Jevric, C. Lapinte, G. J. Perkins, R. L. Roberts, B. W. Skleton, A. H. White, *Organometallics*, 2005, **24**, 5241.

58. A. Klein, O. Lavastre, J. Fiedler, *Organometallics*, 2006, **25**, 635.

59. M. I. Bruce, K. Costuas, T. Davin, B. G. Ellis, J. –F. Halet, C. Lapinte, P. J. Low, M. E. Smith, B. W. Skelton, L. Toupet, A. H. White, *Organometallics*, 2005, **24**, 3864.

60. M. I. Bruce, B. C. Hall, N. N. Zaitseva, B. W. Skelton, A. H. White, *J. Organomet. Chem.*, 1996, **522**, 307.

61. I. R. Whittall, M. P. Cifuentes, M. G. Humphrey, B. Luther-Davies, M. Samoc, S. Houbrechts, A. Persoons, G. A. Heath, D. C. R. Hockless, *J. Organomet. Chem.*, 1997, **549**, 127.

62. I. R. Whittall, M. G. Humphrey, D. C. R. Hockless, B. W. Skelton, A. H. White, *Organometallics*, 1995, **14**, 3970.
63. M. I. Bruce, R. C. Wallis, *J. Organomet. Chem.*, 1978, **161**, C1.
64. M. I. Bruce, B. C. Hall, B. D. Kelly, P. J. Low, B. W. Skelton, A. H. White, *Dalton Trans.*, 1999, 3719.
65. A. Wong, P. C. W. Kang, C. D. Tagge, D. R. Leon, *Organometallics*, 1990, **9**, 1992.
66. C. Gauss, D. Veghini, H. Berke, *Chem. Ber.*, 1997, **130**, 183.
67. M. I. Bruce, B. K. Nicholson, and O. bin Shawkataly, *Inorg. Synth.*, 1989, **26**, 325.
68. C. Bitcon, M. W. Whiteley, *J. Organomet. Chem.*, 1987, **336**, 385.
69. M. I. Bruce, C. Hameister, A. G. Swincer, R. C. Wallis, *Inorg. Synth.*, 1982, **21**, 78.
70. B. Cetinkaya, M. F. Lappert, J. McMeeking, D. E. Plamer, *J. Chem. Soc., Dalton Trans.*, 1978, 381.
71. R. Nast, L. Dahlenburg, *Chem. Ber.*, 1972, **105**, 1456.
72. O. M. Abu Salah, M. I. Bruce, *Aust. J. Chem.*, 1976, **29**, 531.
73. M. I. Bruce, O. M. Abu Salah, *J. Organomet. Chem.*, 1974, **64**, C48.
74. O. M. Abu Salah, M. I. Bruce, *J. Chem. Soc. Chem. Commun.*, 1972, 858.
75. J. A. McGinnety, R. J. Doedens, J. A. Ibers, *Inorg. Chem.*, 1967, **6**, 2243.
76. M. I. Bruce, B. C. Hall, P. J. Low, B. W. Skelton, A. H. White, *J. Organomet. Chem.*, 1999, **592**, 74.
77. C. A. Reed, W. R. Roper, *J. Chem. Soc., Dalton Trans.*, 1973, 1370.
78. M. I. Bruce, B. C. Hall, P. J. Low, M. E. Smith, B. W. Skelton, A. H. White, *Inorg. Chim. Acta*, 2000, **300**, 633.
79. W. H. Baddley, G. B. Tupper, *J. Organomet. Chem.*, 1974, **67**, C16.
80. K. Osakada, M. Kimura, J. –C. Choi, *J. Organomet. Chem.*, 2000, **602**, 144.
81. K. Vrieze, J. P. Collman, C. T. Sears Jr., M. Kubota, *Inorg. Synth.*, 1968, **11**, 101.
82. M. I. Bruce, D. A. Harbourne, F. Waugh, F. G. A. Stone, *J. Chem. Soc. A*, 1966, 356.
83. M. V. Russo, A. Furlani, *J. Organomet. Chem.*, 1979, **165**, 101.

84. O. M. Abu Salah, M. I. Bruce, *Aust. J. Chem.*, 1976, **29**, 73.

85. M. Mayor, C. von Hänisch, H. B. Weber, J. Reichert, D. Beckmann, *Angew. Chem. Int. Ed.*, 2002, **41**, 1183.

86. A. J. Deeming, G. Hogarth, M. –Y. V.Lee, M. Saha, S. P. Redmond, H. Phetmung, A. G. Orpen, *Inorg. Chim. Acta*, 2000, **309**, 109.

87. R. D'Amato, A. Furlani, M. Colapietro, G. Portalone, M. Casalboni, M. Falconieri, M. V. Russo, *J. Organomet. Chem.*, 2001, **627**, 13.

88. F. Takei, S. Tung, K. Yanai, K. Onitsuka, S. Takahashi, *J. Organomet. Chem.*, 1998, **559**, 91.

89. R. Ettorre, A. S. González, *Inorg. Chim. Acta*, 1990, **168**, 221.

90. K. Osakada, T. Takizawa, T. Yamamoto, *Organometallics*, 1995, **14,** 7, 3531.

91. S. J. La Placa, J. A. Ibers, *J. Am. Chem. Soc.*, 1965, **87**, 2581.

92. M. S. Weininger, E. A. H. Griffith, C. T. Sears, E. L. Amma, Inorg. Chim. Acta, 1982, 60, 67.

93. H. –H. Wang, L. H. Pignolet, P. E. Reedy, M. M. Olmstead, A. L. Balch, *Inorg. Chem.*, 1987, **26**, 377.

94. K. Campbell, R. McDonald, M. J. Ferguson, R. R. Tykwinski, *J. Organomet. Chem.*, 2003, **683**, 379.

95. M. Ravera, S. D'Amato, A. Guerri, *J. Organomet. Chem.*, 2005, **690**, 2376].

96. J. Vicente, M. –T. Chicote, M. M. Alvarez-Falcón, P. G. Jones, *Chem. Commun.*, 2004, 2658.

97. K. Angermaier, E. Zeller, H. Schmidbaur, *J. Organomet. Chem.*, 1994, **472**, 371.

98. E. Hernandez, P. Royo, *J. Organomet. Chem.*, 1985, **291**, 387.

99. M. I. Bruce, C. Hameister, A. G. Swincer, R. C. Wallis, *Inorg. Synth.*, 1990, **18**, 270.

100. M. I. Bruce, B. G. Ellis, P. J. Low, B. W. Skelton, A. H. White, *Organometallics*, 2003, **22**, 3184.

101. M. I. Bruce, N. J. Windsor, *Aust. J. Chem.*,1977, **30**, 1601.

102. G. B. Kaufmann, L. A. Teter, *Inorg. Synth.*, 1963, **7**, 245.

103. J. G. Evans, P. L. Goggin, R. J. Goodfell, J. G. Smith, *J. Chem. Soc. A, Inorg. Phys. Theoret.*, 1968, 464.

104. M. J. Mays, P. L. Sears, *J. Chem. Soc., Dalton Trans.*, 1973, 1873.

105. M. I. Bruce, E. Horn, J. G. Matisons, M. R. Snow, *Aust. J. Chem.*, 1984, **37**, 1163.

106. M. I. Bruce, D. N. Duffy, *Aust. J. Chem.*, 1986, **39**, 1697.

107. K. Sonogashira, T. Yatake, Y. Tohda, S. Takahashi, N. Hagihara, *J. Chem. Soc. Chem. Commun.*, 1977, 291.

108. M. A. Fox, R. L. Roberts, W. M. Khairul, F. Hartl, P. J. Low, *J. Organomet. Chem.*, 2007, **692**, 3277.

109. *SHELXTL, version 6.14,* Bruker AXS, Madison, Wisconsin, USA, 2000.

Chapter 7 Conclusion and Future Work

7.1. Conclusion

The preparation, physical and chemical characterisation of long rigid-rod organic molecules with extended π-conjugated systems is of interest within the field of molecular electronics as such systems are thought to have potential to act as "molecular wires". In this thesis, oligo-phenylene ethynylene compounds, specifically tolan and 1,4-bis(phenyl ethynyl)benzene derivatives, have been prepared, characterised and used in the preparation of metal complexes. The tolans contain either donor and acceptor groups, and the transmission of this electronic information from one end of the tolan to the metal centre located at the other has been investigated.

Auration of these ligands afforded the gold(I) oligo-phenyelene ethynylene complexes in good yields. The solid-state structures of these gold(I) complexes were determined, revealing that the bulkiness of the phosphine supporting ligands bound to the gold centre prevents aurophilic interactions between molecules; however, in some molecules there are various π-π and C-H..π interactions between the organic ligands.

The electrochemical properties of ruthenium acetylide complexes featuring simple phenyl, tolan, oligo-phenylene ethynylene moieties have been described. It may be concluded that in the case of simple phenyl derivatives the frontier orbitals contain appreciable metal character, which in the case of the HOMO is also admixed with the ethynyl and aromatic π system. However, in the case of the ethynyl anthracene, the frontier orbitals are largely localised on the anthracene moiety. The characteristics of the simple phenyl derivatives are quite similar to those of the tolan and and the extended "three-ring" derivatives. There is little to suggest that the extended phenylene ethynylene system is a suitable bridging moiety for promoting electronic interactions between metal centres located at the ligand termini. In addition, it can be

noted that there is little if any, influences of the donor or acceptor groups on the electronic properties of these system.

The rich coordination chemistry of C≡CH groups to clusters offer an attractive entry point for further development of the clusters as surface model in molecular electronics and both the terminal alkynes tolans and the analogous gold tolan complexes have been used in the preparation of tolans bearing heterometallic cluster end-caps. Several clusters of the triruthenium carbonyl systems have been prepared and the photophysical characterisation of these clusters revealed that there is a mixing of the electronic states between the cluster and phenylene ethynylene moieties in the excited state. In the electrochemical studies, the phenylene ethylene moieties does not act as a particularly efficient conduit to permit the passage of the electronic effect of either the electron donating or withdrawing groups to cluster core.

The readily available gold acetylide complexes $Au(C{\equiv}CR)(PL_3)$ (L = Ph, Cy) have been used in a novel route to the preparation of several inorganic and organometallic acetylide compounds $M(C{\equiv}CR)L_n$ [M = metal, L_n = supporting ligands]. Simple reactions to investigate the mechanism involved in the reaction also have been carried out. The absence of any detectable protio-vinylidene in the reaction suggests that the transmetallation proceeds perhaps *via* a transient gold vinylidene $[Ru(C{=}C(AuPR_3)R(dppe)Cp^*]^+$ with the position of the equilibrium being solvent / proton dependent. The role of free $AuCl(PPh_3)$ in the reaction is interesting, but clearly more work remains to be done to elucidate the mechanism of this process.

7.2. Future Work

The work carried out in this thesis has been concerned with aspects of the synthesis, physical structures and electronic structures of oligophenylene ethynylene complexes. The combination of phenylene based spacers within the π-conjugated "wire" and ruthenium centres does not appear suitable developing "molecular wires" with extended, delocalised d-π electronic structures. In order to tune the properties

and promote "wire-like" behaviour within ruthenium-based wires, it may be beneficial to explore the greater use of anthrylene moieties within the ligand structure with a view to promoting longer-range, electron transfer via hopping mechanisms. Interestingly, whilst numerous organic polymers containing anthracene moieties are known, there are, to the best of the author's knowledge, only a very limited number of M-C≡C-Anth-C≡C-M systems, and to date no examples of M-C≡C-Anth-C≡C-Anth-C≡C-Anth-C≡C-M based complexes are known. Comparisons of the electronic structures of such systems with those of the analogous phenylene complexes would likely repay investigation. A considerable amount of interest in the organic 1,4-bis(phenylene)ethylene system arises from the fluoresecent behaviour of these compounds, which may serve both as a probe of molecular structure in the ground and excited states and as a molecular property which might be exploited in devices, such as OLEDs. Given the highly fluorescent nature of the anthracene moiety, and the redox chemistry that can be expected from metal complexes of ethynyl anthrancenes, investigations of the redox-switchable fluorescent properties of ruthenium acetylide complexes featuring anthracene moieties could also be profitable.

One of the major challenges in molecular electronics is the self-organisation of molecular materials onto, or in close proximity to, solid state electrode surfaces. With a view to exploiting both the π-π interactions that can occur between oligo(phenylene ethynylene) moieties in the solid state and the aurophilic interactions well-known for gold, the preparation of new series of gold(I) complexes featuring $AuPMe_3$, AuNCR and AuCN-Ar end-caps with reduced steric bulk at the Au centres should be undertaken. The reduced bulk at the gold centres could allow Au...Au interactions and by exploiting the aurophiclic interactions together with the organic π-π type interactions, supramolecular assembly of phenylene ethynylenes on what would amount to a mono-layer of gold can be explored. In addition, the linear –(AuC≡C)- moiety makes this fragment an attractive candidate to prepare multilayer Langmuir-Blodgett films of phenylene ethynylene derivatives molecules that connect not only to the LB substrate but also to each other by various intermolecular interactions. Thus these 'aggregation' suitably functionalised to allow the assembly

of multi-nanometre long molecules onto metallic or semi conducting on metal surfaces.

In general terms, transmetallation reactions are well-known and increasingly important in the area of transition metals in organic synthesis. The demonstration of successful and simple transmetallation reactions in **Chapter 6**, has provided an opportunity to explore a wide range of novel chemistry. For example, gold catalysis is becoming a topic of a considerable body of interest. The development of transmetallation pathways from gold(I) acetylides hints at opportunities for further investigation. Taking advantage of readily prepared gold complexes, further studies could include development of simple cross-coupling protocol based upon the formal elimination of $AuX(PR_3)$ during the Pd/Cu catalysed cross-coupling an organometallic complexes. Bruce has indicated some of these reactions proceed using readily isolable $[(Ph_3P)Au\text{-}\{C{\equiv}C\}_n\text{-}Au(PPh_3)]$, which are not stable as either the terminal or Cu(I) derivatives. Such a useful cross-coupling approach promises much in the preparation of not only metal complexes featuring "all-carbon" ligands but also in the preparation of highly conjugated organic compounds.

Finally, it should be noted that the nature of the metal-molecule junction is not fully understood and the role of the metal-molecule contact on the properties of molecular electronic devices not yet completely described. Longer term goals could centre on an extension of the cluster-surface analogy with a view to better understanding this vital contact.

Appendix. Compounds Numbering Scheme

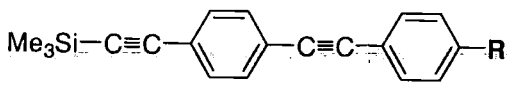

R = Me (**1**), OMe (**2**), CO_2Me (**3**), NO_2 (**4**), CN (**5**)

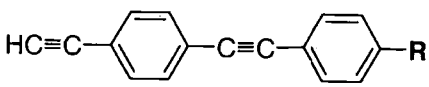

R = Me (**6**), OMe (**7**), CO_2Me (**8**), NO_2 (**9**), CN (**10**)

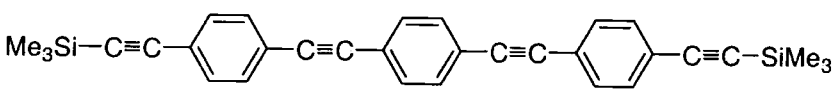

(**11**)

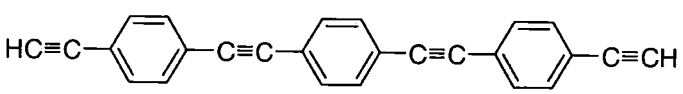

(**12**)

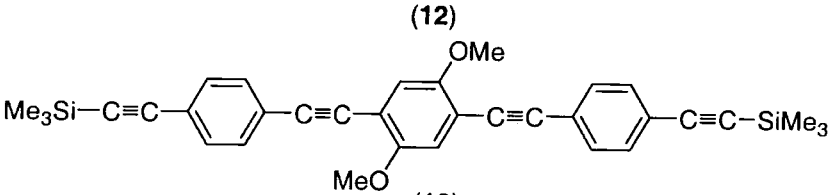

(**13**)

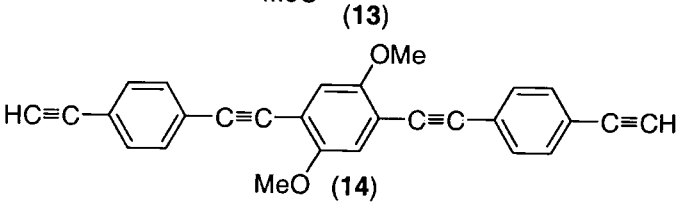

(**14**)

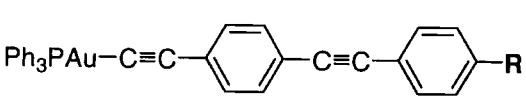

R = Me (**15**), OMe (**16**), CO2Me (**17**), NO_2 (**18**), CN (**19**)

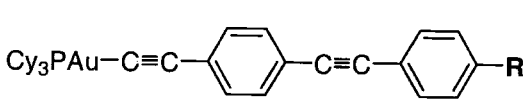

R = Me (**20**), OMe (**21**), NO_2 (**22**)

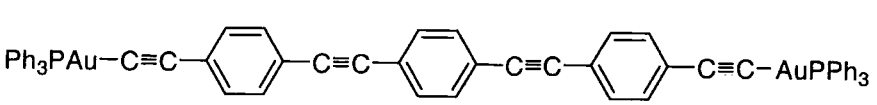

(**23**)

Appendix. Compounds Numbering Scheme (cont.)

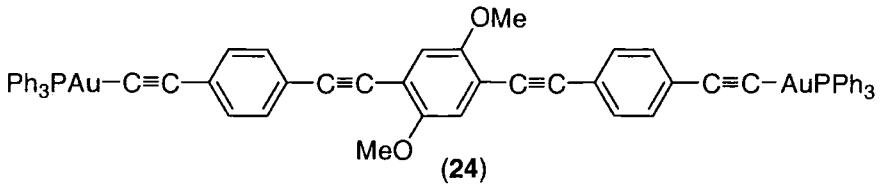

(24)

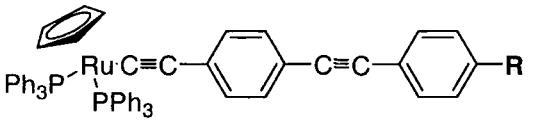

R = Me (**25**), OMe (**26**), CO_2Me (**27**), NO_2 (**28**)

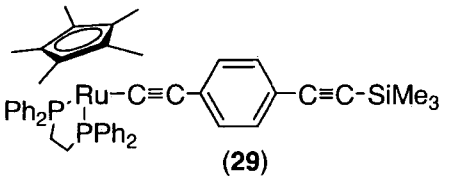

(29)

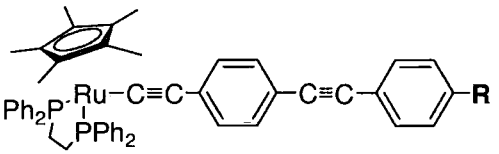

R = Me (**30**), OMe (**31**), CO_2Me (**32**), NO_2 (**33**)

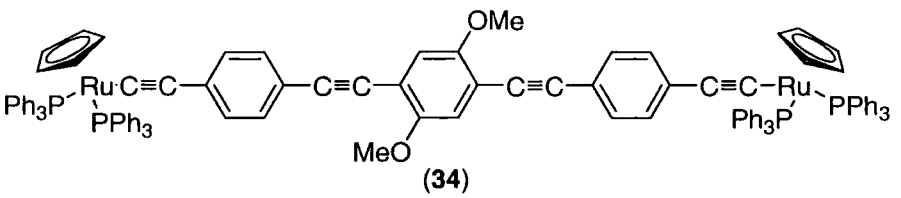

(34)

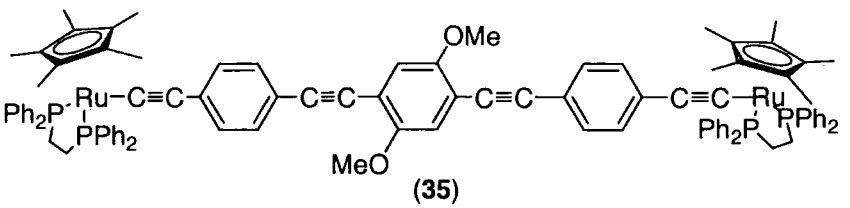

(35)

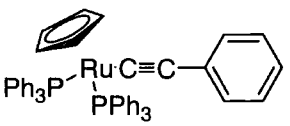

(**Ru1a**)

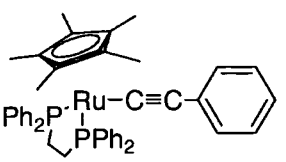

(**Ru1b**)

Appendix. Compounds Numbering Scheme (cont.)

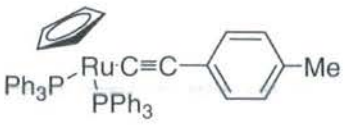

(**Ru2a**)

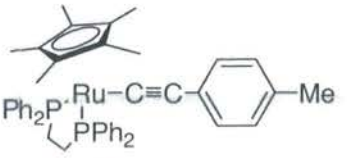

(**Ru2b**)

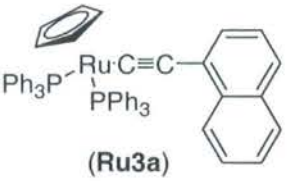

(**Ru3a**)

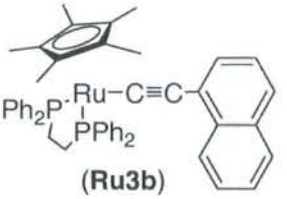

(**Ru3b**)

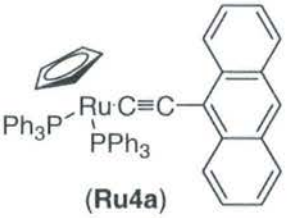

(**Ru4a**)

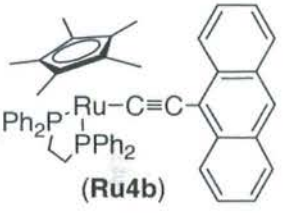

(**Ru4b**)

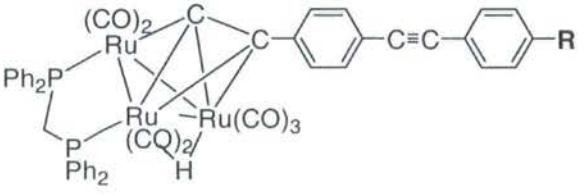

R = Me (**36**), CO_2Me (**37**)

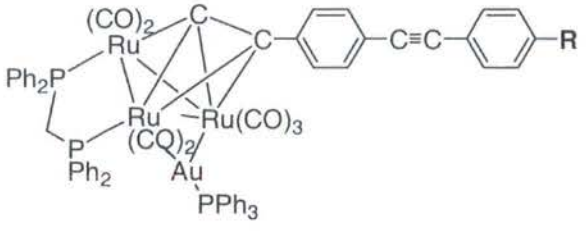

R = Me (**38**), OMe (**39**), CO_2Me (**40**), NO_2 (**41**), CN (**42**)

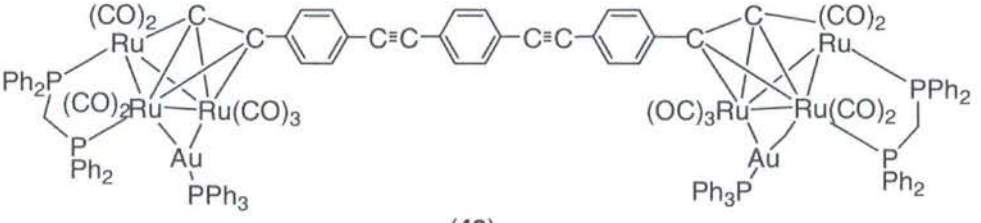

(**43**)

Appendix. Compounds Numbering Scheme (cont.)

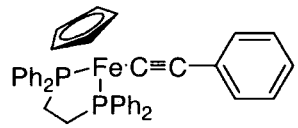

(44)

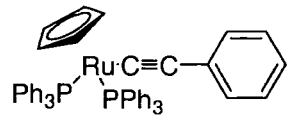

(45)

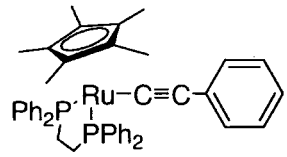

(46)

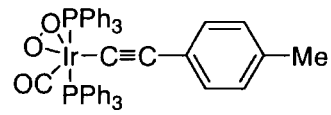

(47)

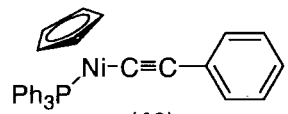

(48)

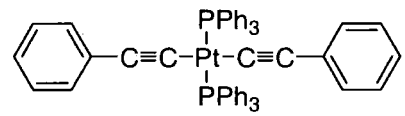

(49)

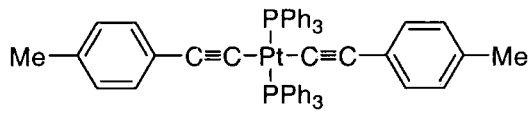

(50)

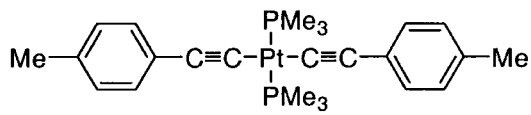

(51)

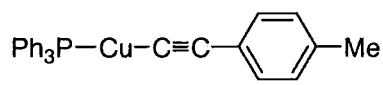

(52)

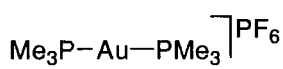

(53)